

The following static magnetization curve given by Praeg of Argonne National Laboratory was used as an input to the GFUN code:

H(oe):	0	7	15	40	1800	6000	100,000
B(gs):	0	10,000	14,000	16,000	20,000	24,000	119,000

Five coils in given locations with a current density of  $1888 \text{ A/cm}^2$  were found to be sufficient to match the given vacuum field distribution. The wall thickness was 6 mm and the axial length which gave the largest average force density was 25 cm. The octagonal shape of the wall was modeled with prismatic finite elements.

The results of the computations may not be very accurate owing to the fact that the net outward pressure is the difference of two large surface force densities computed using finite elements with an awkward aspect ratio. This was dictated by program limitations. Therefore only an estimate is deduced from the results: The net average outward pressure due to static magnetic forces is about one-half atmosphere. By comparison the vacuum magnetic pressure of the 4.2 tesla applied field is

$$\frac{B^2}{2\mu_0} = 7.10^6 \text{ n/m}^2 \approx 1000 \text{ psi} \approx 69 \text{ atm.}$$

The net outward pressure appears as the difference of two (integrated) numbers of this size.

It is concluded that since the outward pressure is of the same order of magnitude as the pneumatic vacuum pressure, no extraordinary engineering problems should result from the use of a magnetic material. However, further analyses is recommended to improve the accuracy of the computations and to study the resulting local stresses.

V.C.2.b. Tritium Breeding Materials.  $\text{Li}_{17}\text{Pb}_{83}$  was chosen as the tritium breeding material because of the following reasons:

1. The chemical activity of the  $\text{Li}_{17}\text{Pb}_{83}$  with water is about four orders of magnitude lower than that of pure liquid lithium.
2. The tritium breeding potential of the  $\text{Li}_{17}\text{Pb}_{83}$  eutectic is excellent due to its intrinsic neutron multiplier, Pb.

3. A liquid heat conduction medium is required in the blanket to reduce the effect of contact resistance.

4. It has the lowest melting point (235°C) among the lithium-lead eutectics.

Lithium and lead were also predicted to be compatible with beryllium metal at 600°C such that the necessity of coating the beryllium with graphite as proposed in the 1979 TMHR molten salt blanket design might be avoided.

The solubility of tritium in the  $\text{Li}_{17}\text{Pb}_{83}$  eutectic was recently found to be very low. A possibility of achieving a very low tritium inventory in this blanket design will be described later.

V.C.2.c Fertile Materials. Candidate thorium fertile materials for fusion-fission hybrid applications were investigated previously.<sup>1</sup> The oxide,  $\text{ThO}_2$ , which has a density of 9.9 g/cm<sup>3</sup> compared to 9.4 g/cm<sup>3</sup> for the  $\text{Li}_{17}\text{Pb}_{83}$  eutectic at 500°C, was chosen as the fertile material to be suspended in the  $\text{Li}_{17}\text{Pb}_{83}$  eutectic because it is expected to be stable in both  $\text{Li}_{17}\text{Pb}_{83}$  and the tritium environment. Due to the necessity of maintaining a suspension equilibrium in the blanket, the density of the suspension particles should be very close to that of  $\text{Li}_{17}\text{Pb}_{83}$  eutectic; the density of  $\text{ThO}_2$  particles should be adjustable during fabrication by introducing controlled amounts of porosity.

Some concern has been raised for the compatibility of beryllium with  $\text{ThO}_2$  and  $\text{UO}_2$  as mentioned in Section V.C.1. A possible solution of that is to coat the  $\text{ThO}_2$  particles with  $\text{BeO}$ ,  $\text{SiC}$  or  $\text{TiC}$ . For a particle of 0.5 mm diameter and a  $\text{SiC}$  coating layer of 10  $\mu\text{m}$ , the coated particle density is 9.5 g/cc which is almost the same as that of  $\text{Li}_{17}\text{Pb}_{83}$  eutectic. The other advantage of coating  $\text{ThO}_2$  particles is that the fission product can thus be well defined in the particle. However, the increase of fabrication cost and fuel reprocessing cost are of concern and cost analysis and comparison are needed.

The separation of  $\text{ThO}_2$  particles of  $\text{Li}_{17}\text{Pb}_{83}$  eutectic can be performed initially using metal screen made of an alloy compatible with  $\text{Li}_{17}\text{Pb}_{83}$  such as the HT-9 steel. Dilute nitric acid can then be used to wash the separated particles to remove lithium and lead wetted on the coating.<sup>49</sup>

## V.D MECHANICAL DESIGN

### V.D.1 Configuration

Figure V-14 shows the central region of the Tandem Mirror Hybrid Reactor where the majority of the power is generated and the breeding and energy recovery is effected. It is divided transversely into 24 identical modules, each 4 m long. Each module is thus a short cylinder standing on its side. It is composed of a series of major annuli around the central bore which is approximately 4 m in diameter. The first of these annuli, the detail composition of which is discussed below, is the blanket zone totaling 0.75 m thickness made in eight separate units forming an octagon around the circular bore (see Fig. V-15). This includes a 0.15 m thick gas distribution plenum behind the blanket proper. The second major annulus is the shield. The latter is of somewhat simpler form, is 1 m thick minimum, and may be up to 1.5 m thick depending on the material chosen. The third annulus, in this case only intermittently occupied along the axial length of the reactor, consists of the central cell magnets (currently at one per 4 m module).

The module has two major circulatory systems, both of which occupy a fraction of the shield space. The first is the gas coolant system described in Section V.E. A distribution ring space is included in the shield annulus to carry the coolant azimuthally around the blanket back plenum from the main connecting pipes. This space is filled by a circular gas distribution plenum which also serves as the backbone on which the submodules are mounted.

Section V.D.3 describes the second circulatory system, which is divided into separate subsystems. This system circulates the blanket working fluid, a liquid lithium-lead eutectic with thoria particles suspended in it, which breeds the tritium and fissile fuel and serves as a contact medium for heat transfer within the blanket. This system also occupies a small part of the shield annulus. The required flows for this system are small, but in the interests of low structure burden this material is not pressurized or confined and every effort is made to restrict its hydrostatic head. Figure V-15 also shows how the shield and magnet rings can be separated from the blanket which has a shorter design life and experiences a more harsh environment than the shield and magnet.

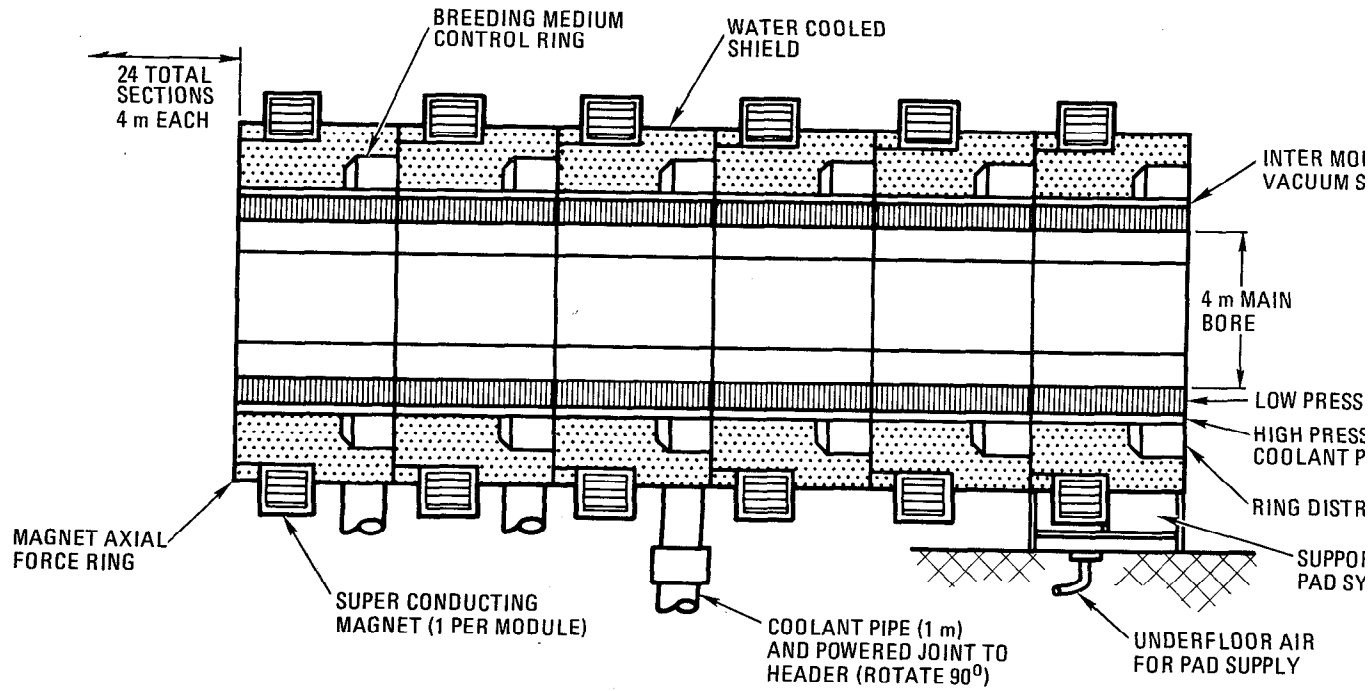


FIGURE V-14. Tandem Mirror Hybrid Reactor body for beryllium/thorium oxide blanket design.

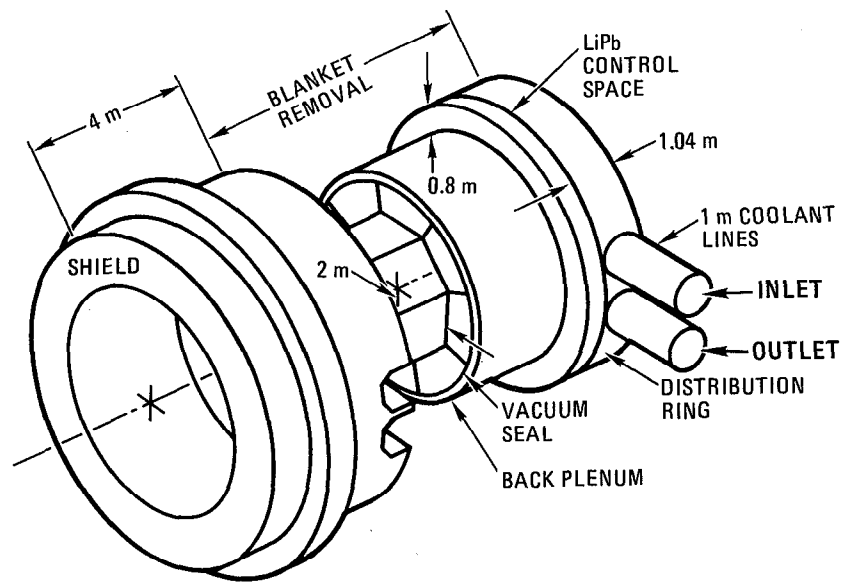


FIGURE V-15. Tandem Mirror Hybrid major module.

V.D.1.a Blanket Submodule Structure. The blanket submodule is shown in Fig. V-1. Its outer base consists of a membrane type pressure vessel furthest from the plasma, the other five walls being corrugated plates with the corrugation blending out at the four front corners leaving simple folded corners. The coolant pressure of 5 MPa requires that the coolant tube be fairly thick. However, since this region is not subject to intensive radiation swelling, it does not produce difficult stressing situations. The sides of the box which is illustrated in Fig. V-16 are oriented towards the plasma and the corrugations are required for two reasons. First, such corrugations provide bending strength to take the box internal pressure, and secondly, they allow the radially nonlinear swelling to produce comparatively small flexure stresses (6 ksi maximum) to deal with their "worst possible" orientation. The first wall is corrugated only to provide bending strength, it should swell uniformly without stress, matching the swelling of the front edges of the box sides. Thus at the beginning of life small wedge shape gaps exist between submodules. As shown in the figure, some internal structures are also required in the low pressure box system to reduce bending on the corrugations, however these also have a separate function as discussed below.

The re-entrant cooling tubes extend towards the plasma from the rear pressure vessel and constitute the majority of the 4% ferritic steel content of the blanket zone. The function and design of these is discussed in Section V.E. It is worthwhile to mention that the design swelling stress of the cooling tube is under 200 psi.

The above components constitute the blanket structure. They are fabricated in HT-9 ferritic steel and are expected to have, as one of their life limiting mechanisms, a radiation swelling limit of  $4 \times 10^{23}$  N/cm<sup>2</sup> (i.e., about 10 years at 2 MW/m<sup>2</sup> neutron wall loading).

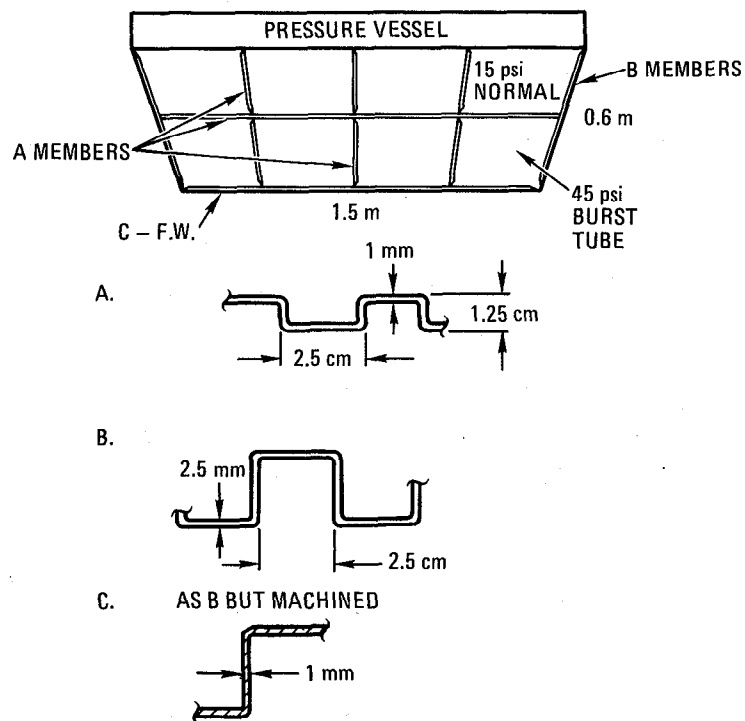


FIGURE V-16. Preliminary low pressure box design.

V.D.1.b Blanket Nuclear Elements. Figure V-17 as well as Fig. V-8 show the front 30 cm long beryllium blocks (see Section V.C for beryllium discussion). These triangular blocks are arranged in such a way that considerable swelling at the front does not inhibit blanket operation (sufficient gap being present for 3-1/4% linear growth). This is done by providing a positive location for the blocks at the first wall only. The rear of the blocks are minimally sprung against the internal membrane mentioned earlier. This membrane completes the restraint necessary to hold the block against flotation forces. The truncated triangular cross section blocks have a small central hole through their hottest region to allow migration of irradiation produced gases out of the beryllium. The only stresses in these blocks are associated with positioning them since their self-induced swelling stress are expected to be small.

The reflector layer is also 30 cm thick and is constructed in a similar manner to the beryllium zone. Due to the swelling resistance of the silicon carbide used and the lower neutron fluence in the reflector zone, this region has no provision for swelling and only flotation forces are expected.

The third significant nuclear component in the blanket is the  $\text{Li}_{17}\text{Pb}_{83}\text{-ThO}_2$  suspension which floods the entire low pressure box, immersing both multiplier and reflector materials. This material, while breeding, transfers heat to the re-entrant cooling tubes.

V.D.1.c Shield and Magnet. The shield and magnet tradeoffs have not been extensively pursued. While the magnet is a considerable design task in its own right, it is not intrusive in the mechanical-structural arrangements, similarly the shield has various feasible configurations where the required thickness is related to the cost of the materials used. The determining factor in the design of these two components is largely that of cost, and feasibility issues are not expected to arise. The cost elements however are not only incurred in the shield-magnet assembly itself. The reactor weight, foundations, building and module mobility are significant drivers in this design.

For the purpose of this design study we have assumed that a lead shield cooled by borated water (20% by volume) will be used. A shield thickness of 1.2 m is assumed. The resulting magnet inner bore is 6.9 m and the magnet pitch is 4.0 m.

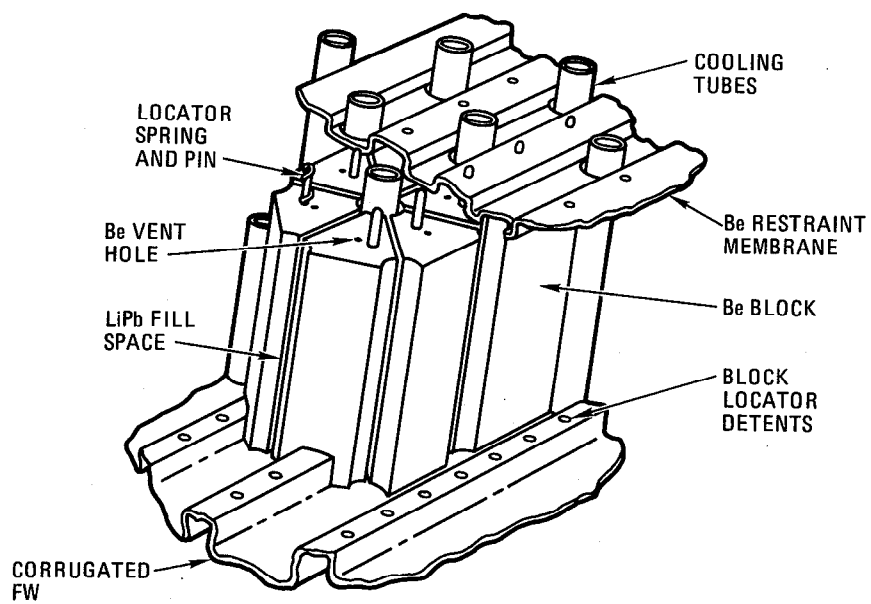


FIGURE V-17. Beryllium zone.

## V.D.2 Maintenance and Accessibility

V.D.2.a Maintenance. For maintenance purposes the reactor central cell is divided into 24 modules, each of which is individually removable and can be replaced while the module requiring maintenance is serviced in a hot cell. In order to take a module off line, which is conceived of as an air-pad job, it must be disconnected from its services and moved to one side. We propose that the normal procedure will then be to remove the blanket from the shield/magnet assembly, place a new blanket in this assembly and replace the module. There will be no possibility of the above tasks being performed hands-on.

Maintenance and service procedures and technologies remain to be engineered, but it does not appear that any uniquely difficult steps will be involved and the required technologies seem to be current state of the art in the automated machine tool industry. The devices produced by this industry are usually dedicated to a certain family of operations, e.g., metal cutting, stamping, welding, subassembly, etc., and carry out those operations very quickly and efficiently. Moreover, in the course of these operations the work has never required much human contact, and over the course of the last two decades this contact has become even less, even being withdrawn, via the use of numerically controlled machines.

The relevance of this to the TMHR operation is that machines are within present technology to make and break pipe joints, electrical connections, move objects, and perform all the module changeout functions. In addition, it is within present technology to record that the above operations are complete and test their function without requiring hands-on work. We thus see the TMHR as a machine programmed to break itself down to the point where the option will exist to scrap the part with no great economic burden, or to apply comparatively new robotic technology to its repair. The breakdown however will not be a high technology operation, neither will it stop the reactor working and cause excessive downtime.

The design and building of such devices as dedicated powered pipe joints is necessarily expensive, however a wide application of such devices is foreseen and the modular reactor approach tends to make them worthwhile. Moreover the technical risk could be much reduced by the use of existing technology or limited extensions of it. The saving in reactor downtime by this

approach is an important as the reduction of technical risk. There seems no reason why the few megajoules of energy required to perform the changeout operation cannot be expended in times of the order of an hour. A motorized self-jointing pipe for instance, is easily envisaged as operating in minutes, perhaps including its self test function and the recording of completion.

An alternate scenario which has been envisaged on some reactor studies involves the modification of present hands-on type connections to interface with man-controlled general purpose manipulators. This has two major disadvantages. The first is that modification of the hands-on connection can leave essentially manual fine adjustments to be made, and the second is that present television-robot links do not give the operator good sensory perception. The lack of inertial input to the balance organs and inappropriate muscular tensions can result in disorientation of the operator. The result is likely to be a slow operation with consequent impact on the plant downtime and many general purpose manipulators and operators could be required.

The present fission reactor scenario where connections are made in marginal radiation conditions by hand, with limited manpower and manually logged and tagged is unlikely to be easily or attractively made remote and thus straightforward application to fusion is unlikely.

V.D.2.b Maintenance Access Summary. The major systems and their characteristics are listed in Table V-17. These systems provide breakdown for maintenance and repair.

TABLE V-17  
MAJOR SYSTEMS SUMMARY

<u>System</u>	<u>Type of Connection or Operation</u>	<u>Power Source</u>	<u>Notes</u>
1. Module mobility	Air pad	Compressor and reservoir	Floor supplied on module.
2. Main coolant	Powered joint*	Air motor	All metal high pressure May be inflated
3. Vacuum seal	Inflatable metal seal	Compressor/reservoir	EPRI Report A 5.3.2 and 5.3.3
4. Shield water coolant	Powered joint*	Air motor	May use organic seals
5. Breeding medium	Powered joint*	Air motor	High temperature Tritium may require joint.
6. Magnet power	Powered connector	Air motor or cylinder	Heavy electrical joint appears
7. Magnet vacuum	Powered joint*	Air motor	Organic seals
8. Magnet refrigerant	Powered bayonet	Air cylinder	Converted existing
9. Thermometry and pressure sensing	Powered connector	Air cylinder	Single multipoint Organics question

\*The powered joints here are expected to be similar in design principles and to be part of standard range.

### V.D.3 Fuel Handling

From the mechanical design standpoint, the most important aspect of the breeding medium system is the control of pressure in the low pressure boxes of the submodules. Figure V-18 shows how this pressure is controlled. The static head of the medium is controlled by free surfaces on the inlet and outlet of each box. For the side boxes of the octagon the maximum static head is 2 atmospheres. A tritium outlet loop is provided to be used as part of the tritium extraction system as described in Section V.F.

Although these surfaces are free, the system must be closed and will be held subatmospheric to both contain the tritium bred in the medium and to lower the box normal operating pressure.

The operating scenario for the medium is discussed in Section V.B. The flow rate required for continuous operation is extremely small 0.25 ( $\text{cm}^3/\text{s}/\text{box}$ ) so electromagnetic effects will not be large if this option is selected. Practical pipes for quick draining and level control will be of the order of 3 - 5 cm diameter in a batch operating mode.

In the event of a tube failure, the contact medium may be pressurized more or less suddenly and in these circumstances the electromagnetic inhibition and inertia of the medium will be important. Figure V-19 shows a burst device intended to allow the gas to escape if the pressure exceeds the box allowable pressure. It should be noted that any small leak occurring, perhaps in manufacture, may well be tolerable. The escaping gas would be gathered and recovered by the tritium control system. The issue of pressurization following a sudden pipe burst requires further study.

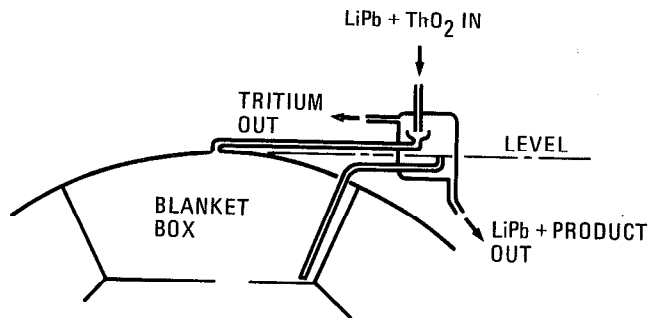


FIGURE V-18. Contact medium level schematic.

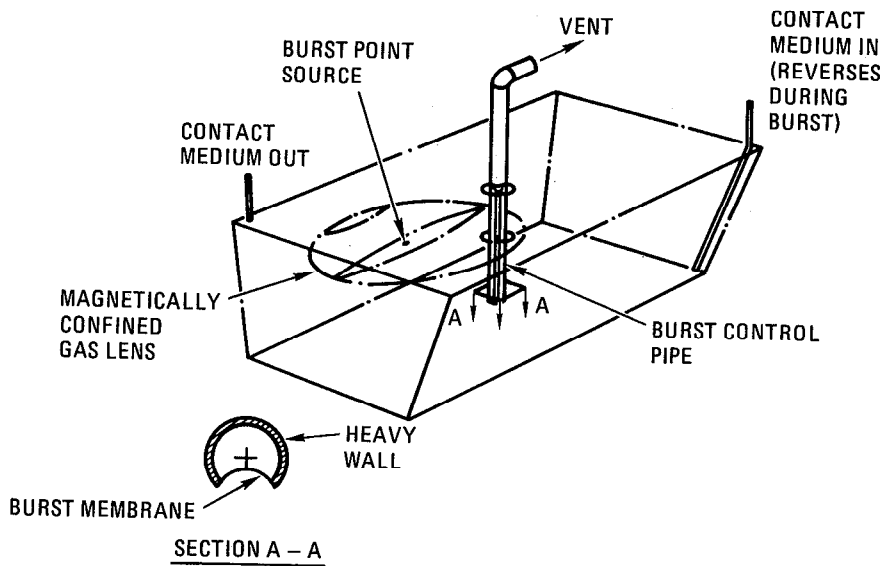


FIGURE V-19. Burst protection system.

## V.E THERMAL-HYDRAULIC DESIGN

### V.E.1 Introduction

Among the general considerations for the thermal-hydraulics design of the TMHR blanket are minimization of structural material, adequate removal of thermal power generated in the blanket (while maintaining acceptable temperature levels for blanket components), and thermal cycle efficiency. Since the principal objective for the TMHR blanket design is to optimize the fissile fuel production rather than to optimize the electrical power production, the emphasis of the thermal-hydraulic design is on the reduction of structural material content in the blanket.

There are some unique features associated with the TMHR blanket which are important to the thermal-hydraulic design. The blanket employs beryllium as the neutron multiplier and a liquid  $\text{Li}_{17}\text{Pb}_{83}$  eutectic (with  $\text{ThO}_2$  particles suspended in it) as the tritium breeding and fissile production medium. Since beryllium swells under neutron irradiation environment, as discussed in Sec. V.C.1, the volume ratio of  $\text{Li}_{17}\text{Pb}_{83}$  and beryllium decreases during blanket life. Also, the volumetric heating in the suspension liquid varies in a wide range as the fissile enrichment in the fertile material increases and the suspension liquid volume fraction decreases. The distinct difference in volumetric heating in the suspension liquid and the solid beryllium metal and their respective thermal conductivities ( $\sim 16 \text{ W/m}^\circ\text{C}$  for  $\text{Li}_{17}\text{Pb}_{83}$  and  $\sim 50 \text{ W/m}^\circ\text{C}$  for 80% dense beryllium metal) further complicates the analysis of a thermal-hydraulic design. Parametric heat transfer analyses were made to justify the recommended heat transfer design such that the maximum temperatures in the blanket components are acceptable under all design conditions.

The aim of the thermal-hydraulic analysis performed here is to identify a feasible pressure tube design by demonstrating that the maximum temperatures expected in various components are within acceptable limits and that pumping power losses in the blanket are not excessive. Important areas considered for the thermal-hydraulic analysis include the temperature distribution in the blanket components along the axis of the pressure tube, the first wall temperature, the power conversion cycle, and the effect of

natural convection of suspension liquid in the magnetic field. Critical areas that require more detailed thermal-hydraulic analysis are also identified.

#### V.E.2 Pressure Tube Design

To minimize the content of structural material in the blanket, a low pressure module design with the concentric pressure tubes as the heat removal unit were selected. Figure V-20 shows schematically the concentric pressure tube design. As shown in this figure, the inlet helium coolant at 250°C flows radially from the inlet plenum through the center of the concentric tube towards the first wall. The coolant, while picking up the nuclear heat, turns around at the tip of the tube and flows along the annulus of the concentric tube towards the reflector and then flows into the outlet plenum. The outlet coolant temperature is 450°C.

The coolant at the tip of the tube will be higher than 250°C because of the recuperation effect from the hot outlet coolant. The recuperation effect may be kept to an acceptable level by introducing in the pressure tube an annular insulation layer of 1 mm thick stagnant helium formed by two thin, 1/4-mm thick tubes. This insulation layer is essential to keep the coolant at the tip of the pressure tube at low temperature for the purpose of reducing the surrounding material to a lower acceptable temperature, since the volumetric heat generation is highest close to the first wall. In particular, all temperatures in the first wall area will, in general, be higher than the coolant temperature at the tip of the tube. To assure a simple design, the pressure tube is also used to cool the first wall.

The thermal-hydraulic calculations are performed by considering a multi-layer concentric cylindrical unit cell. The mass flow rate in the pressure tube is determined by thermal power balance. The coolant velocity and the heat transfer coefficient in the outlet annular region of the pressure tube are then calculated after the annular region geometry is defined.

Figure V-21 shows the cylindrical unit cell modeled for the thermal-hydraulic calculations, where region I is the annular outlet helium zone.

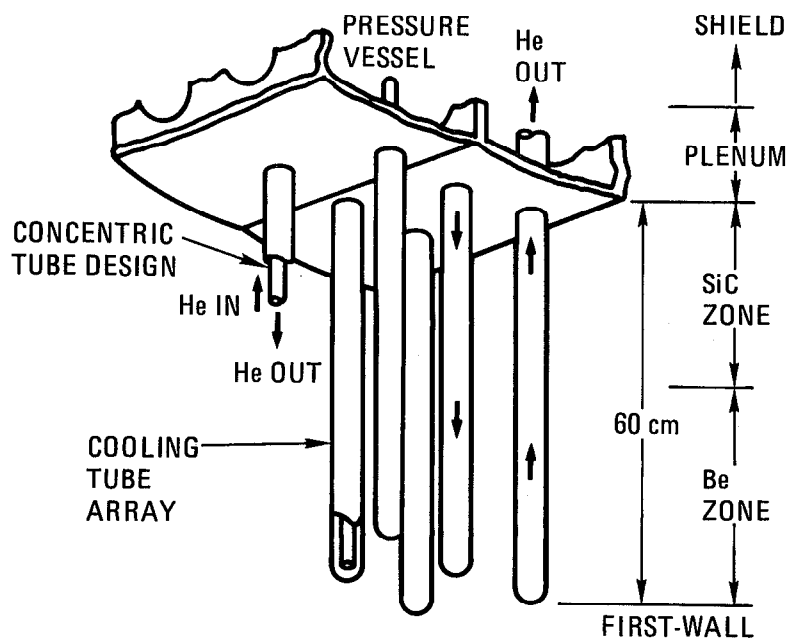


FIGURE V-20. Pressurized tube designs.

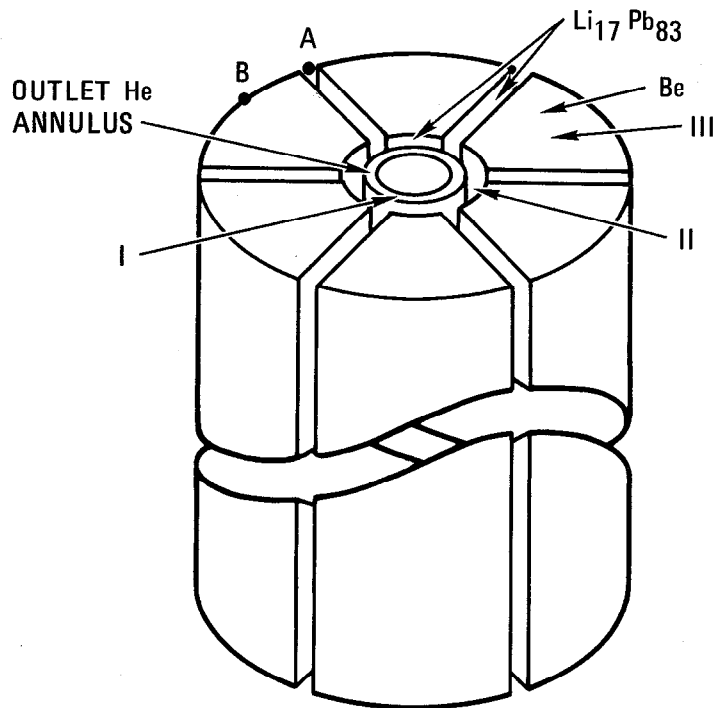


FIGURE V-21. Cylindrical unit cell.

Region II is the  $\text{Li}_{17}\text{Pb}_{83}$  zone, and Region III is the combined zone formed by the beryllium blocks and the  $\text{Li}_{17}\text{Pb}_{83}$  radial sheets. The film drop temperature and the solid temperature drop in the three zones are calculated using equations providing for the multi-concentric layer cylindrical geometry,<sup>51</sup> including volumetric heat generation from the individual zones and the appropriate surface heat flux from the adjacent zones. The average volumetric heat generation in Zone III is represented by the weighted sum of volumetric heat generation in the  $\text{Li}_{17}\text{Pb}_{83}$  suspension liquid and beryllium block multiplied by their respective volume fractions. This assumption is reasonable because of the intimate contact of the  $\text{Li}_{17}\text{Pb}_{83}$  eutectic with the beryllium and the excellent thermal conductivity of the beryllium metal. This weighted volume fraction approach was used because overly conservative results leading to much smaller tube pitch spacing would be obtained when the higher volumetric heat generation and low thermal conductivity of  $\text{Li}_{17}\text{Pb}_{83}$  used were in the calculation. The maximum temperature for the beryllium at location B is thus calculated using the average heat generation and the thermal conductivity of beryllium metal. Similarly, for the calculation of the maximum temperature in the  $\text{Li}_{17}\text{Pb}_{83}$  eutectic at location A, the thermal conductivity of the  $\text{Li}_{17}\text{Pb}_{83}$  is used.

Although the one-dimensional model described here is sufficient to provide adequate information for the preliminary blanket design, more detailed multi-dimensional models should be considered in future studies.

### V.E.3 Pressure Tube Recuperation Temperature

One of the important considerations in the concentric pressure tube design is the recuperation effect. This effect, shown schematically in Fig. V-22, is the heating up of the cold inlet coolant by the hot outlet coolant as it is flowing through the inside of the pressure tube. The recuperation temperature  $\Delta T_{\text{recup}} = T_x - T_i$  should be minimized to keep the coolant and structure temperature reasonably low at the first wall. Physically one can expect that the recuperation temperature,  $\Delta T_{\text{recup}}$ , increases with larger inlet to outlet temperature differential,  $|T_o - T_i|$ , and decreases with better and thicker thermal insulation. The insulation

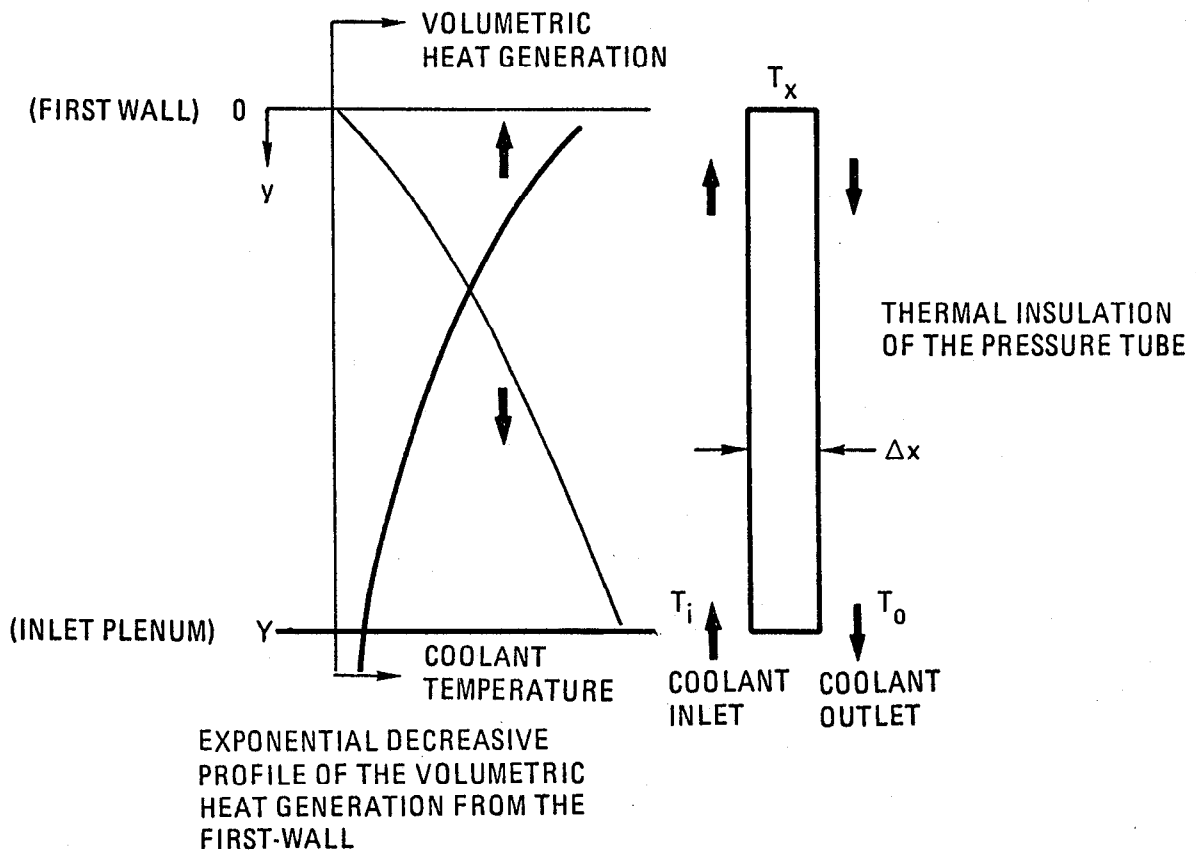


FIGURE V-22. A schematic description of the pressure tube recuperation effect.

material used here is stagnant helium which has a very low thermal conductivity of 0.3 W/m°C and is also transparent to neutrons.

In selecting a suitable design, the crucial temperature to be estimated is  $T_x$ , the temperature at the location closest to the highest nuclear heating. In the following we derive equations for the solution of the temperature  $T_x$ . By assuming an exponential dependence of the volumetric power generation in the blanket and noting that the inlet to outlet coolant temperature differential in the tube is proportional to the integrated heat input, the radial temperature gradient as a function of axial position  $y$  in the tube can be approximated by:

$$\frac{dT}{dx}(y) = \frac{T_o - T_i}{\Delta x} \frac{(1 - e^{-\alpha y})}{(1 - e^{-\alpha Y})}, \quad (V-4)$$

where  $T_i$  and  $T_o$  are the coolant inlet and outlet temperatures,  $\alpha$  is the attenuation coefficient, and  $\Delta x$  is the thickness of the thermal insulation layer, and  $Y$  is the length of the pressure tube. The total power transferring into the inlet coolant can then be calculated by integrating the heat flux along the tube:

$$Q_i = 2\pi R_o k \frac{(T_o - T_i)}{\Delta x} \left[ \frac{Y}{(1 - e^{-\alpha Y})} - \frac{1}{\alpha} \right]. \quad (V-5)$$

Using the equation,

$$\frac{T_x - T_i}{T_o - T_i} = \frac{Q_i}{Q}, \quad (V-6)$$

where  $Q_i$  is the power transferring into the inlet coolant and  $Q$  is the total power deposited in the unit cell around a pressure tube, the recuperation temperature,  $\Delta T_{recup} = T_x - T_i$ , can be calculated.

Results obtained using the above equations indicate that for a stagnant helium layer thickness of 1 mm, with inlet and outlet coolant temperatures of 250°C and 450°C, respectively, the recuperation temperature is 13°C, which is acceptable.

#### V.E.4 Pressure Tube Parametric Heat Transfer

In designing the pressure tube, the first thing to define is the unit-cell and pressure tube geometry. A critical parameter for the neutronics performance of the TMHR is the structure volume fraction  $f_s$ , which is defined as:

$$f_s = \frac{\text{Volume of structure}}{\text{Volume of unit cell including structure, suspension liquid and beryllium}}$$

Figure V-23 illustrates a 5 cm diameter unit cell.

The selection of 0.25 mm inner wall thickness is based on reasonably thin HT-9 tubing that can be manufactured. The 1 mm thick stagnant helium thickness is determined by reasonably adequate thermal insulation required as discussed earlier. The 1 mm thick coolant outlet annular gap is defined by minimum gap width to enhance convective heat transfer, yet within the range of manufacturing feasibility to maintain the required gap dimension.

Figure V-24 shows the structure volume fraction as functions of inner tube radius  $R_o$  and outer tube thickness  $\Delta x$ . Within the proposed structure volume fraction range of 3 - 5% as discussed in Section V.B, a recommended tube internal radius of 0.4 cm combined with an outer tube wall thickness of 0.5 mm can allow a structure volume fraction close to 3%, thus allowing some margin for the necessary additional structural requirement in the low pressure blanket. Since the design tensile stress limit for HT-9 at 550°C is 151 MPa, the outer wall thickness of 0.5 mm for the 1.5 cm diameter tube is reasonable to withstand the hoop stress of 78 MPa on the HT-9 outer tube, with 5 MPa (50 atm) helium as the coolant.

With the unit-cell and pressure tube dimensions specified, parametric results are then obtained for the maximum temperatures in the outer pressure tube wall and in the beryllium metal as functions of the volumetric power generation and the  $\text{Li}_{17}\text{Pb}_{83}$  layer thickness. Figure V-25 shows these results. With reference to Fig. V-23, the  $\text{Li}_{17}\text{Pb}_{83}$  layer thickness  $\Delta x_{\text{Li-Pb}}$ , is defined as the annular  $\text{Li}_{17}\text{Pb}_{83}$  layer next to the pressure tube and the six radial slot thicknesses as indicated in that figure. Figure V-25 also shows the corresponding volume fractions of the  $\text{Li}_{17}\text{Pb}_{83}$  suspension liquid and beryllium components as the  $\text{Li}_{17}\text{Pb}_{83}$  layer thickness varies. Using the parametric results shown in Fig. V-25, the operating temperature ranges in

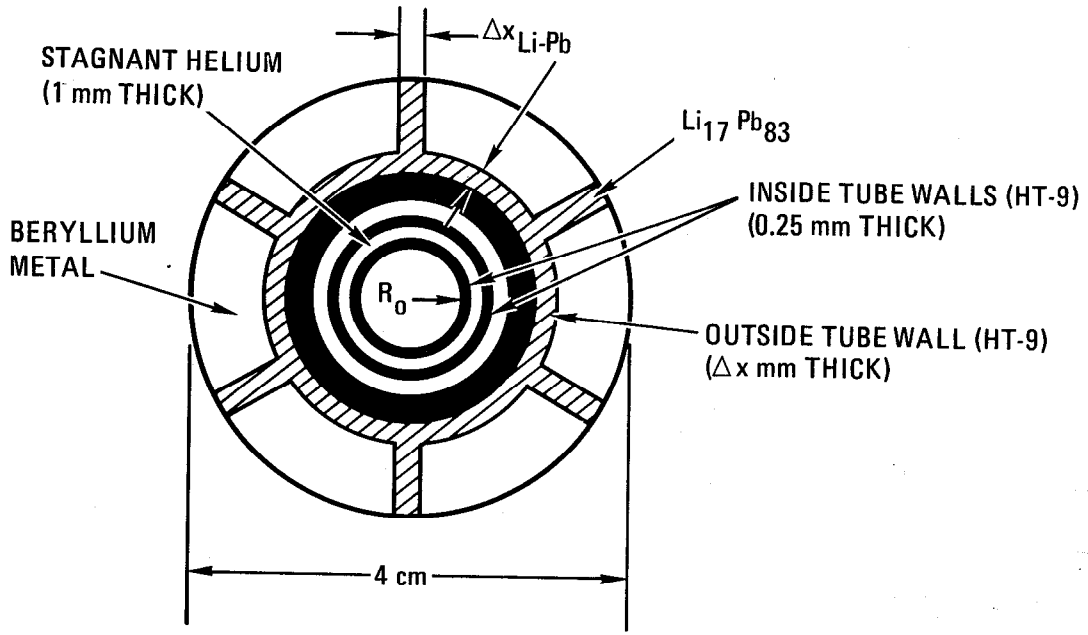


FIGURE V-23. Illustration of a 4 cm diameter unit cell.

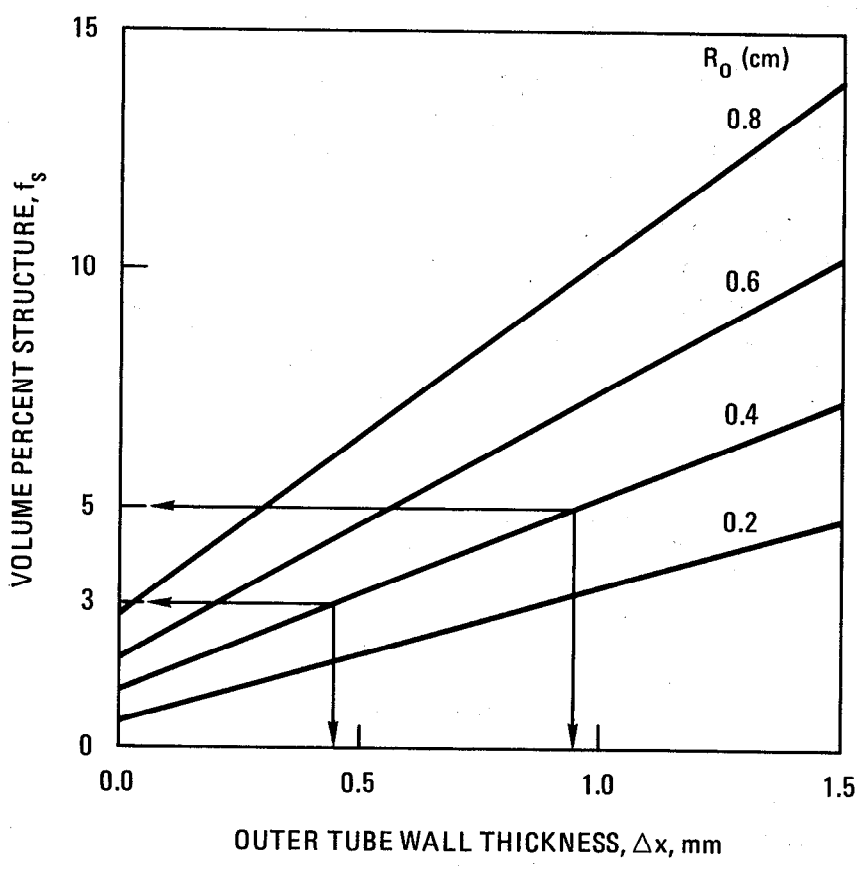


FIGURE V-24. Structural volume fraction of unit cell as a function of inner tube radius  $R_0$  and outer tube wall thickness  $\Delta x$ .

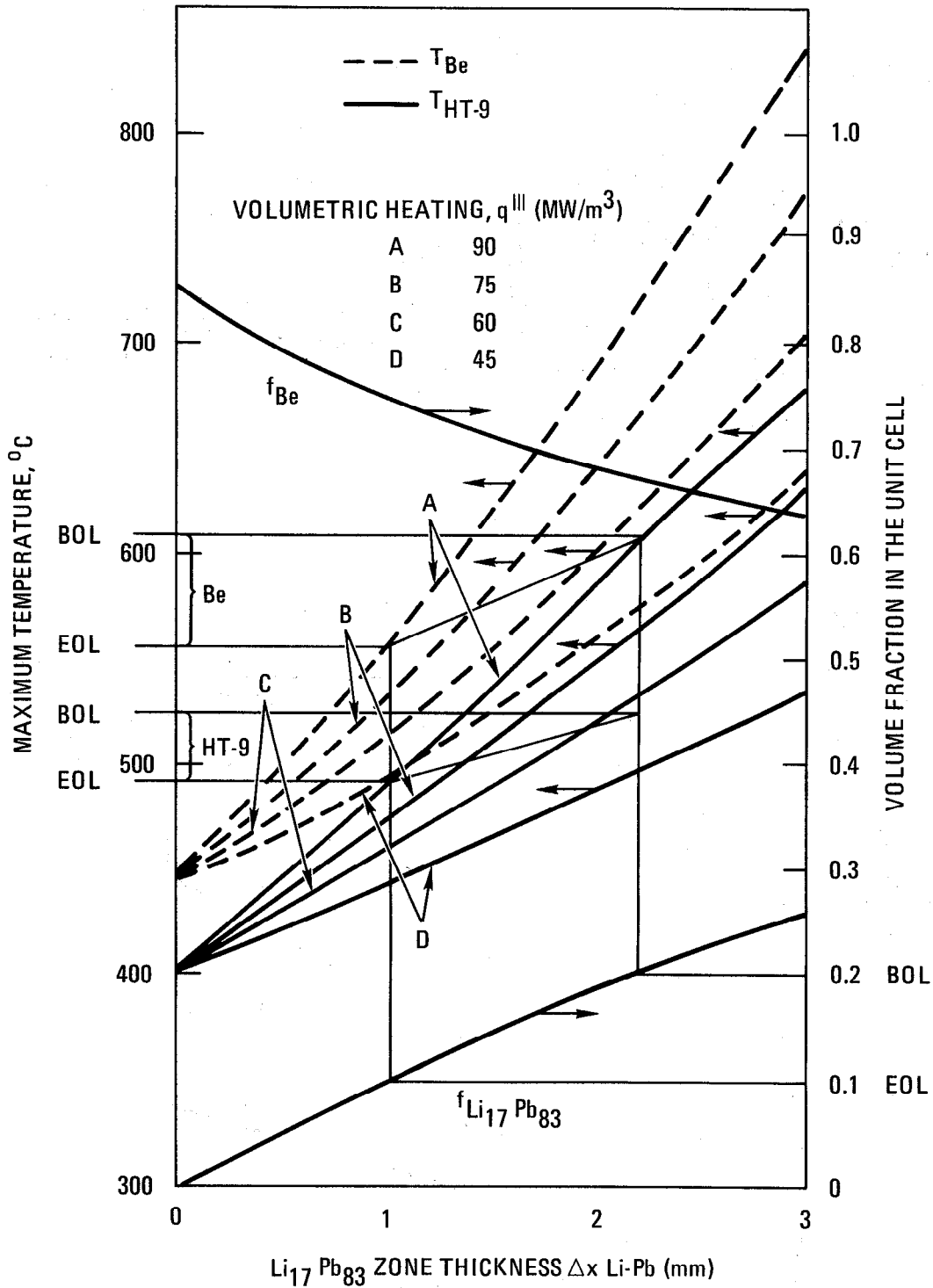


FIGURE V-25. Parametric results for the volume fractions and maximum temperature of HT-9 and beryllium metal in the pressure tube design for the TMHR gas-cooled blanket at beginning of life (BOL) and end of life (EOL).

the HT-9 ferritic steel pressure tube and in the beryllium component can then be determined. As mentioned earlier, the volume fraction of the suspension liquid,  $\text{Li}_{17}\text{Pb}_{83}$  eutectic, varies from 20% to 10% and the volumetric power generation varies from 56 to 90  $\text{MW/m}^3$  in the suspension liquid during the blanket life. The corresponding maximum temperature in the beryllium component varies from  $610^\circ\text{C}$  to  $550^\circ\text{C}$  and in the HT-9 tube component from  $520^\circ\text{C}$  to  $490^\circ\text{C}$ , respectively. It is of interest to note that the volumetric heat generation is higher at the end of blanket life (EOL), however the temperatures in the blanket components are lower than at the beginning of blanket life (BOL). The reason for this is that the suspension liquid layer is thicker at the beginning of life, which results in relatively poor conductivity. Nevertheless, the above operating temperatures are acceptable for both beryllium metal and HT-9 tube components.

#### V.E.5 Reference Pressure Tube Design

Table V-18 summarizes the design characteristics for the reference pressure tube design. The coolant inlet and outlet temperature difference is  $200^\circ\text{C}$  which is relatively low. This is selected to reduce the recuperation loss to a low value of  $13^\circ\text{C}$ . The resulting steam cycle thermal efficiency is ~36%.

The pumping power required for the helium coolant to flow through the pressure tube is less than 0.5% of the thermal power deposited in the unit cell. This is not small, yet acceptable for the hybrid design.

Figure V-26 displays the axial maximum temperature distributions in the HT-9 tube and beryllium metal components. It shows in this figure that the helium temperature rises from  $263^\circ\text{C}$  to  $450^\circ\text{C}$  as it flows from the tip of the tube toward the outlet. It is interesting to note that the temperature in the beryllium metal and HT-9 tube components drops rapidly with distance from the first wall. This is because of the rapid decrease of the volumetric power generation in the blanket components.

**TABLE V-18**  
**DESIGN CHARACTERISTICS FOR THE REFERENCE PRESSURE TUBE DESIGN**

<b>PRESSURE TUBE DIMENSIONS</b>	
(WITH REFERENCE TO FIG. V.E-4)	
INNER TUBE DIAMETER .....	.0.8 cm
OUTER TUBE DIAMETER .....	.1.4 cm
PITCH SEPARATION BETWEEN TUBES .....	~4 cm
TUBE LENGTH .....	.60 cm
INNER WALL THICKNESS .....	.0.25 mm
OUTER WALL THICKNESS .....	.0.5 mm
STAGNANT HELIUM GAP .....	.1 mm
OUTLET HELIUM GAP .....	.1 mm
<b>COOLANT .....</b>	
	<b>5 MPa (50 atm.) HELIUM</b>
T <sub>IN</sub> .....	.250°C
T <sub>OUT</sub> .....	.450°C
OUTLET COOLANT VELOCITY .....	33 m/sec
REYNOLD'S NUMBER .....	.6604
CONVECTIVE HEAT TRANSFER COEFFICIENT .....	.2804 W/m <sup>2</sup> °C
RECUPERATION TEMPERATURE DROP .....	.13°C
<b>MAXIMUM VOLUMETRIC POWER GENERATIONS</b>	
Li <sub>17</sub> Pb <sub>83</sub> SUSPENSION LIQUID .....	
BOL .....	56 MW/m <sup>3</sup>
EOL .....	90 MW/m <sup>3</sup>
BERYLLIUM-METAL (80% DENSE) .....	14 MW/m <sup>3</sup>
<b>VOLUME FRACTIONS</b>	
Li <sub>17</sub> Pb <sub>83</sub> .....	18.7%
BERYLLIUM-METAL .....	69.1%
STRUCTURAL MATERIAL, HT-9 .....	2.9%
HELIUM .....	9.3%
<b>MAXIMUM TEMPERATURES</b>	
Li <sub>17</sub> Pb <sub>83</sub> SUSPENSION LIQUID .....	663°C
BERYLLIUM-METAL .....	596°C
HT-9 PRESSURE TUBE .....	514°C
<b>POWER CONVERSION SYSTEM</b>	
STEAM CYCLE THERMAL EFFICIENCY, $\epsilon_{th}$ .....	~36%
<b>PUMPING POWER</b>	
COOLANT PRESSURE LOSS THROUGH THE CONCENTRIC PRESSURE TUBE .....	16.4 kPa
PUMPING POWER/UNIT CELL THERMAL POWER .....	<0.5%
NUMBER OF PRESSURE TUBE/AREA .....	~800/m <sup>2</sup>

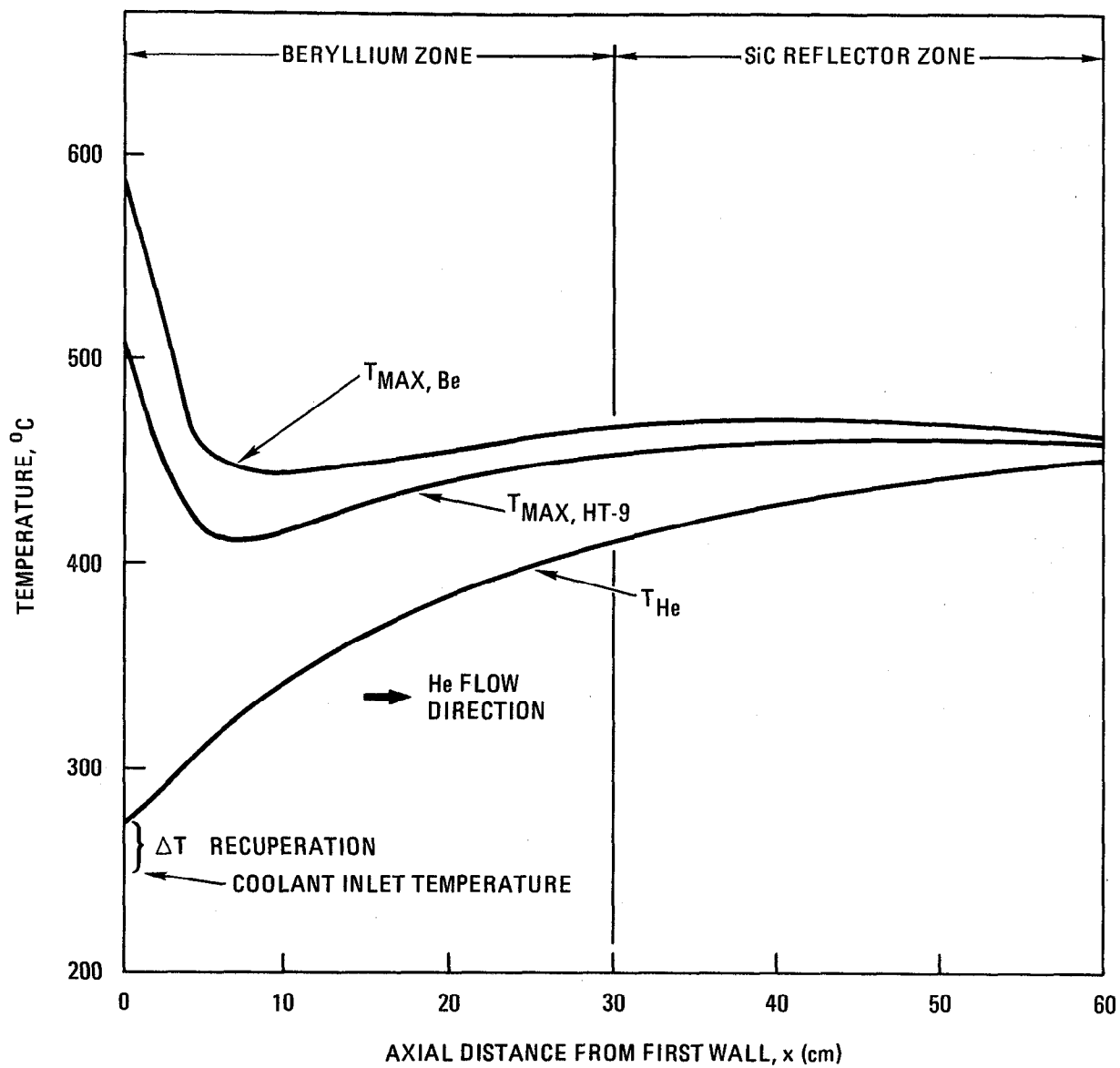


FIGURE V-26. Axial temperature distributions in the pressure tube and beryllium components defined in a unit cell.

#### V.E.6 First Wall Temperature Estimate

To simplify the blanket design, a corrugated first wall design is proposed. It is cooled by the pressure tubes. A simple model is used to estimate the maximum first wall temperature. Figure V-27 illustrates the model under consideration, which allows the pressure tube to insert into the corrugated space.

Because of its high thermal conductivity, the beryllium metal is designed to fill in as much space as possible close to the first wall to enhance heat conduction. With reference to Fig. V-27, the maximum temperature of the tube at location A was calculated using the mechanism described in Section V.E.5. The maximum temperatures at locations B and C were calculated by simple conduction path consideration for the slab geometry with volumetric power generation along distances AB and BC.

The volumetric power generation in the first wall is  $19 \text{ MW/m}^3$  as described in Section V.B. With the inclusion of a surface wall loading of 0.5% of the neutron wall loading and the tapered geometry of the unit cell, the maximum temperature calculated at the first wall is  $600^\circ\text{C}$ , which is above the recommended maximum operating temperature for HT-9 ferritic steel. However, because of the low pressure module design the required strength of the first wall material is much less than that required for the pressure vessel wall. The reduced strength at higher temperature can be compensated by reducing the distance of the supporting span in the blanket, yet conserving the amount of structural material. The first wall temperature may be lowered to about  $550^\circ\text{C}$  if design considerations for the first wall such as the addition of fins to the tip of the tubes are taken to optimize the design. This can be investigated in the future detailed blanket designs.

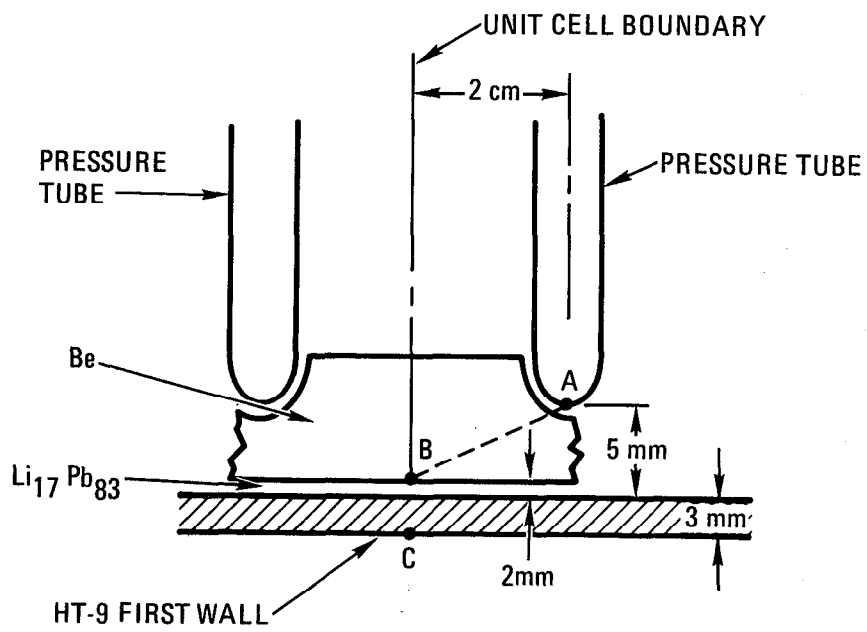


FIGURE V-27. Schematic of a first wall pressure tube model for temperature calculations.

### V.E.7 Natural Circulation in Uniform Magnetic Field

Because of the high volumetric power generation and relatively low thermal conductivity in the  $\text{Li}_{17}\text{Pb}_{83}$ , it is expected that the temperature differential across the  $\text{Li}_{17}\text{Pb}_{83}$  layer can be as large as  $\sim 50^\circ\text{C}$ . It is of interest to investigate the effect of natural convection for  $\text{Li}_{17}\text{Pb}_{83}$  under a uniform magnetic field.

Gierszewski, *et al.*,<sup>52</sup> showed by dimensional analysis that for liquid metal in the presence of uniform magnetic field, the effective thermal conductivity  $k_{\text{eff}}$  can be approximated by:

$$k_{\text{eff}} = \frac{\psi}{k_{\text{eff}}} + k, \quad (\text{V-7})$$

$$\text{where } \psi = \frac{C_p^2 g C_p L^2 \beta \dot{q}'''}{2\sigma B^2}$$

with  $k$  - thermal conductivity,  $16 \text{ W/m}^\circ\text{C}$

$C_p$  - specific heat,  $160 \text{ J/sec m}^\circ\text{C}$

$\rho$  - density,  $9400 \text{ kg/m}^3$

$g$  - acceleration due to gravity, usually  $9.8 \text{ m/sec}^2$

$L$  - characteristic dimension,  $\Delta x_{\text{Li-Pb}}$ ,  $2 \text{ mm}$

$\beta$  - thermal coefficient of volume expansion: assumed to be  $2 \times 10^{-4} \frac{1}{\text{K}}$

$\dot{q}'''$  - volumetric power generation,  $\text{MW/m}^3$

$\sigma$  - electrical conductivity,  $0.93 \times 10^6 \Omega^{-1} \text{ m}^{-1}$

$B$  - magnetic field strength  $3 \text{ tesla}$

Note that all the above parameters except  $\sigma$  and  $\beta$  were obtained for  $\text{Li}_{17}\text{Pb}_{83}$ . The values for  $\sigma$  and  $\beta$  were obtained for lead because they are not available for  $\text{Li}_{17}\text{Pb}_{83}$ .  $C$  is a constant taken to be  $0.3$  to correlate to experimental results. Equation (V-7) can be solved for  $k_{\text{eff}}$  and it gives

$$k_{\text{eff}} = \frac{k + \sqrt{k^2 + 4\psi}}{2}. \quad (\text{V-8})$$

As seen from Eq. (V-7) it turns out that the value  $\psi$  is very sensitive to the characteristic dimension  $L$ . For a gap width of 2 mm, the effective thermal conductivity is improved by <4% at a magnetic field strength of 3 tesla. Thus natural convection is not very effective in reducing temperature differentials. This also implies a minimum internal circulation of the  $\text{ThO}_2$  particles in the  $\text{Li}_{17}\text{Pb}_{83}$  suspension.

#### V.E.8 Observations and Recommendations

From the above considerations, we may conclude that the low pressure blanket module design with the pressure tube as the heat removal element is feasible for the TMHR from the thermal-hydraulics point of view. However, detailed multi-dimensional heat transfer calculations are required to confirm the design characteristics of the blanket and the first wall. Further design optimization of the component configuration is needed to reduce the maximum temperature level in the blanket and the first wall.

An example of the improved unit cell configuration is given below. This unit cell is composed of an annular beryllium-metal cylinder instead of several triangular blocks. The inner and outer layers are filled with  $\text{Li}_{17}\text{Pb}_{83}$  suspension liquid. For the same volume fractions of materials as in the reference pressure tube design, the maximum temperatures in the blanket components can be reduced by  $\sim 50^\circ\text{C}$ . By adopting this design approach the tube pitch separation can be increased, thus the number of tubes per unit area and the probability of tube failure can be reduced. The credibility of the pressure tube blanket design can therefore be enhanced.

More detailed thermal-hydraulic analysis in other areas are also needed. For example, the heat removal performance at the tip of the pressure tube where the radial coolant flow changes direction, and the heat transfer analysis between the  $\text{ThO}_2$  particles and the  $\text{Li}_{17}\text{Pb}_{83}$  eutectic are all essential in the future study.

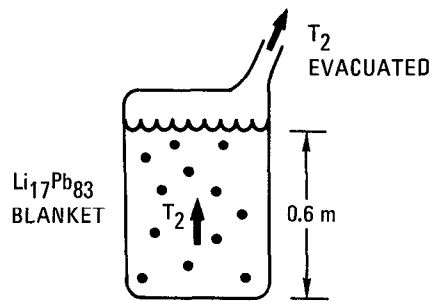
## V.F TRITIUM HANDLING

One area which becomes more critical as the design of fusion power reactor becomes more mature is the confinement and extraction of tritium bred in the blanket. The tritium production rate in the TMHR blanket is estimated to be 487 grams per day, or  $4.7 \times 10^6$  curies per day. At equilibrium this must be equal to the extraction rate from the blanket. Four options were considered for tritium removal from the TMHR blanket: (1) bulk diffusion, (2) side stream extraction, (3) helium percolation and (4) release to the main coolant as illustrated schematically in Fig. V-28.

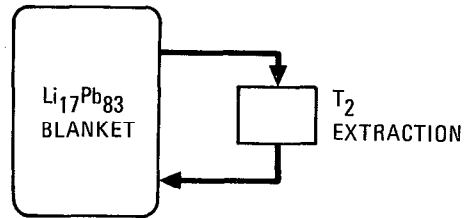
The bulk diffusion extraction method relies on the diffusive property of tritium in  $\text{Li}_{17}\text{Pb}_{83}$  such that the bred tritium diffuses to an evacuated region in the blanket module where it can be extracted. The extraction region has to have a pressure lower than the partial pressure of  $\text{T}_2$  in the blanket as defined by the solubility of  $\text{T}_2$  in  $\text{Li}_{17}\text{Pb}_{83}$  at  $7.25 \text{ appm/torr}^{\frac{1}{2}}$ .<sup>53</sup>

By assuming a simple slab model of 0.6 m thick corresponding to the blanket thickness, a tritium diffusion coefficient of  $10^{-3} \text{ cm}^2/\text{sec}$ ,<sup>46</sup> a total blanket volume of  $125 \text{ m}^3$  and a  $\text{T}_2$  generation rate of  $5.6 \times 10^{-6} \text{ kg/sec}$ , the  $\text{T}_2$  inventory in the blanket was calculated to be 11 kg. This inventory is relatively high for the TMHR which has a nuclear power output of  $\sim 4700 \text{ MW}_{\text{th}}$ .

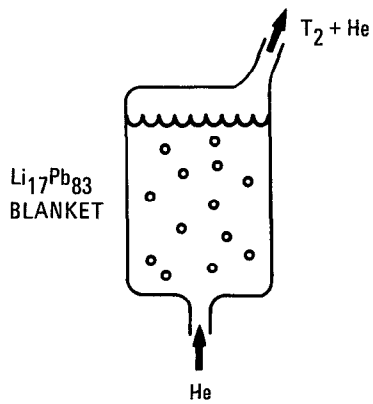
The second option of tritium extraction is to extract the bred tritium from a side stream of  $\text{Li}_{17}\text{Pb}_{83}$  outside the blanket as illustrated in Fig. V-28b. The blanket tritium inventory is a function of  $\text{Li}_{17}\text{Pb}_{83}$  circulation rate and the efficiency of the extraction system. Using the molten salt extraction model presented in Section IV.F, we are able to calculate the required processing rate as a function of the desired tritium inventory in the  $\text{Li}_{17}\text{Pb}_{83}$ . In this case we assume a more favorable volumetric distribution coefficient for Li-Pb than for liquid lithium<sup>46</sup> and assume that  $D_v$ ,  $\epsilon$ , and  $\eta$  are 100, 0.3, and 0.3, respectively. For a 487 gram per day tritium production rate and a 1 kg tritium inventory in the  $\text{Li}_{17}\text{Pb}_{83}$ , the fractional processing rate is 0.54 of the  $\text{Li}_{17}\text{Pb}_{83}$  blanket inventory per day. Conversely, if the Li-Pb is to be processed on a 30 day time scale (more representative of the fuel residence time), the resulting tritium inventory would be about 16 kg. Since the latter value is, most likely excessive, this option requires an active circulation system to continuously extract the suspension from the blanket



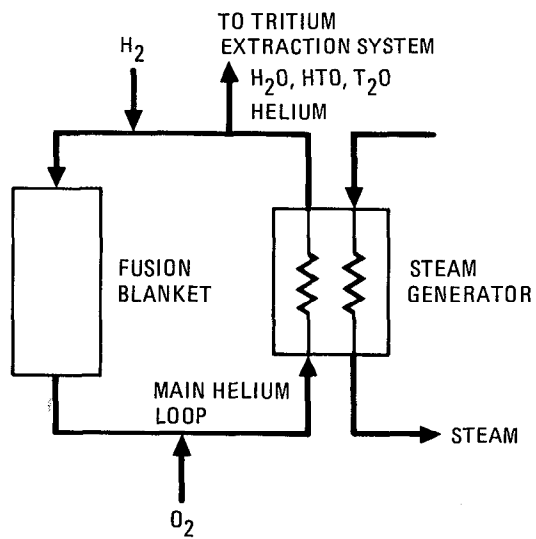
(a) BULK DIFFUSION



(b) SIDE STREAM EXTRACTION



(c) HELIUM PERCOLATION PRESSURE



(d) RELEASE TO MAIN COOLANT

FIGURE V-28. Options for tritium removal from the TMHR blanket.

and return it via a side stream. Such a process would also be useful with respect to circulation of the suspension to assume mixing in the blanket, but concerns associated with circulating the  $\text{ThO}_2$  in the suspension outside of the blanket require further study.

The third option of tritium extraction is to percolate flow of low pressure helium through the  $\text{Li}_{17}\text{Pb}_{83}$  eutectic. Due to the low solubility of  $\text{T}_2$  in  $\text{Li}_{17}\text{Pb}_{83}$ , the bred tritium can be carried away in the helium bubbles, as illustrated in Fig. V-28c. The blanket tritium inventory depends on the volume flow rate of the percolating helium. Assuming a percolating helium pressure of  $2 \times 10^5$  Pa (2 atmospheres) and a solubility value of  $7.25 \text{ appm/torr}^{1/2}$  for  $\text{T}_2$  in  $\text{Li}_{17}\text{Pb}_{83}$ , for helium volume flow rates of 0.28 and  $2.8 \times 10^{-3} \text{ m}^3/\text{sec}$ , the blanket tritium inventories were calculated to be 0.1 and 1 kg. These are acceptable flow rates and tritium inventories. However, because of the small gap sizes ( $\sim 2$  mm) associated with the TMHR blanket and the potential flow path for helium bubbles in the blanket, it is difficult to have a design that has evenly distributed percolating bubbles in the blanket.

The last option of tritium removal is to release the bred tritium into the main helium coolant. This method of releasing tritium into the main coolant utilizes the low solubility property of tritium in the  $\text{Li}_{17}\text{Pb}_{83}$  eutectic which leads to high tritium partial pressure in the blanket and therefore enhances the permeation of tritium into the helium coolant from the  $\text{Li}_{17}\text{Pb}_{83}$  through the HT-9 ferritic steel pressure tube wall.<sup>54</sup>

Figure V-28d shows schematically the power cycle and tritium flow diagram which is applicable for the TMHR gas cooled blanket.<sup>55</sup> As shown in this figure, the high temperature helium ( $\sim 450^\circ\text{C}$ ) is circulating into the steam generator to deliver heat to the steam. The helium coolant contains a tritium concentration such that the steam in the steam generator may be contaminated with tritium which results in tritium release to the environment. The addition of oxygen in this loop will maintain an oxide layer on the tube wall and can reduce the tritium permeation into the steam cycle. The tritium, mostly in the form of HTO and  $\text{T}_2\text{O}$ , is then extracted from the helium stream after passing through the steam generator. There is a concern regarding the addition of oxygen in the cooling loop that the inner side of the pressure tube wall may be oxidized to form an oxide layer

on the wall which reduces the permeation rate of tritium into the helium coolant. This concern can be alleviated by maintaining a positive hydrogen pressure in the coolant as shown in Fig. V-28d.

A preliminary analysis of the tritium inventory in the blanket was performed utilizing data provided in Refs. 54 and 56. Based on the assumption that the maximum tritium release to the environment (mainly through the steam generator) is 10 curies per day per gigawatt electric power, the gas-cooled TMHR shall release no more than 15 Ci per day tritium into the steam generator since its power rating is about 1500 MW electric. Using the data and calculational technique provided in Ref. 56, the tritium partial pressure in the helium coolant should be limited to  $1.1 \times 10^{-3}$  torr which implies a tritium inventory in the helium loops of about 3 grams. The tritium partial pressure above the  $\text{Li}_{17}\text{Pb}_{83}$  will be about  $1.3 \times 10^{-3}$  torr, which corresponds to about 5 Wppb tritium in  $\text{Li}_{17}\text{Pb}_{83}$ , in order to release a total amount of  $4.8 \times 10^6$  curies per day tritium into the helium coolant. This estimate makes use of the tritium permeation data provided in Ref. 54, and a wall thickness of 0.5 mm, a total surface area of  $2.2 \times 10^4 \text{ m}^2$  and at  $550^\circ\text{C}$ . The tritium inventory in the liquid  $\text{Li}_{17}\text{Pb}_{83}$  eutectic is about 6 grams.

Based on the above estimate, the amount of tritium to be treated and extracted from the breeding material circulating out of the blanket is about 0.2 grams per day since the fertile material residence time in the blanket is 30 days. The rest of that, about 513 grams per day, must be vented to the main helium coolant. To extract this amount of tritium releasing into the helium coolant, the tritium extract system requires a helium flow rate of  $5.18 \times 10^5$  kg per hour, which is about 3.4% of the main coolant flow rate.

In conclusion, among the four options investigated for the release of tritium bred in  $\text{Li}_{17}\text{Pb}_{83}$ , the options using bulk diffusion and helium percolation would either lead to a blanket tritium inventory greater than 10 kg or have operating difficulties. The methods of venting the tritium into the main coolant for tritium removal and side stream extraction look promising for the gas-cooled TMHR blanket design. However, many areas associated with the properties of tritium behavior in the lithium-lead eutectic suspension liquid and in other blanket materials such as beryllium, HT-9 ferritic steel

and SiC need to be investigated in detail. The concept of adding oxygen and hydrogen into the helium coolant at various stages of the power cycle may play an important role in the control of tritium flow and inventory in the system and is obviously worthwhile to look into in the future. Also, the safety impact of circulating small quantities of  $\text{ThO}_2$  outside of the blanket requires consideration.

## V.G ALTERNATIVE MATERIALS FOR REFERENCE CONCEPT

### V.G.1 UO<sub>2</sub> Fertile Fuel

Although the thorium-uranium cycle is considered in this design, the uranium-plutonium cycle is an alternative for the hybrid application. In this subsection we investigate the potential of adopting the U-Pu cycle in the gas-cooled TMHR blanket design. The approach for the investigation was to replace the thorium fertile material by the uranium fertile material in the suspension liquid. Since the blanket mechanical configuration does not change at all, the design areas we are interested in are therefore neutronics performance and heat transfer.

The oxide form of the uranium fertile material was selected for this study for the same reason as we chose the ThO<sub>2</sub> fertile material for the Th-U cycle design. The material compatibility with the Li-Pb and beryllium material also remains to be studied in the future. We have performed neutronics calculations using the reference gas-cooled TMHR blanket at the beginning of life for various UO<sub>2</sub> volume percents in the suspension Li<sub>17</sub>Pb<sub>83</sub> liquid and for various <sup>6</sup>Li atom percent in lithium. Note that all neutronics calculations were performed using the one-dimensional ANISN code with P<sub>3</sub>S<sub>6</sub> approximation and the DLC-37 nuclear cross section library. Consequently, corrections for 2-D and other effects (see Section V.B.3.e) are not included. Figure V-29 displays the fissile fuel (plutonium in this case) production rate as functions of volume percent UO<sub>2</sub> in the suspension liquid and percent <sup>6</sup>Li in lithium for a fixed tritium breeding ratio of 1.1 tritons per D-T neutron. Also shown in this figure is the fissile <sup>233</sup>U production rate for the reference ThO<sub>2</sub> system. They are given at the beginning of life and cycle. However, the general features will also be valid for the rest of design life and cycle.

The most important feature of the UO<sub>2</sub> system as observed from Fig. V-29 is that a lower oxide volume fraction in the Li<sub>17</sub>Pb<sub>83</sub> suspension liquid is needed in the UO<sub>2</sub> system compared to the ThO<sub>2</sub> system. This is because the integrated resonance capture cross section of uranium-238 is about a factor of 3 higher than that of thorium-232. This implies that the fertile inventory in the UO<sub>2</sub> system can be reduced by about a factor of three lower as compared to that in the ThO<sub>2</sub> system. Hence the fissile (plutonium) enrichment

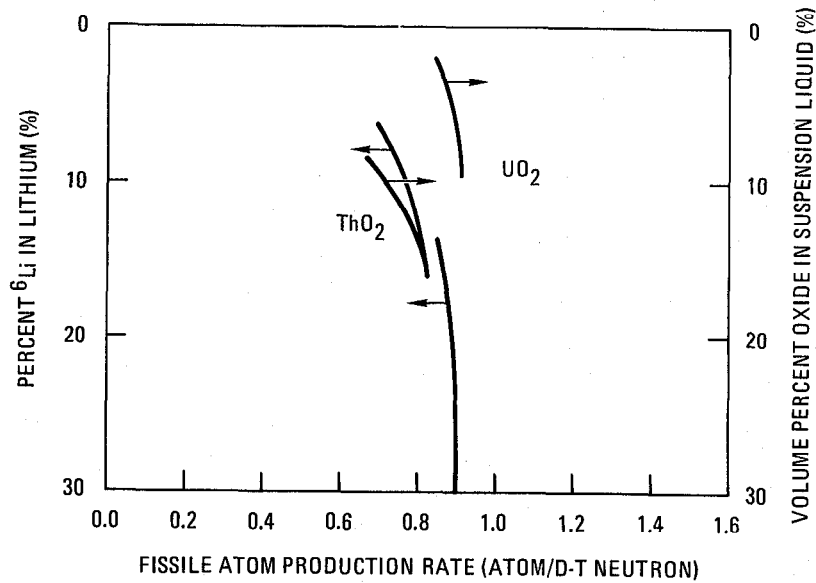


FIGURE V-29. Fissile atom production rates for ThO<sub>2</sub> and UO<sub>2</sub> systems as functions of both <sup>6</sup>Li enrichment in lithium and volume percent oxide fertile material in the suspension Li<sub>17</sub>Pb<sub>83</sub> liquid. A tritium breeding ratio of 1.10 tritons per D-T neutron is assumed for these curves shown in this figure.

rate is greatly enhanced. It takes only about 12 days for the  $\text{UO}_2$  system to reach 0.6% fissile enrichment in the fertile material, whereas it takes about 36 days for the  $\text{ThO}_2$  system to reach the same level of enrichment.

Table V-19 further summarizes the neutronic performance for the  $\text{ThO}_2$  and  $\text{UO}_2$  systems compared here. The  $\text{ThO}_2$  system, which is composed of 15%  $\text{ThO}_2$  in the suspension  $\text{Li}_{17}\text{Pb}_{83}$  liquid, with 15%  $^6\text{Li}$  in lithium and 0.2%  $^{233}\text{U}$  in thorium, represents the reference TMHR gas-cooled blanket design at the beginning of life. The tritium breeding ratio (T/n), net overall fissile atom production rate (U/n) and blanket nuclear heating (MeV/n) are 1.10, 0.82 and 26.01, respectively, as shown in Table V-19. The  $\text{UO}_2$  system shown here is a system corresponding to the reference  $\text{ThO}_2$  system. It has only 5% by volume  $\text{UO}_2$  in the suspension  $\text{Li}_{17}\text{Pb}_{83}$  liquid. The  $^6\text{Li}$  enrichment in lithium is also 15%. However the  $^{239}\text{Pu}$  concentration in uranium of 0.6%, the overall fissile fuel ( $^{233}\text{U} + ^{233}\text{Pa}$ ) enrichment expected in the reference  $\text{ThO}_2$  system. This assumption was made because precursor atom,  $^{239}\text{Np}$  is only 2.4 days. This is considerably shorter than the  $^{239}\text{Pu}$  27 day half life of  $^{233}\text{Pa}$  in the  $\text{ThO}_2$  system. Thus we assume that in the  $\text{UO}_2$  system most of the neutron capture reactions with uranium would produce the fissile plutonium atoms directly. The tritium breeding ratio, net fissile (Pu) production rate and blanket nuclear heating for the  $\text{UO}_2$  system are 1.16, 0.78 and 26.02, respectively, as also shown in Table V-19. It is of interest to mention that the blanket nuclear heatings for these two systems are about the same. Therefore the thermal-hydraulic design aspect for the  $\text{UO}_2$  system will be very similar to that for the  $\text{ThO}_2$  system. Note that the  $\text{UO}_2$  system displayed in Table V-19 does not include the  $^{235}\text{U}$  material which is normally expected to exist in the natural or depleted uranium. If the  $^{235}\text{U}$  material is included in the blanket, it may not alter the tritium breeding and fissile atom production rate too much. However, the blanket nuclear heating will be affected depending on the concentration of  $^{235}\text{U}$  in the fertile uranium material because of the thermal fissioning of  $^{235}\text{U}$  atoms and the increase of the blanket nuclear heating depends on the concentration of  $^{235}\text{U}$  in the fertile uranium material.

In summary, the replacement of thorium  $\text{ThO}_2$  fertile material by  $\text{UO}_2$  fertile material does not alter the fissile atom production rate and the blanket nuclear heating in the TMHR gas-cooled beryllium blanket if the tritium breeding ratio

TABLE V-19  
 COMPOSITIONS OF SUSPENSION  $\text{Li}_{17}\text{Pb}_{83}$  LIQUID, TRITIUM BREEDING  
 RATIOS FISSILE ATOM PRODUCTION RATES AND BLANKET NUCLEAR  
 HEATING RATES FOR  $\text{ThO}_2$  AND  $\text{UO}_2$  REFERENCE BLANKET SYSTEMS

	Th-U Cycle	U-Pu Cycle
Composition of Suspension Liquid	15% $\text{ThO}_2$ + 85% $\text{Li}_{17}\text{Pb}_{83}$ (15% $^6\text{Li}$ in Lithium 0.2% $^{233}\text{U}$ in Thorium)	5% $\text{UO}_2$ + 95% $\text{Li}_{17}\text{Pb}_{83}$ (15% $^6\text{Li}$ in Lithium 0.6% $^{239}\text{Pu}$ in Uranium)
<u>Tritium Breeding (T/n)</u>		
$^6\text{Li}(n,\alpha)\text{T}$	1.0743	1.1345
$^7\text{Li}(n,n'\alpha)\text{T}$	0.0070	0.0079
$\text{Be}(n,\text{T})$	0.0161	0.0160
Tritium Breeding Ratio	1.0974	1.1584
Fissile Atom Production (F/n)	0.8384	0.8006
Fissile Destruction Rate ( $^{233}\text{U}$ or $^{239}\text{Pu}/\text{n}$ )	0.0155	0.0208
Net Fuel Production (F/n)	0.8229	0.7798
T + F/n	1.9203	1.9383
<u>Nuclear Heating (MeV/n)</u>		
Fission	3.88	4.12
Non-fission	22.13	21.90
TOTAL	26.01	26.02

is kept constant. However the fissile material enrichment rate in the  $\text{UO}_2$  system is improved by about a factor of 3 because of the reduced fertile inventory in the  $\text{UO}_2$  blanket due to the improved neutron capture cross section of U-238 compared to that of Th-232. A shorter fertile material residence time in the  $\text{UO}_2$  system than in the  $\text{ThO}_2$  system is expected for achieving the same level of overall fissile atom enrichment.

## V.H BLANKET TECHNOLOGY ASSESSMENT

### V.H.1 Blanket Technology

The reference gas-cooled beryllium blanket incorporates the following design features:

- Low pressure blanket modules
- High pressure helium re-entrant cooling tubes
- Non-stressed, straightforwardly configured beryllium blocks
- Slowly circulating liquid  $\text{Li}_{17}\text{Pb}_{83}$  eutectic with pressure tubes and beryllium or SiC blocks immersing in it
  - $\text{ThO}_2$  particles suspended in the  $\text{Li}_{17}\text{Pb}_{83}$  eutectic
  - Th-9 ferritic steel first wall and tubing.

Most of these features can be achieved within the scope of existing technologies.

Technologies that need development are primarily in the materials area. For the reference beryllium blanket design, we believe that more in-depth investigation on the Li-Pb eutectic is needed, particularly in the areas of compatibility with other blanket materials and tritium behavior. The understanding of radiation damage on the beryllium blocks with 14 MeV neutron at a fluence comparable with the hybrid blanket environment must be confirmed experimentally. An integral experiment to test behavior of the blocks considering the temperature and flux profile in the blanket is also needed. The effects of volumetric swelling of the beryllium can thus be more precisely predicted. The suspension of  $\text{ThO}_2$  particles in the  $\text{Li}_{17}\text{Pb}_{83}$  eutectic needs to be demonstrated in a bench scale test.

The primary mechanical technologies that need development are related to the pressure tube, which requires a high reliability. The long term strength of the tube as designed requires some practical as well as theoretical evaluation. The ability of the design to handle a slowly leaking tube requires assessment as does the effect of a large leak into the magnetically constrained lithium-lead contacting medium. More detailed thermal-hydraulic modeling (i.e., multi-dimensional) is needed to better predict operating temperatures.

Among the above technology and materials development, the beryllium and suspension of  $\text{ThO}_2$  particles in the  $\text{Li}_{17}\text{Pb}_{83}$  eutectic are unique with the fusion-fission hybrid design. Most others can probably be developed along the pure fusion design program such as the (HT-9) ferritic steel development program supported by the Department of Energy.

## REFERENCES

1. R. W. Moir, et al., "Tandem Mirror Hybrid Reactor Design Study Final Report," UCID-18808, Lawrence Livermore National Laboratory (1980).
2. D. K. Sze, R. Clemmer, E. T. Cheng, "LiPb, A Novel Material For Fusion Applications," Proc. Fourth Topical Meeting on the Technology of Controlled Nuclear Fusion, October 1980, King of Prussia, Pennsylvania (1981).
3. W. W. Engle, Jr., "ANISN: Multigroup One Dimensional Discrete Ordinates Transport Code With Anisotropic Scattering," K-1693, Oak Ridge National Laboratory (1967).
4. "ENDF-102: Data Formats and Procedures for the Evaluated Nuclear Data File, ENDF," BNL-NCS-50496 (ENDF 102), Brookhaven National Laboratory (1975).
5. "AMPX-II: A Modular Code System for Generating Coupled Multigroup Neutron-Gamma Libraries from ENDF/B," Radiation Shielding Information Center, Oak Ridge National Laboratory, PSR-63 (1978).
6. D. M. Plaster, et al., "Coupled 100 Group Neutron and 21 Gamma-Ray Cross Section for EPR Calculations," ORNL-TM-4873, Oak Ridge National Laboratory (1975).
7. R. W. Roussin, C. R. Weisbin, J. E. White, N. M. Greene, R. Q. Wright, and J. B. Wright, "VITAMIN-C: 171 Neutron, 36 Gamma-Ray Group Cross Sections in AMPX and CCCC Interface Formats for Fusion and LMFBR Neutronics," DLC-41, Oak Ridge National Laboratory (1979).
8. Y. Gohar and M. A. Abdou, "MACKLIB-IV: 171 Neutron, 36 Gamma-Ray Group Nuclear Response Function Library Calculated with MACK-IV from Cross-Section Data in ENDF/B-IV," DLC-60, Oak Ridge National Laboratory (1979).
9. T. K. Basu, et al., "Neutron Multiplication Studies in Beryllium for Fusion Reactor Blankets," Nucl. Sci. Engr., 70, 3 (1979).
10. R. J. Howerton, et al., "An Integrated System For Production of Neutronics and Photonics Computational Constants," UCRL-50400, Lawrence Livermore National Laboratory (1972-1981 revisions).
11. R. G. Young and L. Stewart, Los Alamos Scientific Laboratory, private communications (1979).

12. D. M. Drake, et al., Nucl. Sci. Fig. 63, 402 (1977).
13. F. O. Purser, Triangle Universities Nuclear Laboratory, private communication (1976).
14. H. H. Hogue, et al., Nucl. Sci. Engr., 68, 38 (1978).
15. D. E. Bartine, et al., "SWANLAKE - A Computer Code Utilizing ANISN Transport Calculations for Cross Section Sensitivity Analysis," ORNL-TM-3809, Oak Ridge National Laboratory (1973).
16. M. Z. Youssef, "Fusion-Fission Systems Analysis and the Impact of Nuclear Data Uncertainties on Design," UWFDM-358, Fusion Research Program, University of Wisconsin (1980).
17. R. G. Alsmiller, et al., "Comparison of the Cross Section Sensitivity of the Tritium Breeding Ratio in Various Fusion Reactor Blankets," Nucl. Sci. Engr., 57 (1975).
18. J. M. Beeston, "Beryllium Metal as a Neutron Moderator and Reflector Material," Nucl. Eng. Des. 14, 445 (1970).
19. M. T. Simnad, "Shielding and Control Materials for the Gas-Cooled Fast Breeder Reactor," General Atomic Report GA-A14478, Chapter 4.
20. U.S. Bureau of Mines, "Mineral Facts and Problems, 1975," USBM Bulletin 650, U.S. Government Printing Office, Washington, D.C. (1975).
21. U.S. Bureau of Mines, "Mineral Commodity Summaries, 1980," U.S. Government Printing Office, Washington, D.C. (1980a).
22. U.S. Geological Survey, "United States Mineral Resources," USGS Professional Paper 820, U.S. Government Printing Office, Washington, D.C. (1973).
23. E. Cameron, R. W. Conn, G. L. Kulcinski and I. Sviatoslavsky, "Materials Resource Implications of a Tokamak Fusion Reactor Economy," UWFDM-313, University of Wisconsin (1979).
24. Argonne National Laboratory, McDonnell Douglas Astronautics Co. - East, General Atomic Company and The Ralph M. Parsons Company, "STARFIRE - A Commercial Tokamak Fusion Power Plant Study," (1980).
25. R. W. Moir, "Hybrid Reactors," Lawrence Livermore Laboratory, UCRL-84826, Rev. 1, Preprint (March 1981).
26. Don L. Hedges, Los Angeles Div., North American Rockwell Corp., "New Approaches to Industrial Hygiene in Beryllium Fabrication," Paper 670802, Trans. of Society of Automotive Engineers Meeting, October 2-6, 1967.

27. T. Y. Sung and W. F. Vogelsang, "DKR: A Radioactivity Calculation Code for Fusion Reactors," UWFDM-170, Nuclear Engineering Department, University of Wisconsin, Madison, Wisconsin.
28. T. Y. Sung and W. R. Vogelsang, "DCDLIB: Decay Chain Data Library for Radioactivity Calculations," UWFDM-171, *ibid.*
29. J. B. Rich, G. P. Walters and R. S. Barnes, "The Mechanical Properties of Some Highly Irradiated Beryllium," *J. Nucl. Mater.* 4, 287 (1961); also in UKAEA Report AERE-R-3449 (1960).
30. R. S. Barnes, "The Behaviour of Neutron-Irradiated Beryllium," The Metallurgy of Beryllium, Proc. of an International Conference by Institute of Metals, Royal Commonwealth Society, London, October 16-18, 1961, p. 372.
31. R. A. Andriyevski, et al., "Properties and Behavior of Moderator Materials Under Irradiation," Fourth Geneva Conference, United Nations, Geneva (1971), Vol. 10, p. 383 (p-452).
32. J. M. Beeston, "Gas Release and Compression Properties in Beryllium Irradiated at 600 and 750C," Effects of Radiation on Structural Metals, Special Technical Publication No. 426, American Society for Testing and Materials (1968).
33. J. B. Rich and G. P. Walters, "The Mechanical Properties of Beryllium Irradiated at 350 and 600°C," The Metallurgy of Beryllium, p. 362.
34. R. S. Barnes, "A Theory of Swelling and Gas Release for Reactor Materials," *J. Nucl. Mat.* 11 (2), 135 (1964).
35. W. N. Beck, R. J. Fousek and J. H. Kittel, "The Irradiation Behavior of High-Burnup Uranium-Plutonium Alloy Prototype Fuel Elements," ANL-7388 (1968).
36. B. Myers, "Some Observations on 14 MeV Neutron Radiation Effects on Reactor Materials," Lawrence Radiation Laboratory, University of California, Livermore, prepared for submittal to the Nuclear Fusion Conference, Abingdon, Berkshire, U.K., September 17-19, 1969.
37. E. E. Hoffman, "Corrosion of Materials by Lithium at Elevated Temperatures," ORNL-2924, Oak Ridge National Laboratory (1960).
38. L. R. Kelman, W. O. Wilkinson and F. L. Yaggee, "Resistance of Materials to Attack by Liquid Metals," USAEC Report ANL-4417, Argonne National Laboratory (1950).

39. G. L. Hanna, "The Compatibility of Beryllium with Oxides of Uranium and Thorium," The Metallurgy of Beryllium, p. 350.
40. H. Migge, "Metallurgical Aspects Concerning the Use of Beryllium in a Thermal Blanket," J. Nucl. Mater. 85&86, 317-321 (1979).
41. W. Vickers, "The Compatibility of Beryllium with Various Reactor Materials," The Metallurgy of Beryllium, p. 335.
42. J. M. Blocher, Jr., M. F. Browning, W. J. Wilson, V. M. Secrest, A. C. Secrest, R. B. Landrigan and J. H. Oxley, Battelle Memorial Institute, "Properties of Ceramic-Coated Nuclear-Fuel Particles," Nucl. Sci. Engr 20, 153-170 (1964).
43. Charles W. Townley, Neil E. Miller, Robert L. Ritzman and Richard J. Burian, Battelle Memorial Institute, "Irradiation Studies of Ceramic-Coated Nuclear Fuel Particles," Nucl. Sci. Engr. 20, 171-179 (1964).
44. R. E. Gold, et al., "Materials Technology for Fusion: Current Status and Future Requirements," Nucl. Tech./Fusion 1, 169 (1981).
45. D. L. Smith, et al., "First Wall/Blanket Materials Selection for STARFIRE Tokamak Reactor," Proc. 4th Topical Meeting on the Technology of Controlled Nuclear Fusion, October 14-17, 1980, King of Prussia, Pennsylvania, p. 1714.
46. B. Badger, et al., "WITAMIR-I, A Tandem Mirror Reactor Study," UWFDM-400, Nuclear Engineering Department, University of Wisconsin, Madison, Wisconsin (1980).
47. S. N. Rosenwasser, et al., "Ferritic Stainless Steels for Fusion Applications," J. Nucl. Matl. 85&86, 177 (1979).
48. A. Armstrong, et al., "GFUN3D USER'S GUIDE," RL-76-029/A, Rutherford National Laboratory, England.
49. L. Yang, General Atomic Company, private communication.
50. D. K. Sze, University of Wisconsin, personal communication.
51. "STARFIRE - A Commercial Tokamak Fusion Power Plant Study," ANL/FPP-80-1, (1980).
52. P. J. Gierszewski, B. Mikic and N. E. Todreas, "Natural Circulation in Fusion Reactor Blankets," ASME/AIChE National Heat Transfer Conference, Orlando, Florida (1980).
53. Preliminary data from Veleckis of ANL, private communication with D. K. Sze, University of Wisconsin.

54. B. Badger, et al., "WITAMIR-I, A Tandem Mirror Reactor Study," UWFDM-400, University of Wisconsin (1980), Sec. XI.C.
55. D. K. Sze and E. T. Cheng, "Tritium Confinement and Recovery Considerations for  $\text{Li}_{17}\text{Pb}_{83}$  Fusion Blankets," A summary accepted for presentation at the ANS Winter Meeting, San Francisco, California, November 29 - December 4, 1981.
56. Fusion Engineering Staff, "Doublet Demonstration Fusion Power Reactor Study," General Atomic Report GA-A14742, Sec. 6.2.2 (July 1978).

## CHAPTER VI

### REACTOR SAFETY CONSIDERATIONS

#### VI.A OVERVIEW AND DESIGN PHILOSOPHY

##### VI.A.1 Introduction

A perceived advantage of suppressed fission blankets for fusion breeders is improved safety features relative to fast fission blankets. This advantage should result from both lower afterheat power levels and lower actinide and fission product generation in the blanket. This might lead to a blanket system which does not require active emergency cooling systems, but can for the most part rely upon semi-active, or passive (e.g., natural convection) cooling in accident situations. In this chapter we discuss and quantify the principal safety aspects of both the beryllium thorium oxide and the lithium/molten salt reference blankets for the Tandem Mirror Hybrid Reactor (TMHR).

For thorium fueled fast-fission hybrid blankets, Schultz, et al.,<sup>1</sup> showed that the principal contribution to the biological hazard potential (BHP) of a hybrid reactor (~75% of the total) is due to the fission products while 24% is due to the actinides. This contrasts with a uranium-fueled blanket where 94% of the total BHP is caused by the actinides. This suggested that fission suppressed blankets (with lower actinide production and fission product yields) should yield even lower BHPs. Maya, et al.,<sup>2</sup> further compared the BHPs of thorium fast fission and thorium suppressed fission blankets and concluded that the thorium suppressed fission blanket offered two orders of magnitude lower risk.

The most significant hazard associated with the TMHR is a release of the radioactivity present in the blanket and surrounding structure. To establish a potential accident situation, a radioactive release first requires an initiating event. Following an initiating event, a release requires that successive failures of inherent systems and barriers, as well as engineered safety features present in the TMHR, continue the accident sequence and provide both the pathway and the mechanism for the physical transport and escape of radioactivity.

For both the gas-cooled and liquid lithium-molten salt blanket concepts, nuclear criticality accidents are impossible because of the low fissile concentrations in the fuel form (with less than 0.25%  $^{233}\text{U}$ ); consequently, the safety issues considered in this chapter involve radiological hazards and the protection of the public (the environment) and the plant operators. This is translated into engineered safety features to prevent any uncontrolled release of radioactivity to the environment under accident conditions.

The remainder of Section VI.A presents the objectives, methodology and figures of merit used to perform and evaluate the safety analysis of the radioactive hazard associated with the TMHR blankets. The rest of Chapter VI performs the following functions for both the gas-cooled and liquid-metal-cooled systems:

- Identifies major accident pathways, barriers and sources of radioactivity.
- Describes accident scenarios and event probabilities.
- Quantifies the isotopic hazard, consequence and thermal analysis.
- Develops major accident sequences in event tree format and qualitatively compares the relatively major contributions to risk.

The chapter concludes with safety-oriented design guidance resulting from this year's study of fission-suppressed blankets, safety conclusions regarding the present designs and the establishment of safety-oriented evaluation criteria.

The fissile fuel reprocessing plant is assumed to be outside the reactor building, enclosed in a separate building on the same site. The accident initiating events, accident pathways and hazards associated with such a reprocessing plant are not treated here. Similarly, the release of tritium from external tritium handling and processing facilities has not been treated.

#### VI.A.2 Objectives

A major feature of the fission-suppressed blanket concept is the reduction of the fission product and actinide inventories and the attendant problems of radionuclide containment and decay heat removal. This reduction translates

into significant advantages from the viewpoints of public safety and engineering design. The goals and objectives of this safety analysis were to:

- Develop safety criteria and figures-of-merit on which to evaluate and compare promising suppressed-fission blanket concepts.
  - Integrate safety considerations into the design process, starting at the conceptual design stage where such integration is apt to be most beneficial.
  - Perform an overall analysis of the safety characteristics of blanket concepts to sufficient depth to evaluate the importance of fission suppression.
- The scope of the overall safety analysis has been to evaluate the important safety features of the TMHR breeding blankets. These features include:
- The quantity, location, and isotopic distribution of the radiologically hazardous material in terms of the four major contributors (i.e., actinides, fission products, activation products, and tritium).
  - The response of the blanket to decay-heat loading during off-normal loss-of-cooling-capability events.
  - The siting and containment implications of the reactor in terms of its potential radiological risk to the population and environment surrounding the site following a severe hypothetical maximum-credible accident.

On the basis of the results of the above analyses, safety criteria and figures-of-merit can be developed and applied to evaluate the effect of design decisions. Safety-motivated design modifications of demonstrated value can then be prepared and incorporated as an integral part of an on-going design process.

### VI.A.3 Methodology and Figures-of-Merit

In performing the safety analysis, the approach is to quantify the major risk contributors using the methods of probabilistic risk assessment (PRA). This involves quantitatively determining the sources of radiological hazard, their location, and the events that are necessary for an accident to continue and provide a pathway for the escape of these sources. Given this information, the probabilities and consequences, and therefore the risks of particular sequences of events can be compared. The high contributors to risk can thus be identified and the design modified accordingly.

A number of figures-of-merit relating to safety can be postulated. These include Biological Hazard Potential (BHP), decay heat power density, time to structural melt, time to fuel melt, relative risk, etc. These quantities are evaluated during the course of performing the safety analysis and provide guidance as to the quantity of the hazard (BHP), the events required to lead to a hazardous condition (relative risk), the time available in which to take corrective action following an event (times to melt), etc. Having these evaluated quantities, safety-oriented criteria such as minimum allowable time to melt or maximum fission power density can be formulated to provide meaning to the term "fission-suppressed" as it relates to safety.

## VI.B SAFETY CONSIDERATIONS FOR GAS-COOLED SYSTEMS

### VI.B.1 Characterization of Principal Accidents and Consequences

VI.B.1.a Introduction. The principal sources of radioactivity to be considered in the characterization of accidents involving the TMHR gas-cooled blanket are:

- Highly mobile tritium used in generating fusion power.
- Mobile Li-Pb-ThO<sub>2</sub> suspension containing actinides, fission products, and bred tritium.

- Relatively immobile activation products in the blanket structure.

Due to the nature of the fertile dilute fission-suppressed concept, significant differences exist between the radioactive inventory in this breeding blanket and previous designs. These differences are discussed in a subsequent section.

A number of reactor systems and design features are present in the design to mitigate the release of radioactivity to the environment. These include:

- Submodule containment of the fertile suspension to limit the amount of suspension that can be spilled in certain events.
- Suspension level control to limit the maximum static pressure and prevent loss of thermal contact in the event of in-flow blockage.
- Preliminary consideration of a submodule pressure relief system to reduce the probability of a submodule overpressurization.
- A fertile suspension drain tank to provide temporary holdup of the actinides and fission products and limit the amount of radioactivity released in a serious accident.
- A "freeze-type drain valve" as described in Section VI.C.1.a to provide a highly reliable drain mechanism.

In addition, the reactor is presumed to have fully developed detection systems (flow, temperature, pressure), plasma shutdown systems, and a secondary containment building with filters and recirculators. These features and those inherent to the gas-cooled blanket, namely low fissile concentration and very low afterheat, provide for very encouraging safety characteristics.

VI.B.1.b Identification of Accident Type and Initiating Mechanisms. To aid in classifying the gas-cooled TMHR accident types and identifying potential initiating mechanisms, the radioactive release pathways and mitigating barriers are depicted in Fig. VI-1. The arrows in Fig. VI-1 indicate the radioactivity release pathways and do not represent a time sequence. The accident initiators are shown adjacent to the source of radioactivity only symbolically to indicate their requirement in creating an accident condition. In fact, the initiating event could occur anywhere, (e.g., a coolant line rupture, pump failure, etc). The barrier and system failures listed are representative and also include valve failures, engineered system failures, failures in sensing equipment, cleanup systems, etc.

In order to result in a release, the sources or radioactivity in the blanket, the Li-Pb-ThO<sub>2</sub> suspension and the activated structure must first breach either the primary coolant boundary, i.e. the pressure vessel helium plena at the back of a module, or a pressure tube, or the first wall. If the pathway is through the first wall, then the fusion vacuum boundary must also be breached for a release to occur, either directly to the secondary containment, as shown in the figure, or indirectly via vacuum components. If the pathway is through the primary coolant boundary, a direct release to the secondary containment could occur, or alternately the release could proceed through the secondary coolant system as shown in Fig. VI-1. Fusion-specific events are not considered except in a synergistic sense since tritium events do not contribute significantly to hybrid reactor risk and are being treated in the fusion program.

On this basis, two types of accidents have been identified involving the gas-cooled TMHR blanket:

- Structural failures
- Loss of heat removal capability events.

These accident types can be initiated by events utilizing stored energy sources present in the TMHR. Potential energy sources include the plasma kinetic energy, the radioactive decay energy, the primary coolant pressure, and the stored energy in the magnets and associated refrigerant system. Potential accident initiating events of these two types are listed in Tables VI-1 and VI-2. The events with major potential consequences are marked with asterisks and developed in event tree format below. Some of these events require thermal

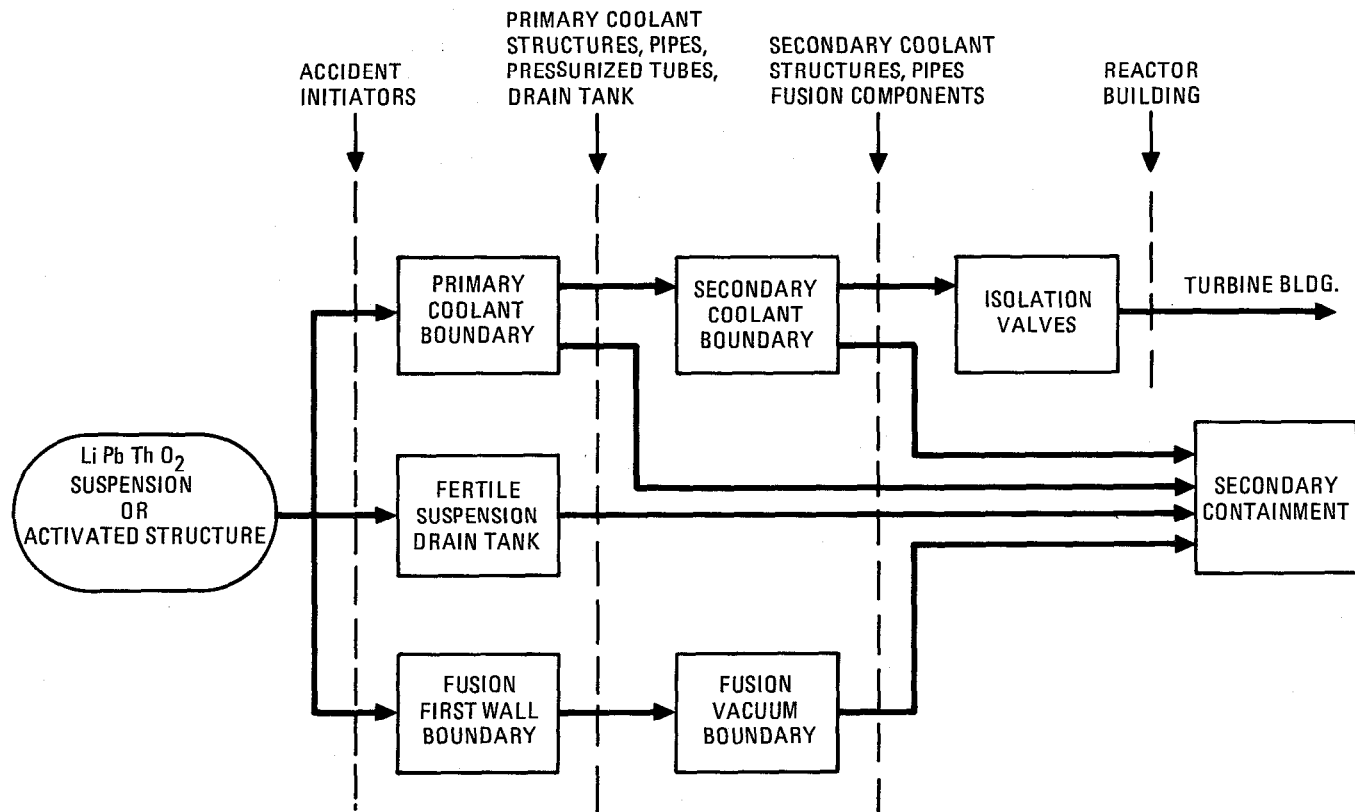


FIGURE VI-1. Radioactivity release pathways and barriers associated with the TMHR gas-cooled blanket.

TABLE VI-1. Potential structural failure events that could lead to a release of radioactivity in the gas-cooled system.

Structural Failure Event	Comments
*1. Plasma disruption with first wall rupture.	Plasma disruption frequency small.
2. Pressure tube circumferential failure with missile generation.	Highly unlikely; sound and demonstrated grounds that failure mode is longitudinal.
*3. Pressure tube longitudinal failure resulting in sub-module overpressurization.	Incorporate burst discs and/or pressure relief system (see Chapter V).
4. Magnet failure with missile generation or box rupture.	Probability of occurrence can be made very small via design.
*5. Component (pipes, pumps, etc.) structural failure	Can lead to a loss-of-cooling capability event.

\* Selected for further development.

TABLE VI-2. Potential loss of heat removal events that could lead to a release of radioactivity in the gas-cooled system.

Loss of Heat Removal Capability Event	Comments
*1. Pressure tube leakage.	Leads to a loss of thermal contact.
2. Pressure tube blockage.	Leads to a local loss of primary cooling.
*3. Heat removal system failure.	Total loss of coolant flow.
4. Fertile suspension in-flow blockage.	Would lead to a loss of thermal contact; can operate suspension on a "spill over" principle.
5. Fertile suspension out-flow blockage.	May exceed design thermal rating or create hot-spots; very slow time scale.

\* Selected for further development.

analyses in order to determine the accident progression, sequence of events and consequences. The thermal analyses are therefore presented first.

VI.B.1.c Thermal Modeling of Accident Scenarios. The events in Table VI-2 selected for further development were chosen on their potential for leading to thermally induced structural failure in the event of loss of heat removal capability. That is to say, an event that does not result in such failure under any postulated sequence of postulated failures is not deemed to result in a release of radioactivity. This section presents the thermal analyses performed in support of the gas-cooled blanket.

The thermally significant design features of the gas-cooled blanket are the use of gaseous helium as a coolant and a liquid suspension of lithium-lead and small solid thorium particles as a thermal contact medium. Most of the afterheat in our analyses was associated with the presence of these thorium particles, principally due to decay of  $\text{Th}^{233}$  to  $\text{Pa}^{233}$  and subsequently to  $\text{U}^{233}$ . Our analysis considered varying degrees of loss of the lithium lead thermal contact medium, with and without helium coolant flow, to bracket the credible accident scenarios.

In these studies, it is assumed that a failure of the helium coolant system involving loss of pressure or flow to several tubes, or a thermal contact medium leak, would be easily detected and would initiate an immediate plasma shutdown. Therefore, emphasis was placed upon "Plasma off" scenarios which included:

1. Loss of helium
2. Loss of thermal contact medium and helium
3. Loss of thermal contact immediately behind the first wall and loss of helium.
4. Loss of thermal contact medium in a small volume behind the first wall with helium flowing.

A fifth case considered an accident scenario not readily detectable (i.e., blockage of a single helium tube) and assumed the reactor would not be shut down.

Results from cases 1 through 4 indicate that accidents involving losses of the He coolant and/or the thermal contact medium should allow for an

attractively long time to initiate corrective measures with the plasma shut off. Results from the loss of helium analysis (case 1) show relatively benign behavior, with the first wall reaching  $1000^{\circ}\text{C}$  after about 30 hours. Case 2 further indicates that if the lithium lead thorium is drained off following the loss of helium, first wall temperatures may be kept below  $700^{\circ}\text{C}$ . (This thermal radiation-dominated problem is highly dependent on the emissivities of the reactor materials.) Case 3 models loss of He with a thin layer of thermal contact medium lost immediately behind the first wall. This forces heat removal from the first wall to be radiation-dominated, but does not remove the heat generating thorium (as in case 1) and is intended to be our (thermally) worst case. Case 3 results indicate temperatures slightly higher than case 1 (loss of helium only) results after the first two hours.

The blocked tube analysis (plasma on) is not adequate for definitive conclusions; however, the results suggest that a blocked tube may be tolerated during operation if the reactor is designed to accommodate a first wall temperature perturbation of  $50^{\circ} - 100^{\circ}\text{C}$  without failure. A more detailed discussion of the modeling methods and results follows.

The Systems Improved Numerical Differencing Analyzer (SINDA) code<sup>3</sup> was used to perform transient two-dimensional analyses of the loss of helium accident (case 1) and the loss of thermal contact medium in a small area accident (case 4). The SINDA transient analysis used a backward differencing implicit method (classical implicit method). SINDA was also used to perform a steady state thermal analysis of the blanket under operating conditions in order to determine initial temperature inputs for the transient afterheat analysis.

As shown in Figs. VI-2 and VI-3, the 1-D unit cell used in the analysis is a cylinder taken about a coolant tube oriented radially with respect to the central cell plasma. Since heat will flow to the nearest cooling tube, forming a hexagonal adiabatic boundary about each tube on the locus of points that are equidistant from the surrounding tubes, an adiabatic boundary condition at the outer radius of the unit cell is used. This assumes homogeneity, and that the tubes maintain the same separation. The outer radius of the unit cell was taken as that of a circle of the same area as the hexagon. The unit cell was broken into 132 nodes, 6 radial by 22 axial. The first wall corrugations were approximated by thickening the first wall and the thermal contact medium region directly behind the first wall. The

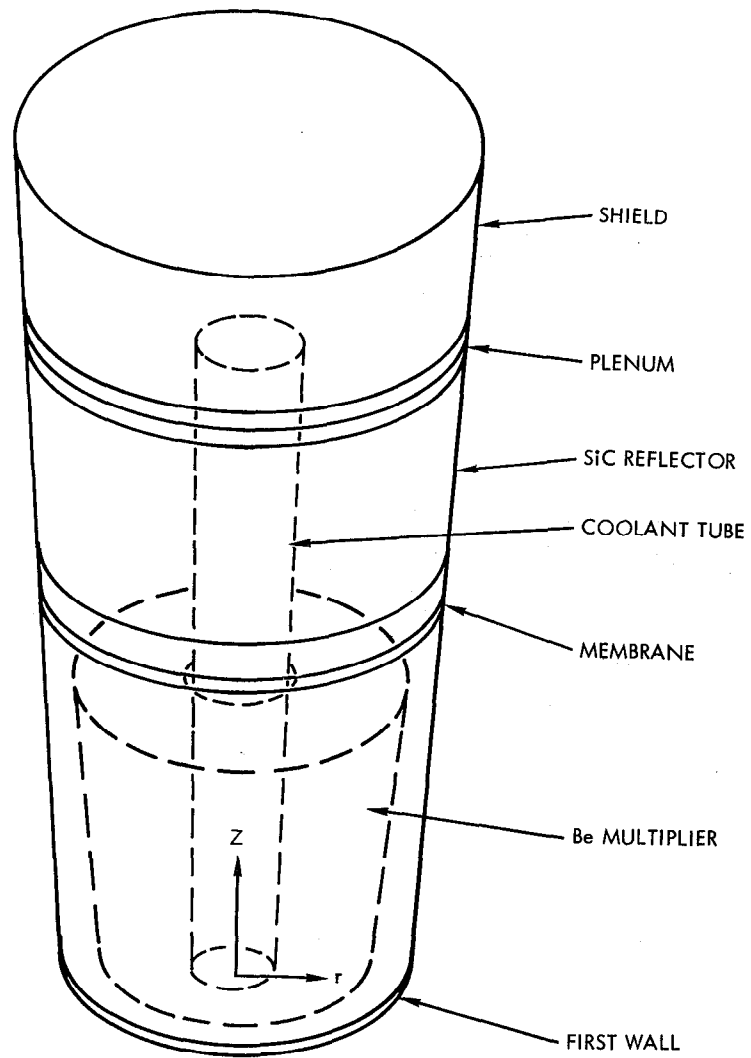


FIGURE VI-2. Heat transfer unit cell.

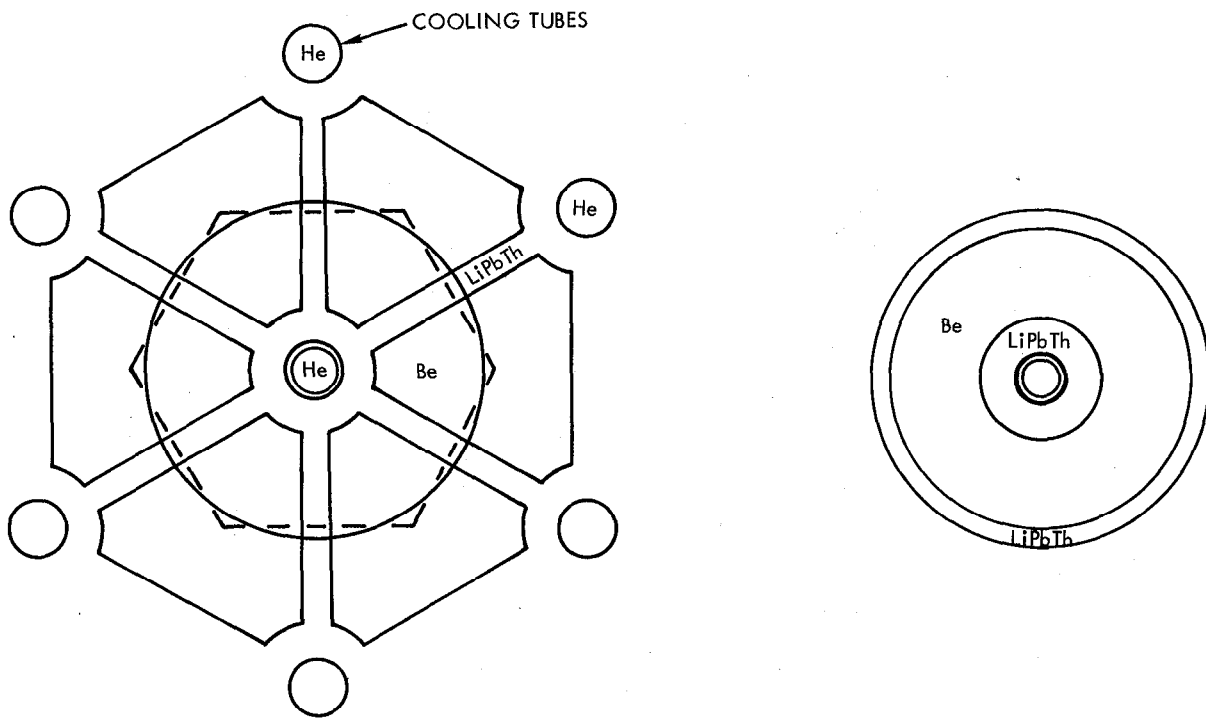


FIGURE VI-3. Heat transfer unit cell cross section.

helium tubes actually are closer packed towards the center of the reactor, distorting the hexagon. This slight distortion is conservatively ignored in the model, resulting in a slightly more heat generating material near the first wall and slightly less heat sink material toward the outside of the blanket.

Case 1, Loss of Helium. The SINDA code was used to perform a 1-D transient analysis of afterheating without helium coolant flow. The unit cell is as described above. The outer radius of the unit cell was chosen to approximate the actual adiabatic boundary, and the plasma side of the first wall (i.e., bottom of the unit cell) is also adiabatic. (This assumes that vacuum is maintained and that all of the first wall is at the same temperature.) The top boundary is also adiabatic, but this makes little difference since the outer blanket and shield regions act as heat sinks. The shield temperature increases by only 72°C after 29 hours of afterheating. Material properties are as shown in Table VI-3, but the time decay term in the heat generation from the HT-9 structural material is not included. (This results, of course, in higher temperatures.) Stagnant helium at one atmosphere was assumed, with thermal radiation across the helium zones neglected. This also results in a conservative model of the heat flux across the plenum.

The transient loss of helium model predicted time dependent behavior up to a period of 22.5 days, beginning with the initial temperatures shown on the temperature map on Fig. VI-4. The initial shield temperature (not shown on Fig. VI-3) was 100°C. First wall (the hottest zone) temperatures reached 1000°C after about 30 hours and leveled off at 1260°C after 16 days (see Fig. VI-5).

This analysis shows that afterheat behavior of the gas-cooled blanket is fairly benign, allowing several hours in which to take action before any damage would occur. It is possible that gas filling the plasma chamber to one atmosphere pressure to relieve the stress on the blanket modules would be sufficient to prevent failure. However, the high (1260°C) temperatures indicated by this analysis would preclude re-using the modules. As shown below, draining off the fuel-bearing thermal contact medium will greatly improve the situation.

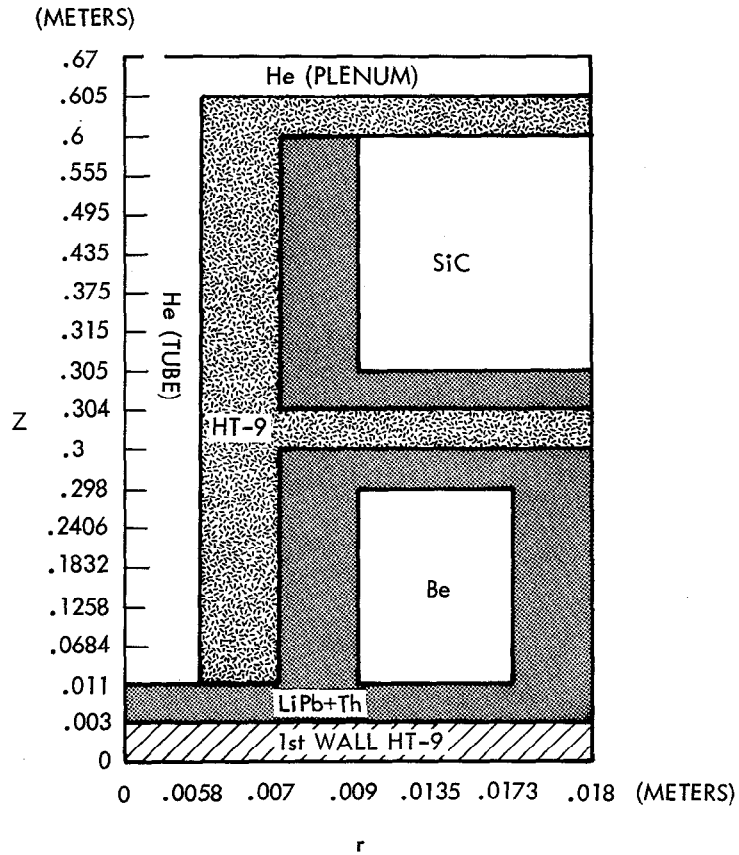
TABLE VI-3. Material properties at EOL.

Material	Conductivity <sup>a</sup> (W/m°C)	Heat Capacity <sup>a</sup> (J/kg°K)	Density <sup>a</sup> (kg/m <sup>3</sup> )	Volumetric Heat Generation <sup>a</sup> (W/m <sup>3</sup> )
LiPb ThO <sub>2</sub>	16	165	9400	$1.40 \times 10^6 e^{-5.204 \times 10^{-4}\tau}$ $+ 0.35 \times 10^6 e^{-2.97 \times 10^{-7}\tau}$
SiC	48.3 - 0.022T	1039 + 0.210T	3200	0
Be <sup>b</sup>	65	2286 + 1.01T	1850	0
HT-9 <sup>c</sup>	29	781 + 0.586T	7776 - 0.307T	$(1 \times 10^{16})^{-11.5r} \times (0.829^{-1.1 \times 10^{-4}\tau}$ $+ 0.121^{-7.75 \times 10^{-8}\tau})$
He	0.0680 + 0.0002T	5200	0.0729 - 3 × 10 <sup>-5</sup> T	0

(a)  $\tau$  is time in seconds. T is temperature in degrees Kelvin.

(b) 80% dense.

(c) r is distance from plasma centerline in meters. HT-9 afterheat generation was decayed with time in cases 2 and 3.



(°C)

470	470	470	470	470	470
468	470	470	470	470	470
467	470	471	471	471	471
466	471	472	472	472	472
463	470	472	472	472	472
459	469	472	473	473	473
452	469	472	474	475	475
451	473	478	481	482	482
451	474	478	482	493	484
450	474	478	482	485	485
450	474	478	484	486	486
438	472	479	483	485	485
421	469	478	484	486	487
394	463	477	486	489	490
352	457	479	493	497	499
270	463	503	531	539	541
675	710	719	720	725	729
698	716	720	726	730	730

(HELIUM TEMPERATURES ARE CONSTANT)

FIGURE VI-4. Steady state operating temperatures.

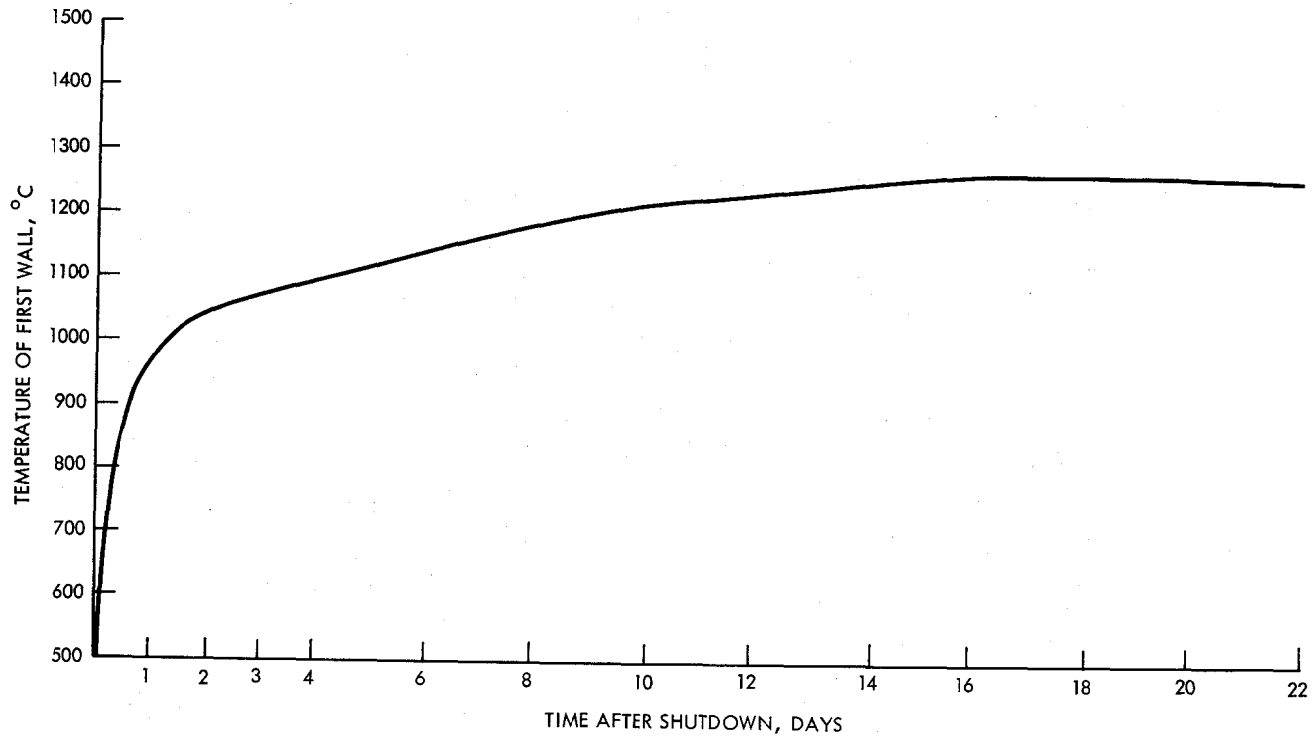


FIGURE VI-5. Loss of He first wall temperatures from SINDA.

Case 2, Loss of Thermal Contact Medium and Helium. This analysis models temperatures in the blanket following a loss of helium coolant accident with the thermal contact medium drained off intentionally or accidentally. A steady state analysis was performed at 0, 2 hours and 24 hours after shutdown of the plasma and the helium system. The unit cell described above was simplified to reduce the problem to a simple hand calculation in one dimension, (i.e., the Z direction in Fig. VI-2), with constant radial properties. (Radial temperature changes from the two dimensional analysis above were generally less than 1°C.) Only decay heating in the HT-9 structural material was assumed present. This source of heat was diminished with distance from the plasma centerline and with time as shown in Table VI-3. In order to preserve the 1-D model and conserve the heat generated in the HT-9 coolant tube, the tube was considered to be cut in half. The material from the outer half (towards the plasma) was added to the first wall and the inner half was added to the membrane (see Fig. VI-6). This increases the thermal resistance path of the heat generated in the tube, making the first wall temperature higher. A constant conductivity of 37 W/mk<sup>0</sup> was taken for the SiC reflector zone. The steady state temperatures given on Table VI-4 (see Fig. VI-6 for temperature locations) were found by setting the backwall temperature to 300°C and calculating conduction and radiation through the layers shown in Fig. VI-6. Emissivities were taken at 0.2, 0.5 and 0.7, and heat generation values (the only time varying term) at time 0, 2 hours and 24 hours. The problem is radiation dominated and results are conservative since the heat generation rates actually decrease in time.

Actual temperatures will lag behind the steady state temperatures given in Table VI-4. If the thermal contact medium were drained off following a loss of helium accident, the reactor temperatures would approach these steady state temperatures. After about two hours following plasma and He system shutdown, the steady state temperatures due to the loss of helium and thermal contact medium fall below the transient temperatures from the loss of helium only case, indicating that the reactor will cool if the thermal contact medium is drained off more than two hours after a loss of helium. Note that the first wall can be kept below 700°C (if the emissivities are 0.5 or greater) at all times by draining off the thermal contact medium about two hours after a loss of He accident.

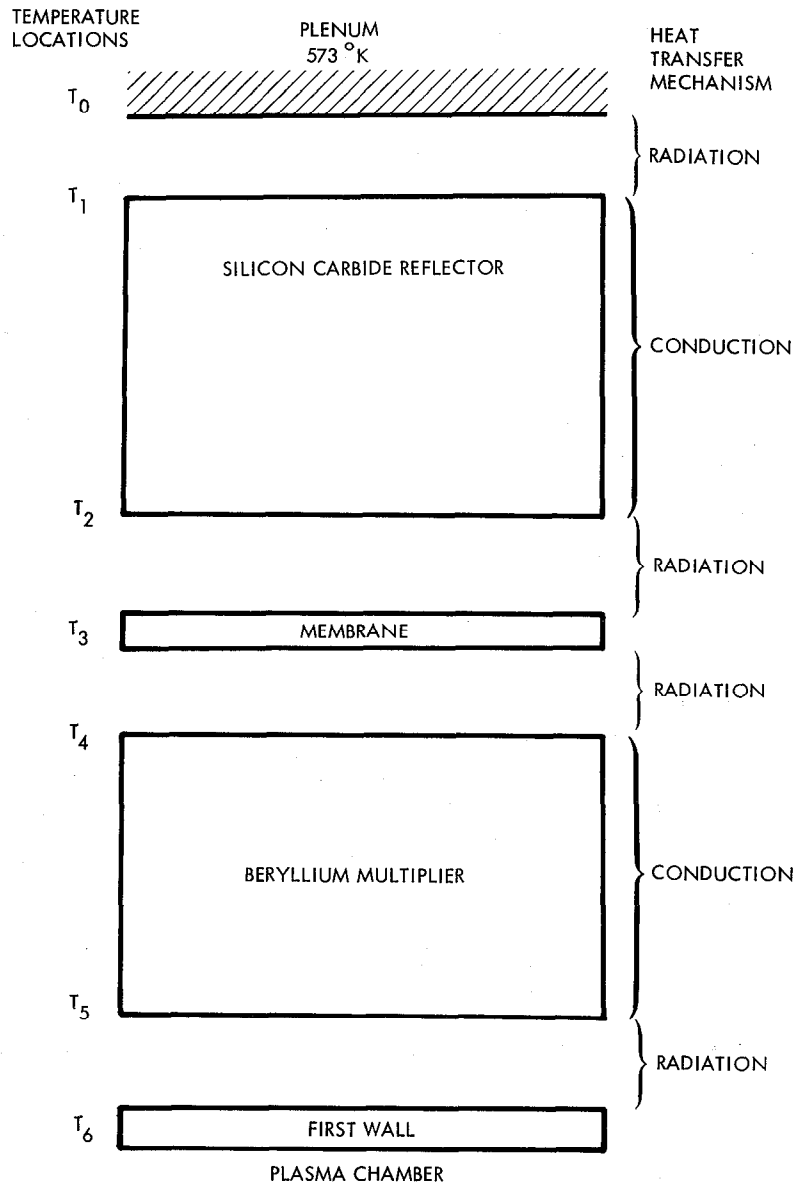


FIGURE VI-6. Loss of thermal contact medium and helium.

TABLE VI-4. Loss of thermal contact medium and helium.

Time	Temperature (°C)	Emissivity		
		0.2	0.5	0.7
0	T <sub>1</sub>	697	531	485
	T <sub>2</sub>	768	602	555
	T <sub>3</sub>	895	690	631
	T <sub>4</sub>	1008	773	703
	T <sub>5</sub>	1051	815	838
	T <sub>6</sub>	1107	856	781
2 hours	T <sub>1</sub>	574	448	415
	T <sub>2</sub>	611	485	452
	T <sub>3</sub>	720	557	517
	T <sub>4</sub>	816	625	570
	T <sub>5</sub>	838	647	592
	T <sub>6</sub>	889	683	623
24 hours	T <sub>1</sub>	401	346	334
	T <sub>2</sub>	410	355	343
	T <sub>3</sub>	469	388	368
	T <sub>4</sub>	527	422	395
	T <sub>5</sub>	532	427	400
	T <sub>6</sub>	564	447	416

Case 3, Loss of Helium and Thermal Contact Medium Immediately Behind the First Wall. Radiation heat transfer between the first wall and the zones behind it with loss of helium was analyzed. A radiation gap behind the first wall is modeled but no appreciable amount of thermal contact medium (containing most of the decay heat generating products) is assumed lost. No heat loss is assumed on the plasma side of the first wall. Considering only radiation, the steady state first wall bulk temperature is given by:

$$T = \left( q''' V / A \sigma \epsilon F + T_s^4 \right)^{1/4} ,$$

where  $q'''$  is the first wall volumetric heat generation rate at the time considered, (assumed to be constant)

$V$  is the first wall volume

$A$  is the area of first wall considered

$F$  is the shape factor (1)

$\sigma$  is the Stefan-Boltzmann constant

$\epsilon$  is the emissivity taken to be 0.2, 0.5 and 0.7

$T_s$  is the sink temperature of the zones behind the first wall.

The sink temperatures were taken at the times indicated from the transient loss of helium analysis (case 1) above. Results are shown in Table VI-5. Note that these equilibrium first wall temperatures result from conservative overestimates of heat generation. The actual temperatures would lag behind and therefore be lower as the temperature is rising.

As mentioned above, this analysis considers heat removal from the first wall by radiation only without removing the heat generating thorium, and is intended to be a worst case analysis involving losses of helium and thermal contact medium. Temperatures are not appreciably higher than those from the loss of helium case (1), especially if the emissivities of the reactor materials can be kept above about 0.5. Accidents involving isolated first wall regions with the plasma and helium coolant system shut off should present no greater problems than the loss of helium coolant only accident.

TABLE VI-5. Isolated first wall temperatures, °C.

T is first wall temperature  
 $\Delta T$  is first wall temperature amount  
 above loss of helium (case 1)

Time After Shutdown	Emissivity					
	0.2		0.5		0.7	
	T	$\Delta T$	T	$\Delta T$	T	$\Delta T$
50 seconds	674	84	627	37	617	27
6.5 minutes	649	90	598	39	588	29
27 minutes	679	70	639	30	631	22
35 minutes	688	64	651	27	644	20
56 minutes	706	53	675	22	669	16
2 hours	736	34	716	14	712	10
6 hours	815	10	809	4	808	3
15 hours	915	5	912	2	911	1
28 hours	998	4	996	2	995	1

Case 4, Loss of Thermal Contact Medium in a Small Area With Helium Flowing.

A transient analysis was performed using the SINDA code. Here flow was modeled by setting He temperatures to the constant values shown in Fig. VI-4. Two gap nodes with radiation transfer across them were taken between the helium tube and first wall. All other properties and assumptions were as in case 1. Results are shown on Fig. VI-7. With the plasma shut off, and helium coolant flowing, the blanket temperatures drop off very rapidly. Thermal problems should not develop in this reactor if the plasma is shut off and the helium cooling system is kept operating.

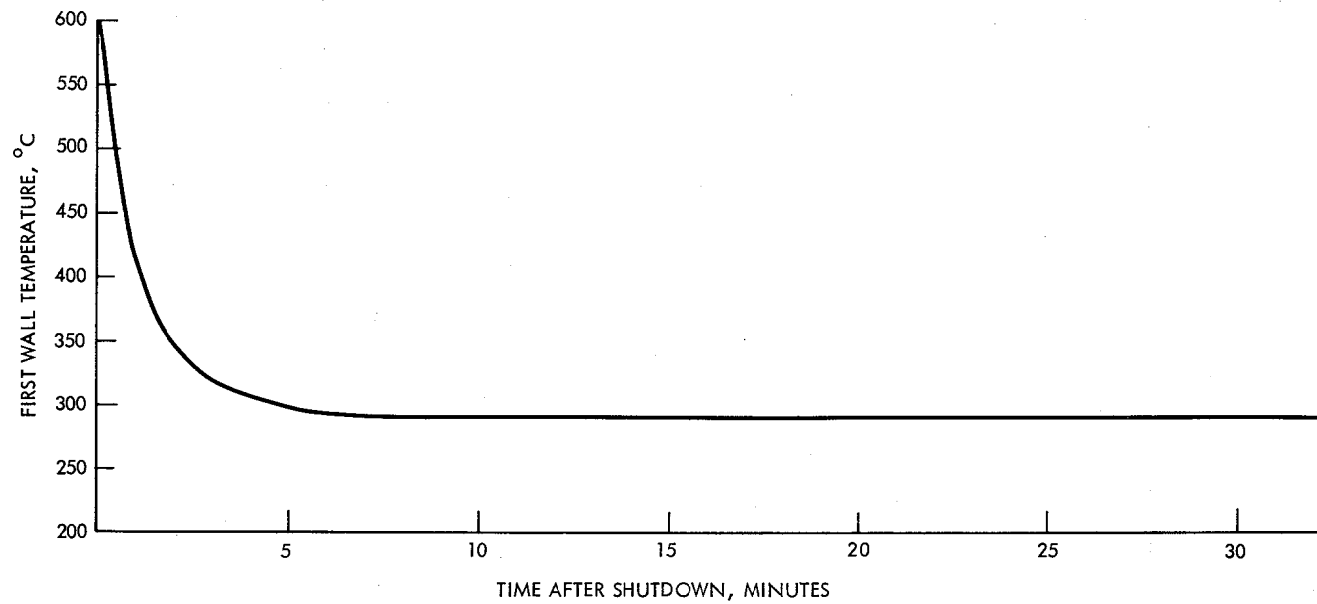


FIGURE VI-7. Loss of  $\text{LiPb ThO}_2$  in a small zone with helium flowing.

Case 5, Helium Flow Blockage in a Single Tube. A one-dimensional analysis of the first wall near a blocked tube with the plasma on was performed. This analysis considers heat conduction only along the first wall toward the nearest working cooling tubes. The plasma side of the first wall is adiabatic if vacuum is maintained and all of the first wall is at the same temperature. This is conservative when considering a hot spot on the first wall as it would radiate heat to cooler areas. Assuming that the blanket side of the first wall is adiabatic is also conservative since it implies a higher temperature in the blanket than would actually exist. Rough calculations indicate that the actual heat flux from the blanket side of the first wall is about 20% of the conduction along the wall. These calculations ignore the first wall corrugations. The adiabatic boundaries reduce the problem to conduction in an infinite cylinder, and the maximum temperatures occur at steady state. The solution to the steady state conduction equation for an infinite cylinder with constant properties is:<sup>4</sup>

$$T - T_o = Q/4k \left( R_o^2 - r^2 \right) ,$$

- where
- $T_o$  = outside cylinder temperature
  - $T - T_o$  is the temperature difference between the cylinder centerline temperature (corresponding to the hottest point below the blocked coolant tube) and the outer temperature
  - $r$  = radius at which temperature  $T$  is found (center temperature at  $r = 0$ )
  - $R_o$  = outside radius
  - $Q$  = heat generation per unit volume
  - $k$  = conductivity.

Results are in Table VI-6. This simple analysis gives only a very general idea of the consequences of a blocked tube. The outside cylinder temperature would also increase above its steady state temperature since the heat formerly carried by the blocked tube must be shared by the neighboring six tubes. Because of the complex geometry of the first wall region a proper analysis of tube blockage will require a detailed 3-dimensional model; however, these results indicate that a reactor operating with sufficient temperature margin could tolerate tube blockage.

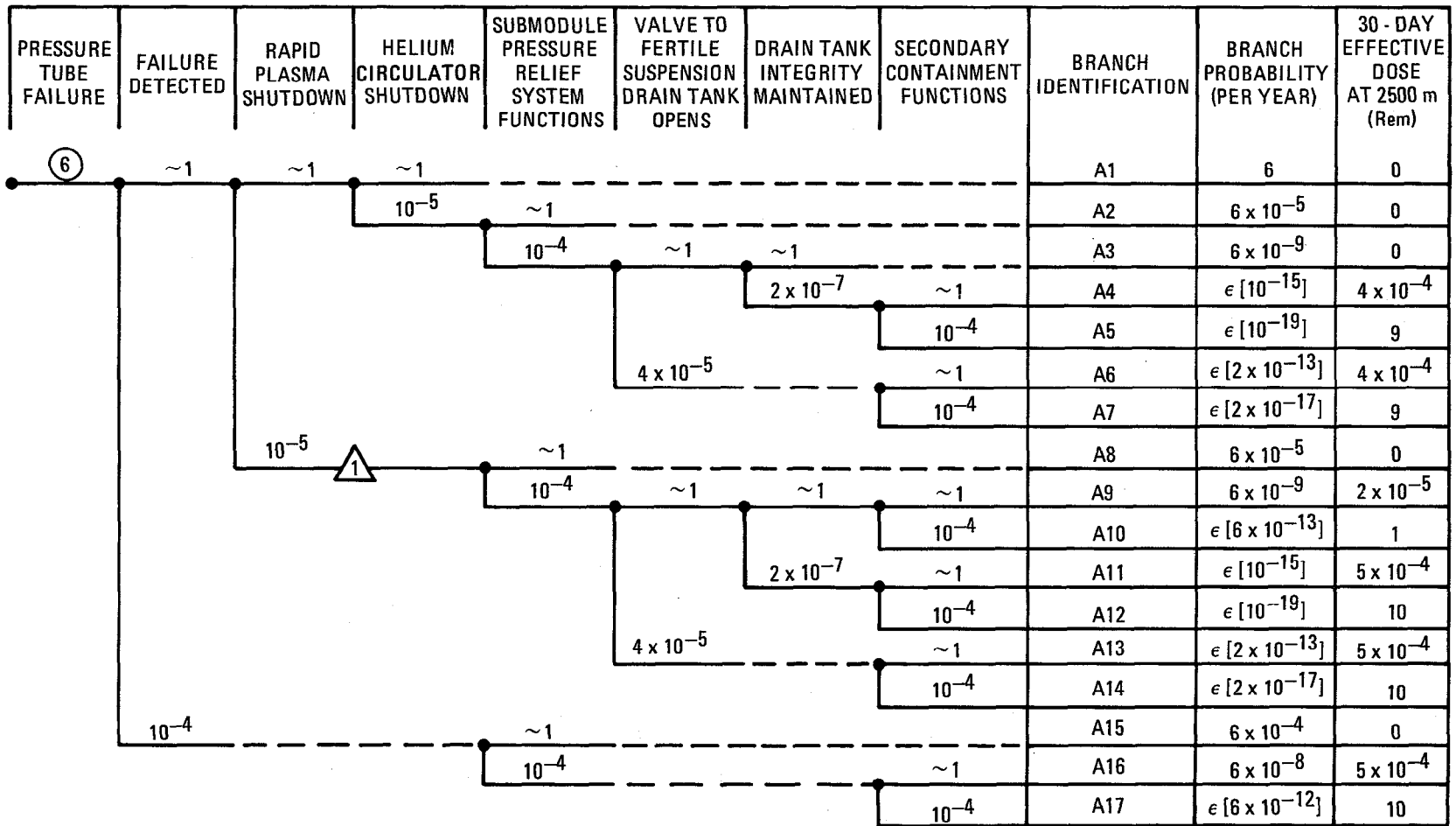
TABLE VI-6. Temperature difference as a function of unit cell radius, blocked tube analysis.

$R_o$ (m)	$T - T_o$ (°C)
0.018	39
0.027	87
0.036	155

In summary, the results of these preliminary analyses show that if the plasma is shut down, the gas-cooled fertile suspension blanket will not melt under the postulated conditions. The question arises as to whether the module would instead buckle and rupture before melting. Preliminary indications are that since the first wall was designed to accommodate long term creep rupture stresses, the short term stresses present during these types of accidents may not exceed the allowable stress at the elevated temperatures. Definitive answers however will require coupled stress and thermal analyses or experiments.

VI.B.1.d Event Tree Construction and Branch Probabilities. On the basis of the release pathways, barriers and sequences developed earlier, coupled with the results of the thermal analysis, event trees can be constructed for selected initiating events. These are presented below, followed by the discussion of the branch probabilities included in the figures. The calculation of the consequences is presented in the next section.

Pressure Tube Leakage (Fig. VI-8). A longitudinal pressure tube failure will result in a partial loss of thermal contact and the overpressurization of the submodule. Upon detection the plasma is shut down and then the helium pressure is relieved. If the helium circulation can't be shut down, then the pressure relief system can either relieve the gas pressure or activate a drain valve to drain the fertile suspension and thereby relieve the pressure. If the pressure relief system fails to function, the valve fails to open, or the



△1 IF THE PLASMA IS NOT SHUTDOWN, MAINTAIN HELIUM FLOW THROUGH BLANKET.

FIGURE VI-8. Pressure tube leakage event tree.

drain tank does not maintain its integrity, a release of the inventory of one submodule to the secondary containment will result. If the plasma does not immediately shut down, the He supply is not shut off, as cooling is required by the rest of the reactor, but the contents of the submodule containing the failed pressure tube are drained in order to limit the magnitude of the release in the event of submodule rupture. Naturally, if the failure is not detected, and the passive pressure relief system fails, the submodule is assumed to rupture.

Heat Removal System Failure (Fig. VI-9). This initiating event is assumed to include catastrophic heat removal system failures from all sources, e.g., pipe ruptures, pump breakdowns, heat exchanger failures, etc. Upon detection, the plasma is shut down. The results of the thermal analyses show that if the plasma is shut down no melting and therefore no release will occur. If the plasma is not shut down, then a fertile suspension dump is performed in order to limit the consequences of a release. If the dump is successful, only activation products and tritium are released. Otherwise the entire reactor radioactive inventory is released. If the failure is not detected, melting occurs, and a release occurs to the secondary containment.

First Wall Failure (Fig. VI-10). The probability of a plasma disruption in the TMHR is not expected to be very high. Nevertheless, in addition to the two accidents discussed above, a plasma disruption was considered another event which could result in first wall failure. If such a failure did occur, a drain of the fertile suspension in the damaged submodule would be initiated. There is no present way to prevent the contents of the submodule from spilling from upper modules, and therefore one-half of the submodule inventory is assumed to leak into the plasma chamber even if the valve to the drain tank operates. No credit was taken for the fusion vacuum boundary barrier and the leak is assumed to lead directly into the secondary containment. If the drain tank fails, the valve does not open or the failure is not detected, the entire submodule inventory is assumed to be released .

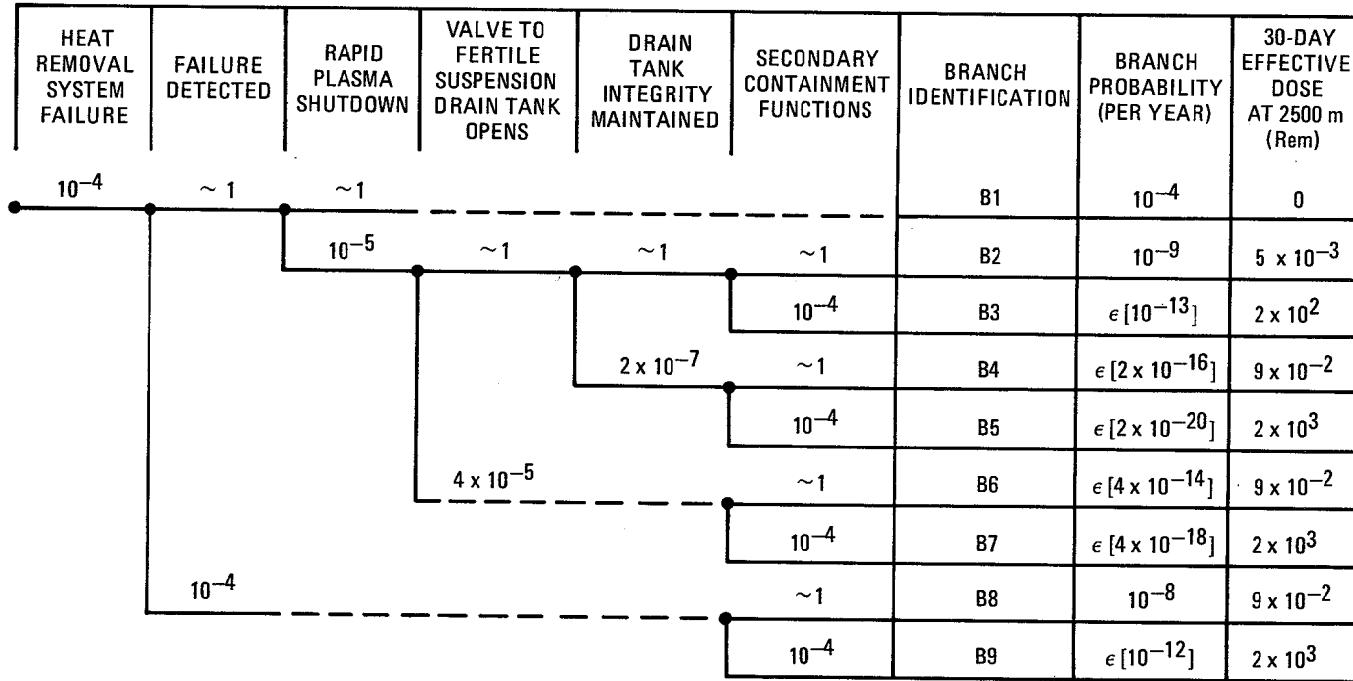


FIGURE VI-9. Heat removal system failure event tree.

PLASMA DISRUPTION-FIRST WALL FAILURE	FAILURE DETECTED	VALVE TO FERTILE SUSPENSION DRAIN TANK OPENS	DRAIN TANK INTEGRITY MAINTAINED	SECONDARY CONTAINMENT FUNCTIONS	BRANCH IDENTIFICATION	BRANCH PROBABILITY (PER YEAR)	30-DAY EFFECTIVE DOSE AT 2500m (Rem)
$10^{-1}$	$\sim 1$	$\sim 1$	$\sim 1$	$\sim 1$	C1	$10^{-1}$	$2 \times 10^{-4}$
				$10^{-4}$	C2	$10^{-5}$	5
			$2 \times 10^{-7}$	$\sim 1$	C3	$2 \times 10^{-8}$	$4 \times 10^{-4}$
				$10^{-4}$	C4	$\epsilon [2 \times 10^{-12}]$	9
		$4 \times 10^{-7}$		$\sim 1$	C5	$4 \times 10^{-7}$	$4 \times 10^{-4}$
				$10^{-4}$	C6	$\epsilon [4 \times 10^{-11}]$	9
	$10^{-4}$			$\sim 1$	C7	$10^{-5}$	$4 \times 10^{-4}$
				$10^{-4}$	C8	$10^{-9}$	9

FIGURE VI-10. First wall failure event tree.

Branch Probabilities. To provide a relative measure of probability among the events described above and presented in Figs. VI-8 to VI-10, a generic data base<sup>5</sup> for gas-cooled reactor components and systems was used. Pressure tube failure data was obtained by applying steam generator tube failure data from the world experience in water-cooled nuclear power reactors in 1976.<sup>6</sup> Table VI-7 represents the probability failure rates resulting from applying the data base, along with conservative engineering judgment and experience. Probabilities less than  $10^{-9}$  are designated as  $\epsilon$  in the event trees. A large uncertainty range can be associated with the probability data. However, important design guidance can still be obtained from the application of the data and is presented in Section VI.B.2.

TABLE VI-7. Failure probabilities for the events of Figs. VI-8 through VI-10.

Event Description	Failure Probability (a)
Pressure tube failure	6/year
Heat-removal system failure	$10^{-4}$ /year
Plasma disruption with first wall failure	$10^{-1}$ /year
Detection system failure	$10^{-4}$
Rapid plasma shutdown	$10^{-5}$
Helium circulator shutdown	$10^{-5}$
Burnt protection system failure	$10^{-4}$
Valve to fertile suspension drain tank failure	$4 \times 10^{-5}$
Drain tank failure	$2 \times 10^{-7}$
Secondary containment failure	$10^{-4}$

(a) Failure probabilities are on a per demand basis unless otherwise stated.

VI.B.1.e Description of Potential Consequences. Having presented event probabilities in the previous section, the next step in computing risk is to obtain the dose consequences at an external site location. The calculation of the radioactive inventory is presented first, followed by the presentation of the consequence analysis.

Radioactive Inventory. The major sources of radioactivity in a hybrid reactor are actinides, fission products, activation products and tritium. The activities and biological hazard potential in air (BHP) contributed from each of these sources are presented in Tables VI-8 through VI-12. The first four tables present the activity and BHP by contributing radionuclide. Table VI-12 presents a summary by source.

The TRW ISOGEN code was used to model actinide production and decay in the TMHR designs. Table VI-8 shows that both the actinide activity and BHP are dominated by the radioisotopes  $^{233}\text{Th}$  and  $^{233}\text{Pa}$ . Since these two nuclides are an inherent part of the fuel production chain, these results signify that this blanket concept does not have any significant parasitic contributors to hazard at shutdown. In addition, after the decay of the two primary contributors (in the time scale of hours to months) the actinide BHP will be reduced by an additional two orders of magnitude. At that time the hazard will be dominated by the relatively long-lived  $^{231}\text{Pa}$ .

Of the 4320 MW of blanket power in the gas-cooled design, 460 MW are contributed from fissions. These fissions as well as reducing the fertile fuel production rate produce fission products. The major contributors to BHP and their activities are shown in Table VI-9. Although one order of magnitude less hazardous than the actinides at shutdown, after the decay of  $^{233}\text{Th}$ ,  $^{233}\text{Pa}$ , the iodine isotopes,  $^{89}\text{Sr}$ , and  $^{140}\text{Ba}$ , the contributions of actinides and fission products are comparable. Since in most cases the inventory of fission products scales with fission power, the value of fission-suppression is evident.

The activation product inventory was obtained from DKR<sup>7</sup> activation and decay calculations. The ferritic steel first wall and structure are the sources of activation products. Due to the low structure fraction of the gas-cooled blanket, approximately 80% of the activity is located at the first wall. Table VI-10 presents the major contributors to activation product hazard.

TABLE VI-8. Major contributors to actinide BHP for the gas-cooled blanket.

Radionuclide	Activity (Ci)	BHP (km <sup>3</sup> )	Half-Life
Th 228	3.6 +01	1.8 +05	1.91 y
232	1.7 +01	1.7 +04	1.4 x 10 <sup>10</sup> y
233	2.0 +10	5.2 +08	22 m
Pa 231	1.3 +03	3.3 +07	3.3 x 10 <sup>4</sup> y
233	1.3 +10	2.1 +09	27 d
U 232	3.0 +03	3.3 +06	72 d
233	3.1 +03	7.8 +05	1.6 x 10 <sup>5</sup> y
TOTAL	3.3 +10	2.7 +09	
TOTAL/module	1.4 +09	1.1 +08	
TOTAL/kg yearly fissile fuel production	5.0 +06	4.0 +05	

TABLE VI-9. Major contributors to fission product BHP for the gas-cooled blanket.

Radionuclide	Activity (Ci)	BHP (km <sup>3</sup> )	Half-Life
Sr 89	5.7 +06	1.9 +07	54 d
90	4.4 +04	1.5 +06	28 y
91	2.3 +07	2.5 +06	9.7 h
Y 91	6.8 +06	6.8 +06	58 d
Zr 95	6.6 +06	6.6 +06	65 d
Mo 99	2.4 +07	3.4 +06	67 h
I 131	1.1 +07	1.1 +08	8.1 d
133	2.6 +07	6.4 +07	2.1 h
135	2.2 +07	2.2 +07	6.7 h
Cs 134	1.4 +06	3.5 +06	2.3 y
Ba 140	2.0 +07	2.0 +07	13 d
La 140	2.0 +07	5.1 +06	40 h
Ce 144	1.5 +06	7.7 +06	285 d
TOTAL	1.7 +08	2.7 +08	
TOTAL/module	7.0 +06	1.1 +07	
TOTAL/kg yearly fissile fuel production	2.5 +04	4.1 +04	

TABLE VI-10. Major contributors to activation product BHP for the gas-cooled blanket.

Radionuclide	Activity (Ci)	BHP (km <sup>3</sup> )	Half-Life
Cr 51	8.8 +07	1.2 +06	27 d
Mn 54	4.0 +07	4.0 +07	300 d
56	2.0 +08	1.1 +07	2.6 h
Fe 55	4.6 +08	1.5 +07	2.9 y
Co 57	8.3 +05	1.3 +05	267 d
58	2.5 +06	1.2 +06	71 d
60	8.3 +05	2.8 +06	5.2 y
Ni 57	1.5 +05	1.5 +06	36 h
W 185	1.3 +07	3.5 +06	74 d
187	6.6 +07	6.6 +06	24 h
TOTAL	8.7 +08	8.3 +07	
TOTAL/module	3.6 +07	3.5 +06	
TOTAL/kg yearly fissile fuel production	1.3 +05	1.3 +04	

TABLE VI-11. Tritium inventory and BHP for the gas-cooled blanket.

Location	Activity (Ci)	BHP (km <sup>3</sup> )
Tritium associated with the blanket	9.0 +04	4.4 +02
Tritium associated with fusion-related fueling, processing, etc.	1.2 +07	6.0 +04
Tritium in storage	6.9 +07	3.4 +05
TOTAL	8.1 +07	4.0 +05
TOTAL/module	3.3 +06	1.7 +04
TOTAL/kg yearly fissile fuel production	1.3 +04	6.0 +01

TABLE VI-12. Total radioactive inventory and BHP for the gas-cooled blanket.

Radioactivity Source	Activity (Ci)	BHP (km <sup>3</sup> )
Actinides	3.3 +10	2.7 +09
Fission products	1.7 +08	2.7 +08
Activation products	8.7 +08	8.3 +07
Tritium	8.1 +07	4.0 +05
TOTAL	3.4 +10	3.1 +09
TOTAL/module	1.4 +09	1.6 +08
TOTAL/kg yearly fissile fuel production	5.1 +06	4.7 +05

The tritium inventories associated with the fusion-producing processes and storage were scaled from the design presented in Ref. 8. The tritium inventory in the blanket was estimated to be 6 g in the LiPbThO<sub>2</sub> suspension liquid. Note that in the event of an accident the tritium in storage is assumed to be secure and therefore not released.

The total inventories from each source are compared in Table VI-12. Actinides dominate by one order of magnitude, but as noted earlier, the major contributors decay rapidly. The tritium contribution is seen to be insignificant. It is noted that actinides and activation products are relatively immobile while gaseous fission products and tritium are relatively mobile. These inventories represent the source terms used in the consequence analysis in the next section.

Consequence Analysis. The calculation of the radiological consequences of the release of the inventories given in the last section is the last step in computing risk. Following a blanket heatup event, submodule rupture or drain tank failure, the radioactivity present is released to the secondary containment. The radionuclide behavior in such situations is a major uncertainty. Potential chemical reactions, product volatilities, plateout and other deposition and escape mechanisms present a major problem in the estimate of consequences. The failure in an engineered safety feature does not necessarily result in an escape. For the purposes of this study, the release fractions were chosen to be consistent with those employed in LWR siting events. These include a 100% release of the noble gases and tritium, 25% release of the halogens, and 1% of all remaining material. The results obtained from the consequence analysis, though potentially overestimating the consequences, is useful in identifying the major consequence contributors.

The computer code TDAC<sup>9</sup> was used to calculate consequence. The radiation path after release from the containment involves meteorological assumptions and intake pathways such as inhalation and ingestion, ground contamination and surface deposition. This analysis assumed direct airborne plume submersion and prompt inhalation and estimated external whole body exposure and internal inhalation-dose commitment to the organs, thyroid, bone and lung. A detailed summary of the reference conditions, parameters and assumptions used in the analysis is found in Table VI-13. An effective dose equivalent accounting for the total risk attributable to the exposures



TABLE VI-13 (Continued)

Parameter	Assumption
DOSE COMPUTATION	
Breathing rate assumed for duration of accident	2.32 x 10 <sup>-4</sup> m <sup>3</sup> /sec.
Inhalation dose commitment effectiveness	Ref. 10 adult inhalation values used. (Note: Ref. 10 has increased the tritium inhalation dose commitment factors by 50% to account for transpiration pathway. Also activation product effectivities developed using Appendix B of Ref. 9 information.)
Wind speed assumed	1.0 m/sec.
Decay and buildup enroute to dose receptor	Considered.
Exposure pathways examined	Prompt inhalation and submersion in the passing plume only.
Dose computation computer program	TDAC/E1 (Ref. 9).

to all the organs irradiated was used in presenting the results. The weight assigned to the exposure of each organ was derived from the ICRP-26<sup>11</sup> recommended values and are shown in Table VI-14. These risk factors are based upon the likelihood of inducing fatal malignant disease, threshold effects and genetic defects.

TABLE VI-14. Dose-equivalent risk weighting factors used in calculating effective dose.

Whole body	0.76
Thyroid	0.04
Bone	0.04
Lung	0.16

Table VI-15 presents the results of the dose consequence calculation. Approximately two-thirds of the effective dose is contributed by the actinides, most of it in the form of lung inhalation commitment. A little less than one-third of the effective dose is attributed to the fission products and a few percent to activation products. The tritium contribution to hazard is negligible. These distributions of hazards presented in these results can be attributed to the 1% of the actinide release assumption. It is noted that ~95% of the total lung dose is contributed by <sup>233</sup>Pa. Though in fact such a release may not be mechanistically possible, the results represent a basis for relative comparisons.

TABLE VI-15. Dose consequence from total gas-cooled blanket involvement events.

Accident Type	Integrated 30-Day Dose (Rem) at 2500 Meters				Effective Dose Equivalent <sup>(a)</sup> (Rem)
	External Whole Body Gamma	Inhalation			
		Thyroid	Bone	Lung	
Secondary containment functional - Contributors (%):	$3.4 \times 10^{-3}$	0.55	0.026	0.38	0.086
Actinides	0.0	0.0	0.8	66.6	67.4
Fission products	2.8	25.5	0.3	2.0	30.6
Activation products	0.2	0.0	0.1	1.8	2.0
Tritium	0.0	0.0	0.0	0.0	0.0
Secondary containment failed - Contributors (%):	30.0	$1.3 \times 10^4$	620.0	$9.1 \times 10^3$	$2.0 \times 10^3$
Actinides	0.0	0.0	0.8	68.0	68.7
Fission products	1.3	25.9	0.3	2.8	30.3
Activation products	0.2	0.0	0.1	1.8	2.0
Tritium	0.0	0.0	0.0	0.0	0.0

(a) See text for development of effective dose equivalent.

VI.B.1.f Risk Plot Analysis. With both event probabilities and consequences in hand, the major risk contributors in the gas-cooled blanket can be identified via the risk plot of Fig. VI-11. A number of observations can be made from the figure. The first observation is that pressure tube leakage, although a high probability event, is not a major contributor to risk since the consequences of such a failure can be constrained to a maximum release of one submodule's inventory. A second observation is that, due to the excellent after-heat thermal response of the blanket, only an undetected failure of the heat removal system with release of the entire reactor inventory to a functional secondary containment system is considered credible. (In general, events with probabilities less than one in a billion are considered inconceivable.) For comparison purposes, this maximum credible release results in consequences well below the 10CFR100<sup>12</sup> limits prescribed for accident situations. A third observation is that, of the limited accidents analyzed, the major risk contributor is first wall failure from a plasma disruption. This is due to a number of factors:

- No credit was taken in the analysis for limiters or plasma energy dump protection devices.
- No methods were devised to prevent the fertile suspension from leaking out from static pressure once a rupture has occurred (e.g., a "fast drain" system).
- No credit was taken for the fusion vacuum boundary as an additional barrier.

The inclusion of these factors would bring the risk of a plasma disruption more in line with those of the other events. From the above observations safety design guidance can be provided and is presented in the last section.

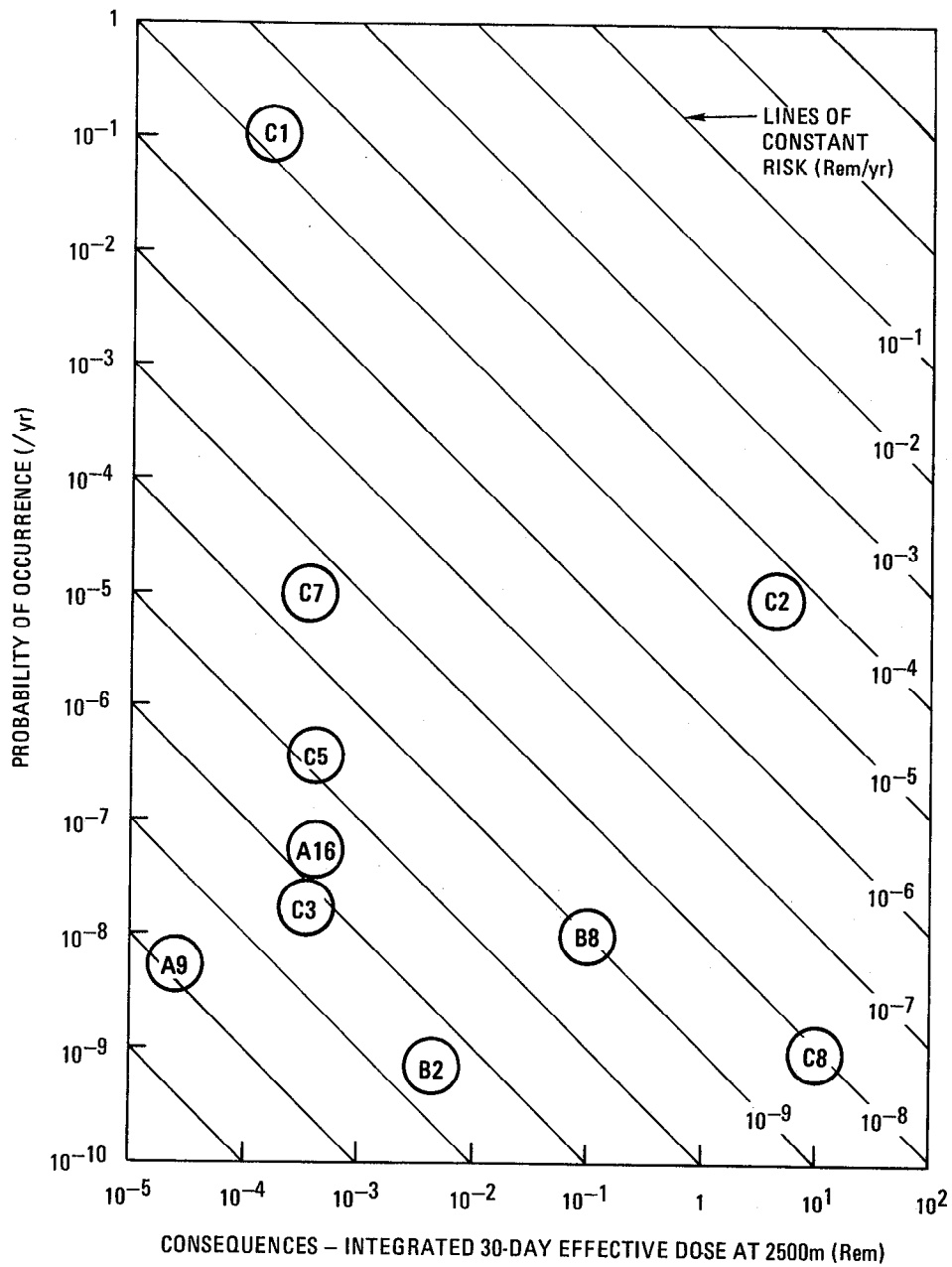


FIGURE VI-11. Major risk contributors of the TMHR gas-cooled blanket.

## VI.B.2 Overview and Comment

The safety features of the TMHR gas-cooled blanket have been evaluated. The results indicate that the fertile-dilute, thorium oxide in suspension blanket possesses very attractive safety characteristics. These characteristics include the following:

- Blanket melting does not occur from decay afterheat under any postulated loss of heat removal capability event. Only as a result of the plasma remaining on during an undetected heat removal system failure will the radioactive inventory be released to a functional secondary containment.
- The BHP present at shutdown in the blanket is approximately one to two orders of magnitude lower than that of an LMFBR. This advantage increases further as the major BHP contributors of the gas-cooled blanket, the iodine isotopes,  $^{233}\text{Th}$  and  $^{233}\text{Pa}$  quickly decay.
- The consequences of the maximum credible release using conservative release fractions and median U.S. site meteorology are below the 10CFR100<sup>12</sup> guidelines for accident conditions.

Having performed the safety analysis integral with the design of the blanket, a number of conceptual engineered safety systems have been incorporated into the design. These include the fertile suspension flow control mechanism, a fertile suspension drain tank with frozen drain valves, and consideration of a submodule pressure relief system. These should be further analyzed and improved in future studies. In addition, the results of the risk analysis demonstrate that adequate plasma disruption protection devices and a method for limiting spills (as in a pipe rupture) of the fertile suspension need to be included and analyzed in subsequent design iterations. Finally, the results of the thermal analyses show that a blocked cooling tube may be tolerable for short periods of time. That analyses should be refined and a detection system to locate such blockages should be devised.

## VI.C CONSIDERATIONS FOR LIQUID METAL COOLED SYSTEMS

### VI.C.1 Characterization of Principal Accidents and Consequences

VI.C.1.a Introduction. The potential sources of radioactivity for hybrid reactors are all of those common to pure fusion reactors plus those sources associated with the fission blanket. The sources that are common to fusion reactors are the activation products and tritium sources, while those that are associated with hybrids result from the actinides and fission products. Accordingly, the principal sources of radioactivity are due to the mobile fluid fuel, the mobile lithium and the immobile activation products.

The blanket concepts considered in Refs. 1 and 2 were based on fixed fueled designs cooled by helium, while the liquid lithium-molten salt blanket concept considered here is a fluid-fueled blanket containing two primary coolants. Significant differences might be expected in the accident pathways and the relative risks of fluid fuel blankets when compared with those of the fixed fuel blankets.

Description of the Reactor Systems and Containment Building Features. A simplified schematic diagram of the primary loops and BOP is shown in Fig. VI-12. As shown in this figure, the blanket consists of two zones; an inner, liquid lithium zone for tritium breeding and an outer, molten salt zone for fissile breeding. The two zones have a common containment wall in certain regions of the blanket. The system contains a molten salt dump tank or dump tanks. In certain accident events, the blanket fluid fuel is dumped to prevent damage (or aggravating the damage) to the blanket and/or the reactor. Up to fifteen separate, parallel, molten salt loops would provide the desired redundancy and minimize any release of radioactivity.

As in the MSBR, the design-basis accident is a rupture of the main fuel circulating lines<sup>13</sup> that occurs while the reactor is in operation, resulting in a spill of the molten salt. Such a rupture could release large quantities of radioactive material to the immediate surroundings. In order to limit the amount of molten salt spilled, multiple parallel molten salt loops and separate primary containments can be incorporated. To prevent the dispersion of the activity throughout the reactor building, the components of the fueled system

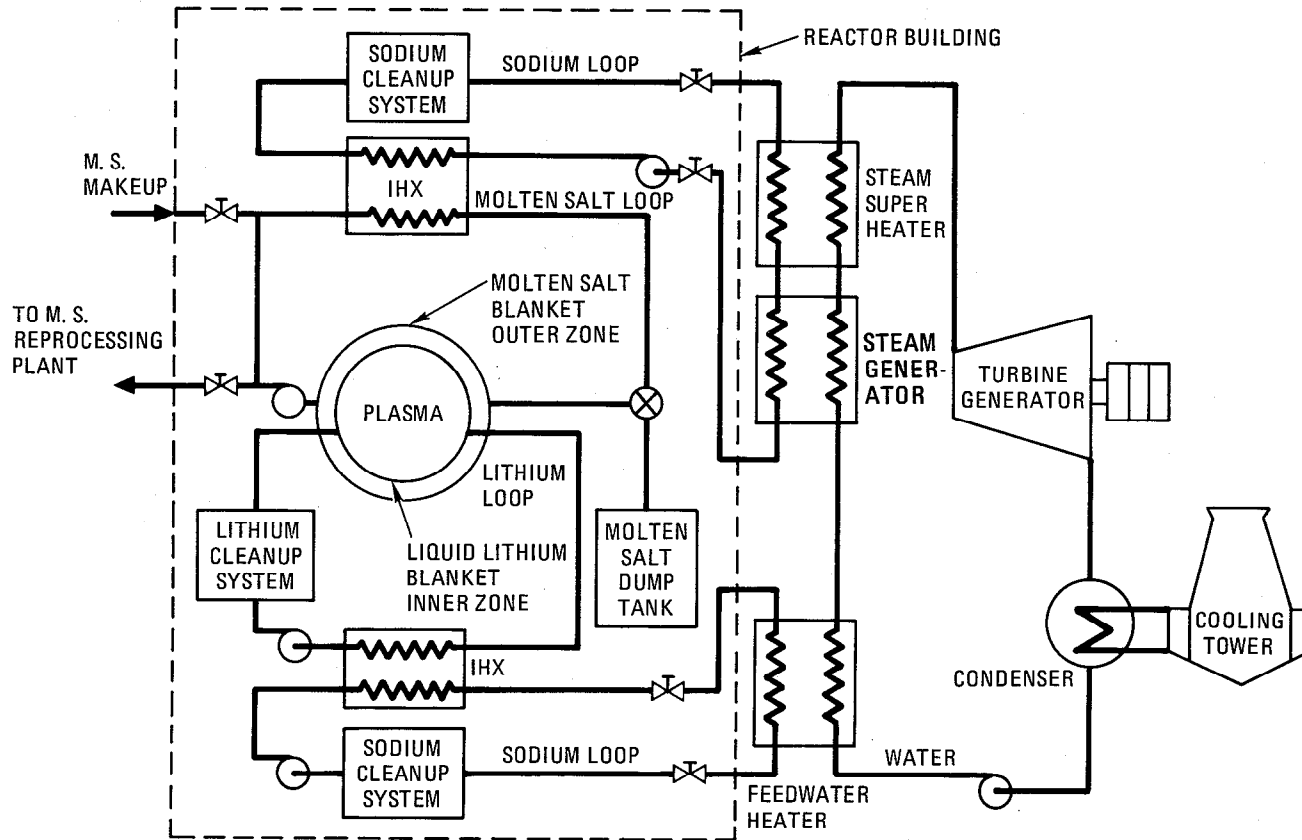


FIGURE VI-12. Schematic diagram of the liquid lithium-molten salt blanket primary loop and BOP components.

are assumed to be enclosed within a primary containment system of sealed cells from which water is excluded. This guards against the generation of large volumes of steam from the sensible heat of the fuel salt and thus limits the increase in the primary containment pressure to small values even in the event of major salt spills.

The prevention of the release of radioactivity to the environment under all possible accident scenarios is a governing principle behind the hybrid plant design. As a consequence, the reactor containment building (the secondary containment) represents the last of a series of defenses in case all precursor safeguards fail. Isolation valves are installed on piping that penetrate the containment building (e.g., the sodium secondary coolant loops that go to and come from the steam generator building) so as to prevent normally radioactive or activated coolant from escaping the secondary containment under certain accident conditions.

Another basic design feature that dictates the design of several major components within the reactor containment building is that all coolants that have common containment walls with the molten salt fluid fuel are designed to have higher pressures than the molten salt. In the event of possible breaches of the common containment wall, coolant(s) will leak into the molten salt rather than vice versa, thus preventing the highly radioactive fluid fuel from entering the secondary coolant system. Accordingly, the liquid lithium in the inner blanket has higher pressures than those of the molten salt. Similarly, the sodium in the sodium-molten salt intermediate heat exchanger has higher pressures than those of the molten salt. In the liquid lithium-sodium intermediate heat exchanger, again sodium has the higher pressure. In this case, the object is to prevent tritium leakage into the secondary coolant which might then find its way into the steam system and escape from the secondary containment. Pressure relief valves and vent systems are installed in the lower pressure flow systems so that the containment systems do not have to be designed for higher pressures.

The reactor building is assumed to be filled with argon at a pressure slightly below atmospheric so as to prevent gaseous leakage out of the containment building. Molten salt is rather inert in air; however, liquid lithium is highly reactive in air and with water. Consequently, it is

proposed that the containment building be filled with argon\* rather than air. The argon atmosphere will prevent fire hazards in case of a lithium spill into the containment building. The containment building is equipped to be purged with argon gas to remove any fission products, fission product gases, off-gases, and tritium that might be leaked into the building. The purge stream flows through a set of traps and through processing equipment for the removal of all radioactive materials.

Fifteen separate, parallel lithium loops are proposed to minimize the potential radioactivity release. This is consistent with the need for fifteen or more separate EM pumps (based on the capacity limit of EM pumps). The components of the plant that are enclosed by the reactor building (the secondary containment) are shown by the enclosures within the dotted area in Fig. VI-12. Two components that are necessary to safeguard the blanket are the dump or "drain" tank and the drain valve.

Molten Salt Dump/Drain Tank. A major safeguard system for the blanket is the use of a molten salt dump (or drain) tanks. The dump or drain tanks are designed to provide temporary holdup of the blanket molten salt as well as the fission products. As a consequence, cooling of the drain tank must be provided. Its design is strongly influenced by the drain system flowsheet and its design is integral to that of the TMHR plant. Active cooling of the drain tank can be effected through the use of a coolant such as NaK, considered in the MSBR program,<sup>14</sup> although passive cooling is a possibility that should be studied. The fission product gases are removed through vent lines for processing.

Drain Valve. The discharge of the blanket molten salt into the dump tank is achieved by thermal activation of the drain valve. The drain "valve" is conceived to be of the freeze type used successfully in the Molten Salt Reactor Experiment (MSRE).<sup>14</sup> The "valve" consists of flattened sections of drain lines

---

\* Nitrogen cannot be considered a candidate atmosphere since nitrogen, in contact with stainless steel, tends to form nitrides which can cause embrittlement and cracking of the structure; moreover, nitrogen is highly reactive with liquid lithium.

provided with external heaters and coolers. The number and size of the drain lines depend on the volume of the blanket discharge and the rate of discharge desired. The actual design of such a valve will have to be established by a detailed design. The valve provides positive shut-off by freezing the salt in the flattened sections. The valves are "opened" by melting out the frozen salt through the activation of the heaters. Although a drain valve for the subsequent Molten Salt Breeder Reactor (MSBR) had not been designed, it was conceived to have the appearance of a small shell-and-tube heat exchanger with the salt flowing through the tubes.<sup>14</sup> A mechanical-type valve with the seat chilled to provide positive shut-off was also considered. The design of a viable drain valve was not considered to be a major uncertainty in the MSBR design. The nature of this type of valve suggests that the valve can be opened only relatively slowly. Consequently, the rate of blanket molten salt temperature rise in case of a loss-of-flow accident can be important; however, the speed of the valve actuation is subject to design. The inherent safety features of the lithium-molten salt blanket include the following:

1. No conceivable possibility for criticality accidents
2. Plasma shutdown shuts down system
3. Relatively low afterheat
4. Low rate of molten salt heatup

The first and last are due to the low fissile concentrations inherent in fission-suppressed hybrid blankets and specifically to the molten salt fuel form. In view of the general difficulty of maintaining a plasma, it is expected that the shutdown of the plasma can be achieved by a variety of methods. Low blanket afterheat is a basic characteristic of fission suppressed blankets. With the very low fission rate, heat producing fission products in this reference molten salt blanket are kept at a minimum so that very low rates of molten salt heatup are anticipated. A calculation based on lumped parameters and adiabatic heating showed that the rate of heatup is  $0.024^{\circ}\text{C/s}$ .

VI.C.1.b Identification of Accident Type and Initiating Mechanisms. The generic accident pathways for this blanket and the TMHR plant and the barriers to the release of radioactivity are summarized in Fig. VI-13. There are a number of possible accident initiating events that have the potential of leading to accidental releases of radioactivity. The potential radioactivity

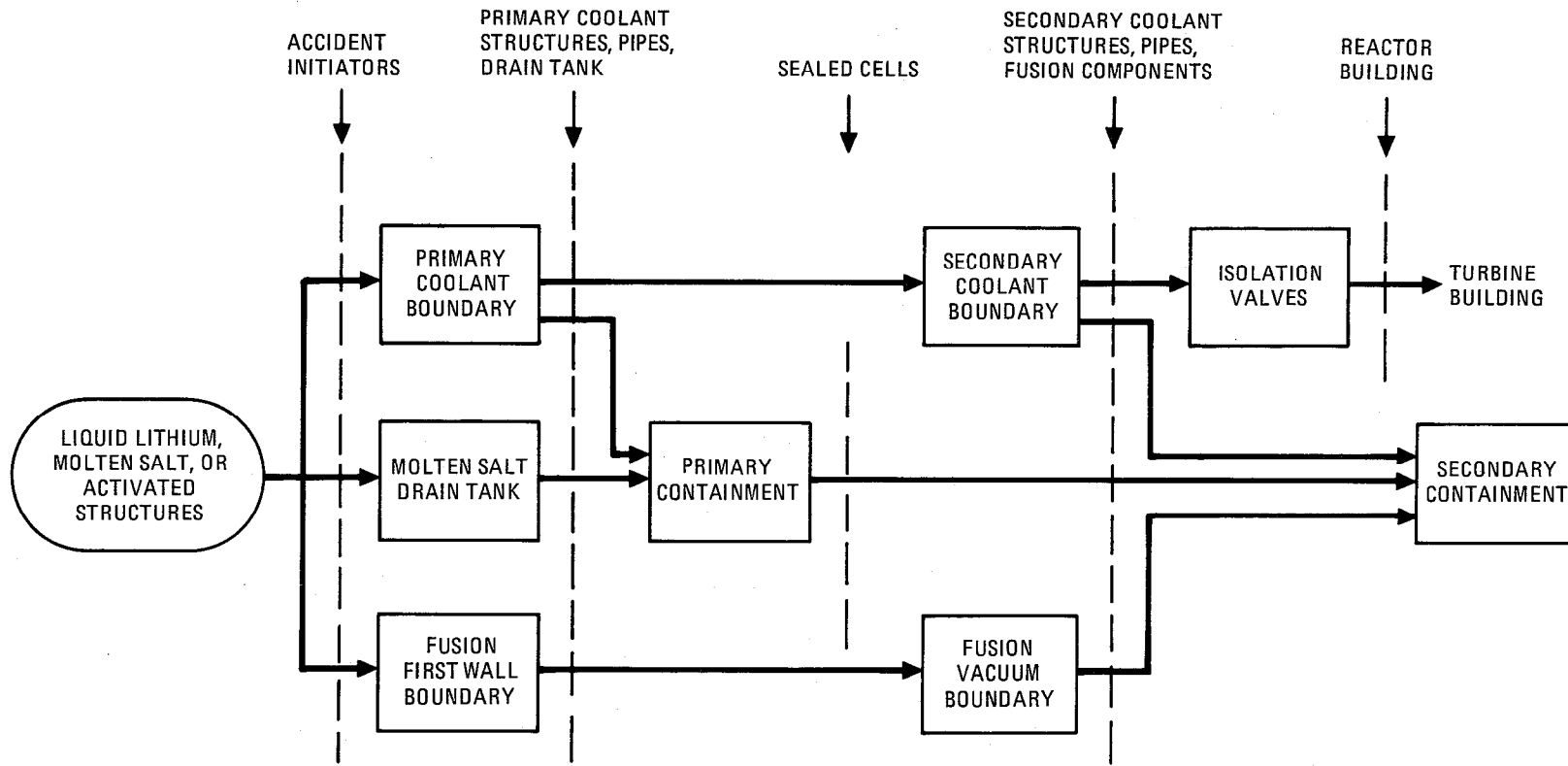


FIGURE VI-13. Radioactivity release pathways and barriers associated with the TMHR liquid metal cooled blanket.

releases from the liquid lithium blanket and flow system arise as a result of the presence of tritium, bred in the lithium blanket. Several of the potential accident initiating events are unique to the reference blanket concept. Ten different events postulated initially are listed in Table VI-16. Accident initiating events other than those listed can be postulated; however, those that are considered to have relatively low consequences and relatively low risks are left out, while others can be fitted into (or are similar to) those events illustrated in Table VI-16.

It is expected that the two primary coolant loops (liquid lithium and molten salt) will have flow, temperature, and pressure sensors so that the various accident events postulated can be rapidly detected and trigger a plasma shutdown. The only accident event that is relatively failsafe is that due to Event 4 in which the first wall is breached; liquid lithium leaks into the plasma and the plasma is quenched automatically.

For most of the accident initiating events, the coolant pressure changes rapidly while the coolant temperature response tends to be relatively slow. Consequently, plasma shutdown is conceived to be activated by more than two different sensors to provide redundancy. For example, in the event the pressure sensing system fails, then the temperature sensors would actuate plasma shutdown and other safeguards.

Among the ten potential accident initiating events, four are expected to have the greatest consequence. These are marked by an asterisk in Table VI-16 and are deemed the major accident initiating events selected for further consideration. The sequence of events and accident pathways for each of the four major accident initiating events are described briefly below.

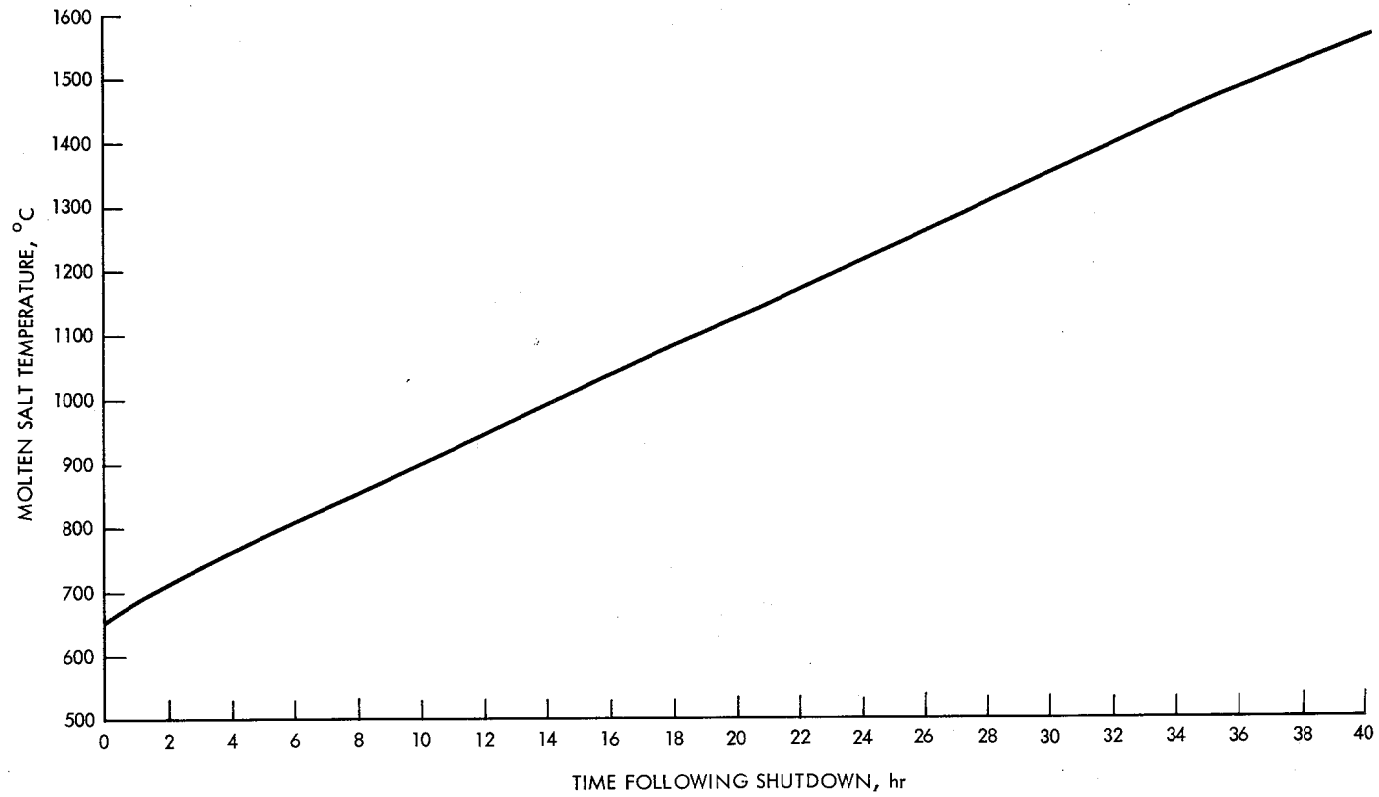


FIGURE VI-14. Molten salt heating following a loss of heat removal capability.

TABLE VI-16. Potential accident initiating events that could lead to a release of radioactivity in the liquid metal cooled system.

- |   |
|---|
| * 1. Molten salt pipe failure                       |
| * 2. Molten salt-liquid lithium common wall failure |
| * 3. Lithium pipe failure                           |
| * 4. First wall failure (lithium blanket breached)  |
| 5. Molten salt pump failure                         |
| 6. Lithium pump failure                             |
| 7. Lithium-sodium IHX tube failure                  |
| 8. Molten salt-sodium IHX tube failure              |
| 9. Sodium pipe failure (for Li-Na IHX)              |
| 10. Sodium pipe failure (for MS-Na IHX)             |

\* Major accident initiating events.

VI.C.1.c Thermal Modeling of Accident Scenarios. To obtain a preliminary feeling for the time in which to take corrective action in an event involving the molten salt blanket, an adiabatic analysis of the molten salt afterheating was performed.  $\text{Pa}^{233}$ ,  $\text{Th}^{233}$  and fission product decay heat raise the molten salt to the boiling point in 36 hours under adiabatic conditions. Results of integrating the following equation are shown in Fig. VI-14.

$$\dot{Q} = \rho c \frac{dT}{dt}$$

where  $\rho$  = molten salt density 3350 kg/m<sup>3</sup>  
 $c$  = heat capacity 1382 W/kg  
 $\dot{Q}$  = the volumetric heat generation rate, W/m<sup>3</sup>.

In this case,

$$\dot{Q} = \dot{Q}_{Pa} + \dot{Q}_{Th} + \dot{Q}_{fission}$$

where  $\dot{Q}_{Pa} = 2.88 \times 10^4 e^{-2.97 \times 10^{-7} \tau}$

$$\dot{Q}_{Th} = 4.40 \times 10^4 e^{-5.204 \times 10^{-4} \tau}$$

$$Q_{fission} = 9.52 \times 10^4 * 0.055 \left[ (\tau - 10)^{-0.2} - 0.87 (\tau - 2.7 \times 10^7)^{-0.2} \right]$$

The adiabatic analysis is extremely conservative because it ignores most of the heat capability of the reactor, and any heat losses such as active cooling of the shield. The results indicate that several hours (and possibly days) would be available to remove the molten salt from the reactor. It is quite possible that a small amount of cooling will cause the molten salt temperature to level off at an acceptable level. This needs to be confirmed by analysis.

VI.C.1.d Event Tree Construction and Branch Probabilities. On the basis of the pathways and barriers identified for the molten salt-liquid lithium blanket, sequences of events can be postulated and event trees constructed. These are discussed below, followed by a presentation of the branch probabilities used in the event trees. The results of the consequence calculations are presented in the subsequent section.

Molten Salt Pipe Failure (Fig. VI-15). This event is the design basis accident, identical to that for the MSBR. Such a failure results in an immediate release of the radioactive molten salt to the primary containment (the sealed cell). It immediately triggers a shutdown of the molten salt pump and a shutdown of the plasma. The pipe failure triggers a loss of molten salt flow to the blanket. The molten salt in the blanket will heat up as a result of actinide and fission product decay. The molten salt temperature rise should cause the dump tank valve to be activated, in this case the molten salt in the blanket is dumped into the dump (drain) tank where it is cooled and the tritium and fission product gases are vented to a cleanup system. If the primary containment is

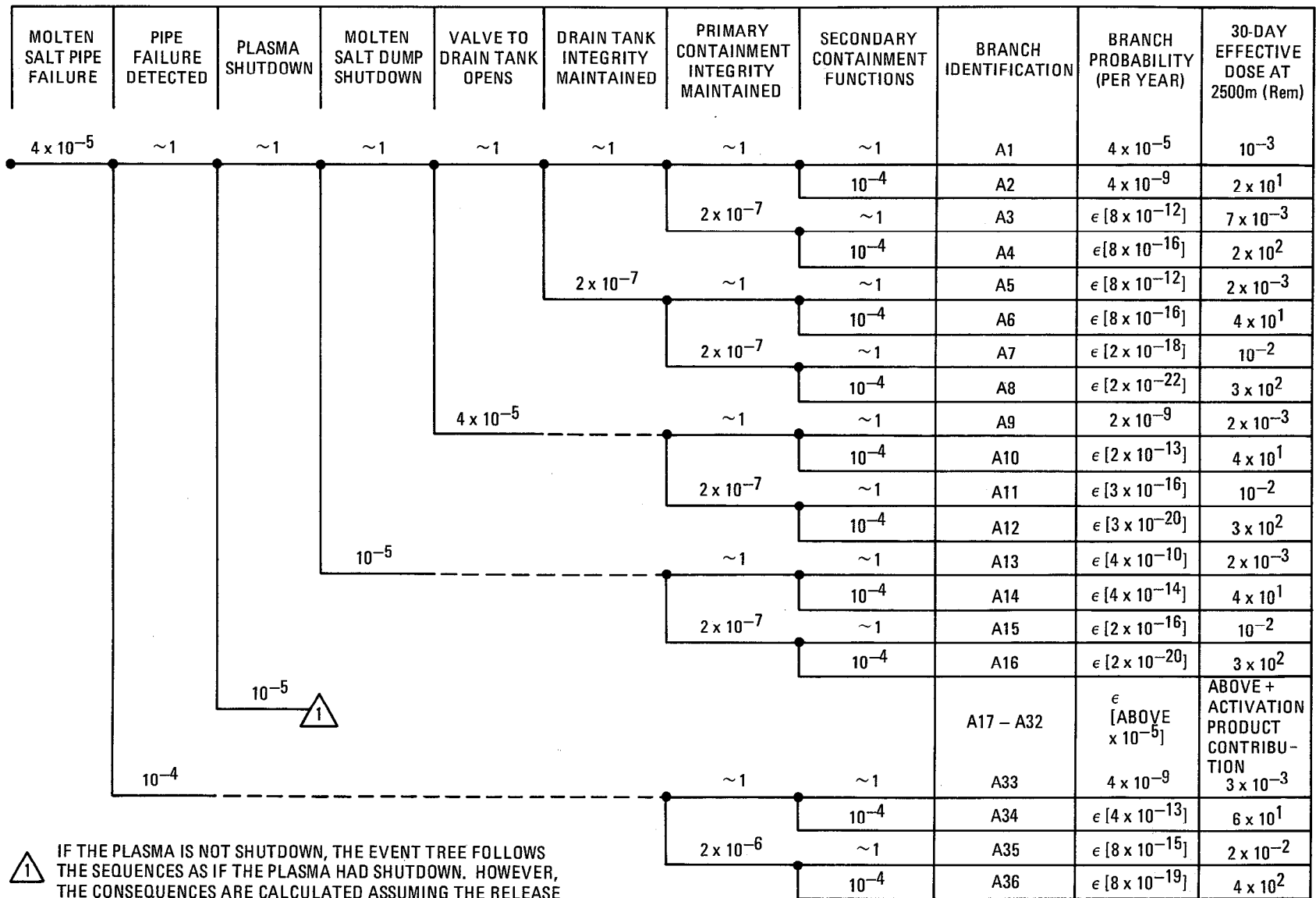


FIGURE VI-15. Logic tree for a molten salt pipe failure event.

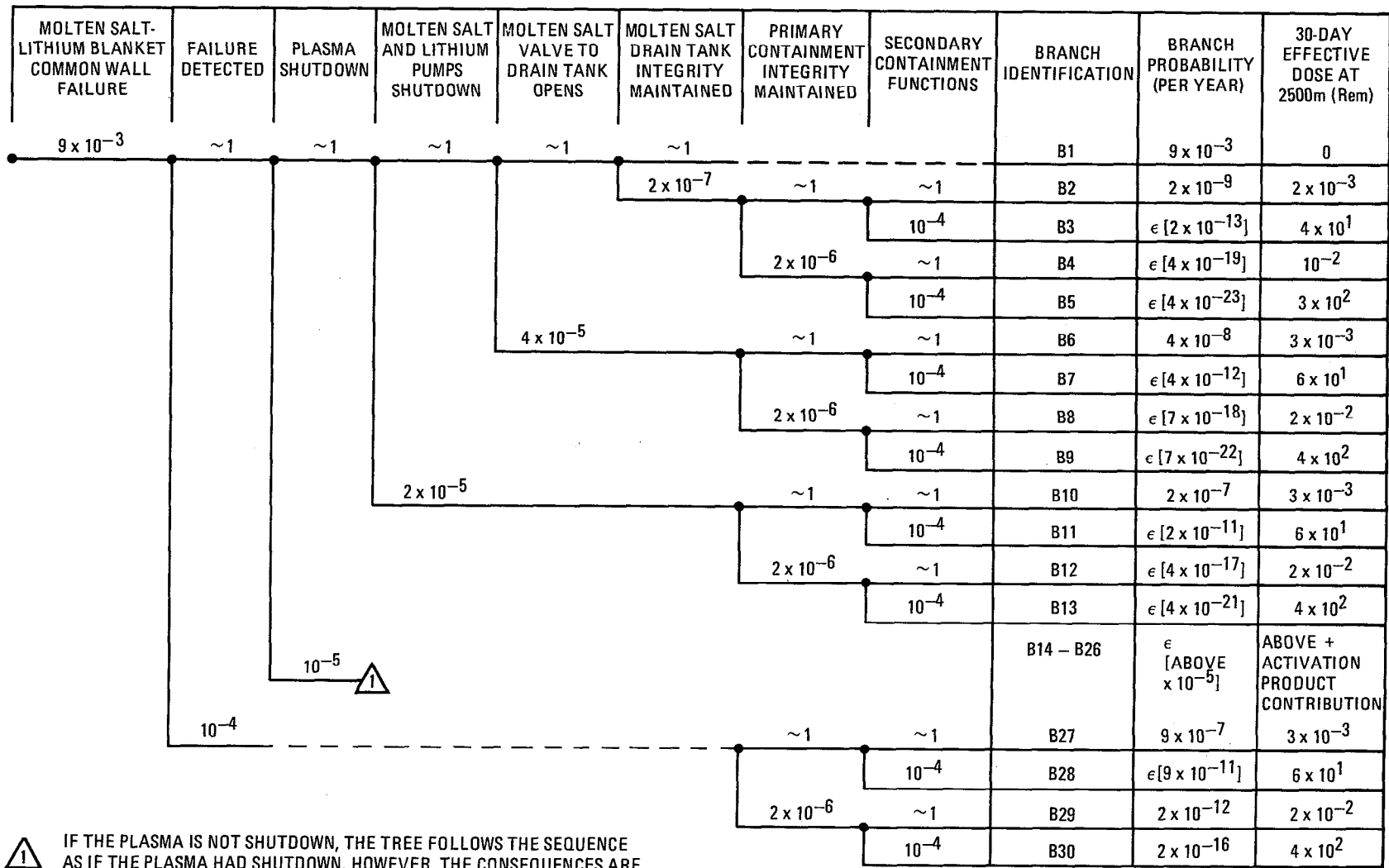
breached, then the molten salt can spill into the secondary containment building. Radioactivity release to the environment could occur only if the secondary containment fails.

In order to minimize the amount of molten salt spilled, the molten salt flow to each blanket module can be designed to be handled by a separate circuit. In addition, for redundancy, more than one drain can be provided.

Molten Salt-Lithium Common Wall Failure (Fig. VI-16). In this event lithium will flow through the breach and into the molten salt blanket. The lithium depressurization would trigger a lithium pump shutdown and a plasma shutdown. The molten salt pressure would rise and the detection of this increase would trigger the molten salt pump shutdown. The lithium and the molten salt in the blanket would then be dumped into their respective dump tanks, except for some lithium which would have flowed into the molten salt blanket (lithium and molten salt are mutually non-reactive). Other events subsequent to these are similar to those for the first case (Fig. VI-15).

Lithium Pipe Failure (Fig. VI-17). In this event, lithium will be spilled into the primary containment (the sealed cells). This should trigger a pump shutdown and a plasma shutdown. The molten salt loop is relatively unaffected, permitting relatively orderly shutdown. For lithium accidents, the molten salt should be dumped. Thus, the accident pathways involve principally the lithium loop. Natural convection in the liquid lithium remaining in the blanket could transfer the afterheat in the blanket structural material to its molten salt loop and to the liquid lithium and molten salt in the adjacent blanket modules for removal through their loops.

First Wall Failure (Fig. VI-18). The fusion reactor first wall is a part of the blanket module containing the liquid lithium. This first wall can fail as a result of plasma impingement, neutron damage, etc. A lithium leak into the plasma would generally quench the plasma. The amount of leakage necessary to accomplish this is expected to be very small; therefore, this accident initiating event applies to small cracks and leaks as well. However, the more severe condition is that due to a large breach in the first wall.



IF THE PLASMA IS NOT SHUTDOWN, THE TREE FOLLOWS THE SEQUENCE AS IF THE PLASMA HAD SHUTDOWN. HOWEVER, THE CONSEQUENCES ARE CALCULATED ASSUMING THE RELEASE OF THE ENTIRE MODULE INVENTORY AS MELTING IS PRESUMED.

FIGURE VI-16. Logic tree for a molten salt-liquid lithium common wall failure event.

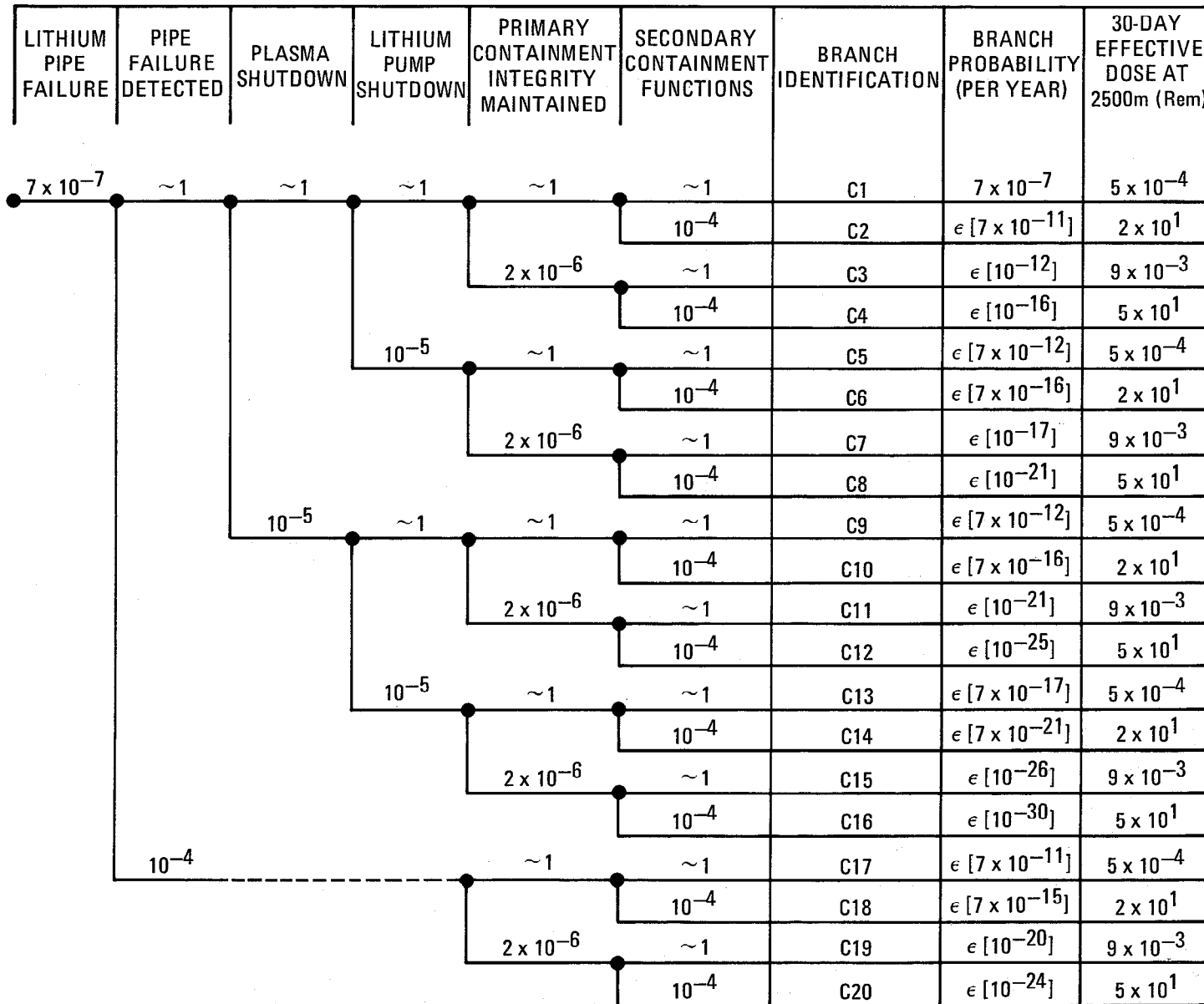


FIGURE VI-17. Logic tree for a lithium pipe failure event.

PLASMA DISRUPTION-FIRST WALL FAILURE	FAILURE DETECTION	LITHIUM PUMP SHUTDOWN	PRIMARY CONTAINMENT INTEGRITY MAINTAINED	SECONDARY CONTAINMENT FUNCTIONS	BRANCH IDENTIFICATION	BRANCH PROBABILITY (PER YEAR)	30-DAY EFFECTIVE DOSE AT 2500m (Rem)
$10^{-1}$	$\sim 1$	$\sim 1$	$\sim 1$	$\sim 1$	D1	$10^{-1}$	$5 \times 10^{-4}$
				$10^{-4}$	D2	$10^{-5}$	$2 \times 10^1$
			$2 \times 10^{-6}$	$\sim 1$	D3	$2 \times 10^{-7}$	$9 \times 10^{-3}$
				$10^{-4}$	D4	$\epsilon [2 \times 10^{-11}]$	$5 \times 10^1$
		$10^{-5}$	$\sim 1$	$\sim 1$	D5	$10^{-6}$	$5 \times 10^{-4}$
				$10^{-4}$	D6	$\epsilon [10^{-10}]$	$2 \times 10^1$
			$2 \times 10^{-6}$	$\sim 1$	D7	$\epsilon [2 \times 10^{-12}]$	$9 \times 10^{-3}$
				$10^{-4}$	D8	$\epsilon [2 \times 10^{-16}]$	$5 \times 10^1$
	$10^{-4}$		$\sim 1$	$\sim 1$	D9	$10^{-5}$	$5 \times 10^{-4}$
				$10^{-4}$	D10	$10^{-9}$	$2 \times 10^1$
			$2 \times 10^{-6}$	$\sim 1$	D11	$\epsilon [2 \times 10^{-11}]$	$9 \times 10^{-3}$
				$10^{-4}$	D12	$\epsilon [2 \times 10^{-15}]$	$5 \times 10^1$

FIGURE VI-18. Logic tree for a first wall failure event.

The depressurization of the lithium coolant, in case of a large breach, triggers the pump shutdown. A termination of forced flow will result in reduced lithium losses from the blanket. The liquid lithium remaining in the blanket modules can be left in the blanket to transport the first wall afterheat (by natural convection) to the molten salt. The molten salt loop can continue to operate until the afterheat becomes completely dissipated as the entire molten salt inventory gets reprocessed.

Lithium escaping to the blanket chamber would probably vaporize and together with the tritium will be pumped out of the vacuum chamber by the vacuum pump; some of it may deposit in the vacuum duct walls. Traps and filters will remove the lithium and other solid particles, while the effluent is treated to remove the tritium. Any release of radioactivity would be limited to the tritium diffusing into the reactor building where it is removed by the inert gas purge. Therefore, no release to the environment would result.

Branch Probabilities. The probabilistic data for the various failures in each accident pathway are summarized in Table VI-17 for the abbreviated event logic trees given in Figs. VI-15 to VI-18 for the four major accident initiating events previously described. The failure probabilities were based primarily on data used in the CRBRP program and on a previous study on TMHR safety.<sup>2</sup> Since reliability data on lithium and molten salt containment/components are virtually nonexistent, the data on sodium was used by applying assumed "severity factors" that ranged up to 100. The selection of the severity factors was based on considerations of relative corrosiveness/erosion/mass transfer, relative temperatures and pressures. The last two factors affect the stresses on the components.

For example, the corrosion rates of stainless steel by lithium, as reported in Ref. 15 is 10 to 100  $\mu\text{m}/\text{y}$  for the temperature range of 500°C to 600°C. This may be compared with an acceptable rate of 1.5  $\mu\text{m}/\text{y}$  in sodium cooled fast breeder reactors. Extrapolation of the lithium data to the maximum blanket liquid lithium temperature of 390°C based on the Arrhenius theory yields 3.9  $\mu\text{m}/\text{y}$ . Thus lithium corrosion of stainless steel under reactor operating conditions is ~2.6 times more severe. However, typical sodium fast breeder reactors are designed with sodium temperatures on the order of 500°C, which is substantially higher than the maximum lithium temperature for the TMHR blanket. The maximum

TABLE VI-17. Failure probabilities for the events of Figs. VI-15 through VI-18.

Event Description	Failure Probability (a)
Molten salt pipe failure	$4 \times 10^{-5}/\text{yr}$
Molten salt-liquid lithium blanket common wall failure	$9 \times 10^{-3}/\text{yr}$
Lithium pipe failure	$7 \times 10^{-7}/\text{yr}$
Plasma disruption with first wall failure	$10^{-1}/\text{yr}$
Detection system failure	$10^{-4}$
Rapid plasma shutdown	$10^{-5}$
Pump shutdown	$10^{-5}$
Valve to molten-salt drain tank failure	$4 \times 10^{-5}$
Drain tank failure	$2 \times 10^{-7}$
Primary containment failure	$2 \times 10^{-7}$
— With potential for lithium fire	$2 \times 10^{-6}$
Secondary containment failure	$10^{-4}$

(a) Failure probabilities are on a per demand basis unless otherwise stated.

coolant system pressures are about the same in the two cases (~200 psia). Consequently, for pipe rupture, an overall lithium severity factor of two was assumed. Where the potential for a lithium fire exists, a severity factor of 10 was applied. Probabilities less than  $10^{-9}$  are designated as  $\epsilon$  in the event trees.

For blanket walls covered with a frozen salt protective layer, a severity factor of 100 was assumed to account for the large uncertainties in frozen salt adherency and required thicknesses for protection.

### VI.C.1.e Description of Potential Consequences

Radioactive Inventory. The computation of safety characteristics and risk continues with the calculation of the radioactive inventory present in the molten salt-liquid lithium blanket. The results are presented in Tables VI-18 through VI-22, the first four tables presenting activity and BHP by contributing radionuclide and Table VI-22 summarizing the results by principal category.

The TRW ISOGEN code was used to calculate the actinide production and decay in the molten salt blanket. Two modes of operation for the molten salt blanket/reprocessing plant are being considered:

- Continuous reprocessing to recover uranium and protactinium. In this case, all isotopes of the above elemental constituents will eventually reach their respective equilibrium concentrations. Although rare earth fission product recovery is possible, the recovery efficiency per pass is only 0.37%, equilibrium would not be reached during the 30 year plant life, and this option has not been adopted.

- Continuous reprocessing to recover uranium only (i.e., fluorination only). All uranium isotopes reach equilibrium in this case, but other stable isotopes continue to build up.

Concerning these modes, the fluorination only mode is the baseline case since it requires the least process development and should be the least expensive. However, the isotopic generation and decay performance for both modes have been investigated and are described here.

As shown in Table VI-18, the fluorination only process results in increased concentrations of  $^{228}\text{Th}$ ,  $^{231}\text{Pa}$ ,  $^{233}\text{Pa}$ , and  $^{232}\text{U}$  after 30 years. However, after the decay of  $^{233}\text{Th}$  and  $^{233}\text{Pa}$ , the dominant hazards are  $^{228}\text{Th}$ ,  $^{231}\text{Pa}$ , and  $^{232}\text{U}$ , and one to two orders of magnitude reduction in the activity and BHP present in the blanket can be attained via protactinium recovery in reprocessing.

The fission product inventory is the result of the 760 MW of power obtained from fissioning of the produced fissile fuel. Notice that although the initial fission product BHP is somewhat lower than that of either actinide processing mode, after the decay of the  $^{233}\text{Th}$  and  $^{233}\text{Pa}$ , the fission product hazard, measured by BHP (and dominated at that time by the  $^{90}\text{Sr}$ ), would be comparable to the actinide hazard.

TABLE VI-18. Major contributors to actinide BHP for the lithium-cooled blanket<sup>(a)</sup>.

Radionuclide	Full Processing		Fluorination Only	
	Activity (Ci)	BHP (km <sup>3</sup> )	Activity (Ci)	BHP (km <sup>3</sup> )
Th 228	5.9 +04	3.0 +08	1.1 +05	5.7 +08
232	1.9 +02	1.9 +05	1.9 +02	1.9 +05
233	6.8 +09	3.4 +08	6.8 +09	3.4 +08
Pa 231	1.6 +03	3.9 +07	8.9 +04	2.2 +09
233	8.1 +09	1.3 +09	9.8 +09	1.6 +09
U 232	5.9 +04	6.6 +07	1.2 +05	1.3 +08
233	1.7 +04	4.3 +06	1.7 +04	4.3 +06
TOTAL	1.6 +10	1.8 +09	1.7 +10	4.8 +09
TOTAL/module	1.1 +09	1.2 +08	1.1 +09	3.2 +08
TOTAL/kg yearly fissile fuel production	2.5 +06	2.8 +05	2.7 +06	7.5 +05

(a) Isotopics at end of life (30 year), 70% average plant capacity factor, total thorium loading =  $1.68 \times 10^9$  grams.

TABLE VI-19. Major contributors to fission product BHP for the lithium-cooled blanket.

Radionuclide	Activity (Ci)	BHP (km <sup>3</sup> )
Sr 89	2.9 +07	9.7 +07
90	1.5 +07	5.0 +08
91	3.9 +07	4.3 +06
Y 91	3.9 +07	3.9 +07
Zr 95	4.2 +07	4.2 +07
Mo 99	4.1 +07	5.9 +06
Ru 103	2.0 +07	6.6 +06
106	2.6 +06	1.3 +07
I 131	2.0 +07	2.0 +08
133	4.4 +07	1.1 +08
135	3.7 +07	3.7 +07
Cs 134	4.4 +07	1.1 +08
Ba 140	4.3 +07	4.3 +07
La 140	4.3 +07	1.1 +07
Ce 144	3.7 +07	1.9 +08
TOTAL	5.0 +08	1.4 +09
TOTAL/module	3.3 +07	9.3 +0
TOTAL/kg yearly fissile fuel production	7.9 +04	2.2 +05

TABLE VI-20. Major contributors to activation product BHP for the lithium-cooled blanket.

Radionuclide	Activity (Ci)	BHP (km <sup>3</sup> )
Cr 51	9.4 +07	1.2 +06
Mn 54	8.6 +07	8.6 +07
56	1.5 +08	7.5 +06
Fe 55	5.0 +08	1.7 +07
Co 57	3.6 +07	6.0 +06
58	1.0 +08	5.0 +07
58m	4.3 +07	1.4 +05
60	1.7 +07	5.7 +07
60m	1.6 +07	4.0 +07
Ni 57	4.0 +06	4.0 +07
TOTAL	1.0 +09	2.7 +08
TOTAL/module	6.7 +07	1.8 +07
TOTAL/kg yearly fissile fuel production	1.6 +05	4.2 +04

TABLE VI-21. Tritium inventory and BHP for the lithium-cooled blanket

Location	Activity (Ci)	BHP (km <sup>3</sup> )
Tritium associated with the blanket	9.6 +06	4.8 +04
Tritium associated with fusion-related fueling, processing, etc.	1.2 +07	6.0 +04
Tritium in storage	6.9 +07	3.4 +05
TOTAL	9.1 +07	4.5 +05
TOTAL/module	6.1 +06	3.0 +04
TOTAL/kg yearly fissile fuel production	1.4 +04	7.1 +01

TABLE VI-22. Total radioactive inventory and BHP for the lithium-cooled blanket, fluorination only.

Radioactivity Source	Activity (Ci)	BHP (km <sup>3</sup> )
Actinides	1.7 +10	4.8 +09
Fission products	5.0 +08	1.4 +09
Activation products	1.0 +09	2.7 +08
Tritium	9.1 +07	4.5 +05
TOTAL	1.9 +10	6.5 +09
TOTAL/module	1.3 +09	4.3 +08
TOTAL/kg yearly fissile fuel production	3.0 +06	1.0 +06

The method used to generate the activation product inventory made use of the first wall radioactivity calculations performed for the UWMAK-I reactor. That reactor has a basic blanket design very similar to the molten salt-blanket in that 316SS and liquid lithium are the main constituents. The results of the estimate are given in Table VI-20. These were obtained by scaling versus blanket thermal power, which was taken to be 3600 MW<sub>t</sub>, and increasing by 25% to include activated structure other than the first wall.

The tritium inventory was estimated to be 1 kg in the liquid lithium coolant. The other tritium sources were scaled from the design of Ref. 8. Again it is noted that in the event of an accident the tritium in storage and the dominant source of tritium is assumed to be secure and not released.

The total inventories from each source are compared in Table VI-22. The actinides and fission products are seen to be comparable and one order of magnitude higher than the activation products. The tritium contribution to the blanket hazard is negligible. As noted earlier, the actinides and activation products are relatively immobile compared to the gaseous fission products. This effect and that due to the variations in half-life are considered in the consequence analysis of the following section.

Consequence Analysis. The calculation of the radiological consequences of an accidental release from the molten salt-liquid lithium blanket is similar to that performed for the gas-cooled blanket with two exceptions. The first is the radionuclide source terms of Tables VI-18 through VI-21. The second is the presence of sealed cells performing as a primary containment and an additional barrier preventing the escape of radioactivity. All other assumptions are the same and reference is made to Tables VI-13 and VI-14.

Table VI-23 presents the results of the dose consequence analysis of the molten salt-liquid lithium blanket. The major contributors to blanket consequences are the actinides, followed by the fission products. The activation products contribute a few percent and the tritium contribution is negligible. The actinide inhalation bone and lung commitments are due mainly to <sup>228</sup>Th, <sup>231</sup>Pa, and <sup>233</sup>Pa. The fission product thyroid commitment is due to the iodine isotopes and the bone dose is due to <sup>90</sup>Sr. The effect of the primary containment, in

TABLE VI-23. Dose consequence from lithium-cooled blanket one-loop involvement events.

Accident Type	Integrated 30-Day Dose (Rem) at 2500 Meters				Effective Dose Equivalent <sup>(a)</sup>
	External Whole Body Gamma	Inhalation			
		Tyroid	Bone	Lung	
Primary containment intact, secondary containment functional, contributors (%):	$2.5 \times 10^{-5}$	$6.1 \times 10^{-3}$	0.015	0.11	$2.6 \times 10^{-3}$
Actinides	0.0	0.0	15.4	47.0	62.4
Fission products	0.6	9.3	7.4	13.0	30.3
Activation products	0.2	0.0	0.0	7.1	7.3
Tritium	0.0	0.0	0.0	0.0	0.0
Primary containment failed, secondary containment functional, contributors (%)	$5.9 \times 10^{-4}$	0.097	0.058	0.053	0.015
Actinides	0.0	0.0	10.3	45.1	55.4
Fission products	2.8	25.7	5.0	5.8	39.3
Activation products	0.2	0.0	0.0	5.1	5.3
Tritium	0.0	0.0	0.0	0.0	0.0
Primary containment intact, secondary containment failed, contributors (%)	0.30	140.0	350.0	270.0	63.0
Actinides	0.0	0.0	15.0	48.1	63.0
Fission products	0.2	8.9	7.2	13.2	29.5
Activation products	0.2	0.0	0.0	7.3	7.5
Tritium	0.0	0.0	0.0	0.0	0.0
Primary containment failed, secondary containment failed, contributors (%)	5.4	$2.3 \times 10^3$	$1.4 \times 10^3$	$1.3 \times 10^3$	360.0
Actinides	0.0	0.0	10.4	41.7	52.0
Fission products	1.0	25.6	5.1	10.9	42.5
Activation products	0.2	0.0	0.0	5.3	5.5
Tritium	0.0	0.0	0.0	0.0	0.0

(a) See Section VI.B.1.e for development of effective dose equivalent.

addition to lowering the probabilities of a radioactivity escape, is approximately an 85% reduction in the consequence of a release. The primary containment is most effective in delaying the release of the iodine isotopes, resulting in their substantial decay before escaping and resultant lower dose consequence.

VI.C.1.f Risk Plot Analysis. The major risk contributors in the molten salt blanket can be identified via the risk plot of Fig. VI-19. A number of observations can be made from the figure. The first observation is that the major risk contributors are events which leak the radioactive inventory as a result of the force exerted by the static pressure of the molten salt. These events include pipe ruptures and first wall failures with or without secondary containment failure. The second observation is that the probability of failure of the primary containment in a postulated sequence of events usually resulted in that sequence of events being inconceivable (i.e., having a branch probability of less than  $10^{-9}$  per year). A third observation regarding plasma disruption is that:

- No credit was taken in the analysis for limiters or plasma energy dump protection devices.
- No credit was taken for the fusion vacuum boundary as an additional barrier.
- As mentioned above, there were no provisions to limit molten salt leakage from static pressure (e.g., via a "fast drain" system).

These factors would decrease the risk of a plasma disruption event. Design guidance and conclusions are presented in the last section of this chapter.

It is noted here that the analysis of Events A, B and C were performed assuming a ten-loop system. Since the final design incorporated fifteen loops, the probabilities and therefore the risk of these events should be increased accordingly.

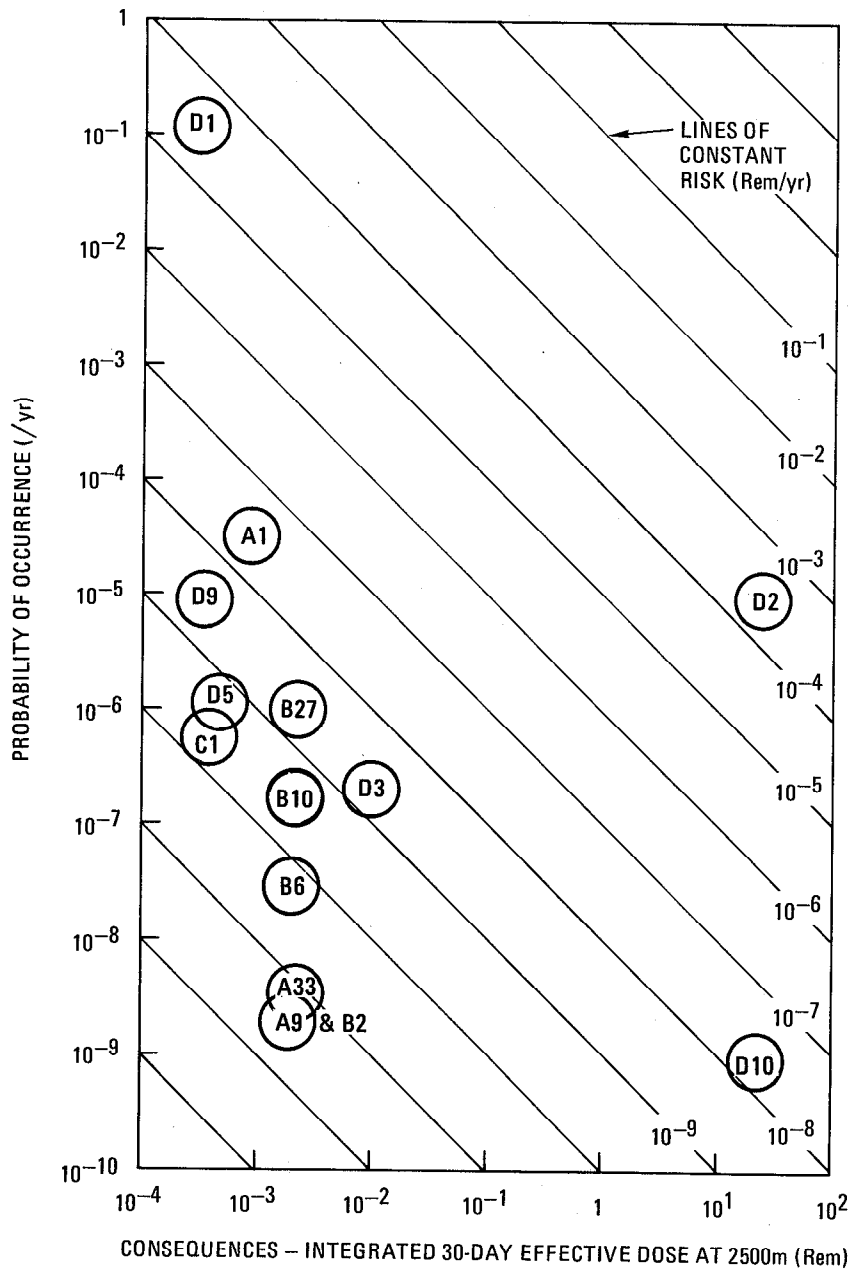


FIGURE VI-19. Major risk contributors of the TMHR molten salt-liquid lithium blanket.

## VI.C.2 Overview and Comment

The engineered safety features incorporated into the TMHR molten salt-liquid lithium blanket result in a design with very low probabilities of radioactivity release. These safety features include:

- Fifteen separate, parallel molten salt loops
- Molten salt and lithium dump tanks
- Freeze type drain valves
- Primary containment (argon-inerted sealed cells) enclosing the components of the fueling system
- Fluid pressure differentials so that potential leaks are into the molten salt.

These features and others present a sequence of barriers whose probabilities of successive failures are in most cases inconceivable.

The BHP present at shutdown is approximately one order of magnitude lower than that of an LMFBR. The use of fifteen separate loops also serves to reduce the consequences of an event an additional order of magnitude. It must be noted that the analysis of loss of cooling capability events outside of the secondary containment, e.g., feedwater flow disruption or steam generator failure, are beyond the scope of the present work. This type of event would have more serious consequences since all fifteen loops would be affected simultaneously. However, a risk analysis of such events would require system definition not presently available in order to compute the probabilities and consequences of the potential combinations of failures and releases.

It has been assumed that accident events involving the liquid lithium loop only would have little effect on the molten salt loop. Lithium burns in air and reacts strongly with concrete. Upper limits on the adiabatic flame temperature of a lithium fire can be computed from thermochemical considerations to be from 2100<sup>o</sup>K to 2500<sup>o</sup>K. Though this temperature range would appear to permit structural failure of stainless steel components, realistic configurations and boundary conditions of heat transport and dissipation may indicate otherwise. The incomplete picture that presently exists on lithium reactions and fires prevents conclusive statements. In addition, the use of inerted, steel lined sealed cells (a common practice in LMFBR and MSBR plant designs) and an inert reactor building reduces the

possibility of a lithium fire and radioactive releases such as those pessimistically assumed and analyzed by Holdren.<sup>16</sup>

The liquid lithium-cooled first wall may have an inherent safety feature; namely, the first wall can be adequately cooled by natural convection in the event of a loss-of-flow. In this case, the afterheat generated in the first wall (estimated to be  $\sim 3.6 \text{ W/cm}^3$ ) could be transferred to the molten salt and to the adjacent modules. The depressurized lithium would reduce the pressure stresses on the containment walls, thereby permitting higher operating temperatures. In the event of a loss of liquid lithium as a result of a large breach of the first wall, the first wall will melt. However, the blanket module affected and the first wall would have to be replaced in any case. The molten stainless steel will flow and contact other integral blankets in which liquid lithium continues to flow. Thus the molten steel would solidify and result in no release of activation products outside the reactor. The possibility that the adjacent integral modules may serve as effective heat sinks needs to be analyzed.

## VI.D CONCLUSIONS REGARDING SUPPRESSED FISSION SAFETY ANALYSIS

On the basis of past works on hybrid reactor safety, a number of safety characteristics were selected for evaluation for the TMHR with the intent of obtaining figures-of-merit and establishing safety criteria. The results of this year's effort is presented in this section.

The figure-of-merit used to quantify the isotopic hazard in the TMHR is the Biological Hazard Potential (BHP). BHP is defined as the ratio of the radionuclide activity to the maximum permissible concentration (MPC) of a specific isotope. Total BHP is the sum of the BHPs of each radionuclide present. Since the MPC accounts for the half-life of the radionuclide, its decay mode and energy, as well as the distribution of the decay and its biological effect to the critical organ, so does BHP, though BHP does not account for the volatilities and solubilities of the materials under consideration, it nonetheless provides an accepted measure of the radiological hazard present in the system. From this point of view, fission suppression has been shown to offer one to two orders of magnitude improvements in shutdown BHP over fast-fission and LMFBR systems.

An additional consideration has emerged as a result of this year's work and that consideration is the isotopic distribution of the hazard. In the production of  $^{233}\text{U}$  fissile fuel from fertile  $^{232}\text{Th}$ , the concomitant production of the intermediate nuclides  $^{233}\text{Th}$  and  $^{233}\text{Pa}$  is inherent. Though these isotopes dominate the BHP at shutdown, they decay away relatively rapidly, leaving the hazard to be dominated by nuclides produced via parasitic captures and fissions. A computation of BHP as a function of time after shutdown would demonstrate this fact and permit comparisons of the hazard subsequent to the initial transient. Alternatively, though the single datum of BHP at shutdown is not sufficient to characterize this behavior, the use of an integrated-BHP,<sup>17</sup> that is an integral BHP over the effective lifetime of an isotope, may serve the same purpose and should be investigated in future safety work.

A second figure-of-merit proposed is the time-to-melt. The results of thermal analyses performed this year and comparisons to past work indicate that the computation of the time-to-melt is sensitive to the assumptions made in formulating the thermal model. Adiabatic models offer overly pessimistic

indications of melting potential and two-dimensional models, although more realistic, are quite costly and do not permit extensive parametric analyses. This year's results have shown that indications of melting obtained with pessimistic assumptions, along with the attendant safety implications, were not obtained after analyses with realistic two-dimensional configurations. The 2-D analyses showed that the gas-cooled blanket in fact does not melt under the postulated loss-of-cooling capability events.

An additional consideration arises in the use of time-to-melt in conjunction with structural members under stress. The allowable material working stress decreases rapidly at elevated temperatures. It is therefore necessary to consider the possibility of a material buckling before it has reached its melting temperature. This is a safety consideration that must enter into the design process, though the analysis is complex.

The time-to-melt (or fail) can still provide a good index of safety. To provide a valid measure of performance, it is recommended that this figure-of-merit be computed under as realistic a configuration as practical. Pessimistic conservative assumptions are not necessarily reflective of worst-case situations. In addition, the results of the thermal analysis should be fed back to the mechanical designer in order to include this failure mode in the structural design.

The third figure-of-merit evaluated is relative risk. Risk being the product of probability and consequence, the latter two quantities are discussed below. Maintenance and availability are intimately tied to the probability of failure. The number of failures per unit of time for a given component for a particular failure mode can be obtained from an analysis of failure histories available in the literature. However, the probability that a component will fail at a particular time when called upon to function depends upon the availability of that particular component. Failures can be subdivided into two classes, announced and unannounced. Announced failures make themselves known via horn blowing, light flashing, etc., and therefore availability depends on the mean time to repair. For unannounced failures, such as a valve left in the wrong position, the calculation of the demand failure probability depends on the maintenance period. That is, a component is unavailable from the time it fails to the time of the next maintenance or

test procedures. The probabilities used in the risk analysis are approximations based on generically similar components, mature instrumentation and detection systems, fission industry service and maintenance procedures, redundancy in the heat removal systems, etc. The results of the event trees show that most sequences of events are inconceivable. This means that either the major risk-contributing sequences have not been identified or that a large margin of safety exists due to the engineered safety systems incorporated in the design. Due to the design dependency of the probabilities, only relative comparisons among themselves are possible. Extensions to comparisons among dissimilar systems is risky. The failure probabilities however can be used as targets as the system definition and design details emerge.

The unit of consequence used in this report is effective dose. The effective dose equivalent assigns a risk factor to the exposure of each organ based upon the likelihood of inducing biological damage. This formulation was used from the need to combine doses to a number of different organs since equal exposures to different organs have significantly different dose consequences. For the purposes of relative biological consequences comparisons this formulation is adequate. An additional measure of consequence however is necessary to account for property damage to the environment as well as damage to the reactor internals. From the experience at Three Mile Island, it is necessary that a consequence unit be employed during the design phase that measures both biological and economic damage. The Reactor Safety Study<sup>18</sup> presents a basis for such a formulation that has subsequently been used.<sup>19</sup>

For the purposes of the present study, the product of probability and consequence can be used to identify the major risk contributors of the present design configurations. Design guidance through which the risk can be reduced has been offered in previous sections for this year's reactor designs. The relative risk has indeed served as a useful figure of merit in the present designs and can continue to serve as the designs evolve and the risk computation refined.

## REFERENCES

1. Hybrid Reactor Safety Study Annual Report, October 1, 1978 – September 30, 1979, General Atomic Report GA-A15578 (1979).
2. I. Maya, et al., "Safety Evaluation of Hybrid Blanket Concepts," General Atomic Report GA-A16101 (1980).
3. J. D. Gaski, L. C. Fink and T. Ishimoto, "Systems Improved Numerical Differencing Analyzer Users Manual," TRW Systems, 11027-6003-RO-00 (1970).
4. J. P. Holman, Heat Transfer, McGraw Hill (1976).
5. G. W. Hannaman, "GCR Reliability Data Bank Status Report," General Atomic Report GA-A14839 (1978).
6. O. S. Fatone and R. S. Pathama, "Steam-Generator Tube Failures: World Experience in Water-Cooled Nuclear Power Reactors in 1976," Nuclear Safety, Vol. 19, No. 6, Nov.-Dec. 1978.
7. T. Y. Sung and W. F. Vogelsang, "DKR: A Radioactivity Calculation Code for Fusion Reactors," UWFDM-170, Nuclear Engineering Department, University of Wisconsin (1976).
8. G. A. Carlson, et al., "Field-Reversed Mirror Pilot Reactor," Lawrence Livermore National Laboratory, UCID-18550 (1980).
9. D. W. Buckley, "TDAC – An Analytical Computer Program to Calculate the Time-Dependent Radionuclide Effects of Radionuclide Release," General Atomic unpublished material (1976).
10. U.S. NRC Regulatory Guide 1.109, "Calculation of Annual Doses to Man From Routine Release of Reactor Effluents," Rev. 1 (Oct. 1977).
11. "Recommendations of the International Commission on Radiological Protection," ICRP Publication 26, Pergamon Press, adopted January 1977.
12. U.S. NRC Rules and Regulations, Title 10, Part 100, "Reactor Site Criteria," (Feb. 1978).
13. A. D. Kelmers, et al., "Evaluation of Alternate Secondary (and Tertiary) Coolants for the Molten-Salt Reactor," Oak Ridge National Laboratory Report, ORNL-TM-5325 (April 1976).
14. J. L. Anderson, et al., "Conceptual Design Study of a Single-Fluid Molten-Salt Breeder Reactor," Oak Ridge National Laboratory Report, ORNL-4541 (1971).

15. D. L. Smith, R. G. Clemmer and D. D. Harkness, "Fusion Reactor Blanket/ Shield Design Study," ANL/FPP-79-1 (July 1979).
16. J. P. Holdren, "Contribution of Activation Products of Fusion Accident Risk in Part 1. A Preliminary Investigation," Nuclear Technology/Fusion, Vol. 1 (January 1981).
17. W. Hafele, et al., "Fusion and Fast Breeder Reactors," International Institute for Applied Systems Analysis, A-2361, Luxemburg, Austria, Report RR-77-8 (Nov. 1976).
18. U.S. NRC, "Reactor Safety Study," WASH-1400 (NUREG-75/014) (Oct. 1975).
19. V. Joksimovic, et al., "HTGR Accident Initiation and Progression Analysis Status Report," General Atomic Report GA-A15000 (April 1978).



CHAPTER VII  
FUEL CYCLE TECHNOLOGIES

VII.A. OVERVIEW OF FUEL CYCLES

VII.A.1. Introduction

The principal role of the fusion breeder reactor is to provide an external source of fissile fuel to support a fission power reactor economy composed of LWRs or other fission reactors. In this role, the fusion breeder is operationally similar to a fissile enrichment plant which requires no fissile feed stream and is an electricity producer rather than a consumer. In contrast with fission breeder reactors (i.e., liquid metal fast breeder reactor (LMRBR) and light water breeder reactor (LWBR)), the neutron rich fusion breeder is a subcritical assembly, produces an order of magnitude more net excess fuel, and is not subject to the neutron balance constraints of conventional fission reactors. As a result, a wide variety of fuel cycles and fuel forms are possible. In particular, the fusion breeder may produce either  $^{233}\text{U}$  or  $^{239}\text{Pu}$  using oxide, metal, carbide, molten salt or other fuel forms.

After the bred fissile material is separated from the fertile fuel form it may be used to provide initial inventories or fissile makeup to fuel conventional light water reactor (LWR) clients operating on one of several possible fuel cycles. Alternatively, the bred fuel could be used to fuel advanced fission converter reactors such as the high temperature gas cooled reactor (HTGR) or the Canadian heavy water reactor (CANDU). If desired, the fusion breeder might also breed fuel to provide initial fissile inventories for liquid metal fast breeder reactors (LMFBR).

Fuel cycle related issues will, in general, depend upon the particular breeding blanket design, the choice of a fertile fuel form, and the choices of a client reactor type and its associated fuel cycle. These issues can have potentially large impact on the cost of bred fuel, the cost of electricity generation, and overall feasibility of the fusion breeder.

In this chapter we first review several candidate fuel cycle options. This review is followed by more detailed discussions relating to the molten salt and thorium oxide suspension blankets considered during this study. Conceptual plant designs and costing analysis relating to molten salt and THOREX fuel reprocessing facilities for TMHR discharge fuel will be presented. These reprocessing technologies are considered to be key elements in the symbiotic electricity generation system. Detailed isotopic generation and depletion results for actinide transmutation species produced in the TMHR blankets will also be presented. The later results have impact upon the possible need to remotely fabricate uranium fuels produced in the TMHR.

#### VII.A.2. Fuel Cycle Options and Issues

A general schematic of the fusion breeder/fission burner reactor fuel cycle is shown in Figure VII.A-1. Although this schematic does not address any specific fuel form, several features are deserving of note. Most importantly, the overall fuel cycle is separated into two distinct fuel cycles which are coupled by the flow of bred fissile material from the fusion breeder to the fission converters. With the exception of issues which bear upon the type of converter fuel fabrication plant required (e.g., the amount of  $^{232}\text{U}$  in bred  $^{233}\text{U}$ ), the breeder and burner fuel cycle issues are entirely separable.

Both the fusion breeder and fission client fuel cycles are closed by reprocessing and recovery of fissile materials. Although direct enrichment, or "refresh" fuel cycles which do not employ reprocessing have been examined in the past,<sup>1,2</sup> these lead to inefficient fissile production in the fusion breeder as well as the disposal and loss of large quantities of valuable fissile resources. Our results indicate that, like the LMFBR, the fusion breeder requires a closed fuel cycle to achieve adequate economic performance. The fusion breeder and fission breeder fuel cycles are also similar in that only small quantities of fertile materials are required for makeup, mining requirements will be minimal, and isotopic enrichment capabilities are not required.

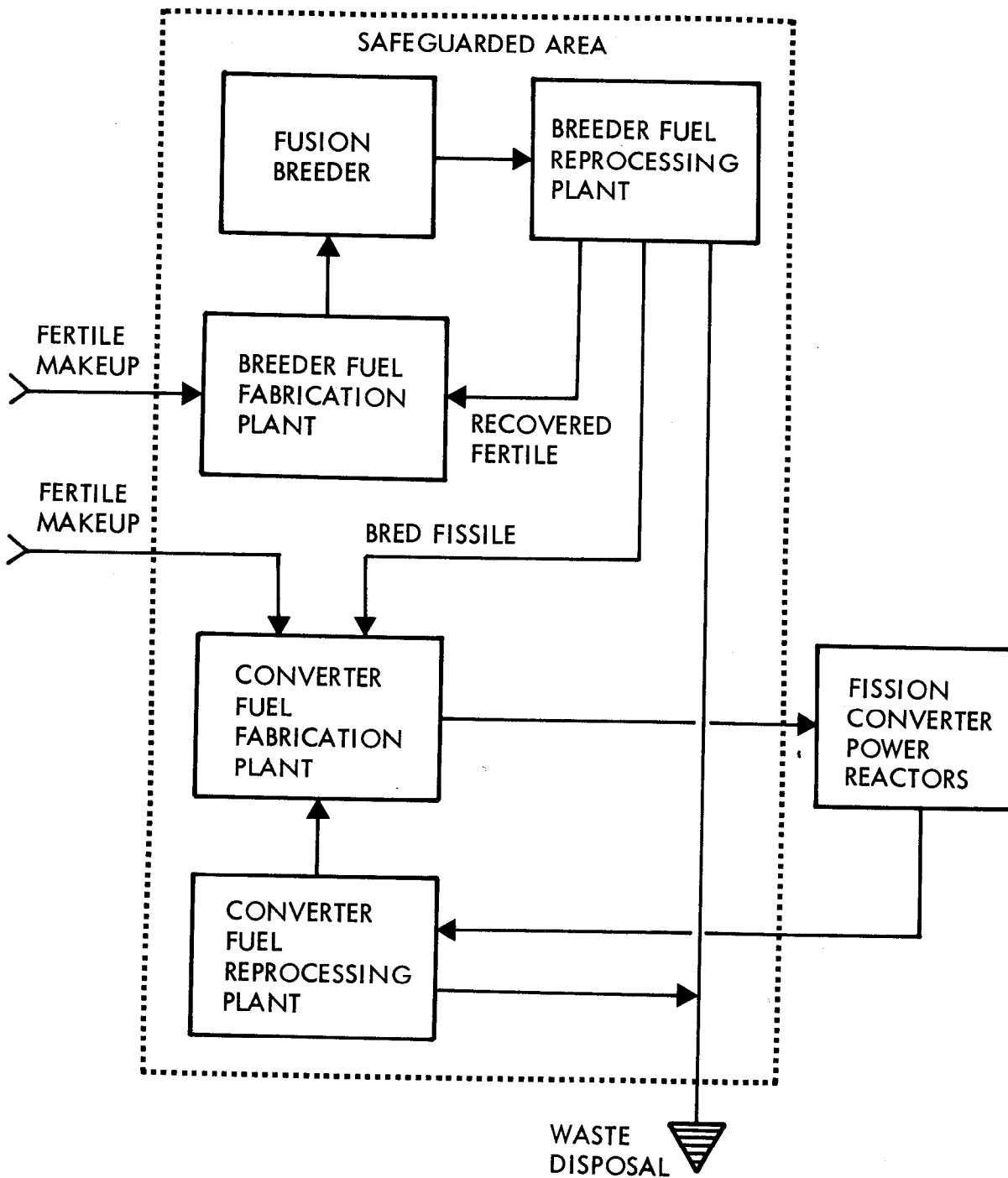


FIGURE VII.A-1. General schematic of the fusion breeder/fission burner reactor fuel cycle.

VII.A.2.a. Overview of Fusion Breeder Fuel Cycles and Issues. Concerning  $^{233}\text{U}$  production from thorium in the fusion breeder, we have considered two fuel cycles. The first of these, chosen for the thorium oxide suspension blanket, requires a THOREX type aqueous chemistry reprocessing plant to extract  $^{233}\text{U}$  from the oxide fuel. A principal concern regarding this technology is cost. In particular, the thorium oxide suppressed fission breeder fuel cycle is unique in the respect that fissile fuel is discharged at very low fission burnup ( $\sim 100$  MWD/MTHM) and at very low concentration ( $\sim 0.6\%$   $^{233}\text{U} + ^{233}\text{Pa}$  in thorium). This leads to an advantage and a disadvantage when the suppressed fission thorium oxide suspension blanket is compared with fast fission blankets. Low burnup, an advantage, leads to lower radioactivity in the discharged fuel with favorable impact on fuel reprocessing and fabrication processes. Conversely, low discharge concentration, can be expected to lead to higher unit costs (i.e.,  $\$/\text{gm}$ ) to recover the bred fuel. This situation is illustrated in Figure VII.A-2 which shows the allowable reprocessing cost to obtain a fixed contribution to the overall cost of bred fuel as a function of the fissile discharge concentration. For instance, in the case of  $\sim 0.5\%$  discharge enrichment, a 20  $\$/\text{gm}$  impact on the cost of bred fissile fuel would require a reprocessing cost of  $\sim 100$   $\$/\text{KgHM}$ . This compares with cost estimates<sup>3</sup> for the reprocessing of high burnup ( $\sim 33,000$  MWD/MTHM) thorium oxide fuels for LWRs which range from 300-500  $\$/\text{KgHM}$ .

Obviously, a major parameter to be optimized in the suppressed fission blanket is the discharge fissile enrichment. As the fissile enrichment builds up, so does the power density and radioactive inventory. The maximum discharge enrichment is constrained by the maximum allowable power density, the design limits of the safety and cooling systems, and the maximum tolerable high level radioactive waste inventory (especially if no emergency cooling system is present). The constraints on fission power density are likely to be quite low in order to capitalize on the improved safety features of suppressed fission blankets. While it is desirable to remove the bred fissile fuel at as low an enrichment as possible, it is more economical to reprocess at higher enrichments.

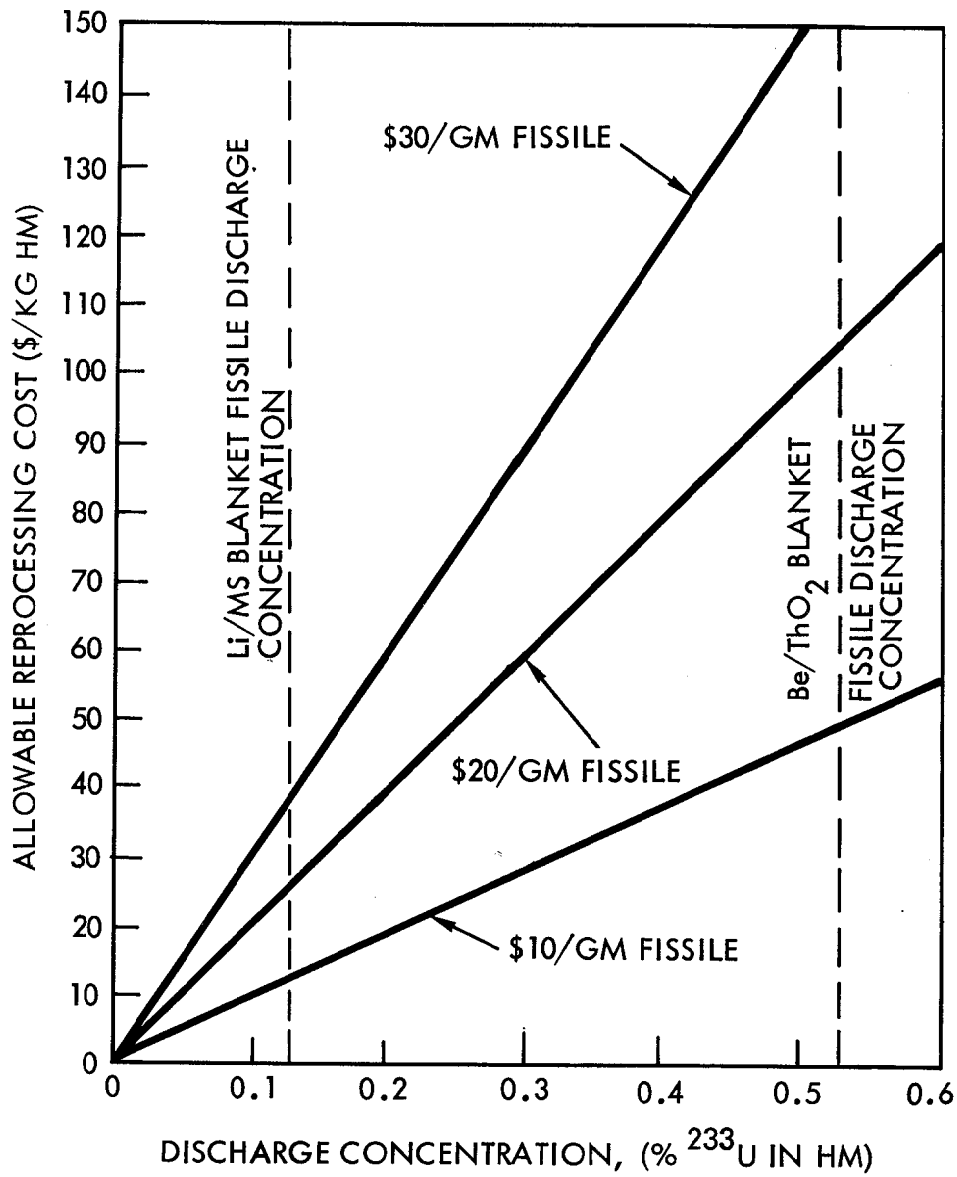


FIGURE VII.A-2. Allowable reprocessing cost to obtain a fixed contribution to the overall cost of bred fuel.

The molten salt reprocessing plant required for the TMHR molten salt blanket is expected to be quite inexpensive and is expected to result in a nearly insignificant increment in the cost of bred fissile from that system. However, the development program required to assure the feasibility of this technology is a concern. The molten salt technology, as adapted to the fusion breeder, is a simplification when compared to the technology requirements for a molten salt breeder reactor (MSBR). In particular, several of the more difficult separation processes can be entirely eliminated and a simple "fluorination only" reprocessing scheme is preferred.

Nevertheless, the use of a molten salt fuel form impacts blanket materials considerations (e.g., corrosion and radiation damage) to the extent that novel approaches are required. These considerations are discussed in detail in Chapter IV.

VII.A.2.b. Overview of LWR Fuel Cycles and Issues. Light water power reactors are expected to dominate nuclear power production when the fusion breeder reactor becomes commercially available and are considered as the principal type of fission client reactor in the symbiotic electricity generation system. The cores of these reactors would be modified to accumulate new types of oxide fuels, but studies suggest that the modified cores might not differ substantially in design or operational characteristics when compared with the current generation of LWRs.<sup>4,5</sup> The fuel cycle facilities required for LWR clients are not generically different than those that would be required to support most other fission reactor clients.

If the fuel bred in the fusion breeder is  $^{233}\text{U}$ , three fuel cycle options are available:

- The thorium fuel cycle (typically 3.3%  $^{233}\text{U}$ , 96.7%  $^{232}\text{Th}$ )
- The denatured thorium fuel cycle (typically 3.2%  $^{233}\text{U}$ , 18%  $^{238}\text{U}$ , 78.8%  $^{232}\text{Th}$ )
- The denatured uranium fuel cycle (typically 2.8%  $^{233}\text{U}$ , 97.2%  $^{238}\text{U}$ )

In comparison, the thorium fuel cycle is most efficient with respect to fissile feed requirements, but the denatured fuel cycles provide some isotopic dilution and have improved intrinsic proliferation resistance.

Regarding fuel processing technologies, both the thorium and denatured thorium LWR fuel cycles will require THOREX fuel reprocessing plant technology as well as a remote and shielded fuel fabrication technology. These technologies have not yet been developed to commercial scale and, although technically straightforward, both processes are expected to result in comparatively high costs per unit of heavy metal throughput. The denatured uranium fuel cycle requires 28% more fissile feed than the denatured thorium fuel cycle, but is compatible with developed PUREX reprocessing plant technology.

If the fuel bred in the fusion breeder is fissile plutonium, denatured fuel cycles are not possible and a mixture of plutonium and  $^{238}\text{U}$  (typically 2.9%  $\text{Pu}_f$ , 97.1%  $^{238}\text{U}$ ) would be used. This fuel cycle is 13% less efficient than the denatured uranium fuel cycle, but circumvents both THOREX and the highly shielded fuel fabrication technology. It is important to note that plutonium burners could be used even if  $^{233}\text{U}$  is bred in the fusion breeder. That is, both the denatured thorium fuel cycle and the denatured uranium fuel cycle produce appreciable quantities of plutonium in the  $^{233}\text{U}$  fueled LWRs.<sup>4</sup> This is a result of neutron absorption in  $^{238}\text{U}$  with subsequent conversion to fissile plutonium. The "secondary" fissile plutonium would, most likely, be recovered and recycled in "secondary" plutonium burning LWRs which might be located within the safeguarded fuel cycle centers.

More detailed information concerning fuel cycle performance and cost estimates as well as the composition of typical symbiotic electricity generation systems is presented in Chapters IX and X. Fuel cycle information for alternate fission reactor clients (i.e., gas cooled pebble bed fission reactors (VHTR and LMFBRs)) is also presented in later chapters.

### VII.A.3. Fuel Cycle Summaries for Reference TMHR Blanket Concepts

In this section important global parameters relating to fuel cycle data for the reference TMHR blanket concepts are presented. Overall fuel cycle parameters for both blankets are presented in Table VII.A-1.

Table VII.A-1. Fuel Cycle Summary for Thorium Oxide and Molten Salt Reference Blanket Designs. (Basis: 3000 MW fusion)

	MOLTEN SALT		
	Thorium Oxide	Fluorination Only <sup>a</sup>	Full Processing <sup>b</sup>
Thorium Inventory, MT	157	1680 <sup>c</sup>	1680 <sup>c</sup>
Fissile Inventories, Kg			
<sup>233</sup> U + <sup>233</sup> Pa In-core	408	2270 <sup>c</sup>	2185 <sup>c</sup>
<sup>233</sup> U + <sup>233</sup> Pa Ex-Core <sup>d</sup>	3315	2225	2225
Fuel Management Mode	Batch	Continuous	Continuous
Fuel Residence Time <sup>e</sup> , yr	0.123	30	30
Net Fissile Production <sup>f</sup> , Kg/yr <sup>233</sup> U	6630	4450	4450
Reprocessing Plant Thorium Throughput <sup>f</sup> , MT/yr	1326	5400	3340
Blanket Discharge Concentrations in Thorium <sup>e</sup> , atom %			
<sup>233</sup> U	0.20	0.107	0.107
<sup>233</sup> Pa	0.32	0.028	0.023
Fission Products	0.025	0.238	0.214
<sup>228</sup> Th	$4.65 \cdot 10^{-8}$	$8.23 \cdot 10^{-6}$	$4.31 \cdot 10^{-6}$
<sup>232</sup> U	$9.78 \cdot 10^{-5}$	$3.28 \cdot 10^{-4}$	$1.64 \cdot 10^{-4}$
Reprocessing Plant Discharge Product Concentrations <sup>e</sup> , atom %			
<sup>232</sup> U in <sup>233</sup> U	0.0157 <sup>d</sup>	0.236	0.099
<sup>228</sup> Th in thorium	$4.67 \cdot 10^{-7}$ <sup>d</sup>	$8.23 \cdot 10^{-6}$	$4.31 \cdot 10^{-6}$

<sup>a</sup>Fluorination only process removes uranium only. Continuous process rate = 0.42 m<sup>3</sup>/hr. Reprocessing plant capacity = 0.60 m<sup>3</sup>/hr.

<sup>b</sup>Full processing removes uranium, protactinium and a small fraction of rare earth fission products. Continuous process rate = 0.24 m<sup>3</sup>/hr. Reprocessing plant capacity = 0.35 m<sup>3</sup>/hr.

<sup>c</sup>In-core fraction = 91%. Fraction in primary loop = 9%.

<sup>d</sup>0.5 yr delay between discharge and reprocessing assumed.

<sup>e</sup>Isotopic accumulation for molten salt blanket based upon 30 year residence time. Thorium is replaced at the rate it is depleted and notes (a) and (b), above, apply.

<sup>f</sup>70% average plant capacity factor included.

VII.A.3.a. Beryllium/Thorium Oxide Blanket Fuel Cycle Summary. The gas-cooled beryllium/thorium oxide suspension blanket operates in a batch fuel reprocessing mode in which the thorium oxide-liquid metal suspension is discharged at relatively frequent intervals of about 45 days (70% average plant capacity factor) when the combined  $^{233}\text{U}$  plus  $^{233}\text{Pa}$  concentration in thorium reaches about 0.52%. Prior to discharge, the suspension may be slowly recirculated within the blanket to insure uniform enrichment and minimize power peaking concerns. Upon discharge, the thorium oxide is separated from the lithium lead heat transfer fluid for reprocessing and the liquid metal is returned to the blanket. This separation may be accomplished using both mechanical and vacuum distillation techniques.

As shown in Table VII.A-1, the 6630 Kg/yr of fissile fuel produced (for a 3000 MW fusion power level) is initially discharged as a mixture of  $^{233}\text{Pa}$  (61%) and  $^{233}\text{U}$  (39%). If the blanket operates at 100% capacity during the fuel residence time, the  $^{233}\text{Pa}$  fraction is even higher (66%), the fuel residence time is reduced from 45 days to 36 days, and the overall fissile discharge enrichment increases to 0.58%. High  $^{233}\text{Pa}$  concentration is considered to be an advantage because less fissioning of bred fissile material is expected.

The amount of fissile material in-core (i.e., the blanket) and ex-core (i.e., the reprocessing loop) is important from the economics perspective. That is, this quantity determines the period of time required before the fusion breeder is able to derive revenues from the sale of its principal product—fuel. Prior to this time, the breeder sells only electricity and accumulates a negative cash flow. The magnitude of this penalty may be put into perspective by assuming that the fusion breeder does not wait the required period before fissile production, but borrows enough fuel to initially operate in steady state on an equilibrium cycle. In this hypothetical case, there is no delay, but the fusion breeder operator would be expected to carry the borrowed resource as a non-depreciating asset and pay an annual carrying charge over the life of the plant.

Assuming typical values for TMHR bred  $^{233}\text{U}$  of 75 \$/gm and a carrying charge of 8.6 %/yr (see Chapter IX), the 3805 Kg inventory associated with the beryllium/thorium oxide blanket would result in a  $25 \cdot 10^6$  \$/yr

operating cost. Typically, over a 30 year plant lifetime, this charge would be about 5% of the overall cost of the TMHR plant capital.

The larger fraction of the total fissile inventory associated with this blanket is the ex-core inventory. This quantity is based upon a 6 month delay prior to reprocessing to allow the fuel to cool and to allow for 99% of the  $^{233}\text{Pa}$  to decay ( $T^{1/2} = 27\text{d}$ ) to  $^{233}\text{U}$  prior to reprocessing. The smaller in-core fissile inventory results from the fertile dilute nature of the blanket (only 157 MT thorium in-core).

Concerning the thorium oxide reprocessing facility, the thorium oxide throughput for a single TMHR will be 1060 MT/yr. This size is comparable to that of typical commercial fuel reprocessing plant designs and is equivalent to the heavy metal throughput rate of about 40 1 GWe LWRs. The above result emphasizes the importance of reprocessing technologies for suppressed fission hybrid blanket concepts.

Additional calculations relating to isotopic generation and depletion as well as the isotopic content of thorium and fissile material discharged from the beryllium/thorium oxide blanket TMHR and its dedicated reprocessing plant will be presented in section VII.C.

#### VII.A.3.b. Lithium/Molten Salt Blanket Fuel Cycle Description.

VII.A.3.b.(1). Batch and Continuous Reprocessing Modes. The lithium/molten salt blanket can operate in either a continuous reprocessing mode or a batch fuel reprocessing mode. In either case, molten salt is removed from the blanket for recovery of bred uranium and (for some processing options), protactinium and, possibly, rare earth fission products.\* All molten salt fuel reprocessing will be performed on-site in a dedicated facility (see Section VII.B).

If batch fuel management is adopted, the molten salt will be charged to the blanket for a fixed period of time required to breed in the desired fissile concentration in the salt. The advantages of this mode of operation are a lower cycle averaged fission rate for the same fissile discharge

---

\*Rare earth fission product removal not proposed for TMHR.

concentration (0.11%  $^{233}\text{U}$ ,  $\approx$  0.03%  $^{233}\text{Pa}$  in thorium) and a possible relaxation in reliability requirements for the molten salt process plant. The disadvantage of this mode of operation is the economic penalty of carrying an entire extra load of molten salt (direct cost  $\approx$  \$200 million for the salt inventory in a 3000 MW fusion TMHR).

Isotopic generation for the batch fuel management mode is shown in Figure VII.A-3. As shown, the time to reach a  $^{233}\text{U}$  concentration in thorium of 0.11% (the design level) is 0.54 years. The same period of time is required for  $^{233}\text{Pa}$  in the blanket to reach its equilibrium level of 0.028% in thorium. Since the total molten salt inventory in the blanket and heat transport loop is about 1150 m<sup>3</sup>, the above results indicate that an average salt processing rate of 2130 m<sup>3</sup>/yr (or 0.243 m<sup>3</sup>/hr) is required to limit the amount of salt in process to one re-load. The above processing rate is reasonable and, as will be discussed later, is similar to the processing rate required for continuous reprocessing modes.

If continuous reprocessing modes are adopted a small slip stream of molten salt will be continuously charged and discharged from the molten salt primary coolant loop. In practice, this slip stream would not have to be continuous, but could operate on a time scale which is short in comparison with the batch irradiation time discussed above to limit the total inventory of salt. In this mode, the  $^{233}\text{U}$  and  $^{233}\text{Pa}$  concentrations will reach equilibrium values determined by the process flow rate, the type of reprocessing employed (i.e., the elements that are removed), and other parameters associated with the blanket and the reprocessing plant.

To model this mode of operation we first consider the protactinium mass balance

$$I \frac{dC_p}{dt} = R_p - F_p \eta_p C_p - \lambda_p I C_p \quad (1)$$

where

- I = Total salt inventory in-core and ex-core (g)
- C<sub>p</sub> = Protactinium concentration in salt (g Pa/g Salt)
- R<sub>p</sub> = Rate of protactinium production via thorium capture and  $^{233}\text{Th}$  decay (g/s)

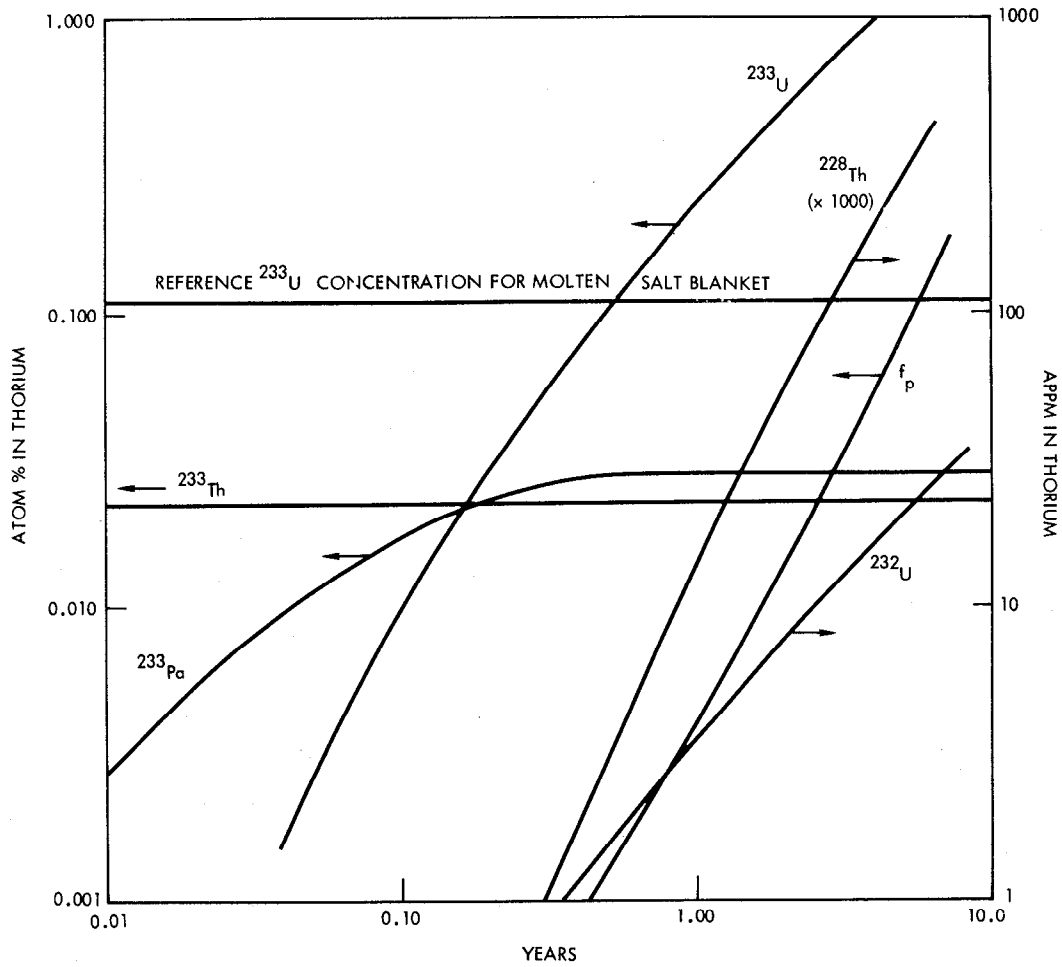


FIGURE VII.A-3. Isotopic generation in molten salt blanket with no fuel reprocessing (batch mode).

$F$  = Salt process rate (g/s)

$\eta_p$  = Protactinium removal efficiency (process dependent)

$\lambda_p$  = Protactinium decay constant ( $s^{-1}$ )

In equation (1), the terms on the right hand side represent nuclear production, process removal, and decay removal, respectively. In equilibrium we have

$$\frac{dC_p}{dt} = 0 \quad (2)$$

and the solution to equation (1) is

$$C_p = \frac{R_p}{F \eta_p + \lambda_p I} \quad (3)$$

To better understand the situation, it is of interest to consider the case where the molten salt process is turned off and the system reaches a natural equilibrium. In this case

$$C_p = \frac{R_p}{\lambda_p I} \quad (4)$$

For the reference lithium/molten salt blanket TMHR (3000 MW fusion) the parameters on the right hand side of equation (4) are

- $R_p = 0.141$  gm/s (at 70% capacity)
- $I = 3.86 \cdot 10^9$  g molten salt ( $1052 \text{ m}^3$  in the blanket,  $100 \text{ m}^3$

in the primary loop)

- $\lambda_p = 2.97 \cdot 10^{-7} s^{-1}$  ( $T^{1/2} = 27d$ )

and the resulting  $^{233}\text{Pa}$  concentration is  $1.23 \cdot 10^{-4}$  gm  $^{233}\text{Pa}$  per gm salt.

A more meaningful quantity, the weight concentration of protactinium in thorium,  $C_p^{\text{Th}}$ , is given by the following

$$C_p^{\text{Th}} = C_p / 0.435 = 2.83 \cdot 10^{-4} \quad (5)$$

where 0.435 is the weight fraction of thorium in the salt. The above quantity represents the equilibrium protactinium concentration in thorium if there were no molten salt process.

We can use equations (3) and (5) to solve for the process flow rate to achieve a specified concentration of  $^{233}\text{Pa}$  in thorium such that

$$F = \frac{1}{\eta_p} \left[ \frac{2.3 R_p}{C_p^{\text{Th}}} - \lambda_p I \right] \quad (6)$$

where  $\eta_p$  is estimated to be 99.5%. For instance, according to equation (6), a slightly reduced  $C_p^{\text{Th}}$  level of 0.023% will require a salt processing rate of 260 gm/s (0.280 m<sup>3</sup>/hr). Since a 70% capacity is assumed, the actual reprocessing capacity should be (0.7)<sup>-1</sup> times larger, or 0.400 m<sup>3</sup>/hr.

Next, consider the uranium mass balance

$$I \frac{dC_u}{dt} = \lambda_p C_p I - F \eta_u C_u \quad (7)$$

where  $F$ ,  $I$ ,  $C_p$ , and  $\lambda_p$  are as previously defined and

$C_u$  = Uranium concentration in salt (g U/g salt)

$\eta_u$  = Uranium removal efficiency (process dependent)

In equation (7), the terms on the right hand side represent protactinium decay to uranium and process removal, respectively. In this analysis, in-core fission as well as the proposed use of small amounts of uranium in the salt to maintain chemical stability are not considered.

Proceeding with equation (7), the equilibrium concentration with the molten salt process is

$$C_u = \frac{\lambda_p C_p I}{F \eta_u} \quad (8)$$

If we use values from above (i.e., a  $^{233}\text{Pa}$  level of 0.023% in thorium, 260 gm/s) and assume a uranium extraction efficiency of 100%, then

$$C_p^{\text{Th}} = C_u / .435 = 0.001 \quad (9)$$

Using the model described above, it is possible to determine the  $^{233}\text{U}$  and  $^{233}\text{Pa}$  concentrations in the molten salt processing loop as a function of the salt processing rate. The results are shown in Figure VII.A-4 for two types of molten salt processing: (1) "full reprocessing" to remove both uranium and protactinium, and (2) a "fluorination only" process to remove

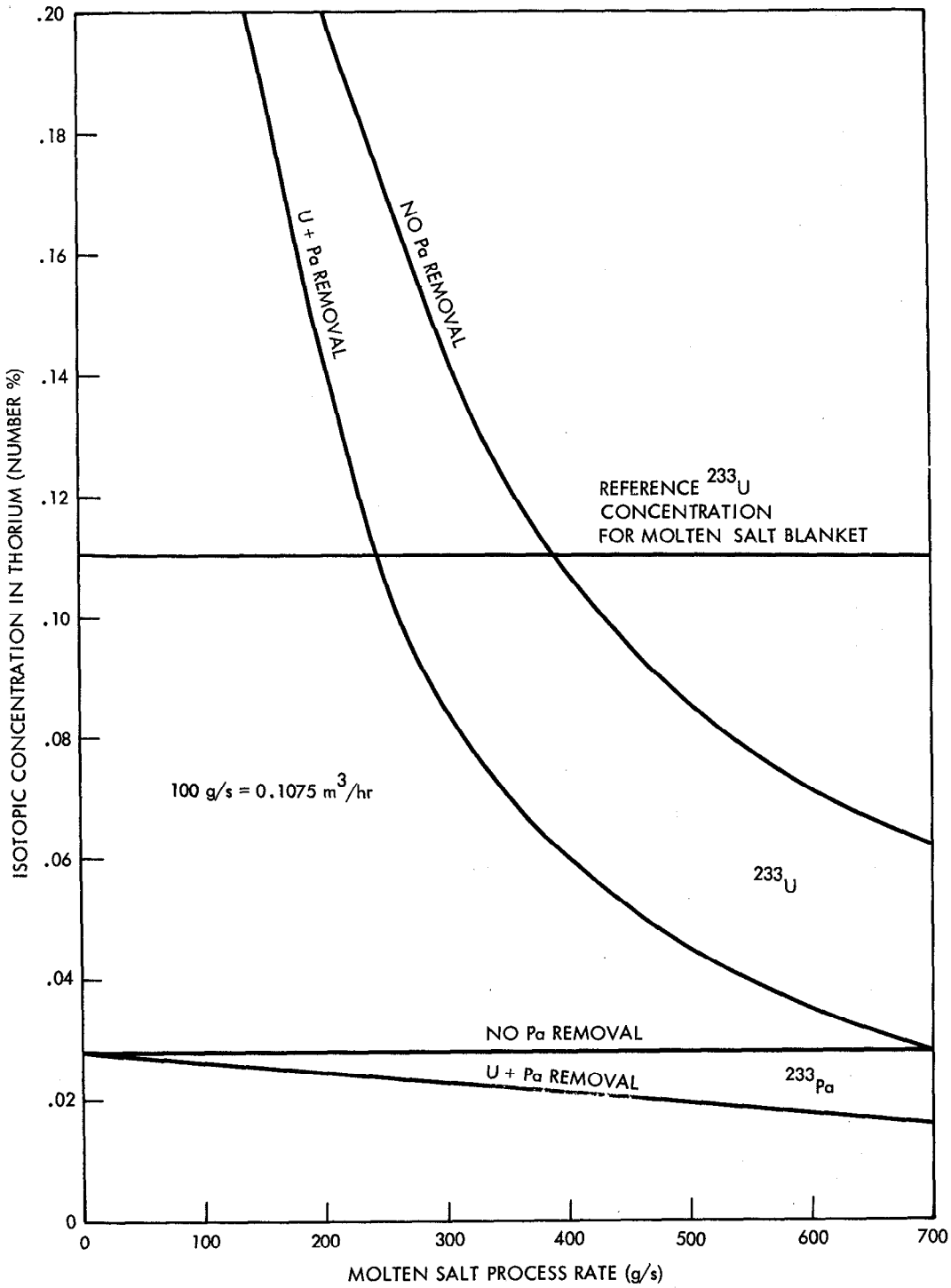


Figure VII.A-4. Equilibrium  $^{233}\text{U}$  and  $^{233}\text{Pa}$  concentrations versus salt process rate.

uranium only with no protactinium removal. The full reprocessing mode is expected to remove 100% of the uranium and 99.5% of the protactinium in the salt per pass through the reprocessing plant, while the less expensive and less technologically demanding fluorination only mode is expected to remove only 75% of the uranium per pass. Both modes are more fully described in Section VII.B.2.

As shown in the figure, for the same processing rate, the U + Pa removal mode results in the lowest  $^{233}\text{U}$  and  $^{233}\text{Pa}$  concentrations in the loop. In this case, a 240 g/s average process rate is sufficient to achieve the reference  $^{233}\text{U}$  concentration of 0.11% in thorium. If the molten salt processing plant has an average capacity factor of 70%, then the design capacity would be about  $240/.7 = 340$  g/s ( $0.365 \text{ m}^3/\text{hr}$ ). For the mode without protactinium removal, a 393 g/s average process rate is required to achieve the reference  $^{233}\text{U}$  concentration and the plant design capacity would be 560 g/s ( $0.600 \text{ m}^3/\text{hr}$ ).

Three considerations are important with respect to a choice between the two possible modes of operation. First, the full processing mode achieves a 20% lower  $^{233}\text{Pa}$  level which should result in marginal increases in fissile breeding (i.e., neutron absorption in  $^{233}\text{Pa}$  is a double loss mechanism) and a small decrease in afterheat due to energy released in protactinium decay. Nevertheless, the  $^{233}\text{Pa}$  concentration is difficult to reduce substantially for reasonable process rates. Second, the fluorination mode is less expensive than the full processing mode despite the much higher process rate. Even so, the more expensive process is estimated to cost less than 5% of the overall direct cost of the reference TMHR. Most importantly, the fluorination only process employs only a batch fluorinator recovery step and eliminates much of the complexity and technological development required for the full process. As a result, the TMHR molten salt processing plant can be less complex than the process required for a Molten Salt Breeder Reactor (MSBR). The choice of the fluorination only process for the TMHR is primarily based upon the later observation. The above considerations are more fully described in Section VII.B.2.

VII.A.3.b.(2). Lithium/Molten Salt Blanket Fuel Cycle Summary. A summary for important fuel cycle parameters for the reference lithium/molten salt blanket TMHR operating in either the fluorination only or full processing mode is given in Table VII.A-1 (Section VII.A.3.a).

As shown, the 4450 Kg/yr of fissile fuel produced is initially discharged as a mixture of  $^{233}\text{Pa}$  (about 19%) and  $^{233}\text{U}$  (about 81%). The fissile inventory associated with either mode of reprocessing is about 4450 Kg and is split about evenly between the ex-core inventory and the in-core inventory. The thorium inventory in the blanket, primary loop, and process plant is 1680 MT. The thorium throughput for a single TMHR will be 5400 MT/yr for the fluorination only process or 3340 MT/yr for the full processing option. Additional calculations relating to isotopic generation and depletion as well as the isotopic content of thorium and fissile material discharged from the lithium/molten salt blanket TMHR and its dedicated reprocessing plant will be presented in Section VII.C.3.

VII.B. THOREX AND MOLTEN SALT FUEL REPROCESSING TECHNOLOGIES FOR TMHR APPLICATION

VII.B.1. Application of Thorex Reprocessing Technology for TMHR Fuel Reprocessing

VII.B.1.a. Overview. As part of the TRW Laser Fusion Breeder Design Study<sup>6</sup> sponsored by DOE during 1980, Bechtel completed a preliminary conceptual re-design and costing study for a THOREX reprocessing plant to address the recovery of fissile material from unclad, low burnup thorium metal fuel discharged from a suppressed fission blanket. The conceptual plant design and process flows were based upon recent commercial reprocessing plant design work<sup>7</sup> (e.g., Barnwell) and plant capital and operating cost estimates were derived as a function of the heavy metal throughput.

Although the thorium metal reprocessing plant technology is not identical to the more difficult technology required to reprocess fuels discharged by the thorium oxide suspension blanket, the technical issues for the metal and the oxide are, for the most part, the same and the description of previous work on thorium metal reprocessing for the fusion breeder in section VII.B.1.b serves as a useful frame of reference. In section VII.B.1.c we use the thorium metal reprocessing plant design and costs as well as other recent reprocessing cost scaling data to obtain a preliminary estimate of the cost to reprocess thorium oxide fuel discharged from a TMHR. The reprocessing plant described in section VII.B.1.b is directly applicable to the thorium metal fueled blanket designs discussed in Appendix A.

Before discussing the plant design it is useful to introduce several design features of the redesigned THOREX plant which could permit substantial reductions in the cost to reprocess thorium metal fusion breeder fuels as opposed to high burnup LWR fuels. These are listed below:

- Lower Burnup ( 100-200 MWd/MT vs 33,000 MWd/MT) - greatly reduces the quantities of fission products and associated effluents.
- Smaller Scope Facility - the reprocessing plant described in Section VII.B.1.a is essentially  $\frac{1}{2}$  the size and has  $\frac{1}{2}$  the equipment of a typical LWR reprocessing plant of similar throughput.

- No High-Enriched Conversion is Required - U is transferred as a solution, hence no calciners and reducers are required.
- Utility Financing Used - considerably lower than usual high risk industry financing.
- Reduced Off-Gas Treatment - due to lower burnup, the off-gas system for this plant is much less extensive than that of typical LWR reprocessing plants.
- No Chop/Shear Equipment - the Th spheres have no cladding and are already in dissolvable size units, hence no shear or clad removal equipment is required.
- No Large Spent Fuel Storage - the spent fuel is stored at the reactor site until ready to be reprocessed. Since the reactors and the reprocessing plant are co-located, only a small surge capacity of spent fuel must be stored at the reprocessing plant.

The above design features will be described in the following discussion.

VII.B.1.b. Thorium Metal Reprocessing Plant. The purpose of the reprocessing plant in the suppressed fission-fusion breeder concept is to recover the fissile uranium ( $^{233}\text{U}$ ) from the irradiated thorium (Th) metal, to transfer the purified uranium product to an on-site light water reactor (LWR) fuel fabricator, to provide for 10-15 years of thorium storage, and to retain, treat, and package the high level waste streams for permanent disposition.\* The basic functions of the reprocessing plant and their interrelations are shown in Figure VII.B.1.

The conceptual design study of a reprocessing plant to accomplish the above objectives was performed by Bechtel as part of the DOE sponsored Laser Fusion Breeder Design Study. The design basis plant was sized to accommodate the fuel discharges from two suppressed fission breeder reactors as described in the study final report.<sup>6</sup> However, the economic

---

\*Low-level liquid and solid waste will be transferred to an on-site waste-handling facility which processes all site-generated (reactors, reprocessing, and Th metal fabrication) low-level waste.

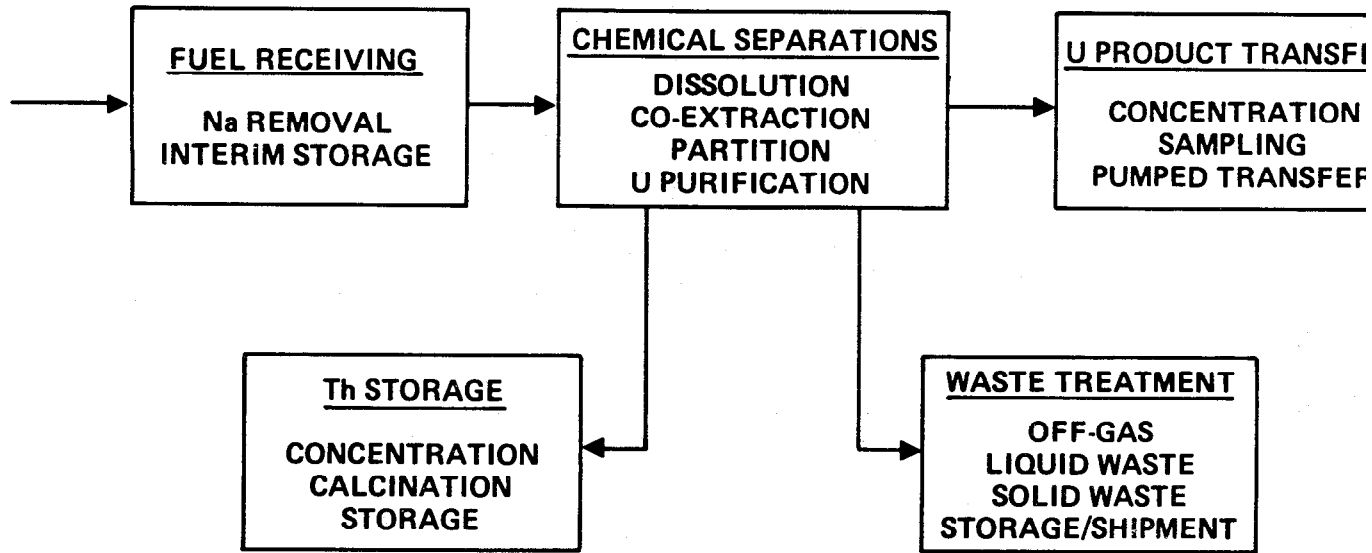


Figure VII.B-1. Thorium blanket reprocessing functions.

impact of smaller and larger reprocessing plants was also determined. The reactors, reprocessing plant, Th metal fabrication plant, and LWR fuel fabrication plant are all assumed to be co-located on the same site.

VII.B.1.b.(1). Reprocessing Plant Design Basis.

Battery Limits. The irradiated thorium fuel storage facilities at the site are not part of the reprocessing plant. Rather, facilities to provide three months of cooling between reactor discharge and chemical processing are assumed to be part of the reactor design. Transfer of the irradiated fuel to the reprocessing plant will be done in a batch operation. Some interim storage of cleaned (Na removed) thorium spheres is provided in the processing plant.

The high-level and intermediate-level liquid waste produced in the reprocessing plant will be concentrated, stored for five years, and solidified prior to shipment to a federal repository. Radioactive solid waste (e.g., spent filters, resin beds, failed equipment) and low-level liquid waste will be transferred to a waste management facility which services the entire complex.

The recovered uranium (essentially 100%  $^{233}\text{U}$ ) will be transferred to the on-site LWR fabrication plant as a concentrated uranyl nitrate solution via a double-walled pipeline. The recovered thorium will be calcined to oxide and stored on-site for 10-15 years.

Reference Plant Design Basis. Several plant designs and flowsheets were surveyed and a composite reference design was selected. To the extent compatible, the fission-fusion hybrid reprocessing plant design, the flowsheet, the equipment, and the operating mode will parallel that described in reference 8 (the flowsheet is a synthesis of those in sections C10 and C12) which is based on the Barnwell Nuclear Fuel Plant (BNFP) design.

Table VII.B-1 lists the design basis and constraints for the fission-fusion hybrid reprocessing plant. These design basis are related to the throughput, the irradiated fuel characteristics, the product specifications, the effluent limits, the allowable personnel exposures, and the structural design criteria.

TABLE VII.B-1. Plant design basis.

Operating Period	300 days/year
Throughput:	
Overall	1220 MTHM/year
Head-End	5 MTHM/day
Solvent Extraction	
Co-Extraction	5 MTHM/day
U Purification	30 KgU/day
Uranyl Nitrate Pumping	4.17 g /hr @ 300 g / g
Th Conversion	5 MTHM/day
Feed Characteristics:	
Physical and Chemical	Th metal spheres 2.54 cm in diameter, containing 0.58% <sup>233</sup> U (average)
Burnup (avg) <sup>a</sup>	200 MWd/MT
Minimum Cooling Time	120 days
Fissile Content (Max. expected)	0.72% <sup>233</sup> U
Product Specifications:	
Recovery Factors	99.5% of U 98% of Th
U Product	Th < 0.01% < 0.08% Others
Th Product	U < 0.001% < 0.008% Others
Effluent Limits	
Liquid	No discharge of radioactive liquids
Gas	Extensive separation of I and Ru from off gases Kr and <sup>14</sup> C (if present) to be vented along with any volatilized <sup>3</sup> H
Solid	HLLW to be converted to borosilicate glass within 5 years after separation. <sup>b</sup>

<sup>a</sup>Based upon fission product generation.

<sup>b</sup>HLLW = High level liquid waste.

Operation and Maintenance. The hybrid fuel reprocessing plant is envisioned to employ a combination of maintenance philosophies similar to those used in recently constructed or designed LWR reprocessing plants.<sup>7,9</sup> This consists of placing all equipment associated with high levels of gamma radiation in fully remote cells. Equipment exposed to intermediate levels of gamma radiation is located in semi-remote cells where both remote and some direct maintenance work can be performed. Direct maintenance is utilized where no or low radiation levels are present or where radioactive materials are well confined and shielded (e.g., storage areas). Due to the radioactivity associated with the uranium and thorium, remote operation is used throughout the plant. All instrument read-out and control locations will be separated and shielded from the process equipment.

Proliferation Considerations. Proliferation deterrence for this reprocessing plant is provided by hardened physical protection (guards, double-fenced site, remote sensing equipment, etc.) and dynamic material accountability systems. The natural radiation associated with  $^{232}\text{U}$  in the  $^{233}\text{U}$  product also enhances the proliferation deterrence of the products of the reprocessing plant. The  $^{233}\text{U}$  could also be diluted with  $^{238}\text{U}$  during reprocessing, but this would significantly increase the required material throughput and hence the cost of the reprocessing plant and therefore is not specified for this plant design.

#### VII.B.1.b.(2). Plant Description.

Process Flowsheet Description. The process flowsheet is shown in Figure VII.B-2 and a description of the various streams is provided in Table VII.B-2. In addition to the systems detailed in Figure VII.B-2, the plant also contains the following systems: Off-gas treatment solvent recovery, acid and water recovery and make-up, waste treatment, ventilation, process cooling and heating, and thorium and waste storage facilities. Complete material balances were not calculated, however, the flowsheet was derived from previously determined flowsheets<sup>8,10</sup> so that the range of flowrates and conditions can be estimated with enough accuracy to specify equipment and facility size, layout, and cost.

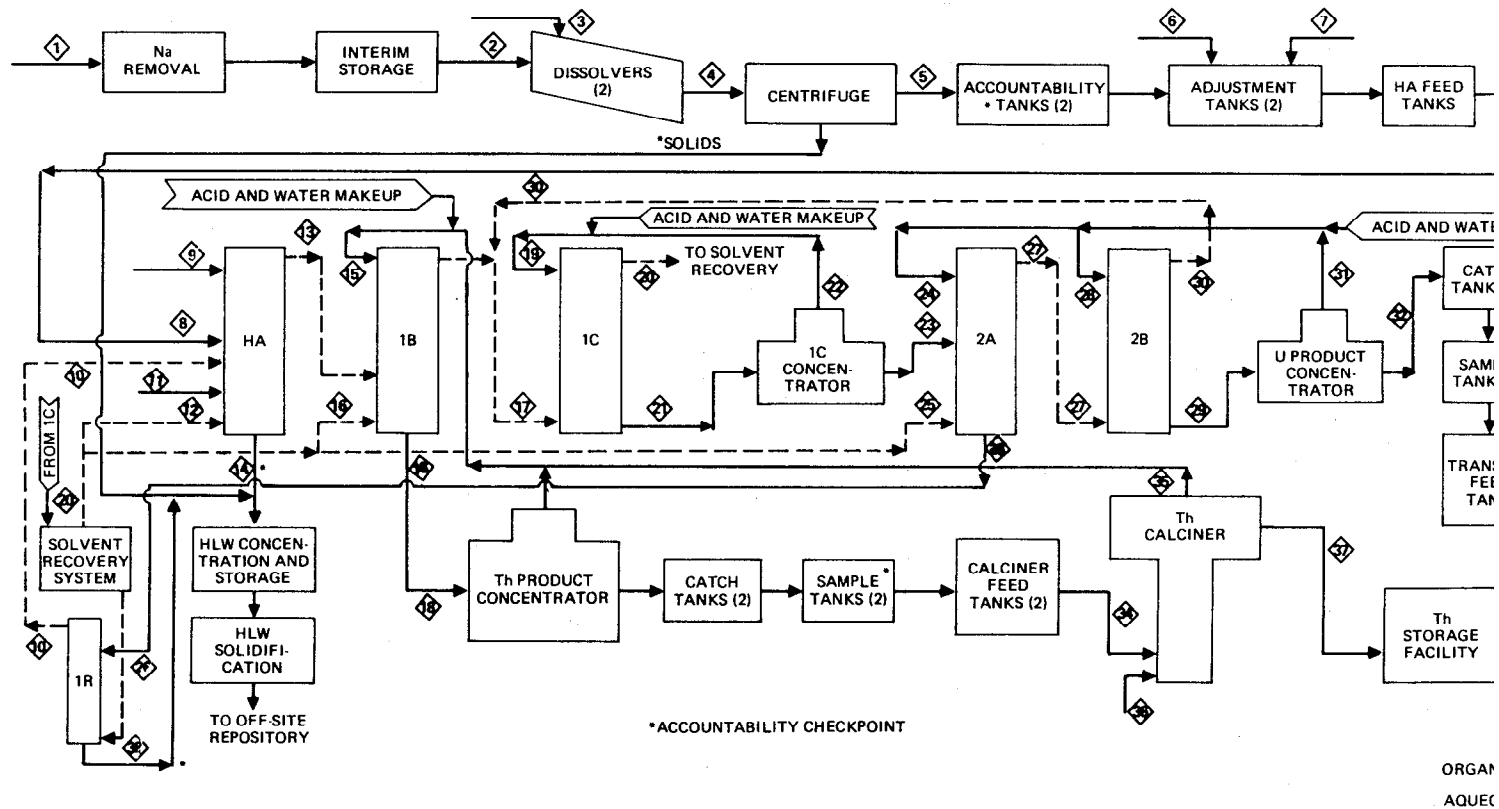


FIGURE VII.B-2. Process flowsheet.

TABLE VII.B-2. Process stream description.

Stream Number <sup>a</sup>	Identification	Description
1	Th sphere transfer	Unclean, Na contaminated spheres
2	Dissolver feed	Cleaned Th spheres
3	Dissolver chemicals	~12M nitric acid with 0.001M HF
4	Dissolver solution	_____
5	Clarified dissolver solution	_____
6	Chemical adjustment lines	Acid and water
8	HA feed	U, Th, FPs in ~ 1M nitric acid
9	Nitric acid scrub	_____
10	Organic solvent from recovery column	30% TPB in hydrocarbon diluent
11	Acid Butt	~12M nitric acid
12	Clean organic solvent	30% TPB in hydrocarbon diluent
13	Loaded organic (U+Th)	_____
14	High-level waste	FPs in nitric acid
15	Nitric acid strip	~0.1M
16	Clean organic solvent	30% TPB in hydrocarbon diluent
17	Loaded organic (U only)	_____
18	Aqueous Th-nitric acid stream	_____
19	Nitric acid strip	0.1M
20	Organic raffinate	_____
21	Aqueous U-nitric-acid stream	_____
22	1C concentrator overheads	_____
23	Concentrated U bearing acid stream	4-5 gU/l

<sup>a</sup> From Figure VII.B-2.

TABLE VII.B-2. (Continued.)

Stream Number <sup>a</sup>	Identification	Description
24	Nitric acid scrub	_____
25	Clean organic solvent	30% TPB in hydro-carbon diluent
26	2A column waste (to recycle)	_____
27	Loaded organic (U only)	_____
28	Nitric acid strip	~0.1M
29	Aqueous U-nitric acid stream	_____
30	Recycle organic	_____
31	U product concentrator overheads	_____
32	U product	300 gU/l
33	U product	300 gU/l
34	Concentrated Th-nitric acid solution	300 gTh/l
35	Th calciner overheads	_____
36	Steam	_____
37	Calcined ThO <sub>2</sub>	2-5 gm/cm <sup>3</sup> ThO <sub>2</sub> powder
38	IR recovery column waste	_____

<sup>a</sup> From Figure VII.B-2.

Thorium metal spheres discharged from a suppressed fission hybrid blanket are loaded from the reactor storage compartments into cylindrical tubes and transferred (1)\* to the sodium removal cell. All operations are carried out in an inert atmosphere to prevent sodium fires. In the sodium

\*Numbers refer to process lines on Figure VII.B-2.

removal cell, the transfer tube is placed in a concentric cylindrical unit where a mixture of water vapor and nitrogen gas is pumped through the sphere bed. Reaction with the water vapor affects the sodium removal. A more detailed discussion of the process (as applied to LMFBR fuel assemblies) can be found in Reference 11. Following sodium removal, the transfer tubes are removed, end fittings are screwed-on, and the tubes are temporarily stored in a water basin. The basin capacity is one month's throughput capacity (~100 MTHM), but is normally kept half-full.

After removal from the interim storage basin, the spheres are loaded into a dissolver feed hopper (2) where they are continuously fed to the rotary kiln dissolver. In the dissolver, the spheres are immersed in a 13M nitric acid solution (3) containing a small amount of fluoride catalyst (~0.001 to 0.005M HF). Upon leaving the dissolver (4), the thorium-uranium bearing nitric acid solution is centrifuged and passed (5) to the accountability tanks. From the accountability tanks, the solution is transferred to adjustment tanks where the chemical content is adjusted to approximately 1.0M nitric acid, 1.07M thorium, and 1.8 gU/ℓ.

The clarified and chemically adjusted solution (8) is fed to the HA pulse column where the uranium and thorium are extracted into an organic phase (13) (30% tri-n-butyl phosphate). The majority of the fission products (FPs) and other impurities remain in the aqueous raffinate stream (14). The thorium is then stripped from the organic phase (13) in the 1B column. The U remains in the organic stream (17). Criticality is prevented by concentration control and neutron poisons (pulse column plates contain a strong neutron absorber).

The aqueous stream (18) containing the thorium is then concentrated, sampled, calcined to oxide (34), and placed in storage for 10-15 years (37). This storage period allows the decay of <sup>228</sup>Th and its daughter products to a level where hands-on chemical conversion to metal (i.e., a "bomb" process) can be performed. If the discharge fuel were thorium oxide rather than thorium metal, the 10-15 year storage might be eliminated and the calcined oxide might be remotely refrabricated back into the blanket fuel form. This operation would be performed on-site.

The organic stream (containing the U) exiting the 1B column is combined with another organic stream (30) which is backcycled from the uranium purification columns. The combined organic stream (17) enters the 1C column where the U is back extracted to the aqueous phase (21). After concentration (23), the uranium is extracted into the organic phase in the 2A pulse column (27) and stripped back to an aqueous phase in the 2B column (29). Criticality control is by concentration and poison plates in the 1C column and by geometry (critically safe column diameters) in the 2A and 2B columns. After concentration in the U product concentrator (32), the uranium solution is sampled and transferred to the LWR fuel fabricator (33). The aqueous raffinate (26) from the 2A column is routed to a recovery column (1R) where any remaining uranium is extracted and backcycled to the HA column (10).

In addition to the processes described above, the plant will also include systems for off-gas treatment, solvent recovery, acid and water recovery, high level liquid waste concentration, storage, and solidification, building ventilation, process cooling and heating, and thorium storage. A detail description of these systems is not provided since they are similar (with the exception of the thorium storage) to the systems in previously design fuel reprocessing plants.<sup>7,8,9,11</sup> However, due to the decreased burnup of the thorium spheres in comparison to LWR fuel, the throughput of all these auxiliary systems will be greatly reduced. The thorium dioxide storage facility is a set of fifteen, buried, carbon steel tanks, approximately 12 m in diameter and 5 meters in depth.

Process Equipment and Facilities. The equipment required for the reprocessing flowsheet described in the previous section is similar to that of the Barnwell Nuclear Fuel Plant (BNFP).<sup>7,8</sup>

The correspondence is:

<u>BNFP Equipment Designation</u>	<u>Figure VII.B-2 Designation</u>
HS	HA
1BX	1B
1C	1C
2A	2A
2B	2B
1S	1R (somewhat smaller than the 1S)
2E Concentrator	Th Concentrator
3P Concentrator	1C and U Product Concentrator
U Calciner (in BNFP UF <sub>6</sub> Plant)	Th Calciner

The equipment will be fabricated from 304 stainless steel with the possible exception of the dissolver, associated tanks, HA column, and parts of the waste treatment system. Other alloys, more resistant to attack by fluoride, could be used for this equipment. Equipment in the auxiliary systems is similar to that described for the corresponding system in references 7 and 8. A brief description of the components in each major system of the reprocessing plant is provided in Table VII.B-3.

The layout of the blanket reprocessing facility is shown in Figure VII.B-3. The materials are basically reinforced concrete with stainless steel liners on the inside of each cell.

The Na removal cell houses the transfer crane, the transfer airlock, the Na removal unit, and the associated chemical feed tanks and equipment. The remote process cell contains the interim water storage tank, dissolvers, crushers, burners, solids handling equipment and high level waste concentrator. All operations and maintenance in the cell are performed remotely.

The high level cell contains the dissolver solution transfer, solution surge, accountability, feed adjustment and HA feed tanks, the centrifuge, the HA column, and their associated piping and auxiliary equipment. The cell is designed for remote operation and contact maintenance after process fluid removal and decontamination of the equipment.

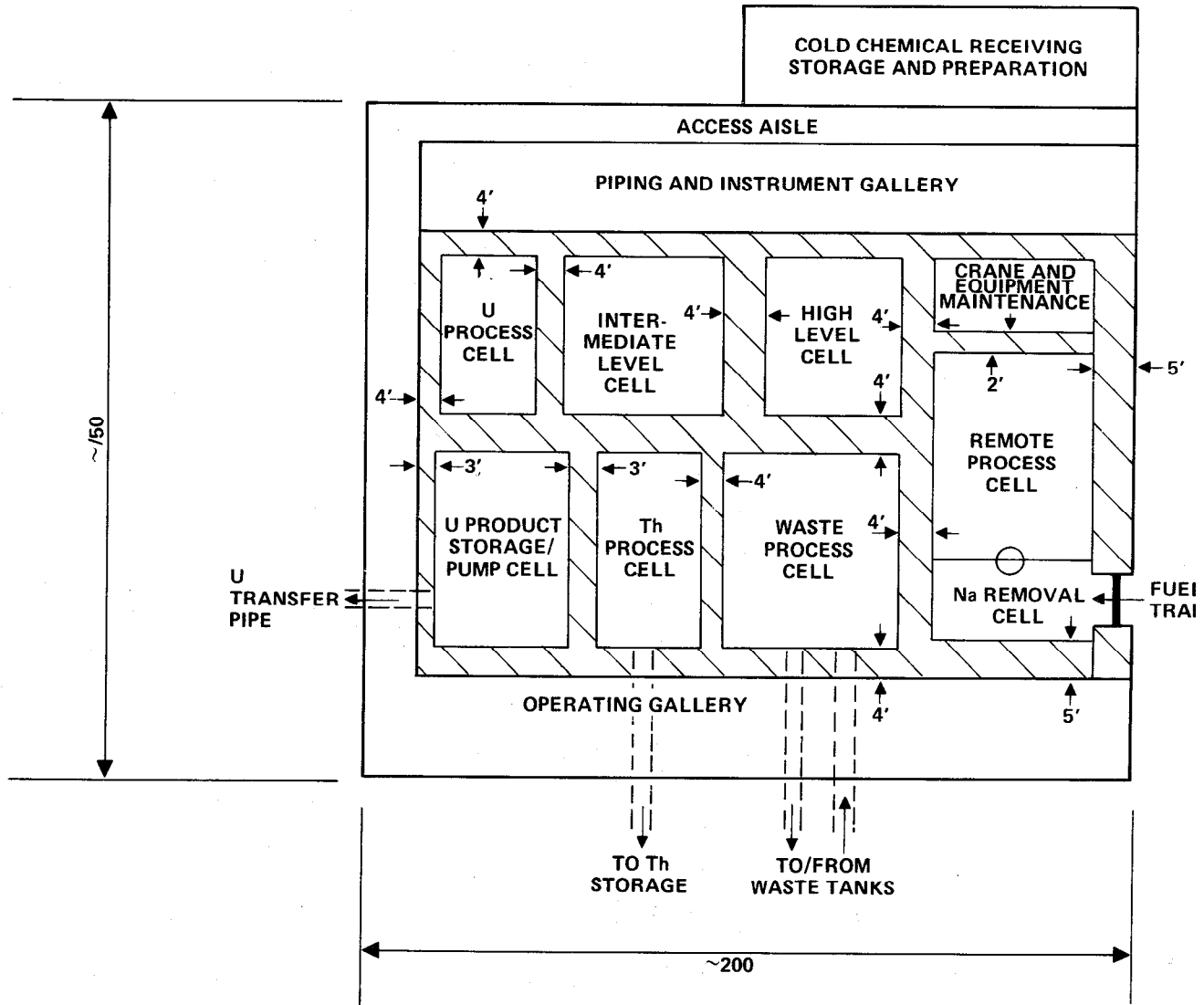


Figure VII.B-3. Facility layout

TABLE VII.B-3. Reprocessing plant components.

Component	Description
1. Head End	
Fuel receiving and sodium removal	Batch operation: cylindrical container with screw-on end fittings
Interim storage	Water basin capacity for 1 mo. operation
Accountability	Weight measurements, gamma scan, neutron measurements
2. Feed Preparation	
Dissolution	Rotary kiln dissolver
Centrifuge	Vertical, solid bowl
Accountability	Tank with weight, gamma, and neutron metering instruments
Feed adjustment	Tank
3. Solvent Extraction	
Pulse columns and associated equipment	(1) large co-extraction column (1) large Th stripping column (1) medium U stripping column (2) small U purification columns (1) medium recovery column (1) intercycle concentrator
4. U Product Preparation	
Concentration and Sampling	U product concentrator U product catch tank U product sample tank U product storage tanks U product pumping system
5. Th Product Preparation	
Concentration, Sampling and Calcination	Th product concentrator Th product catch tank Th product sample tank Th fluidized bed calciner ThO <sub>2</sub> storage transfer system
6. Th Storage	
Storage and Recovery	ThO <sub>2</sub> storage tank ThO <sub>2</sub> slurring and pumping system

TABLE VII.B-3. (Continued.)

Component	Description
7. Off-Gas Treatment	
Dissolver Off-Gas (DOG)	Particulate, ruthenium, iodine and nitrogen oxides removal
Vessel Off-Gas (VOG)	Particulate, ruthenium, iodine and nitrogen oxides removal
8. Acid Recovery	
Capture, Treatment and make-up	Concentrator overhead catch tanks, chemical adjustment system
9. Solvent Recovery	
Treatment and make-up	Filtration, aqueous wash column, ion exchange column, catch and feed tanks
10. High-Level Waste Treatment	
Concentration, storage and solidification	Waste feed tanks, concentrator, underground storage tanks, spray calciner and glass melter
11. Low-Level Waste Treatment	
Collection and Transfer	Transfer cask, 55 gal. drums, boxes, etc.

The intermediate level cell houses the 1B, 1C, and 1R columns, the 1C concentrator, and their associated piping and auxiliary equipment. This cell also contains the off-gas treatment and solvent recovery equipment. The cell is remotely operated and contact maintained.

The U process cell is also remotely operated and contact maintained and houses the 2A and 2B columns and the U product concentrator. The U product storage/pump cell contains the catch, sample storage and transfer tanks and the U solution pumps for transfer to the LWR fuel fabricator.

The Th process cell houses the Th product concentrator, the catch, sample and calciner feed tanks, and the Th calciner. This cell also utilizes contact maintenance and remote operation.

The waste process cell contains the waste calciner, the glass melter, the transfer equipment (liquid to and from storage and solid to storage and shipment) and a water-cooled storage basin. The cell is remotely operated and maintained.

VII.B.1.b.(3). Process Cost. The unit cost (\$/KgHM processed) was determined by estimating the capital and operating cost of the facility. These capital and operating costs were estimated on a modular basis in a manner similar to that described in reference 3. The economic assumptions used are:

- 1980 dollars (end of second quarter)\*
- 15.2% fixed charge rate on capital (typical utility financing)\*

Table VII.B-4 provides a breakdown on the capital and operating cost and the resulting unit price for three different size reprocessing facilities.

TABLE VII.B-4. Cost summary for thorium metal reprocessing plant.

Plant Throughput (MTHM/YR)	600	1200	1800
Head End, \$/M <sup>a</sup>	81	137	185
Solvent Extraction, \$/M	19	26	32
Waste Treatment (including Th calcination and storage), \$/M	26	37	45
Balance of Plant, \$/M	68	103	131
Total Equipment and Facility Direct Cost, \$/M	194	303	393
Field Indirect Cost, \$/M	39	61	79
Home Office Cost, \$/M	47	73	94
Contingency, \$/M	56	87	113
Owners Cost, \$/M	23	37	48
Time Value of Money During Construction, \$/M	48	75	97
Total Indirect Cost, \$/M	213	333	431

<sup>a</sup> 1980 Dollars.

\* Both compatible with Chapter IX assumptions.

TABLE VII.B-4. (Continued.)

Plant Throughput (MTHM/YR)	600	1200	1800
Total Capital Investment, \$/M	407	636	824
Levelized Annual Capital Cost, \$/M <sup>a</sup>	62	97	125
Levelized Annual Operating Cost, \$/M <sup>b</sup>	43	57	67
Levelized Total Annual Cost, \$/M	105	153	192
Levelized Cost Per Kilogram Thorium, \$/Kg	175	127	107

<sup>a</sup> Based upon 15.2%/yr capital charge (typical of utility financing).

<sup>b</sup> Operating cost levelizing factor = 2.038.

Useful scaling relationships can be generated using the information in Table VII.B-4.

Referring to Table VII.B-4, the total capital investment scales with throughput as follows:

$$I = 407 \cdot 10^6 (T/611)^{0.653} \quad (1)$$

where T (MT/yr) is the annual heavy metal throughput. The levelized annual capital cost for a 15.2% annual change rate (typical of utility financing) is then given by

$$A = 62.0 \cdot 10^6 (T/611)^{0.653} \quad (2)$$

Similarly, the levelized annual operation and maintenance cost scales with throughput as follows:

$$B = 4.28 \cdot 10^6 (T/611)^{0.411} \quad (3)$$

Concerning the levelized cost method, operating and maintenance costs escalate with time due to inflation and other factors. As a result, a factor (greater than unity) is included in Table VII.B-4 and equation 3 to adjust the first year operating cost estimates upwards to reflect such increases over the operating life of the plant<sup>12</sup>. The levelizing factor represents a disconnected average contribution for each year and is given by

$$\ell = \frac{\sum_{n=1}^N \left( \frac{1+e}{1+d} \right)^n}{\sum_{n=1}^N \left( \frac{1}{1+d} \right)^n} \quad (4)$$

where

N = financial life of the plant (yr)

e = average cost escalation

d = discount rate (cost of financing equity and debt).

If we again assume typical utility financing with a 30 year plant life and an 11.35%/year discount rate, then  $\ell = 2.038$ .

Therefore, the total levelized annual cost of reprocessing plant operation, as a function of throughput, is given by

$$L = [62.0 (T/611)^{0.653} + 42.8 (T/611)^{0.411}] \cdot 10^6 \quad (5)$$

The levelized cost per kilogram of thorium is then given by

$$K = \frac{L}{1000T} \quad (6)$$

and the levelized cost per gram of  $^{233}\text{U}$  is given by

$$G = \frac{K}{1000 a_{23}} = \frac{L}{10^6 T a_{23}} \quad (7)$$

Where  $a_{23}$  is the discharge assay of  $^{233}\text{U}$  (including  $^{233}\text{Pa}$ , if any) in thorium. For example, for  $T = 1200 \text{ MT/yr}$  and  $a_{23} = 0.0055$  (0.55%) the above equations give  $L = 153 \cdot 10^6 \text{ \$/yr}$ ,  $K = 127 \text{ \$/KgHM}$ , and  $G = 23.18 \text{ \$/g}$ .

As discussed earlier, these unit prices are considerably lower than most reference LWR reprocessing plants due to the numerous differences between the conceptual design outlined in this section and standard LWR reprocessing facilities. Nevertheless, there is considerable uncertainty

associated with the cost due to the thorium metal fuel form. If greater levels of fluoride are required to dissolve the thorium metal and more extensive off-gas treatment is required, the cost could increase substantially. However, if the thorium metal dissolves easily in nitric acid, and no fluoride is required, the cost could decrease. An experimental program to better understand the dissolution rate will be required.

VII.B.1.c. Considerations for Thorium Oxide TMHR Fuel Reprocessing. A conceptual design and cost study of a reprocessing plant for low burnup thorium oxide fuels of discharge concentration similar to the thorium metal fuels discharged by the beryllium/thorium oxide TMHR is not available. Nevertheless, a recent Exxon study<sup>3</sup> did compare reprocessing plants and costs for ThO<sub>2</sub> versus UO<sub>2</sub> fuels discharged by LWRs. Their principal conclusion relating to this comparison was as follows:

"The increased costs of processing thorium-based fuels result primarily from the relatively refractory nature of thoria which necessitates the use of more dissolvers (16 vs 4 hours dissolution time); more evaporation load because of the dilute flowsheets; more frequent equipment replacement because of corrosion from the fluoride catalyst used to accelerate dissolution and from the equipment erosion caused by small particles of undissolved thoria; the increased volume of high-level wastes resulting from the presence of fluoride ion and its metallic complexants."

These increased costs were expressed in their work as relative scaling factors. In particular, Exxon concluded that for LWR fuels, the capital cost of a ThO<sub>2</sub> reprocessing plant would be 1.9 times that of a UO<sub>2</sub> reprocessing plant. Similarly, they conclude that the operation and maintenance cost ratio would be 1.7.

The Bechtel thorium metal reprocessing plant design is expected to be very similar to a similar plant design for unclad, low burnup UO<sub>2</sub> fuel under similar discharge conditions. This results because the thorium metal with only minimal amounts of fluoride added is expected to dissolve as easily as uranium oxide. Therefore, a crude estimate of the reprocessing for low burnup thorium oxide fuels discharged by the TMHR may be deduced based upon the Bechtel plant costs<sup>6</sup> and the Exxon scaling factors.<sup>3</sup>

Such an estimate may be conservative for three reasons:

- The  $\text{ThO}_2$  proposed for use in the TMHR may dissolve more easily than LWR  $\text{ThO}_2$ . This could result from either smaller  $\text{ThO}_2$  particle size or the use of an uncalcined  $\text{ThO}_2$  fuel form.<sup>13</sup>
- The possible use of KF instead of HF to aid dissolution.<sup>13</sup>
- NASAP results<sup>5</sup> indicate that thorium oxide is only about 20% more costly to reprocess than uranium oxide.

In contrast, such an estimate could be optimistic. In the case of the Bechtel process, sodium coolant is stripped from the thorium metal by use of a straightforward process involving contact with steam.<sup>11</sup> If the TMHR thorium oxide is mixed with Pb-Li, both lead contamination and tritium could complicate the process. The following cost estimate is, therefore, inadequate and will be only indicative of thorium oxide reprocessing costs.

Applying the Exxon cost factors directly to Eq. (5), we obtain

$$L = [118 (T/611)^{.653} + 73 (T/611)^{0.411}] \cdot 10^6 \quad (8)$$

where T is the heavy metal throughput and the quantities K and G are calculated as before. Using the same example of  $T = 1200$  MT/yr and  $a_{23} = 0.0055$  we obtain the following:  $L = 280 \cdot 10^6$  \$/yr,  $K = 233$  \$/Kg, and  $G = 42.42$  \$/g. This conservative model is compared with a less conservative model of the thorium oxide reprocessing costs based upon NASAP data in Table VII.B-5. As expected, the conservative model results in unit processing costs which are about 50% higher than those predicted using the less conservative model. However, the high cost and large uncertainties associated with both models strongly suggest the need to perform further analysis with regards to  $\text{ThO}_2$  reprocessing if this option is retained.

TABLE VII.B-5. Estimates of thorium oxide reprocessing costs.<sup>a</sup>

Plant Throughput (MTHM/YR)	600	1200	1800
Conservative projections based upon Exxon/Bechtel Work (1.9 X Capital, 1.7 X Operating)			
Levelized Annual Capital Cost, \$/M	116	183	239
Levelized Annual Operating Cost, \$/M	73	97	114
Levelized Total Annual Cost, \$/M	189	280	353
Levelized Cost Per Kilogram Thorium, \$/KgHM	315	233	196
-----			
Less conservative projections based upon final NASAP report (1.2 X uranium oxide reprocessing costs)			
Levelized Cost Per Kilogram Thorium, \$/KgHM	210	152	128
-----			
Range of Levelized Cost Per Kilogram Thorium, \$/KgHM	210-315	152-233	128-196

<sup>a</sup>See Table VII.B-4 notes.

## VII.B.2 Application of Molten Salt Reprocessing for TMHR Fuel Reprocessing

VII.B.2.1 Overview. Many aspects of molten salt technology were developed, or were under study, over a more than 20-year period at the Oak Ridge National Laboratory.<sup>14,15</sup> The object of that development program was to have been a Molten Salt Breeder Reactor (MSBR) to produce an appreciable excess of  $^{233}\text{U}$ , through the intermediate  $^{233}\text{Pa}$ , from  $^{232}\text{Th}$ . The proposed MSBR was to have been a high-temperature reactor constructed of modified Hastelloy N; the fuel was to have been a molten mixture of  $^7\text{LiF}$ ,  $\text{BeF}_2$ ,  $\text{ThF}_4$ , and  $^{233}\text{UF}_4$  (71.7, 16, 12, and 0.3 mole %, respectively) pumped through a core containing unclad graphite as the neutron moderator and through an external heat exchanger for removal of the 2250  $\text{MW}_{\text{th}}$  produced by fission of  $^{233}\text{U}$ .<sup>16</sup>

Results from this large, though still incomplete, development effort suggest that a molten fluoride blanket for a TMHR could be maintained and that continuous reprocessing of such a blanket could be developed and demonstrated. The following subsections present (1) characteristics of the TMHR blanket system, (2) the chemistry of salt processing and salt maintenance, (3) descriptions of two alternative processes for the TMHR blanket, (4) estimates of capital and operating costs for the processes and (5) a description of the development program required to demonstrate such reprocessing for TMHR applications.

VII.B.2.2. Characteristics of the Molten Salt TMHR Blanket. The reference molten salt TMHR blanket (described more fully in Chapter IV) is to contain a molten mixture of  $\text{LiF}$ ,  $\text{BeF}_2$ , and  $\text{ThF}_4$  with the composition and physical properties<sup>17</sup> shown in Table VII.B-6 below. This salt, for which the  $\text{LiF}$  is to be prepared from 99.8%  $^7\text{Li}$ , contains 44% Th by weight. It is estimated that a total of 1152  $\text{m}^3$  (3860 metric tons) of this salt is required.

TABLE VII.B-6  
COMPOSITION AND PROPERTIES OF TMHR BLANKET SALT

Composition (mole %)	LiF	72
	BeF <sub>2</sub>	16
	ThF <sub>4</sub>	12
Liquidus (°C)		500
Properties at 600°C		
Density (g/cm <sup>3</sup> )		3.35
Heat capacity (cal/g°C)		0.33
Viscosity (centipoise)		12
Vapor pressure (torr)		Negligible
Thermal conductivity (W/°C cm)		0.011

Such a blanket, with a fusion driver of 3000 MW<sub>th</sub>, is estimated to produce 0.202 grams of <sup>233</sup>Th per second and to produce <sup>3</sup>H at a rate of 2.654 x 10<sup>-4</sup> grams per second. The blanket is assumed to be processed at a rate such that the concentration of <sup>233</sup>U is maintained at 1.1 x 10<sup>-3</sup> times the concentration of Th. Such a processing rate corresponds to an inventory of 1870 kg <sup>233</sup>U in the blanket salt, with 4.845 x 10<sup>-4</sup> grams <sup>233</sup>U per gram of salt and with 0.202 grams <sup>233</sup>U (or equivalent) generated and removed each second. Under such conditions the fission rate in the blanket is estimated to be about 800 MW<sub>t</sub>. This fission heat along with decay heat from the <sup>233</sup>Th and <sup>233</sup>Pa, is removed by circulating the salt at a rate of 3.75 x 10<sup>4</sup> metric tons per hour (186.6 m<sup>3</sup>/min) through external heat exchangers of Hastelloy N where the heat is transferred to metallic sodium.

Molten fluoride mixtures for MSRE and for many chemical and engineering experiments have been prepared by treating batches of the mixed materials in the molten state at about 600°C with anhydrous H<sub>2</sub>-HF mixtures and, subsequently, with H<sub>2</sub>.<sup>18-20</sup> Such treatment should certainly suffice for initial preparation of the TMHR blanket salt, though countercurrent (continuous) procedures would seem necessary for preparation of quantities as large as those required. Costs of the materials and of the necessary conversion and purification steps to provide the initial blanket salt are shown in Table VII.B-7 below. The initial charge of TMHR salt (1152 m<sup>3</sup>) would entail a cost of about \$192 x 10<sup>6</sup>; this cost represents a relatively small fraction of that of the total system, but advantages can clearly accrue if a smaller volume of blanket salt can suffice.

Table VII.B-7  
COST (PER CUBIC METER) OF INITIAL CHARGE OF TMR BLANKET SALT\*

Initial blanket salt	Cost, dollars/m <sup>3</sup>
<b>Materials</b>	
<sup>7</sup> Li (267.13 kg at \$160/kg)	42,745
Th (1679.3 kg ThO <sub>2</sub> at \$33/kg)	55,415
BeF <sub>2</sub> (398.6 kg at \$33/kg)	13,155
<b>Conversion and Purification</b>	
<sup>7</sup> Li (992.2 kg LiF at \$2.20/kg)	2,183
Th(1959.1 kg ThF <sub>4</sub> at \$4.40/kg)	8,620
LiF-BeF <sub>2</sub> -ThF <sub>4</sub> (3350 kg at \$13.25/kg)	44,388
<b>Total</b>	<b>166,500</b>

\*The <sup>6</sup>Li depleted lithium (99.8% <sup>7</sup>Li) cost of 160 \$/kg is based upon work performed by McGrath and assumes a 20 \$/kg cost of natural lithium with a 50 \$/kg separative work cost for lithium isotope separation. Other costs from ref. 21, page 124.

#### VII.B.2.C Chemistry of Salt Maintenance and Processing

VII.B.2.C.(1) Fission Product Behavior. Since the MSBR was not built and operated, most of the (still incomplete) understanding of fission product behavior in molten fluoride systems was obtained during operation of the Molten Salt Reactor Experiment (MSRE). The observed behavior has been described in detail;<sup>22</sup> a few pertinent points are noted below.

Fission products that originate in a well mixed molten salt (as in MSRE or TMHR) must come to a steady state as commonly encountered chemical entities. The valence states that they assume in the liquid are presumably defined by the requirements that cation-anion equivalence be maintained and that redox equilibria be established among the components of the melt and between the melt and the surface layers of the container metal.<sup>17,23</sup> Early assessments<sup>19,24</sup> suggested that fission product cations would be equivalent to the fission product anions plus the fluoride ions released by fission only if some of the cations assumed oxidation states corrosive to Hastelloy N. Inclusion, and

maintenance, of a small quantity of  $UF_3$  in the MSRE fuel was adopted to avoid the possibility of corrosion from this source.

The fission product gases Kr and Xe form no compounds under conditions existing in a molten salt reactor or in TMHR, and these gases are only sparingly soluble in molten fluorides.<sup>25,26</sup> Neither of these gases diffuse appreciably through metals, and they can be removed from molten fluorides by sparging with He. Such sparging was done for MSRE,<sup>27</sup> and was to be done for MSBR.<sup>16,28,29</sup>

The fission products Rb, Cs, Sr, Ba, yttrium, the rare earths, and Zr all form quite stable fluorides that are soluble in the molten fuels of MSRE, MSBR, and in the very similar salt to be used as the TMHR blanket. Consideration of solubility relationships among the actinide and rare earth trifluorides for an unprocessed version<sup>21</sup> of a large molten salt reactor, indicates that 30 years operation of TMHR should not result in precipitation of any of the fluorides of these elements.

The fission products Ge, As, Nb, Mo, Ru, Rh, Pd, Ag, Cd, Sn, Sb, Se, and Te were expected to exist in MSRE largely, if not entirely, in the elemental state and to precipitate within the reactor circuit.<sup>17,19</sup> This behavior seems to have been confirmed during MSRE operation,<sup>22</sup> but additional study will be required before details of their behavior can be predicted with confidence for TMHR (or for MSBR). Precipitation of these species within MSBR was adjudged to be tolerable,<sup>16,29,30</sup> and problems posed by these species should prove manageable in TMHR.

However, operation of MSRE led to embrittlement of the grain boundaries of Hastelloy N exposed to the molten fuel; shallow cracks were observed in the heat exchanger. Early studies<sup>31</sup> suggested, and subsequent work<sup>32</sup> has shown, that fission product Te is responsible for this embrittlement. Hastelloy N modified by addition of 1 to 2% Nb appears markedly more resistant than unmodified or Ti-modified Hastelloy.<sup>32</sup> However, a reasonably small change in fuel chemistry has been shown to be even more markedly beneficial.<sup>32-34</sup> Careful experiments have shown that crack frequency and crack depth both decrease markedly in Hastelloy specimens exposed to tellurium-bearing salts as the  $UF_3/UF_4$  ratio is increased (that is, as the melt is made more reducing). Additional study will be required, but it seems likely that use of a moderate  $UF_3/UF_4$  ratio in the fuel, perhaps combined with use of the Nb-modified Hastelloy-N, will alleviate the Te problem for TMHR.

In brief, the ability of molten fluorides to withstand irradiation, fission, and grow-in of fission products appears to be demonstrated. As indicated above, not all details of fission product behavior are understood, and further study is necessary. It is not, however, considered likely that deleterious effects of fission products would prejudice operation of a molten-salt blanket for TMHR.

VII.B.2.C.(2). Chemistry of Molten Fluoride Processing. The proposed MSBR required processing of about 190 grams of fuel salt per second to pass its entire inventory (49 m<sup>3</sup>) through its processing plant each ten days. It was necessary<sup>35,36</sup> that the process remove soluble fission product fluorides (notably those of the rare earths) that are important neutronic poisons and remove the <sup>233</sup>Pa from the fuel for decay to <sup>233</sup>U outside the neutron flux. Removal of these species required prior removal of <sup>233</sup>U from the fuel, and the process had to include steps to return most of this <sup>233</sup>U to the purified fuel stream. In addition, the MSBR process was required to perform several fuel maintenance functions (see VII.B.2.C.(3), below). Several of these operations will be required in management and processing of the TMHR blanket salt.

Key features of the proposed MSBR process were studied for several LiF-BeF<sub>2</sub>-ThF<sub>4</sub>-UF<sub>4</sub> compositions, but most of the studies, and essentially all of the conceptual designs, assumed use of LiF, BeF<sub>2</sub>, ThF<sub>4</sub>, and UF<sub>4</sub> (71.7, 16, 12, 0.3 mole %, respectively). Accordingly, most of what is known about MSBR processing is directly applicable to the salt for the reference design THMR. However, it must be noted that fuel processing for MSBR was far from a demonstrated reality at the termination of that effort. All of the key chemical separations had been repeatedly demonstrated on a small scale, and the process chemistry was well understood. However, much work (especially on suitable materials of construction and upon engineering development) remains to be done before overall feasibility can be assured.<sup>14,15</sup>

Uranium can be recovered from solutions in molten fluorides by fluorination to produce volatile UF<sub>6</sub>. Batch fluorinations can reduce the uranium concentration of the molten fluoride to less than one part per million by weight.<sup>36,37</sup> Such batch fluorinations were proposed<sup>36</sup> for recovery of uranium from salt to be discarded (as waste) from the <sup>233</sup>Pa decay system of the MSBR

processing plant. A continuous fluorinator<sup>14,15,36</sup> was to be used to remove most of the uranium from the MSBR fuel. Such fluorination was conservatively assumed to remove 95 to 99% of the uranium from a feed stream containing 0.3 mole % UF<sub>4</sub>.<sup>14,23</sup>

Fluorination also serves to remove fission product halogens (as volatile BrF<sub>5</sub> and IF<sub>5</sub>) from the molten fluoride and removes the oxide ion, which might be present as an inadvertent contaminant, by volatilization as O<sub>2</sub>. Any tritium present in the molten fluoride would be converted to <sup>3</sup>HF and partially removed with the UF<sub>6</sub> and excess F<sub>2</sub>. The small quantities of Kr and Xe would also be removed in that gas stream. In addition, several fission product species (including Se, Mo, Tc, Ru, Sb, and Te) would be partially converted to volatile fluorides and be removed with the uranium;<sup>23</sup> however, these species largely precipitate within the reactor circuit (see VII.B.2.C.(1), above) and their concentrations in the molten salt to be processed should be very small. Fluorination will not remove protactinium, nor will it remove transuranic elements, such as Pu, or nonvolatile fission product compounds, such as the rare earth fluorides, from the molten fluoride stream.

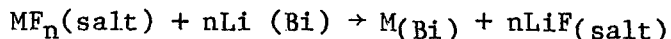
After fluorination, the molten fluoride would contain a small quantity of fluorine, some dissolved UF<sub>5</sub> and oxidized states of some fission product species. This salt stream would require treatment with gaseous H<sub>2</sub> for reduction of these oxidized and oxidizing species before return to the active circuit or before passage to other processing steps.

The fluorinator and the H<sub>2</sub> purge column could be constructed of Ni or a high Ni alloy but these pieces of equipment would require protection by a layer of frozen salt on all wetted surfaces of the units.<sup>36</sup> Development of continuous fluorination equipment was underway in the MSBR program,<sup>14,15</sup> but was still incomplete at the termination of that effort.

Recovery of protactinium and of uranium remaining in salt streams after fluorination can be accomplished by reductive extraction into alloys of bismuth containing lithium and thorium metals. Fission product Zr can also be removed, and (with more difficulty) fission products such as the rare earths and the alkaline earths can also be removed.<sup>14,15,36</sup> Early studies<sup>17,38,39</sup> showed the versatility of such reductive extractions, but most of the definitive studies of selective reductions from fluoride mixtures, however, are due to Ferris et al.<sup>40-46</sup>

Bismuth is a low-melting (271°C) metal that is essentially immiscible with molten halides. Its vapor pressure is negligible over the required temperature interval (500–700°C), and it can dissolve adequate quantities of Li, Th, U, Pa, and the fission product elements of interest. Fortunately, Be is essentially insoluble in Bi and is not appreciably extracted.

Reductive extraction equilibria between materials in salt and metal phases can be represented by the reaction:



in which the fluoride of metal M in the salt phase reacts with lithium from the bismuth phase to produce metal M dissolved in the bismuth and n moles of LiF in the salt. It has been found<sup>14,43</sup> that the distribution coefficient (D) for metal M depends on the mole fraction of lithium ( $X_{\text{Li}}$ ) in the metal phase:

$$\log D = n \log X_{\text{Li}} + \log K_M$$

where  $X_{\text{Li}}$  is the concentration (in mole fraction) of Li in the Bi after equilibrium is established. The quantity  $K_M$  for each element depends only upon the temperature and D (the distribution coefficient) is defined by the relationship

$$D = \frac{\text{mole fraction of M in metal phase}}{\text{mole fraction of } MX_n \text{ in salt phase}}$$

The separation factor for any pair of elements is the ratio of their distribution coefficients.

Table VII.B-8 shows values of n (the effective valence of fluorides involved in the reduction) and  $K_M$  for a number of pertinent species at 600°C along with the distribution coefficient for each at that temperature for a typical lithium concentration ( $X_{\text{Li}} = 1.22 \times 10^{-3}$ ). Such reductive extraction affords an excellent separation of U (and fission product Zr) from Th and a good separation of Pa from Th. For example, extraction with three equilibrium stages and flows such that 5 moles of salt are equilibrated with 1 mole of Bi alloy results in removal of 99.5% of the <sup>233</sup>Pa and essentially 100% of the <sup>233</sup>U and Zr from the salt. Good recovery (and separation from Th) of the transuranics can be obtained but such recovery is of little consequence to TMHR. However, the lanthanide and the alkaline earth elements are poorly extracted from the molten fluoride and are poorly separated from thorium by such extraction.

Table VII.B-8. VALUES FOR n, log K, AND D FOR REDUCTIVE EXTRACTION  
FROM 72LiF-16BeF<sub>2</sub>-12ThF<sub>4</sub> AT 600°C\*

Specie	n	log K	D <sup>†</sup>
U	3	11.056	561
Pa	4	12.467	24.5
Th	4	9.082	0.0101
Zr	4	14.683	4045
Np	3	10.514	161
Pu	3	9.979	47.0
La	3	6.628	0.021
Nb	3	6.801	0.024
Pm	3	6.575	0.019
Sm	2.6	5.734	0.034
Eu	2	3.740	0.016
Ba	2	4.049	0.032

\*Values for n and log K from references 34 and 38.

†Values for D at  $X_{Li} = 1.22 \times 10^{-3}$ .

All of the dissolved metals (including the Li and Th) can be completely and rapidly transferred from the Bi phase to a molten fluoride by treatment of the Bi alloy with anhydrous HF in the presence of the salt.

The fraction of lanthanides and alkaline earths that are extracted can be improved by use of large volumes of Bi alloy with small volumes of salt though the factors for separation of these species from Th are not affected. Smith and Ferris<sup>44</sup> observed that the lanthanides are well separated from Th when Bi alloys are equilibrated with molten LiCl. With this information McNeese<sup>14,47,48</sup> was able to devise a reductive extraction, metal transfer process for removal of lanthanides and other fission product species from molten fluorides along with the <sup>233</sup>Pa and <sup>233</sup>U. The proposed processing plant for MSBR was quite small; processing at about 0.9 gallons/minute (0.205 m<sup>3</sup>/hr) served to pass the entire fuel volume through the plant each 10 days. A conceptual design and a preliminary cost estimate for such a reductive extraction, metal transfer plant was prepared by Carter and Nicholson.<sup>36</sup>

It should be possible to develop and adapt the reductive extraction, metal transfer process for removal of rare earth and other fission product species to the TMHR blanket system, and it is possible that such processing (which could effect some improvement in blanket safety problems) should be considered in further studies. For the present study, however, the reductive extraction of  $^{233}\text{Pa}$ ,  $^{233}\text{U}$ , and zirconium only has been considered.

Elimination of the metal-transfer steps considerably simplifies the proposed<sup>36</sup> process. It needs to be emphasized, however, that much research and development is still necessary (see VII.B.2.f, below) before the reductive extraction process can be engineered and its overall feasibility assured.<sup>14,15</sup> Even for the process as simplified for TMHR, three key problem areas are evident. The first lies in the scarcity of materials capable of containing both molten salts and bismuth alloys as required by the extractor assembly and by the hydrofluorinator which removes  $^{233}\text{Pa}$ ,  $^{233}\text{U}$ , etc. from the Bi alloy and transfers it to the  $^{233}\text{Pa}$  decay system salt. Graphite, molybdenum, and tungsten appear to be capable of long-term service in such environments,<sup>14,15</sup> but all these are very difficult to fabricate into complex assemblies. Tantalum and some of its alloys are easily fabricated and appear to be capable of withstanding the Bi alloys, but their resistance to the salt is questionable. It seems likely that recent advances in coating technology (i.e., plasma spraying, etc.) would permit coating of alloys, such as stainless steel or carbon steel, with adherent, stable coatings of the resistant metals.

A second, though less fundamental, problem area lies in the lack of engineering-scale testing of the several unit processes and, especially, in the lack of operation of such processes as a closely-coupled integrated system. Such studies were barely beginning when the MSBR program was terminated.<sup>15</sup>

Waste disposal may represent a third area of difficulty. Whether the solidified fluoride mixture with contained fission products will be an acceptable waste form is unknown (and, at present, probably unknowable). No studies of conversion of the fluoride mixture into another form, if required, have been attempted. For this study it is assumed that such a solid (and relatively insoluble) material can be considered an acceptable waste form.

VII.B.2.C.(3) Molten Salt Maintenance Functions. Several maintenance functions were required for the MSBR fuel and will be required for the TMHR blanket salt. Two of these, which can be performed in the fuel reprocessing plant and which are described (in VII.B.2.d, below) as part of the process alternatives, are:

- Adjustment of the salt composition to compensate for changes due to burnup, to transmutation, and to addition of reagents required by the process.
- Removal of oxide ion, should any be inadvertently introduced into the molten fluoride, to avoid precipitation of very sparingly soluble  $\text{ThO}_2$ ,  $\text{PuO}_2$ , and  $\text{UO}_2$ .<sup>24</sup> Fluorination of the blanket salt, proposed in both process alternatives, should effectively perform this maintenance function.

However there are two additional maintenance functions, related to fuel processing, that cannot be performed in the processing plant. These functions, described below, must be performed by equipment added as part of the system for removal of heat from the circulating blanket salt.

Maintenance of Required  $\text{UF}_3/\text{UF}_4$  Ratio. The deleterious effect of fission product Te on Hastelloy N appears to be markedly diminished if an appreciable fraction (perhaps 5%) of the uranium is maintained as  $\text{UF}_3$  (see VII.B.2.C.(2), above). This  $\text{UF}_3$  must be replenished at intervals since the fission of U and Th as tetrafluorides is oxidizing<sup>19,20</sup> as is the generation of  $^3\text{HF}$  from transmutation of LiF. Fission (see VII.B.2.b, above) at a level of about 800  $\text{MW}_T$  would be responsible for oxidation of about 3 moles of  $\text{UF}_3$  per day while generation of  $1.95 \times 10^{-3}$  grams of  $^3\text{HF}$  per second would oxidize an additional 7 moles of  $\text{UF}_3$  per day. Maintenance of the desired concentration of  $\text{UF}_3$  in MSRE was readily accomplished by reaction of metallic Be with dissolved  $\text{UF}_4$ ; solid rods of metallic Be in perforated baskets of Ni were lowered through the sampler system into the flowing fuel in the pump bowl.<sup>17</sup> For TMHR, addition of about 45 grams of Be per day would suffice to maintain the  $\text{UF}_3$  concentration after steady state conditions (and reduction of 5% of the uranium inventory) are reached. Though initial startup of the assembly will be more complex (and might necessitate addition of 25 kg of  $^{233}\text{U}$  to the blanket), maintenance of the required  $\text{UF}_3/\text{UF}_4$  ratio in TMHR seems to be a relatively trivial problem.

Removal of Tritium, Kr, and Xe from Blanket Salt. A purge system using He gas was to be used to remove fission product Kr and Xe from the MSBR fuel.<sup>16,28,29</sup> About 1% by volume of He was to be maintained as small bubbles in the circulating fuel, and 10% of the fuel flowing through the heat exchangers was passed through an assembly that included a gas separator and a He bubble generator. Helium was removed and added at a rate of 4.7 liters per second (10 cfm) to the 350 liters per second of molten salt; average residence time of a He bubble in the fuel was near 140 seconds. This system was adjudged adequate to keep the  $^{135}\text{Xe}$  poisoning in MSBR to an acceptable level,<sup>28</sup> and a similar system operating on a modest fraction of the total heat exchanger flow should prove adequate for Kr and Xe removal from TMHR.

Removal and recovery of tritium from TMHR (and MSBR) is more difficult. Tritium is, in principle, generated from LiF as TF, but this compound is largely reduced to the elemental form by the  $\text{UF}_3$  necessarily maintained in the salt. If a generation (and removal) rate of  $2.654 \times 10^{-4}$  grams/sec (22.93 grams per day) is assumed, more than 90% of the tritium atoms will be present in elemental form in salt with 5% of the uranium present as  $\text{UF}_3$ . Elemental tritium diffuses readily through hot metals; it was estimated that nearly 2000 Ci per day of tritium might diffuse (at an effective pressure of  $1.28 \times 10^{-6}$  atmospheres) through the MSBR heat exchangers<sup>49</sup> with the purge system described. It is clear that TMHR will require a more rapid purge rate than that proposed for MSBR if losses of tritium to the sodium coolant system are to be kept to tolerable limits.

The flow of salt to the proposed TMHR heat exchangers totals about 3.1  $\text{m}^3$  per second. It should prove possible (though demonstration would be required) to maintain 1% by volume of He bubbles in the blanket salt and to remove and add this gas (31 liters per second at  $600^\circ\text{C}$ ; equivalent to about 22.5 standard cubic feet per minute) from the total flow prior to passage of the heat exchangers. The mean residence time for He bubbles in the blanket system would be near 367 seconds. Equipment for removal and addition of the bubbles would be similar (though some nine-fold larger) than that described for MSBR.<sup>28,29</sup>

Operation of such a system under steady state conditions would lead to an inventory of about 0.12 grams of T<sub>2</sub> and 0.04 grams of TF in the blanket. The salt plus gas bubbles fed to the stripper each hour would contain 1.2 grams of T<sub>2</sub> and 0.4 grams of TF; of this, some 80% of the T<sub>2</sub> and very little of the TF would be stripped. With tritium-free He reinjected prior to passage of the heat exchanger, the effective pressure of T<sub>2</sub> in the salt within the heat exchanger would be near  $2 \times 10^{-5}$  atmospheres. Tritium diffuses at a rate dependent upon the square root of its effective pressure, and the TMHR heat exchanger is smaller and its top temperature is lower than that of MSBR. It seems likely that less than 4000 Ci per day would diffuse through the TMHR heat exchanger and contaminate the sodium coolant. Escape of 4000 Ci/day to the environment may not be tolerable. Escape of this small quantity could presumably be minimized (at some cost) by cold trapping in the sodium system or, possibly, by processing of the sodium.

If further study should show that an intolerable quantity would escape, the sodium coolant could be replaced by the molten salt coolant mixture (sodium fluoride-sodium fluoborate) proposed<sup>14-16</sup> for use in MSBR and shown experimentally<sup>50</sup> to be capable of trapping diffused tritium for recovery.

Use of such a large purge system would ensure that Kr and Xe isotopes were essentially completely removed from the blanket salt at each pass.

The contained tritium would have to be recovered from the He purge gas and the short-lived isotopes of Kr and Xe would have to be held up for decay. Modifications of the system proposed<sup>28</sup> (but not designed in detail) for MSBR could presumably accomplish these functions. In addition, the long-lived isotopes (largely <sup>89</sup>Kr) might have to be retained and bottled for disposal. Cryogenic systems or fluorocarbon processing could certainly be adapted if necessary.

VII.B.2.d Alternative Processes for TMHR Blanket. The TMHR blanket is to be processed at a rate that will maintain the <sup>233</sup>U concentration at  $1.1 \times 10^{-3}$  times the Th concentration. Such processing will lead to an inventory of 1870 kg of <sup>233</sup>U within the 1152 m<sup>3</sup> of blanket salt ( $4.846 \times 10^{-4}$  gram <sup>233</sup>U per gram of salt), and will require removal of 0.202 grams per second of <sup>233</sup>U or <sup>233</sup>U plus <sup>233</sup>Pa from the salt. Two process alternatives are presented. The simpler process, chosen as the reference process, uses fluorination alone to

recover  $^{233}\text{U}$  from the blanket salt by volatilization as  $\text{UF}_6$ . The alternative process uses a similar fluorination combined with reductive extraction to remove both  $^{233}\text{U}$  and  $^{233}\text{Pa}$  from the processed salt. Both of the processes will receive salt from the external heat exchanger system of the TMHR; such salt will have passed the helium purge system described above. Both of the processes are adapted from those proposed for MSBR fuel and use equipment similar to that described for processing that fuel.<sup>36</sup>

VII.B.2.d.(1). Processing by Fluorination Only. Fluorination readily removes uranium from molten fluoride solutions but is incapable of removal of Pa and most of the fission product species (see VII.B.2.C.(2), above). If complete removal of the contained  $^{233}\text{U}$  were attained, the required 0.202 grams  $^{233}\text{U}$  per second could be obtained by processing at a rate of 417 grams of salt per second. Continuous fluorination in equipment of reasonable size cannot, however, be expected to approach complete removal of  $^{233}\text{U}$  from solutions so dilute as these. If, as seems reasonable, 75% removal can be realized, the required processing rate is about 560 grams of salt per second, corresponding to 0.6 m<sup>3</sup> per hour or to 2.63 gallons per minute. Such a processing rate, which is about three times that proposed<sup>36</sup> for MSBR fuel, would pass the entire blanket inventory through the process each 80 days. The required processing rates are further discussed in Section VII.A.3.6.(1).

The salt received by this process will contain (in grams per cubic meter) about 0.334 of  $^{233}\text{Th}$ , 590 of  $^{233}\text{Pa}$ ,  $3 \times 10^{-5}$  of tritium, and concentrations of stable fission product fluorides (see VII.B.2.C.(1) above) that will increase during the lifetime of TMHR. Since the efficiency of the He purge system for stripping Kr and Xe isotopes is very high, only trivial quantities of these gases will be received by the process. Initial heat generation levels would be near 160 KW/m<sup>3</sup> corresponding to an adiabatic temperature rise of about 2.1°C/minute; of this heat generation about 42, 91, and 27 KW/m<sup>3</sup> would be due to  $^{233}\text{Pa}$ ,  $^{233}\text{Th}$ , and fission products, respectively.

As shown in Figure VII.B-4, the salt is received in a recirculating feed tank capable of effective holdup of the salt for 90 minutes to drop the heat load on the salt to less than 60 KW/m<sup>3</sup>. The salt is then pumped to the primary fluorinator where it descends countercurrent to a stream of fluorine added at a rate of 5 liters (stp) per minute. The salt leaving the fluorinator passes directly to the H<sub>2</sub> purge column where it descends countercurrent to a stream of

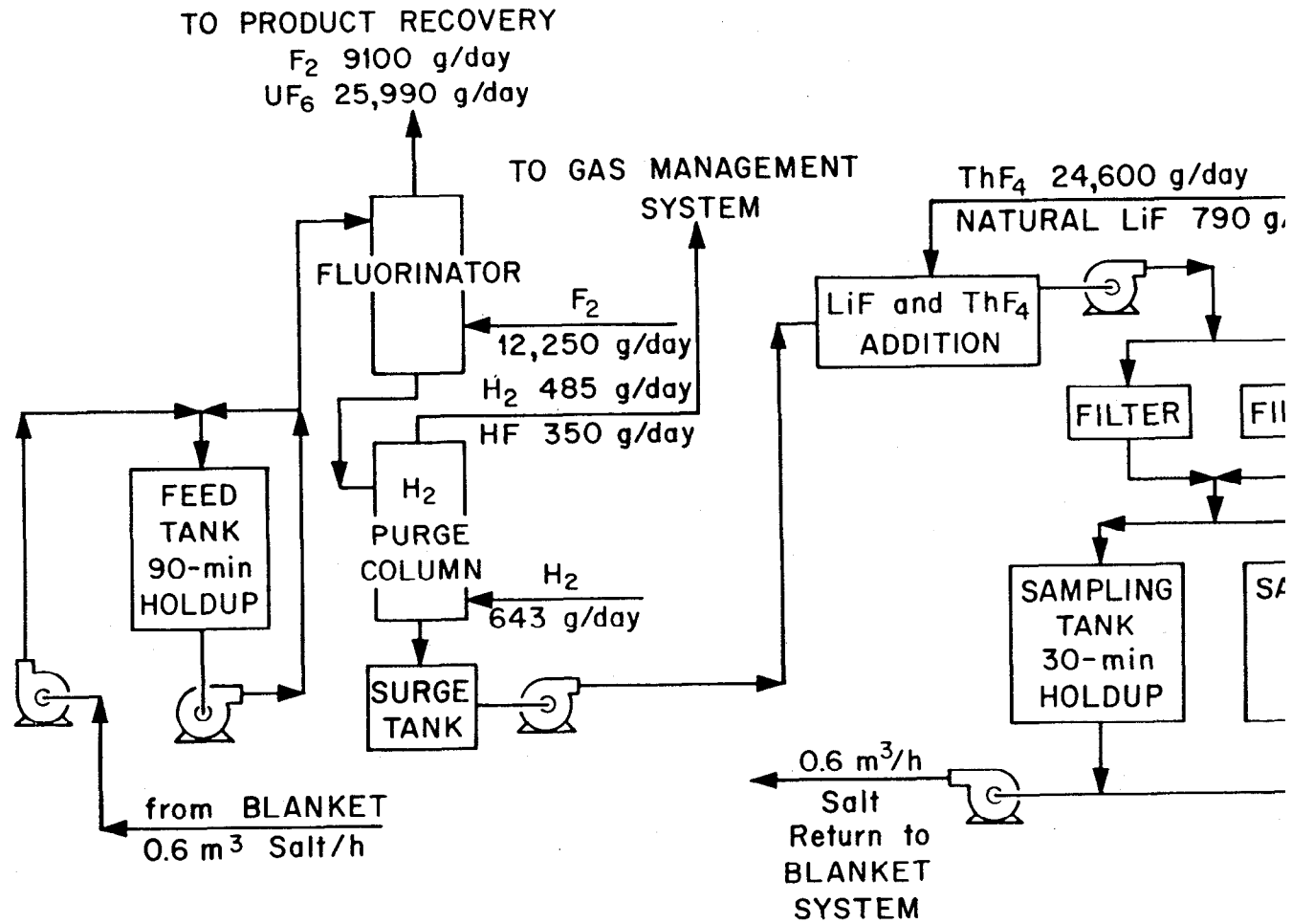


Figure VII.B-4. Salt Flow System for Reference (Fluorination Only) Process.  
 (Reagent usage in grams per full-power day.)

H<sub>2</sub> fed at 5 liters (stp) per minute. Treatment of the gases from the fluorinator and from the H<sub>2</sub> purge column is briefly described below.

Salt from the purge column passes to equipment where solid reagents are added for adjustment of the salt composition. Maintenance of the desired UF<sub>3</sub> concentration (see VII.B.2.C.(3), above) requires addition of 45 grams of Be each full power day. This is equivalent to generation of 235 grams of BeF<sub>2</sub> per day and compensation for this (if necessary) would require addition of 585 grams of LiF and 1.16 kg of ThF<sub>4</sub> each full power day. In addition, transmutation of Li isotopes requires addition of about 200 grams of LiF, and transmutation and fission of <sup>232</sup>Th requires addition of about 23.5 kg of ThF<sub>4</sub> per full power day. Addition of 4.1 kg of ThF<sub>4</sub> at four hour intervals and of about 393 grams of LiF each 12 hours would certainly keep the composition in balance. The additional salt volume produced through compensation of added Be would total 4.4 m<sup>3</sup> in 30 years of operation at 70% plant factor; this quantity should be readily accommodated within the TMHR blanket drain tanks. The LiF additions might be prepared from Li enriched in <sup>6</sup>Li if the isotopic composition within the blanket is to be kept at 99.8% <sup>7</sup>LiF. It seems likely, however, that addition of LiF prepared from normal Li will suffice.

The salt leaving the composition adjustment equipment is filtered and fed to a tank where it is held for 30 minutes for sampling before its return to the TMHR blanket circuit.

All of the process vessels and piping described above are constructed of Hastelloy N, but the fluorinator and the H<sub>2</sub> purge column require protection of all wetted surfaces by a film of frozen salt.<sup>36</sup> Heat removal from each of the assemblies is accomplished (as proposed for MSBR) by circulating liquid NaK. The feed tank heat removal system is of tube and shell construction, while the fluorinator and the purge column are cooled by NaK circulating between the vessel and a complete jacket of Hastelloy N.

Management of the gaseous streams, containing the product <sup>233</sup>UF<sub>6</sub> and fission products volatilized by fluorination, will be accomplished by modifications of the processes used to recover uranium from spent MSRE fuel<sup>37</sup> and of that proposed<sup>36</sup> for MSBR. As shown in Figure VII.B-5, the gas stream from the fluorinator (containing about 9100 g F<sub>2</sub> and 25,990 grams <sup>233</sup>UF<sub>6</sub> per full power day) would pass NaF traps at 425°C for retention of any volatile ruthenium, niobium and antimony fluorides and then through a series of five NaF traps maintained at 100°C for complete sorption of the product <sup>233</sup>UF<sub>6</sub>.

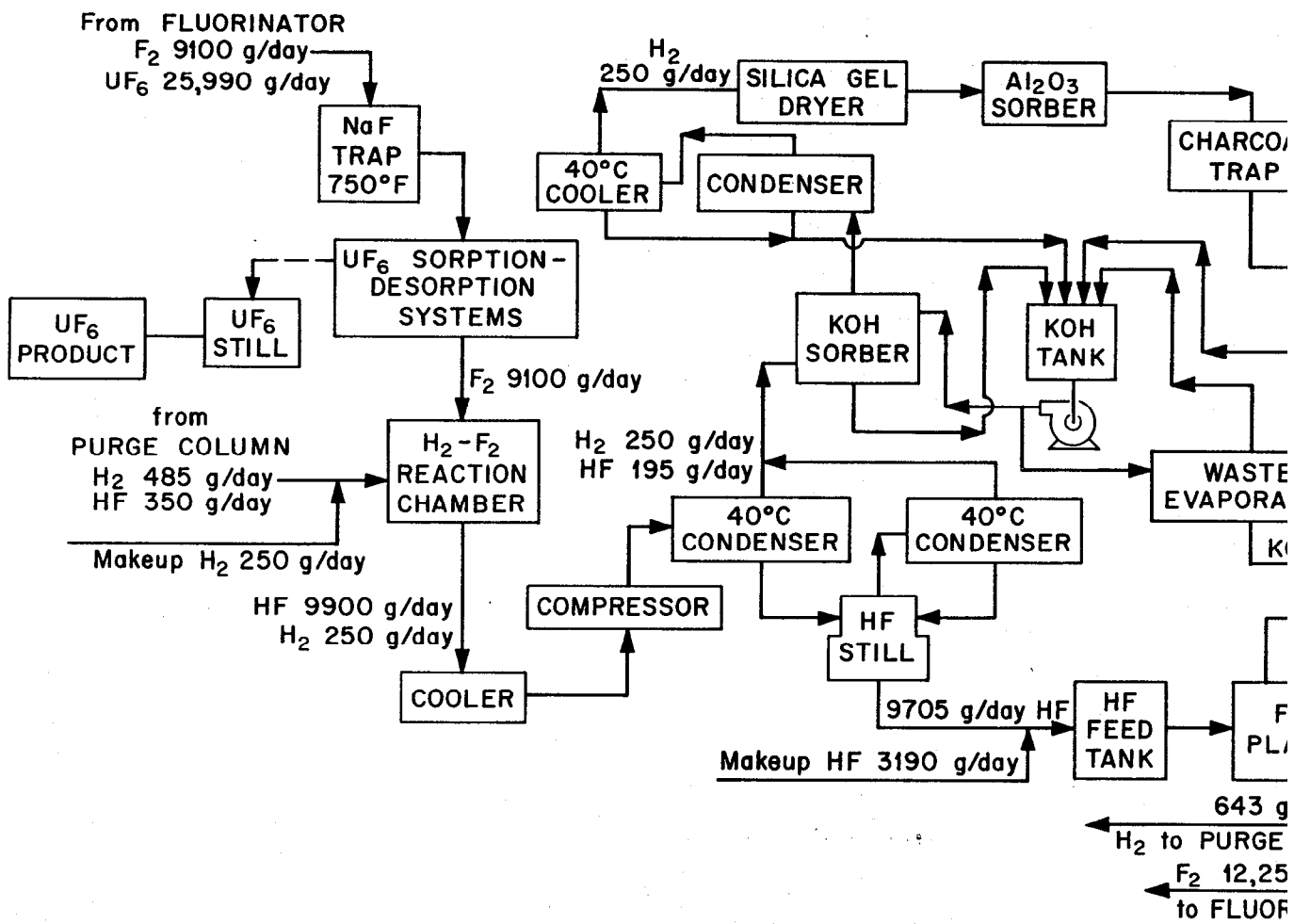


Figure VII.B-5. Gas and Product System for Reference (Fluorination Only) Process.  
 (Reagent usage in grams per full-power day.)

The F<sub>2</sub>, along with fission product fluorides such as IF<sub>5</sub>, TeF<sub>6</sub> and most of the MoF<sub>6</sub>, pass through these traps. The gas from the H<sub>2</sub> purge system (containing about 485 grams H<sub>2</sub> and 350 grams HF per full power day) plus an additional 250 grams of H<sub>2</sub> per day is reacted with the F<sub>2</sub> stream to produce a gas containing about 9900 g HF and 250 grams H<sub>2</sub>/day. This gas is chilled, compressed to 2 atmospheres pressure, and sent to a HF distillation column. The still bottoms (9705 gram HF/day) are sent along with 3190 grams of makeup HF to produce the 12,250 grams per day of F<sub>2</sub> and the 643 grams per day of H<sub>2</sub> required as feed for the fluorinator and H<sub>2</sub> purge system. The HF distillation overheads (250 g H<sub>2</sub> and 195 grams HF per day) are neutralized with 10 molar KOH solution and the H<sub>2</sub> (about 0.07 scfm) is vented and burned after passage through traps of silica gel, Al<sub>2</sub>O<sub>3</sub>, and activated charcoal. Such venting would release about 6 Ci of tritium and trivial quantities of Kr and Xe per full power day.

The product <sup>233</sup>UF<sub>6</sub> is desorbed from the 100°C NaF traps by heating. Fission product contamination (largely from traces of MoF<sub>6</sub>) seems unlikely to be such as to require additional purification, but purification by distillation could be performed if required. The desorbed UF<sub>6</sub> is transferred to product cylinders for shipment to fuel fabrication plants.

Such a process would produce small quantities of waste contaminated with fission products. Evaporation of the 10 M KOH neutralizer solution would produce about 0.5 m<sup>3</sup> of solid waste per year. The condensate from the evaporation would be used to prepare the 10 M KOH solution for the neutralizer. Additional solid wastes would result from occasional replacement of the 425°C NaF trap, of the NaHF<sub>2</sub> electrolyte from the small F<sub>2</sub> production cell, and of the silica gel and Al<sub>2</sub>O<sub>3</sub> sorbers. These are estimated to total about 5 m<sup>3</sup> of contaminated solid per year.

VII.B.2.d.(2). Processing by Fluorination and Reductive Extraction. Reductive extraction with alloys of Li and Th in Bi is capable (see VII.B.2.C.(2), above) of removing Pa and Zr (and, with more difficulty) other fission products along with U from molten fluorides. With essentially complete removal of <sup>233</sup>U and <sup>233</sup>Pa from the salt, processing at a rate of 325 grams of salt per second (0.349 m<sup>3</sup>/hr or 1.535 gallons per minute) would be required to maintain the <sup>233</sup>U at the desired concentration of 4.846 x 10<sup>-4</sup> grams per gram of salt. Such a processing rate (about 1.75 times that proposed for MSBR) would pass the TMHR blanket salt through the plant each 138 days. The <sup>233</sup>U inventory within the

blanket system would again be 1870 kg while the maximum  $^{233}\text{Pa}$  inventory would be 530.1 kg if the TMHR plant operates for several months at full power. The heat generation rate in the fuel received by the plant would be near  $150 \text{ kW/m}^3$ , and as for the fluorination only plant, trivial quantities of tritium (3.2 Ci/day) and Kr and Xe isotopes would be present in the salt for processing.

The salt would be received in a recirculating feed tank and would be sent to a primary fluorinator and a  $\text{H}_2$  purge column very similar to, but somewhat smaller than, those described for the fluorination only process above. Fluorine feed of 3 liters (stp) per minute is again assumed to remove 75% of the uranium, and a similar  $\text{H}_2$  feed rate should suffice for the purge. Blanket salt from the purge column, containing (in grams/ $\text{m}^3$ ) 405.8 of  $^{233}\text{U}$  and 466.2 of  $^{233}\text{Pa}$  passes a small surge tank and is pumped to the bottom of the primary extractor where it passes countercurrent to an alloy of Li and Th in Bi fed at  $0.0794 \text{ m}^3$  per hour. This extractor is scaled from that proposed for MSBR,<sup>36</sup> but we have assumed only 3 (instead of 5) equilibrium stages capable of extracting 99.5% of the  $^{233}\text{Pa}$  along with essentially all of the  $^{233}\text{U}$ . Estimated concentrations of the entering and exit streams are shown in Table VII.B-9.

The TMHR blanket salt from the extractor is passed through a large bed packed with Ni wool for removal of traces of Bi and through a filter system for removal of possible particulate materials. Finally the salt passes, as in the fluorination process above, equipment for adjustment of its composition and through a 30-minute holdup tank for sampling prior to its return to the TMHR blanket system.

The quantities of  $\text{LiF}$  and  $\text{ThF}_4$  that must be added per full power day to compensate for transmutation, for fission, and for the necessary Be addition are, of course, the same as those described for the fluorination process above. However, the reductive extraction process adds 63 grams of lithium and 7130 grams of Th per day to the blanket. As a consequence, addition of 275 grams of  $\text{LiF}$  each 12 hours and 2.33 kg of  $\text{ThF}_4$  each 4 hours should keep the blanket at the desired composition. Again, it would seem reasonable to add the  $\text{LiF}$  (as well as the  $\text{Li}^0$  in the Bi) as normal lithium.

TABLE VII.B-9. QUANTITIES OF PERTINENT SPECIES IN ENTERING AND EXIT STREAMS OF PRIMARY EXTRACTOR (MOLES PER HOUR)

Specie	Salt streams		Bi streams	
	Entering	Exit	Entering	Exit
Salt	18,500	18,500	3700	3700
$^{233}\text{U}$	0.608	0	0	0.608
$^{233}\text{Pa}$	0.689	0.003	0	0.686
Zr	0.045	0	0	0.045
Sr and Ba*	2.13	2.13	0	0.005
Lanthanides*	10	9.96	0	0.04
$\text{Li}^{\circ}$		0.38†	4.90	4.51
$\text{Th}^{\circ}$		1.28†	5.79	4.48

\*Estimated equilibrium values obtained only after many years operation.  
 †Moles/hr of Li and Th transferred to the salt (as LiF and ThF<sub>4</sub>).

The Bi alloy from the primary extractor, containing (see Table VII.B-9) the extracted  $^{233}\text{U}$  and  $^{233}\text{Pa}$ , passes a surge tank and is pumped at 600°C through an assembly similar to that proposed for MSBR<sup>36</sup> in which it passes countercurrent to captive salt and to a stream of anhydrous HF fed (2-fold excess) at 21 liters (stp) per minute. The captive salt, in a circuit isolated from the TMHR blanket, has a composition (in mole %) near 71 LiF-29 ThF<sub>4</sub>, is prepared from LiF containing natural Li, and flows at 0.25 m<sup>3</sup> per hr through the hydrofluorinator. In this assembly, all of the active metals (including U, Pa, Zr, Li and Th) are stripped completely into the captive salt. The essentially pure Bi is pumped to a recirculating pump-tank system where the Bi is brought to the required concentration (73 mole per m<sup>3</sup> of Th and 61.7 moles per m<sup>3</sup>) of Li for return to the primary extractor.

The captive salt receives the active metals from the Bi alloy in the hydrofluorinator and flows in a separate circuit to permit decay of  $^{233}\text{Pa}$  and recovery of the  $^{233}\text{U}$  produced. This salt passes from the hydrofluorinator through a secondary fluorinator, fed with F<sub>2</sub> at 2 (stp) liters per minute, where 75% of the uranium is assumed to be removed and through a purge column where it flows countercurrent to 2 (stp) liters of H<sub>2</sub> per minute. Captive salt from the purge column enters the  $^{233}\text{Pa}$  decay tank from which it is pumped to the hydrofluorinator.

The captive salt increases in volume from 10 m<sup>3</sup> to 11.9 m<sup>3</sup> over a 220-day cycle due largely to accumulation of LiF and ThF<sub>4</sub> from the hydrofluorinator and to addition of 4 kg of normal LiF per day to maintain a usefully low melting salt composition. The inventories of <sup>233</sup>U and <sup>233</sup>Pa near the end of each 220-day cycle are about 12.4 kg and 149.4 kg, respectively. On the average, about 301 grams of <sup>233</sup>U per hour are recovered from the secondary fluorinator. At the end of each cycle, 1.9 m<sup>3</sup> of the captive salt are transferred to a secondary (static) decay system where the <sup>233</sup>Pa is allowed to decay for an additional 220 days. This 1.9 m<sup>3</sup> of salt initially contains about 1.98 kg of <sup>233</sup>U and 23.86 kg of <sup>233</sup>Pa. After 220 days all except 84 grams of the <sup>233</sup>Pa have decayed and the 25.76 kg of <sup>233</sup>U are recovered by fluorination in a batch fluorinator and the salt containing the residual <sup>233</sup>Pa and about 10 grams of <sup>233</sup>U is transferred to waste storage. Since the salt is to be stored on site for some years, a very large fraction (90%) of the discarded 95 grams of <sup>233</sup>U could be recovered by batch fluorination if desired.

All of the equipment and piping intended to handle only salt is, as for MSBR,<sup>36</sup> to be fabricated of Hastelloy N, but as described previously, the fluorinators and the H<sub>2</sub>-purge columns require protection by a film of frozen salt. Equipment intended to handle Bi alloys only (such as the Li and Th makeup tanks) may be constructed of tantalum alloys jacketed with Hastelloy or steel. Equipment such as the primary extractor and hydrofluorinator that must handle both Bi alloys and salts must be of special construction. For this study it is assumed that suitably protective coatings of Mo or W can be emplaced on steel or Hastelloy assemblies. The large (15 m<sup>3</sup>) <sup>233</sup>Pa decay tank is assumed to be of Hastelloy N. It will require equipment for addition of about 4 kg per day of normal LiF. The heat load on this decay tank will be near 10.50 MW<sub>t</sub> from <sup>233</sup>Pa decay and perhaps an additional 5 MW<sub>t</sub> from fission products. It is, accordingly, assumed to be passively cooled by a system in which NaK is moved by thermal convection to an air-cooled radiator in a simple natural convection stack; a generally similar system was proposed for cooling the MSBR drain tank.<sup>16,29</sup> All of the other systems are to be cooled by forced circulation of NaK through tube and shell heat exchangers or vessel jackets.

Management of the gas streams, containing the product <sup>233</sup>UF<sub>6</sub> and volatile fission products, would be accomplished by processes identical to those of the reference fluorination plant described above. The necessary incorporation of the

hydrofluorinator in the reductive extraction process slightly increases the size of some of the equipment. Material balances for the gaseous  $F_2$ ,  $H_2$ , and HF indicate that 465 grams of HF must be neutralized by KOH, 825 grams of  $H_2$  must be vented, and 13,150 grams of makeup HF must be purchased for each full power day of plant operation. Venting of the  $H_2$  at about 6.4 liters (0.23 scf) per minute would result in release of about 4 Ci of tritium and trivial releases of Kr and Xe isotopes per full-power day.

This process, like the reference fluorination only process above, would produce small quantities of solid waste contaminated with fission products. Evaporation of the neutralizer solution would yield about  $1.2 \text{ m}^3$  of waste per year and replacement of traps and adsorbers would add about  $5 \text{ m}^3$  per year. In addition, the discard ( $1.9 \text{ m}^3$  per 220 days) from the captive salt circuit would add about  $3.2 \text{ m}^3$  per year of solid waste for eventual discard to a repository.

#### VII.B.2.e. Estimates of Capital and Operating Costs of Alternative Processes.

Estimation of cost for the MSBR<sup>16,29</sup> and for its complicated processing plant<sup>36</sup> were performed many years ago, were presented in 1969 dollars, and were based upon conceptual rather than detailed and final designs. Several features of the salt maintenance systems and of the processing plants for TMHR differ substantially from those proposed for MSBR. For purposes of this study, the pertinent estimates made for the MSBR systems were accepted; they were updated to 1981 dollars by assuming 6% inflation for five years and 10% inflation for seven years. In addition, they were scaled to the TMHR capacity by assuming that equipment costs scale as the 0.5 power of the throughput. The estimates presented here in 1981 dollars, represent only the direct cost of the system, and include no contingency.

VII.B.2.e.(1) Costs for Salt Maintenance Functions. The operations required for maintenance of the required  $UF_3/UF_4$  ratio in the blanket salt and for removal and recovery of  $^3H$ , Kr, and Xe must be performed by systems associated with the primary heat exchanger system and outside the processing plant.

Maintenance of the required  $UF_3/UF_4$  ratio (VII.B.2.C.(3), above) is most important but is easily accomplished by periodic addition of metallic Be. For this purpose, one of the TMHR blanket salt pumps would require addition of an assembly to permit lowering of a small basket containing Be into the circulating salt in the pump bowl. This relatively small addition to the pump is assumed to

involve a direct capital cost of \$225,000; its operation, requiring the part time service of one operator, is assumed to cost \$25,000 per year. The (trivial) cost of the added Be is included in the reagent cost for the processing plants.

Removal and retention of  $^3\text{H}$ , Kr, and Xe (VII.B.2.C.(3), above) is a much more difficult operation. The similar operations for MSBR<sup>16,28,29</sup> were performed on six-fold smaller salt flow and involved more Kr and Xe but far less  $^3\text{H}$ . Moreover, the MSBR system, though it proposed<sup>14</sup> to retain the  $^{89}\text{Kr}$  cryogenically, did not recover the tritium separately. The MSBR system,<sup>14</sup> after adjustment for inflation and twelve-fold scaleup to TMHR size, would entail a direct capital cost of  $7 \times 10^6$ . It is not, at present, clear how this system would be modified to permit recovery of a large fraction of the tritium. Such a system, capable of recovery of a large fraction of the 20+ grams of  $^3\text{H}$  per day and of bottling the noble gases for disposal, might entail a direct capital cost of  $18 \times 10^6$  and an annual operating cost of \$200,000.

VII.B.2.e.(2). Costs for the Reference Fluorination Only Process. The process for recovery of  $^{233}\text{U}$  from the TMHB blanket by fluorination alone is to operate upon  $0.6 \text{ m}^3$  of salt per hour (VII.B.2.d.(1), above). This reference process is considerably simpler than the MSBR process, though the proposed throughput of salt is three-fold higher, and all equipment in the blanket salt circuits can be of Hastelloy N. The TMHR process is required to handle less  $^{233}\text{UF}_6$  than did that for MSBR, but it must purify a much larger quantity of  $\text{UF}_6$  as product. Direct capital costs (no contingency) have been estimated (after detailed listing of the equipment required) by scaling, wherever possible, from the costs estimated by Nicholson and Carter.<sup>36</sup> Costs for auxiliary equipment, piping, thermal insulation, process instrumentation, etc. were then estimated by the methods used for the MSBR process.<sup>36</sup> Results of this estimate of the direct capital cost of the reference processing system are shown in Table VII.B-10. To the total direct capital cost (with no contingency) of \$17,025,000 must be added the direct capital costs (\$18,225,000) for the salt maintenance functions described in VII.B.2.e.(1) above. On this basis the direct capital costs associated with maintenance of the  $\text{UF}_3/\text{UF}_4$  ratio, removal and recovery of  $^3\text{H}$ , Kr and Xe, and the total direct cost of the reference process would be about \$35,250,000.

At the end of its life, the TMHR will contain about 1160 m<sup>3</sup> of blanket salt contaminated with fission products. It is possible that this still valuable salt can be transferred, at that time, to another TMHR at the same site. However, at some time this large volume of salt must be discarded, presumably as high-level waste. About 8,850 cannisters (10 inches in diameter, 10 feet in length, filled to a depth of 8.5 feet) would be required for disposal if the solidified salt can be considered an acceptable waste form. Such disposal (at \$9000 per cannister) plus transportation would be expected to cost about \$85 x 10<sup>6</sup>. It should be noted, however, that a THOREX plant processing 1500 MgHM per year at 3 ft<sup>3</sup> of high-level waste per MgHM would produce more than three times as much waste for disposal.

VII.B.2.e.(3). Costs for the Fluorination and Reductive Extraction Process.

The process using fluorination and reductive extraction (VII.B.2.d.(2)) is to operate upon 0.349 m<sup>3</sup> of blanket salt per hour. This rate is 1.75 times that proposed for MSBR,<sup>36</sup> but the process is simpler since no provisions are made for removal of alkaline earth and rare earth fission products. However, this alternative process is required, as was the reference process, to purify a much larger quantity of <sup>233</sup>UF<sub>6</sub> product than did the MSBR process. In addition, this alternative process will require special materials or special coatings to protect the equipment that must handle both Bi alloys and molten salts.

As before, the direct capital cost estimates have used the methods of, and have been scaled from the results of, Carter and Nicholson.<sup>36</sup> While it seems likely that ultra-modern techniques can apply suitably resistant coatings of (for example) molybdenum to base metals, we have assumed that costs of such equipment (in 1969 dollars) would be those estimated<sup>36</sup> for fabrication from molybdenum. Results of this estimate of direct capital cost (with no contingency) are shown in Table VII.B-12. As for the reference process, the direct capital costs (\$18,225,000) for the salt maintenance functions must be added to the total from the table. The combined direct costs of the processing plant plus the maintenance operations is, therefore, \$74,703,000.

Table VII.B-10. DIRECT CAPITAL COST OF REFERENCE PROCESSING PLANT FOR FLUORINATION OF 0.6 m<sup>3</sup> OF SALT PER HOUR

Item	Cost (\$1000)
Hastelloy and stainless equipment	5,648
Auxiliary equipment	2,441
Hastelloy and stainless piping	2,591
Thermal insulation	582
Fluorine plant	395
Process instrumentation	2,397
Cell electric connections	255
Sampling stations	1,148
Radiation monitoring	318
Waste handling and storage	1,250
Total direct cost	17,025

Table VII.B-11 shows the estimated annual operating cost of the reference processing plant. Reagents used in the blanket salt maintenance functions previously described are included in this total, but other operating costs are not. As a consequence, to the total of \$1,386,500 shown in the table must be added some \$225,000 for the UF<sub>3</sub>/UF<sub>4</sub> ratio maintenance and the <sup>3</sup>H, Kr and Xe removal functions. Operating costs, assuming 70% plant factor, accordingly, total \$1,611,500 per year.

TABLE VII.B-11. ESTIMATED ANNUAL OPERATING COSTS FOR REFERENCE PROCESSING PLANT FOR FLUORINATION OF 0.6 m<sup>3</sup> OF SALT PER HOUR

Item	Cost (\$ per year)
Reagent use*	
ThF <sub>4</sub> (6.3 metric tons)	205,500
Be (11.5 kg)	2,000
LiF (normal; 201 kg)	8,800
H <sub>2</sub> (64 kg)	1,250
HF (816 kg)	3,000
KOH (200 kg)	1,000
Total	221,550
Plant payroll†	700,000
Waste disposal*	325,000
Total operating cost	1,386,550

\*Calculated for 70% plant factor.

†Does not include blanket salt maintenance operations.

TABLE VII.B-12. DIRECT CAPITAL COST OF PLANT FOR PROCESSING BY  
 FLUORINATION AND REDUCTIVE EXTRACTION (0.349 m<sup>3</sup> SALT PER HOUR)

Item	Cost (\$1000)
Hastelloy and stainless equipment	15,486
"Molybdenum" equipment	5,901
Auxilliary equipment	4,860
Hastelloy stainless piping	9,527
"Molybdenum" piping	1,770
Thermal insulation	1,397
Fluorine plant	410
Process instrumentation	8,962
Cell electric connections	750
Sampling stations	2,870
Radiation monitoring	795
Waste handling and storage	3,750
Total direct cost	56,478

Table VII.B-13 shows the estimated operating costs, assuming a 70% plant factor, for the alternative processing plant. Reagents used in the salt maintenance functions are included, but other costs of operating the maintenance systems are not. Some \$225,000 must be added for those systems leading to a total of \$2,279,000 as the operating cost of the processing and maintenance functions.

As for the reference process, the blanket salt inventory (about 1160 m<sup>3</sup>) of the TMHR at its end of life must - possibly after re-use in subsequent TMHR's - be disposed of as high-level waste. Costs for this disposal would be very similar to those presented above for the reference process.

TABLE VII.B-13. ESTIMATED ANNUAL OPERATING COSTS FOR ALTERNATIVE PROCESSING PLANT (0.349 m<sup>3</sup> SALT PER HOUR)

Item	Cost (\$ per year)
Reagent use*	
Li (natural, 16.1 kg)	2,700
<sup>232</sup> Th (1.82 metric tons)	99,000
Be (11.5 kg)	2,000
LiF (1.2 metric tons)	52,500
ThF <sub>4</sub> (3.0 metric tons)	128,000
HF (3.36 metric tons)	12,400
KOH (480 kg)	2,400
Total	299,050
Plant payroll†	1,200,000
Waste disposal*	555,000
Total operating cost	2,054,000

\*Calculated for 70% plant factor.

†Does not include salt maintenance operations.

VII.B.2.f. Special Development Needs in Molten Salt Technology. The staff of the MSBR program at the Oak Ridge National Laboratory prepared in 1974 a detailed program plan for development of Molten Salt Breeder Reactors.<sup>15</sup> That document described the gaps and uncertainties in the data base, as did a previous study,<sup>14</sup> presented in detail an 11-year program for the required development effort, and estimated the costs of each individual research and development item. Costs of the required MSBR technology effort, in 1975 dollars, were presented for each of the 11 years. The operating fund requirements (excluding reactor design and analysis) averaged about \$6.6 x 10<sup>6</sup> per year for the first five years and about \$13.9 x 10<sup>6</sup> per year for the final six years. Capital equipment funds to support that effort averaged \$1.6 x 10<sup>6</sup> per year over that period. In addition, a total of 104 x 10<sup>6</sup> of capital project funds (not including a test reactor) were identified as necessary during that period. It was not presumed that MSBR technology development would be completed at the end of the 11-year period, but it was believed that such expenditures would permit a MSBR test reactor to be authorized at the end of the fifth year and to be adequately supported during its design and construction phases.

The MSBR program included some items (such as graphite development) that are not germane to the present TMHR. [It should be noted, however, that subsequent TMHRs may include graphite.] However, most of the general classes of needed MSBR development items will be required for the TMHR. A brief description of key items that concern the molten salt portion of TMHR is presented and estimates of the operating and capital equipment costs (scaled from the MSBR estimates<sup>15</sup>) are tabulated in the following.

- Hastelloy-N and its modifications seem likely to prove adequate, but these alloys are not yet approved reactor materials, and expensive development is needed. Some of the MSBR program concerned interaction with the sodium fluoborate coolant (which might be adopted by TMHR), but, in any event, testing of Hastelloy-N with the chosen coolant will be required.
- Basic chemistry of molten  $\text{LiF-BeF}_2\text{-ThF}_4$  mixtures is relatively well known, but better physical property measurements, better understanding of  $^3\text{H}_2$  solubility and behavior, and, especially, better understanding of fission product behavior is needed.
- A few on-line instruments for chemical analysis are well along in development, but several others are needed both for the TMHR blanket and for its processing plant.
- The development requirements in reactor safety (hot-spot analysis, consequences of flow blockage in fuel channels, leaks in heat exchangers, and consequences of primary system leakage may be less serious for TMHR, but they are not trivial.
- Graphite development, including development of less permeable graphites with increased radiation stability, will be required for TMHR if graphite is to be used in contact with molten salts.
- Molten salt reactor technology needs for TMHR, as for MSBR, include development of improved pump and heat exchanger designs, and of improved flow, level, and other monitoring equipment. TMHR may not require development of salt-steam heat exchangers but it must develop and demonstrate stripping, recovery, and control of large quantities of tritium.

- Development of improved instruments and control systems is probably of less consequence to TMHR than to MSBR, but, again, the problems are not trivial.
- If the reference TMHR process (fluorination only) proves satisfactory, a smaller effort in processing technology than that required for MSBR will suffice. Key items for the reference process include the degree of protection afforded the fluorinator by frozen salt films and the efficiency of continuous fluorination in removal of  $^{233}\text{U}$  from very dilute molten salt solutions. An especial need is for demonstration of, and improvement on, the system for recovery, purification, and handling of large quantities of  $^{233}\text{UF}_6$  and for management of the appreciable quantities of fission products volatilized in the fluorinator. If the alternative process is to be preferred, a program of the magnitude of that proposed for MSBR is necessary. In any event, a relatively expensive demonstration facility for the integrated process will be required.
- The program of materials development for the processing plant depends markedly upon whether the reference process or some variant of the alternative process is chosen. If it is the latter, a difficult, and necessarily rapid, development program is necessary to provide and demonstrate compatibility of a metal or coating with combined Bi alloys and salts.

Table VII.B-13 presents an estimate of the total operating fund and capital equipment fund requirements (in 1981 dollars) required over a ten-year period to provide adequate support to a molten-salt blanketed TMHR. As the table shows, a development effort averaging about  $\$15 \times 10^6$  per year and with capital equipment funds of about  $\$2.7 \times 10^6$  per year would be required for a ten-year period to provide support for a test of a TMHR using a molten salt blanket. [It should be noted that the capital equipment requirement is likely to be much higher than above, since the MSBR estimates<sup>15</sup> presumed, as is no longer the case, that ORNL's 1974 pool of test stands and equipment were available.] Research and development on molten salt technology for TMHR would certainly be required beyond this ten-year period, as detailed problem areas indicated by the test design and subsequent designs are identified. Indeed it

seems certain that expenditures beyond this ten-year period would increase substantially (in constant dollars). A recent examination of MSBRs<sup>21</sup> suggests that with development beginning in 1980, a molten salt fission reactor could be made commercial in 30 years and that the research and development costs (including several expensive facilities but not the intermediate scale reactors) would be near  $\$700 \times 10^6$ . It is not apparent that a molten salt version of a TMHR could be built in a shorter period or with development costs markedly less than could a molten salt fission reactor.

TABLE VII.B-13. ESTIMATED OPERATING FUND AND CAPITAL EQUIPMENT FUND REQUIREMENTS FOR DEVELOPMENT OF MOLTEN SALT BLANKETS FOR TMHR (1981 DOLLARS)

	Operating Fund Requirements ( $10^6$ dollars)	Capital Equipment Requirement ( $10^6$ dollars)
Development of Structural Materials	24.6	6.7
Chemical Research and Development	16.9	3.2
Analytical Chemistry Development	8.0	1.7
Reactor Safety	9.6	-
Graphite Development	16.2*	4.2*
Reactor Technology	44.6	6.1
Maintenance	4.4	1.1
Instrumentation and Controls	2.9	0.3
Blanket Processing	20.1†	2.8†
Processing Material Development	1.2**	0.5**
Total	148.5	26.6

\*If graphite is to be used in contact with molten salts in TMHR.

†If the alternative process is chosen, these numbers become 31.6 and 4.8, respectively.

\*\*If the alternative process is chosen, these numbers become 4.0 and 1.7, respectively.

## VII.C ISOTOPIC CONSIDERATIONS

### VII.C.1 Overview

The generation and depletion of actinide and fission product isotopes in suppressed fission blankets is an important concern which impacts the overall economics of three areas:

- The reprocessing of discharge fuel from the TMHR
- The recovery and re-use in the TMHR of fertile thorium discharged from the blanket
- Shielding requirements for fabrication of the bred  $^{233}\text{U}$  for use in an LWR

Concerning the first of these, minimizing the fission product and actinide generation also minimizes the hazard of high level wastes. The second and third areas are most applicable to thorium metal and thorium oxide fuels and are impacted by the generation of  $^{232}\text{U}$  ( $T_{1/2} = 72 \text{ y}$ ) which decays to  $^{228}\text{Th}$  ( $T_{1/2} = 1.9 \text{ y}$ ).  $^{228}\text{Th}$  ultimately decays to  $^{208}\text{Tl}$  with the resultant production of a 2.6 MeV gamma for 36% of all  $^{228}\text{Th}$  decays.

Although fully remote fuel reprocessing operations are required, savings in shielding thicknesses for various other processes, including thorium and thorium oxide fuel fabrication, may be possible by minimizing the generation of  $^{232}\text{U}$ ,  $^{228}\text{Th}$ , and the resulting 2.6 MeV gamma activity. For example, the inventory of thorium required for the lifetime of the hybrid will be determined by how long it will be stored to allow the  $^{228}\text{Th}$  content, produced by the decay of  $^{232}\text{U}$  prior to the separation of uranium at thorium in reprocessing, to decay to acceptable levels for economically reforming it into hybrid fuel. If hands-on processing of the thorium after a 10-15 year cooling period is more economical than immediate remote processing for re-introduction into the hybrid, a 10 to 15 year supply of thorium and storage facilities will be required.

Isotopic generation and depletion during and following irradiation in the TMHR has been estimated from an ORIGIN-like calculation<sup>51</sup> which follows both the fission rate and the production of  $^{232}\text{U}$  and other isotopes as a function of time. The computer program, ISOGEN, developed for this application,

uses the same matrix exponential method as ORIGIN for the production and loss of the isotopes of interest. Figure VII.C-1 shows the isotopes of interest and their production and loss mechanisms.  $^{233}\text{U}$  is produced when a neutron is captured in  $^{232}\text{Th}$  and there are two successive beta decays:  $^{233}\text{Th}$  to  $^{233}\text{Pa}$ , and then to  $^{233}\text{U}$ .  $^{232}\text{U}$  can be produced from (n, 2n) reactions in the bred  $^{233}\text{U}$ . A second important path to  $^{232}\text{U}$  is as follows: A  $^{232}\text{Th}$  (n, 2n) reaction produces  $^{231}\text{Th}$ ,  $^{231}\text{Th}$  decays to  $^{231}\text{Pa}$ ,  $^{231}\text{Pa}$  captures a neutron becoming  $^{232}\text{Pa}$ ,  $^{232}\text{Pa}$  then decays to  $^{232}\text{U}$ . Both production mechanisms require two neutron induced reactions and both have high neutron energy thresholds, so moderating the neutron spectrum before entering the fertile fuel reduces the  $^{232}\text{U}$  production as well as the fission rate.

ISOGEN computes the time-dependent concentrations of  $^{232}\text{Th}$ ,  $^{233}\text{U}$ ,  $^{232}\text{U}$ ,  $^{231}\text{Pa}$ ,  $^{233}\text{Pa}$ ,  $^{228}\text{Th}$ , and fission products. Other intermediate isotopes (e.g.,  $^{231}\text{Th}$ ,  $^{233}\text{Th}$ ,  $^{232}\text{Pa}$ ) have half-lives which are short compared with the irradiation time, so they are assumed to be in equilibrium with their parents and go directly to their longer-lived daughters in the calculation. Averaged isotopic transfer probabilities are input for relevant transfer mechanisms including nuclear reactions ( $\langle\sigma\phi\rangle \text{ s}^{-1}$ ), nuclear decays ( $(\lambda)\text{ s}^{-1}$ ) and continuous chemical removal of selected elements ( $(F\eta/I)\text{ s}^{-1}$ ) by the molten salt processing loop, as applicable. The reaction probabilities are computed from the average flux and activation rates in the blanket as calculated using the ANISN and TARTNP codes for neutron transport calculations.<sup>52,53</sup> The chemical processing transfer rates for the molten salt blanket are based upon the molten salt plant operating point. (See section VII.A.3.6)

### VII.C.2 Isotopic Considerations for the Reference Beryllium/Thorium Oxide Blanket

The time-dependent concentrations of several important isotopes were computed for the reference beryllium/thorium oxide blanket. In this analysis, a 1.8 month irradiation (at 70% capacity factor) was required to build up a fissile enrichment of 0.62 (54%  $^{233}\text{Pa}$ ). A 6 month delay was then allowed before reprocessing to permit most of the  $^{233}\text{Pa}$  present when irradiation was discontinued to decay to  $^{233}\text{U}$  (final  $^{233}\text{Pa}$  concentration of 0.003%). At the time of discharge from the reprocessing plant, uranium

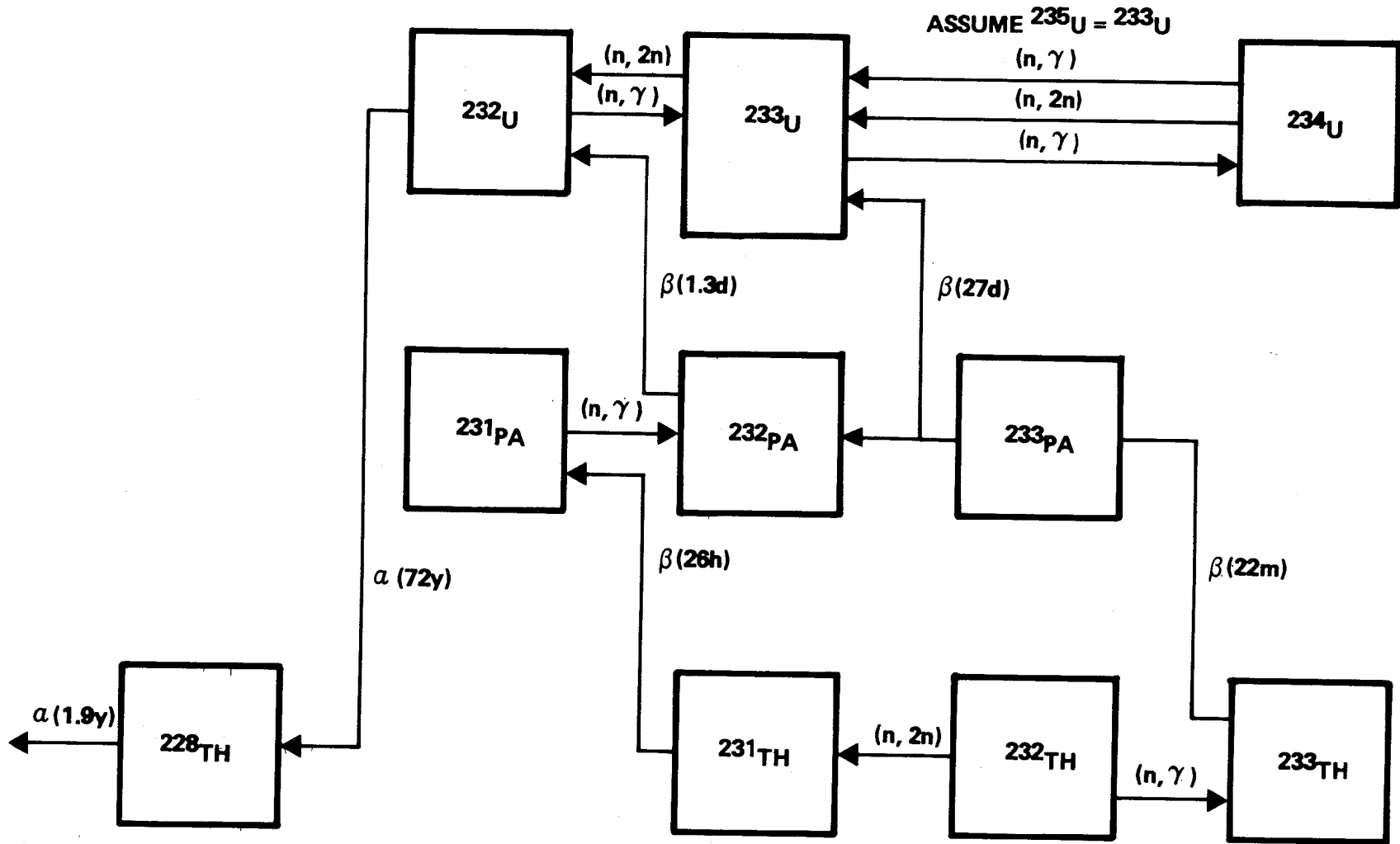


Figure VII.C-1. Production and decay chain for thorium fuel hybrid blankets.

isotopes and thorium isotopes were assumed to be partitioned from each other and the waste stream. Figure VII.C-2 shows the calculated buildup of various isotopes and fission products during the irradiation and 6 month decay period prior to reprocessing.

After reprocessing, the uranium fuel is assumed to be fabricated into LWR fuel. At the time of separation from the thorium isotopes, the uranium is relatively free of penetrating gamma activity and, therefore, relatively easily handled. As the  $^{228}\text{Th}$  buildup from the decay of  $^{232}\text{U}$ , there is a corresponding buildup of 2.6 MeV gamma activity which makes handling necessarily remote and well shielded. At the time of separation from the thorium, the uranium bred in the suppressed fission hybrid is composed of 99.98%  $^{233}\text{U}$  and 0.017%  $^{232}\text{U}$  (173 appm). Table VII.C-1 shows the buildup of  $^{228}\text{Th}$  in the uranium fuel as a function of time and the activity of the 2.6 MeV gamma in the fuel. The activity builds roughly linearly to 40  $\mu\text{Ci/g}$  of uranium in one month. An LWR fuel assembly contains about 12-14 kg of fissile fuel, so the 2.6 MeV gamma activity of a fuel assembly builds to about 0.5 Ci in the one month. Routine handling of this quantity of radioactivity requires remote techniques for shielding.

TABLE VII.C-1. Density of  $^{228}\text{Th}$  and associated 2.6 MeV gamma activity in bred  $^{233}\text{U}$  fuel.

Weeks From Separation	Density of $^{228}\text{Th}$ (appm)	2.6 MeV- $\gamma$ Activity ( $\mu\text{Ci/g-U}$ )
0.25	0.0080	2.31
0.5	0.0161	4.66
0.75	0.0241	6.97
1.0	0.0321	9.28
2.0	0.0642	18.6
4.0	0.1284	37.1
6.0	0.1926	55.7

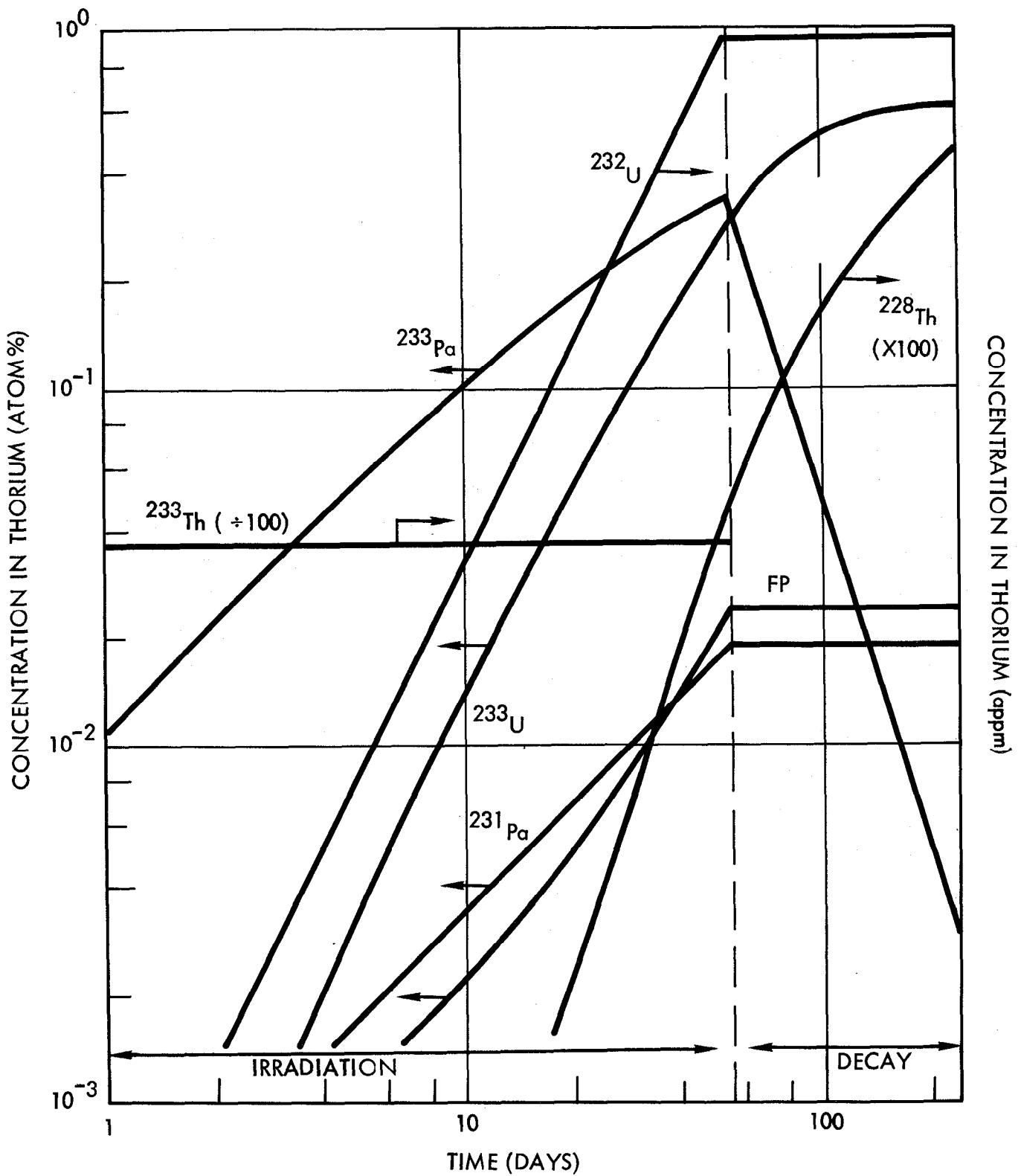


FIGURE VII.C-2. Concentration buildup of important isotopes and fission products during irradiation and six month cooling period for beryllium/thorium oxide blanket.

After reprocessing, the recovered thorium oxide may be stored to allow the  $^{228}\text{Th}$  and associated gamma activity to decay to levels where "hands-on" techniques for refabrication into TMHR fuel are possible. However, more detailed analysis is required to determine if such a procedure would be more economical than the use of remote handling or the simple disposal of the thorium. Table VII.C-2 shows the  $^{228}\text{Th}$  concentration and associated 2.6 MeV gamma activity in the thorium from the time of discharge from the reprocessing stream. The table gives only the  $^{228}\text{Th}$  bred in the hybrid, and not the natural occurrence of  $^{228}\text{Th}$  and other gamma activities associated with the natural decay chain of the fertile  $^{232}\text{Th}$  in the blanket.

TABLE VII.C-2. Radioactivity due to artificially produced  $^{228}\text{Th}$  in reprocessed thorium.

Time From Separation (Yrs)	Density of $^{228}\text{Th}$ (appm)	2.6 MeV- $\gamma$ Activity ( $\mu\text{Ci/g-Th}$ )
0	0.00464	1.334
0.25	0.00424	1.219
0.5	0.00387	1.113
0.75	0.00353	1.015
1.0	0.00322	0.926
2.0	0.00224	0.644
5.0	0.00075	0.216
10.0	0.00012	0.035
15.0	0.00002	0.006
Natural Thorium	0.000136	0.039

Table VII.C-3 gives the natural decay chain of  $^{232}\text{Th}$ . Besides having a constant 2.6 MeV gamma activity, other penetrating gammas are present due to the decay of  $^{228}\text{Ac}$  which is not present in the decay chain after  $^{228}\text{Th}$ . Computing the relative doses from the natural decay chain of  $^{232}\text{Th}$  and the

TABLE VII.C-3. Decay chain for natural thorium showing significant gamma lines and entry point from  $^{232}\text{U}$  decay.

HEAVY NUCLIDE DECAY CHAIN THORIUM SERIES (4n)				
NUCLIDE	ELEMENT NAME	HALF-LIFE	$\lambda$ ( $\text{s}^{-1}$ )	MAJOR GAMMA ENERGIES (MeV) AND INTENSITIES
$^{232}_{90}\text{Th}$	THORIUM - 232	$1.41 \times 10^{10} \text{ y}$	$1.56 \times 10^{-18}$	-----
$^{228}_{88}\text{Ra}$	RADIUM - 228	6.7y	$3.29 \times 10^{-9}$	-----
$^{228}_{89}\text{Ac}$	ACTINIUM - 228	6.13h	$3.14 \times 10^{-5}$	0.34 (15%) 0.908 (25%) 0.96 (20%)
$^{232}_{92}\text{U} \rightarrow ^{228}_{90}\text{Th}$	THORIUM - 228	1.9107	$1.15 \times 10^{-8}$	0.084 (1.6%) 0.214 (0.3%)
$^{224}_{88}\text{Ra}$	RADIUM - 224	3.64d	$2.20 \times 10^{-6}$	0.241 (3.7%)
$^{220}_{86}\text{Rn}$	RADON - 220	55s	$1.26 \times 10^{-2}$	0.55 (0.07%)
$^{216}_{64}\text{Po}$	POLONIUM - 216	0.15s	4.62	-----
$^{212}_{82}\text{Pb}$	LEAD - 212	10.64h	$1.81 \times 10^{-5}$	0.239 (47%) 0.300 (3.2%)
$^{212}_{83}\text{Bi}$	BISMUTH - 212	60.6m	$1.91 \times 10^{-4}$	0.040 (2%) 0.727 (7%) 1.620 (1.8%)
$^{212}_{84}\text{Po}$ (64.0%) $^{208}_{81}\text{Tl}$ (36.0%)	POLONIUM - 212	304ns	$2.28 \times 10^3$	-----
$^{208}_{81}\text{Tl}$	THALLIUM - 208	3.10m	$3.73 \times 10^{-3}$	0.511 (23%) 0.583 (86%) 0.860 (12%) 2.614 (100%)
$^{208}_{82}\text{Pb}$	LEAD - 208	STABLE		-----

hybrid produced  $^{228}\text{Th}$ , it appears the hybrid contributed dose is about equal to the natural dose after only about 10 years. This calculation is conservative since, in equilibrium, the natural chain has a 60% higher dose due to the  $^{228}\text{Ac}$  gammas. Therefore, storage of the reprocessed thorium for about 10-15 years would probably be satisfactory to allow use of whatever handling procedures were used initially for the natural thorium.

Also shown in Figure VII.C-2 is the equilibrium concentration of  $^{233}\text{Th}$  in the blanket. Since this isotope has a 22 m half-life, its concentration will quickly increase and decrease with the reactor operating power level. Therefore, while all other isotopic concentrations are calculated using the average plant capacity factor of 70%, the  $^{233}\text{Th}$  level is a conservative estimate based upon full power operation. This isotope is particularly important as it dominates the short term afterheat level in the blanket. The  $^{233}\text{Pa}$  ( $T_{1/2} = 27$  d) level is similarly important as it dominates the long term afterheat level.

Typical isotopic afterheat contributions for a beryllium/thorium oxide suppressed fission blanket (but not the reference blanket) are shown in Figure VII.C-3. As shown,  $^{233}\text{Th}$  dominates the afterheat for 0.7 hours,  $^{233}\text{Pa}$  dominates for the next 0.35 years, and fission products can be expected to dominate the afterheat only for longer periods. A more detailed discussion of afterheat safety considerations may be found in Chapter VI.

### VII.C.3 Isotopic Calculations for Reference Lithium/Molten Salt Blanket

Isotopic generation and depletion calculations for the fluorination only and full molten salt reprocessing modes were performed using the ISOGEN code. In both cases, the isotopic content of the blanket and primary loop was tracked over the 30 year operating life of the plant. The continuous removal of uranium and protactinium (as applicable) via reprocessing was also modeled. For this purpose, the process flow rates discussed in Section VII.A.3.b were used.

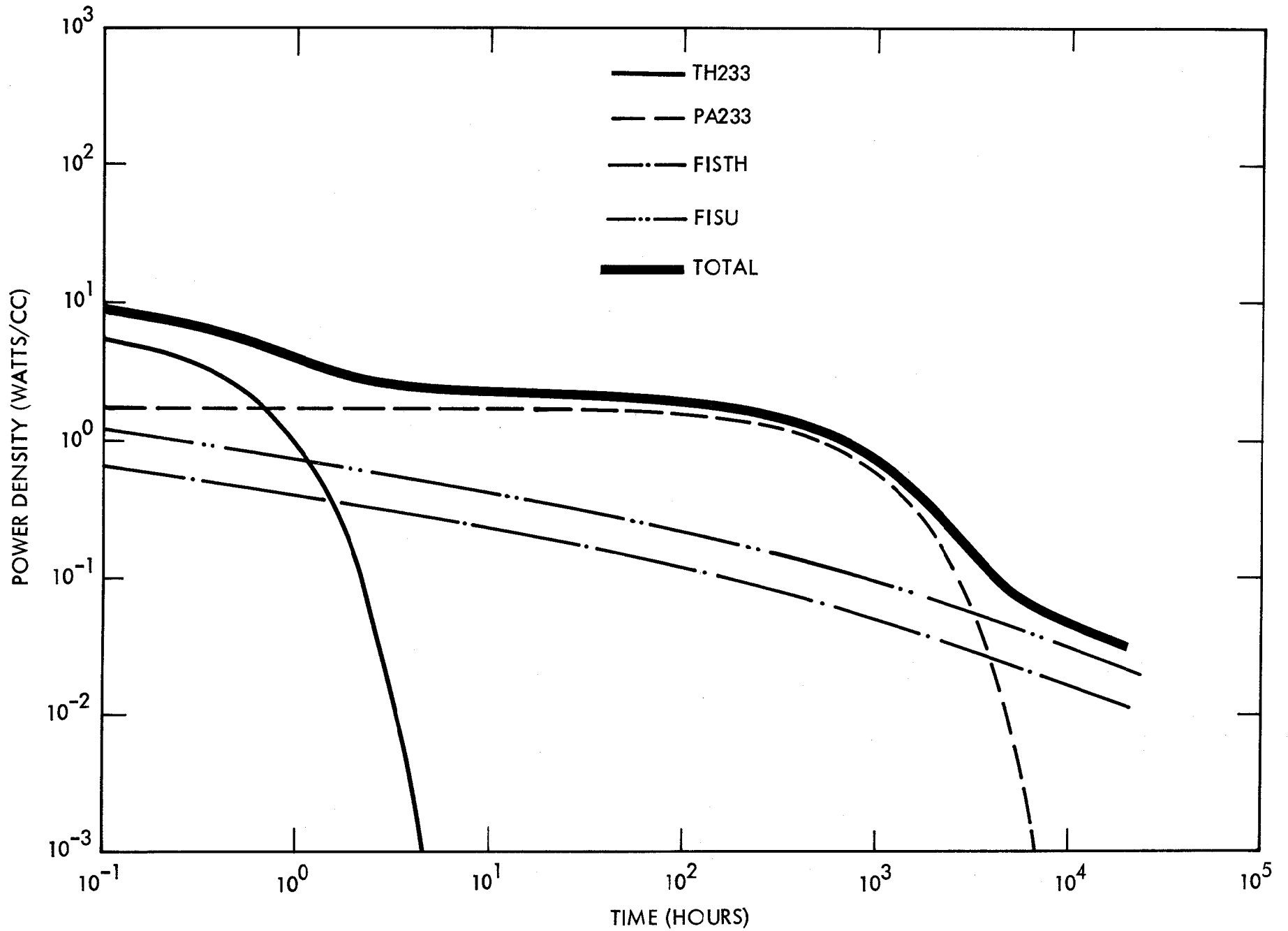


FIGURE VII.C-3. Typical suppressed fission blanket afterheat sources.

VII.C.3.a. Isotopics for Fluorination Only Reprocessing Mode. Figure VII.C-4 shows the calculated buildup of various isotopes and fission products during the 30 year plant lifetime. In this mode,  $^{233}\text{Pa}$  is not removed, but reaches its equilibrium concentration of 0.028% in thorium in only about 0.5 years. The  $^{233}\text{U}$  is removed, and its removal causes it to reach a process equilibrium concentration of about 0.11% in thorium in about 2 years. Concerning  $^{232}\text{U}$ , an equilibrium is almost attained in the 2-6 year period, but for later periods the  $^{232}\text{U}$  level continues to increase due to the continued buildup of  $^{231}\text{Pa}$  (see Figure VII.C-1) which is not removed. The  $^{232}\text{U}$  level after 30 years is  $3.28 \cdot 10^{-4}\%$  in thorium (3065 appm in  $^{233}\text{U}$ ). This level of  $^{232}\text{U}$  results in a  $^{228}\text{Th}$  level of 0.0823 appm in thorium. A maximum  $^{233}\text{Th}$  level of 0.23 appm in thorium was calculated based upon the assumption of short term operation (~several hours) at the full rated capacity of the plant (i.e., 100% plant factor).

Finally, a lumped estimate of fission product generation was made based upon the rate of  $^{232}\text{Th}$  and  $^{233}\text{U}$  fissions in the blanket. For the fluorination only process, the fission products accumulate linearly to a level of 0.24% in thorium in 30 years. However, it should be noted that this calculation does not account for losses of gaseous fission products which are not retained by the fuel. Also, since these fission products accumulate over the life of the plant (rather than during a short period as in an LWR) the associated radiological hazard is expected to be greatly reduced relative to that of the same quantity of "fresh" fission products. The particular makeup of these species is, however, unknown and this topic requires further investigation.

Since thorium recycle is continuously accomplished in the molten salt system, the principal isotopic issue associated with this blanket is the  $^{232}\text{U}$  level in the bred  $^{233}\text{U}$  discharged from the molten salt reprocessing plant. As shown in Table VII.C-4, the  $^{232}\text{U}$  discharge level increases during the plant lifetime to a level of 2400 appm after 30 years. The principal cause of this increase is an increasing  $^{232}\text{U}$  level in the molten salt primary loop (see Figure VII.C-4) which, in turn, results from a continuous buildup of  $^{231}\text{Pa}$  in the system.

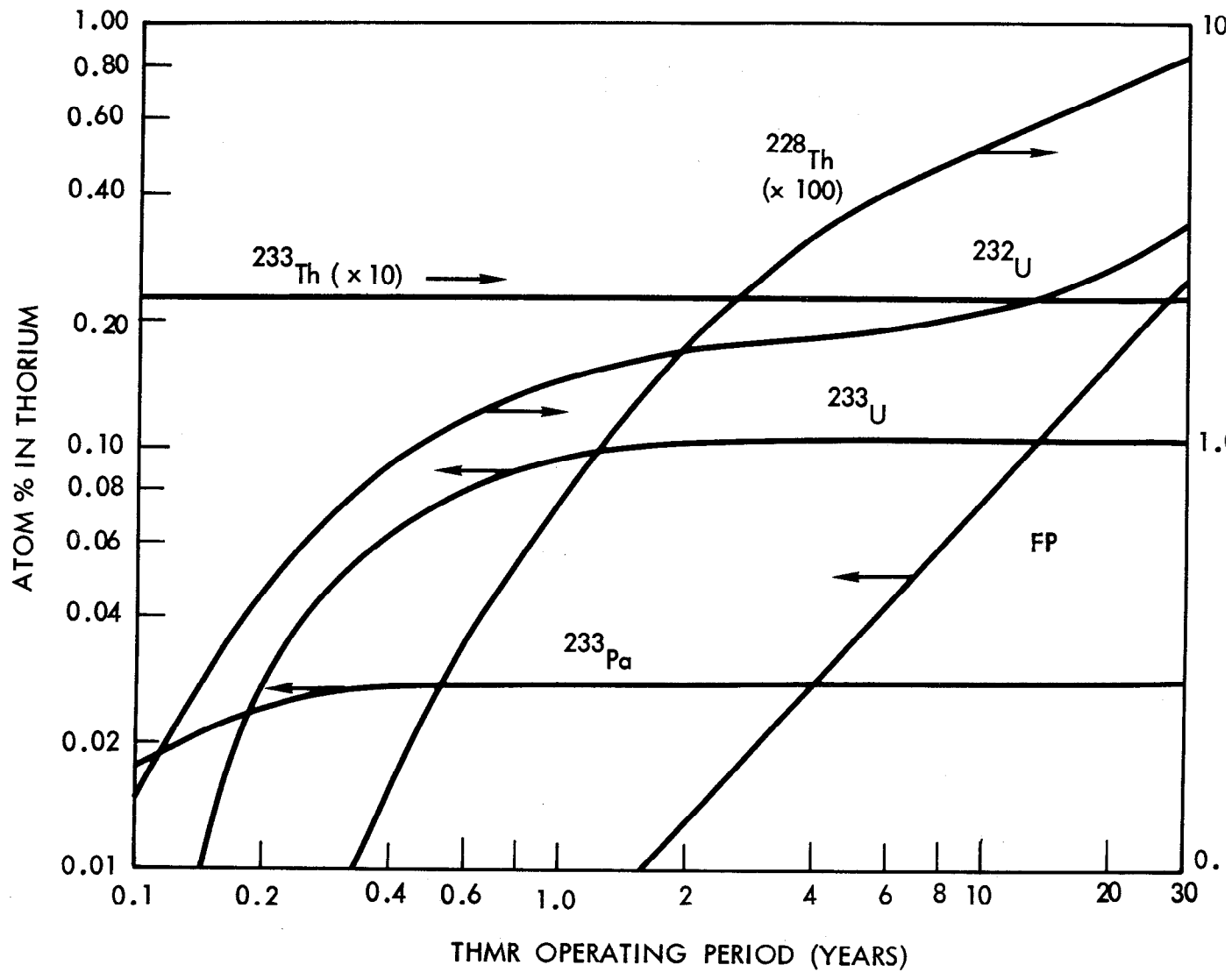


FIGURE VII.C-4. Isotopic generation in the molten salt blanket TMHR for fluorination only

TABLE VII.C-4.  $^{232}\text{U}$  discharge concentrations in  $^{233}\text{U}$  for the molten salt reprocessing plant.

<u>Year</u>	<u>Concentration (appm)</u>	
	<u>Fluorination Only</u>	<u>Full Processing</u>
5	1600	1250
10	1770	1250
15	1950	1250
20	2120	1250
25	2270	1250
30	2400	1250

Since the  $^{232}\text{U}$  level above is considerably higher than the  $^{232}\text{U}$  level discharged from the beryllium/thorium oxide system (175 appm in  $^{233}\text{U}$ ), the concerns related to shielding requirements for LWR fuel fabrication will be magnified. In particular, the results given in Table VII.C-1 would be multiplied by a factor of 13.9 for the molten salt blanket with fluorination only.

VII.C.3.b. Isotopics For Full Reprocessing Mode. Figure VII.C-5 shows the calculated buildup of various isotopes and fission products during the 30 year plant lifetime. In comparison with the fluorination only mode of fuel processing, the full processing option can remove protactinium and (possibly) some fission products from the primary molten salt loop. This results in the following features relating to isotopic generation:

- The equilibrium  $^{233}\text{Pa}$  level in the primary molten salt loop is about 20% lower.
- $^{231}\text{Pa}$  equilibrates in about 3 years to a 0.002% level in thorium. This results in lower  $^{232}\text{U}$  and  $^{228}\text{Th}$  generation.

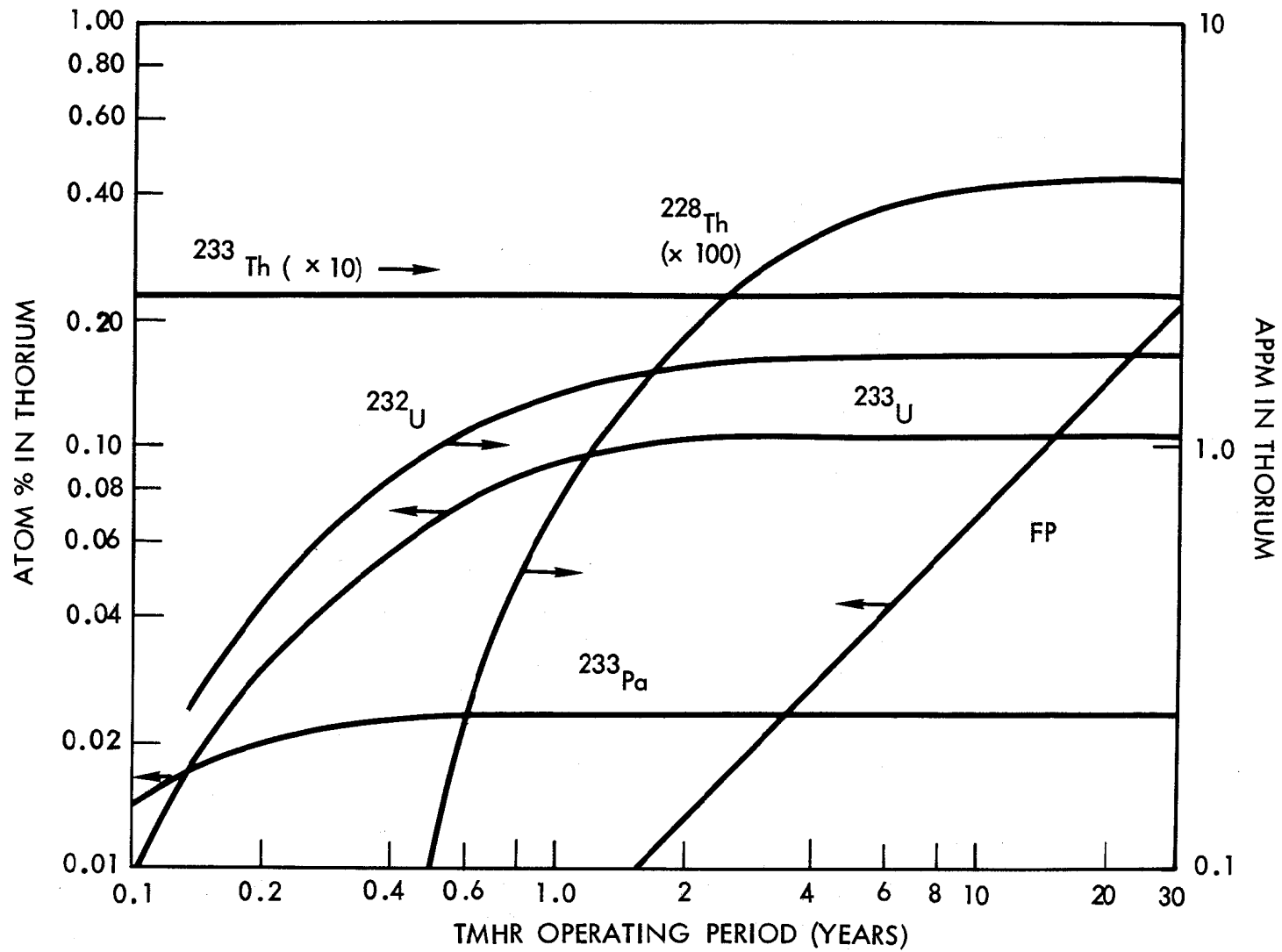


FIGURE VII.C-5. Isotopic generation in the molten salt blanket for full reprocessing mode.

• Fission product concentrations in the primary loop can, at most, be reduced about 10%. This results because the low rare earth fission product extraction efficiency (assumed to be 0.004) as well as the fission rate are both quite low. Since fission product removal requires a more sophisticated molten salt process with more required development (see section VII.B.2.C), this option has not been pursued.

As a result of  $^{231}\text{Pa}$  control for this process,  $^{232}\text{U}$  concentrations is the bred  $^{233}\text{U}$  are expected to be reduced up to 50% over the life of the plant (see Table VII.C-4). However, the calculated  $^{232}\text{U}$  levels are still about 7 times higher than those of the beryllium/thorium oxide blanket. Further reductions might be achieved by increasing the molten salt processing rate to further reduce the levels of  $^{231}\text{Pa}$  and  $^{233}\text{U}$  (both are parents of  $^{232}\text{U}$ ), by reducing the molten salt inventory in the primary loop by the use of reflector materials (e.g., graphite), and by the use of a thicker multiplier region to further soften the neutron energy spectrum. Further studies are required to determine realistic goals with respect to tolerable levels of  $^{232}\text{U}$  which reflect practical considerations regarding remote and shielded fuel fabrication activities.

## VII.D. CONCLUSIONS

### VII.D.1. Fuel Reprocessing Costs

Commercial introduction of the TMHR will certainly be paced by the price of bred fissile fuel as compared with the price of natural uranium ores. Since the bred fuel cost is substantially influenced by the cost of extracting the fissile fuel from the hybrid fertile fuel, reprocessing costs can be a major determinant in the viability of the suppressed fission hybrid. Our results indicate that acceptable fuel cycle costs (consistent with the timeframe for the development of commercial fusion applications and the depletion of inexpensive sources of natural uranium) appear possible.

Table VII.D-1 compares reprocessing costs for the thorium metal, oxide, and salt cases. The unit costs to reprocess thorium oxide fuels using the THOREX process are expected to be most expensive (28-42 \$/gm) while the cost to reprocess thorium metal fuels is expected to be significantly less (23 \$/gm) and the expected cost of molten salt reprocessing (2-4 \$/gm) is greatly reduced when compared with the other options. For the reference lithium/molten salt and beryllium/thorium oxide blankets, the fraction of the overall levelized bred fuel cost (see Chapter IX) attributable to reprocessing is 1.15% and 30% (worst case), respectively. The low cost of molten salt reprocessing is a significant economic advantage, but molten salt technology is less developed than the THOREX-based options and has a greater impact upon the blanket design itself (i.e., materials issues and design fixes to circumvent such issues).

### VII.D.2 Isotopic Considerations

The quality of bred fuel and the effect upon fuel cycle costs depends on the concentrations of contaminant isotopes. A previous study of the quality of hybrid produced fuel suggested that  $^{233}\text{U}$  production was unattractive because of the high  $^{232}\text{U}$  concentrations.<sup>54</sup> Figure VII.D-1 compares the  $^{232}\text{U}$  concentrations in hybrid bred  $^{233}\text{U}$  between the fast fission and suppressed fission cases. As shown, each of the suppressed

TABLE VII.D-1. Comparative results for various fuel forms and reprocessing technologies.

	Fuel Type/Reprocessing Option			
	Thorium Metal	Thorium Oxide	Reference Molten Salt <sup>b</sup>	Molten Salt with Pa Recovery
Total fissile discharge assay in thorium <sup>a</sup>	0.55%	0.55%	0.14%	0.13%
Uranium discharge assay in thorium	0.25%	0.25%	0.11%	0.11%
Process rate, MT/yr	1200	1200	5440	3160
Levelized cost per Kg thorium	\$127	\$152-233	\$1.59	\$5.06
Levelized cost per gm uranium	\$23	\$28-42	\$1.93	\$3.90

<sup>a</sup>Uranium plus protactinium.

<sup>b</sup>For this system only uranium is recovered and recovery efficiency is 75%. So cost per gram =  $1.59 / (1.1 \cdot 0.75) = 1.93$  \$/gm.

fission cases results in a lower <sup>232</sup>U concentration than the fast fission case of equivalent fissile discharge enrichment - a factor of 45 lower for the reference beryllium/thorium oxide blanket.

Reference 54 suggests that for <sup>232</sup>U concentration below ~ 400 appm, shielding and remote handling requirements may be reduced, and that up to 1200 appm the technology developed for HTGR reprocessing applies. If this assertion is correct, the discharge fuel from the reference beryllium/thorium oxide blanket would not require fully shielded fabrication facilities with remote handling and the discharge fuel from a lithium/molten salt blanket with a molten salt process to remove both uranium and protactinium could utilize already developed HTGR fuel fabrication technology.

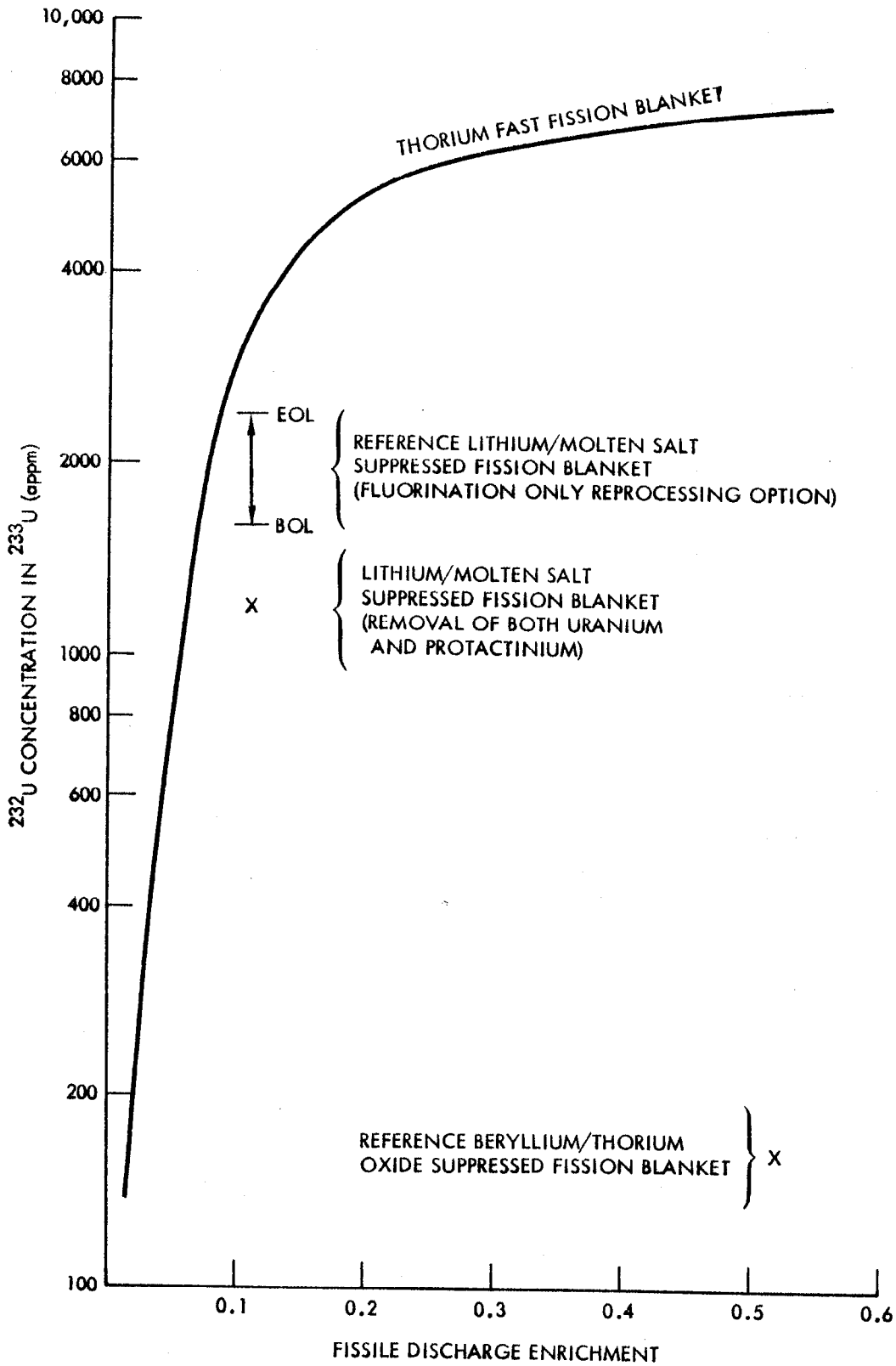


FIGURE VII.D-1. Comparison of  $^{232}\text{U}$  generation for fast and suppressed fission blankets.

In contrast, for the molten salt blanket with uranium recovery only (the reference reprocessing option for this blanket), the expected  $^{232}\text{U}$  levels are higher than 1200 appm (i.e., 1600-2400 appm) an increase over the life of the plant due to the accumulation of  $^{231}\text{Pa}$  in the blanket (see Section VII.C.3.a). The impact of these  $^{232}\text{U}$  generation levels is unknown and further studies are required.

Concerning the buildup of  $^{228}\text{Th}$  activity in fertile thorium to be refabricated and recycled back to the blanket following reprocessing and recovery of the bred fissile fuel, we have shown (in Section VII.C.2) that a 10-15 year cooling period will suffice to reduce the radioactivity level below the natural background level associated with unirradiated thorium. This concern is irrelevant to the molten salt blanket since these systems avoid fuel fabrication steps. Its impact on fuel fabrication for the thorium oxide blanket is unknown, but the worst case (i.e., 15 years cooling), is not prohibitive.

### VII.D.3. Proliferation Resistance

Diversion or proliferation resistance is an issue of some interest and the hybrid offers unique features in this respect. For example, the 2.6 MeV gamma associated with the  $^{232}\text{U}$  decay chain is always present in some quantity and we can consider some amount to be beneficial. Hopefully, the suppressed fission hybrid will have enough penetrating gamma to afford some degree of proliferation resistance without requiring excessive shielding. The presence of penetrating radioactivity in the fissile fuel makes the diversion of the fuel difficult, provided the activity is high enough to require remote handling while moving the fuel assemblies and removing the fissile material. Diversion resistance due to high radioactivity is not considered to render the fuel proliferation-proof, so isotopic denaturing and institutional safeguards are still desirable for proliferation-resistance.  $^{232}\text{U}$  can be isotopically denatured by the addition of  $^{238}\text{U}$  in the fabricated fuel. If the uranium contains less than 20% fissile isotopes, it is considered to be isotopically denatured.<sup>4,55</sup> Fabricated fuel for use in LWRs could contain 3%  $^{233}\text{U}$  and a minimum of 18%  $^{238}\text{U}$  and be considered denatured. The remaining 79% of the fuel could be either  $^{238}\text{U}$  or  $^{232}\text{Th}$ .

Fuel containing 79% thorium might be desirable because it would convert thorium to  $^{233}\text{U}$ , which would be isotopically denatured in the spent fuel. The  $^{238}\text{U}$  will convert to  $^{239}\text{Pu}$  which is not isotopically denatured in the spent fuel. While some  $^{239}\text{Pu}$  will be bred in both fuel types, about seven times as much will be bred in the 97%  $^{238}\text{U}$  fuel. If  $^{239}\text{Pu}$  can be burned only in safeguarded reactors, then it may be advantageous to breed the minimum amount of  $^{239}\text{Pu}$ .

One advantage of the 3%  $^{233}\text{U}$ , 97%  $^{238}\text{U}$  fuel is that the reprocessing of  $\text{UO}_2$  is easier, less expensive, and a better established technology than reprocessing  $\text{ThO}_2$ . Thorium oxide is difficult to dissolve and requires the addition of corrosive fluorine which increases the cost of reprocessing (see Section VII.B). Also, this denatured fuel cycle option provides an additional margin of denaturing for the fresh fuel charged to the LWR. Fusion fuel factories, distributed LWRs, and safeguarded plutonium burners will require tradeoff analyses of reprocessing economics and proliferation-resistance.

## REFERENCES FOR SECTION VII

1. K. R. Schultz, et.al., "A U-233 Fusion—Fission Power System Without Reprocessing", GA-A14635, General Atomic Co. (1977).
2. R. W. Conn, et.al., "SOLASE-H:A Laser Fusion Hybrid Study", UWFD-270, University Wisconsin (1979).
3. Exxon Nuclear Co., Inc., "The Economics of Reprocessing Alternative Nuclear Fuels," ORNL/Sub-7501/4, Oak Ridge National Laboratory (1979).
4. Y. I. Chang, et.al., "Alternative Fuel Cycle Options: Performance Characteristics and Impact on Nuclear Power Growth," ANL-77-70, Argonne National Laboratory (1977).
5. "Nuclear Proliferation and Civilian Nuclear Power: Report of the Nonproliferation Alternative Systems Assessment Program," DoE/NE-0001, U. S. Department of Energy (1979).
6. J. A. Maniscalco, et.al., "Laser Fusion Breeder Design Study Final Report," DoE contract DE-AC08-79DP40-11, TRW (1980).
7. Allied-General Nuclear Services, Barnwell Nuclear Fuel Plant Final Safety Analysis Report, Docket #50-332 (1973).
8. U.S. DoE, "Barnwell Nuclear Fuels Plant Applicability Study," DoE/ET/0040/3, Washington, D.C. (1978).
9. Exxon Nuclear Co., Inc., "Nuclear Fuel Recovery and Recycling Center Preliminary Safety Analysis Report," Docket #50-564 (1977).
10. Burns and Roe Industrial Services Corp., International Fuel Service Center Study, Burns and Roe Industrial Services Corp., Paramus, NJ (1978).
11. Oak Ridge National Laboratory and Bechtel National, Inc., "Hot Experimental Facility Interim Design Report," ORNL/AFRJP-78/6 Oak Ridge National Laboratory (1978).
12. D. H. Berwald and J. A. Maniscalco, "An Economics Method for Symbiotic Fusion-Fission Electricity Generation Systems," Nuclear Technology/Fusion, 1 128 (1981)
13. E. T. Cheng, General Atomic Company, TMHR Monthly Technical Report, May 1981.

14. M. W. Rosenthal, P. N. Haubenreich, and R. B. Briggs, The Development Status of Molten Salt Breeder Reactors, ORNL-4812 (August 1972).
15. L. E. McNeese, Editor, Program Plan for Development of Molten Salt Breeder Reactors, ORNL-5018 (December 1974).
16. R. C. Robertson, Editor, Conceptual Design Study of a Single-Fluid Molten-Salt Breeder Reactor, ORNL-4541 (June 1971)
17. W. R. Grimes, "Molten Salt Reactor Chemistry," Nuclear Applications and Technology 8, 137 (February 1970)
18. G. J. Nessel and W. R. Grimes, Chemical Engineering Progress Symposium Series, 56, 28 (1960)
19. E. R. Grimes, "Materials Problems in Molten Salt Reactors," in Materials and Fuels for High Temperature Nuclear Energy Applications, M.T. Simnad and L. R. Zumwalt, Editors, The M.I.T. Press, Mass. (1964).
20. J. H. Shaffer, Preparation and Handling of Salt Mixtures for the Molten-Salt Reactor Experiment, ORNL-4616 (January 1971).
21. J. R. Engel et.al., Conceptual Design Characteristics of a Denatured Molten-Salt Reactor with Once-Through Fueling, ORNL/TM-7207 (July 1980).
22. E. L. Compere et.al., Fission Product Behavior in the Molten Salt Reactor Experiment, ORNL-4865 (October 1975).
23. W. R. Grimes, "Chemical Basis for Molten Salt Reactors," Molten-Salt Reactor Program, Semiannual Progress Report for Period Ending July 31, 1964, ORNL-3708, p. 214.
24. C. F. Baes, Jr., "The Chemistry and Thermodynamics of Molten Salt Reactor Fuels," J. Nuclear Materials, 51 (1), (May 1974).
25. W. R. Grimes, N. V. Smith, and G. M. Watson, "Solubility of Noble Gases in Molten Fluorides. 1. In Mixtures of NaF-ZrF<sub>4</sub> (53-47 mole %) and NaF-ZrF<sub>4</sub>-UF<sub>4</sub> (50-46 mole %)," J. Phys. Chem. 62, 862 (1958).
26. G. M. Watson, W. R. Grimes, and N. V. Smith, Solubility of Noble Gases in Molten Fluorides. In Lithium-Beryllium Fluoride," J. Chem. Eng. Data 7, 285 (1962).
27. P. N. Haubenreich and J. R. Engel, "Experience with the Molten Salt Reactor Experiment," Nuclear Applications and Technology, 8, 118 (February 1980).

28. D. Scott and W. P. Eatherly, "Graphite and Xenon Behavior and Their Influence on Molten-Salt Reactor Design," Nuclear Applications and Technology, 8, 179 (1970)
29. E. S. Bettis and R. C. Robertson, "The Design and Performance Features of a Single-Fluid Molten Salt Breeder Reactor," Nuclear Applications and Technology, 8, 190 (1970)
30. A. M. Perry and H. F. Bauman, "Reactor Physics and Fuel Cycle Analysis," Nuclear Applications and Technology, 8, 208 (1970).
31. H. E. McCoy, Jr. and B. McNabb, Integranular Cracking of INOR-8 in the MSRE, ORNL-4829 (November 1972)
32. H. E. McCoy, Jr., Status of Materials Development for Molten Salt Reactors, ORNL/TM-5920 (January 1978)
33. D. L. Manning and G. Mamantov, "Electrochemical Studies of Tellurium in Molten  $\text{LiF}-\text{BeF}_2-\text{ThF}_4$  (72-16-12 mole %)," Molten Salt Reactor Program Semiannual Progress Report for Period ending February 29, 1976, ORNL-5132, p. 38.
34. J. R. Keiser, Status of Tellurium-Hastelloy-N Studies in Molten Fluoride Salts, ORNL/TM-6002 (October 1977).
35. L. E. McNeese, Engineering Development Studies for Molten Salt Breeder Reactor Processing, No. 8, ORNL/TM-3528 (May 1972)
36. W. L. Carter and E. L. Nicholson, Design and Cost Study of a Fluorination-Reductive Extraction-Metal Transfer Processing Plant for the MSBR, ORNL/TM-3579 (May 1972).
37. R. B. Lindauer, Processing of the MSRE Flush and Fuel Salts, ORNL/TM-2578 (August 1969).
38. J. H. Shaffer, W. R. Grimes, F. A. Boss, W. K. R. Finnell, and W. P. Teichert, Reactor Chemistry Division Annual Progress Report, December 31, 1965, ORNL-3913, p. 42.
39. J. H. Shaffer, W. P. Teichert, D. M. Moulton, F. F. Blankenship, W. K. R. Finnell, and W. R. Grimes, Reactor Chemistry Division Annual Progress Report, December 31, 1966, ORNL-4076, pp. 34-6.

40. L. M. Ferris, J. F. Land, J. J. Lawrence, and C. E. Schilling, Molten-Salt Reactor Program, Semiannual Progress Report, February 29, 1968, ORNL-4254, pp. 241-47.
41. L. M. Ferris, J. C. Mailen, E. D. Nogueira, D. E. Spangler, J. J. Lawrence, J. F. Land, and C. E. Schilling, Molten Salt Reactor Program, Semiannual Progress Report, August 31, 1968, ORNL-4344, pp 292-97.
42. L. M. Ferris, J. C. Mailen, J. J. Lawrence, F. J. Smith, and E. D. Nogueira, Trans. Am. Nucl. Soc. 12, 26 (1969).
43. L. M. Ferris, J. C. Mailen, J. J. Lawrence, F. J. Smith, and E. D. Nogueira, J. Inorg. Nucl. Chem., 32, 2019 (1970)
44. J. F. Smith and L. M. Ferris, Molten Salt Reactor Program, Semiannual Progress Report for Period Ending February 28, 1969, ORNL-4396, p. 285.
45. L. M. Ferris, F. J. Smith, C. T. Thompson, and J. F. Land, Molten Salt Reactor Program, Semiannual Progress Report for Period Ending February 28, 1970, ORNL-4558, p. 389.
46. L. M. Ferris, F. J. Smith, J. C. Mailen, and M. J. Bell, J. Inorg. Nucl. Chem., 34, 2921 (1972).
47. L. E. McNeese, Engineering Development Studies for Molten Salt Breeder Reactor Processing, No. 5, ORNL-TM-3140 (October 1970).
48. L. E. McNeese, Engineering Development Studies for Molten Salt Breeder Reactor Processing, No. 8, ORNL-TM-3258 (May 1972).
49. G. T. Mays, Molten Salt Reactor Program. Semiannual Progress Report for Period Ending February 28, 1975, ORNL-5047, p. 8.
50. G. T. Mays, A. N. Smith, and J. R. Engel, Distribution and Behavior of Tritium in the Coolant-Salt Technology Facility, ORNL/TM-5759 (April 1977).
51. M. J. Bell, "ORIGEN - The ORNL Isotope Generation and Depletion Code," ORNL-4628, Oak Ridge National Laboratory (1973).
52. W. W. Engle, Jr., "ANISN: Multigroup One Dimensional Discrete Ordinates Transport Code with Anisotropic Scattering," K-1693, Oak Ridge National Laboratory (1967).

53. R. J. Howerton, et.al., "An Integrated System for Protection of Neutronics and Photonics Constants," UCRL-50400, Vol. 14, Lawrence Livermore National Laboratory (1976).
54. B. R. Leonard and U. P. Jenquin, "The Quality of Fissile Fuel Bred in a Fusion Reactor Blanket," BNWL-SA-5750, presented at 2nd ANS Topical Meeting on Controlled Nuclear Fusion, September 1976.
55. T. H. Pigford, et.al., "Denatured Fuel Cycles for International Safeguards," Nuclear Technology, 41, 46 (1978).



CHAPTER VIII  
TMHR PLANT DESCRIPTION

VIII.A OVERVIEW OF TMHR MODELING

A principal result of the Tandem Mirror Hybrid Reactor (TMHR) design study has been the development of two suppressed fission hybrid reactor designs based upon the lithium/molten salt and beryllium/thorium oxide breeding blankets discussed in Chapters IV, V, VI, and VII. As part of the design process detailed information has been developed for each of the two reference design concepts. Performance and cost parameters, describing the two design concepts, are presented in this chapter.

Two computer models were used to generate the tandem mirror hybrid reactor performance and cost data. The first of these, the LLNL Tandem Mirror Physics Code (TMPC),<sup>1</sup> was used to estimate the fusion and injected power flow and the central cell configuration given the fusion power, neutron wall loading, end plug configuration and other quantities. The fusion power flow and configuration are input to the Tandem Mirror Reactor Design Code (TMRDC)<sup>2</sup> which, in turn, provides estimates of the plant capital cost as well as power flow parameters associated with the fusion driver, first wall/blanket/shield, power conversion, and balance of plant systems. TMRDC was developed as part of the EPRI-sponsored "Preliminary Feasibility Assessment of Fusion-Fission Hybrids"<sup>2</sup> and has been modified during the TMHR study to better represent the two reference blanket concepts and their power conversion systems. The original plasma engineering model was removed from TMRDC, as this function is now provided by TMPC.

The TMRDC cost and performance estimates, which relate to a tenth-of-a-kind commercial fusion facility, are highly uncertain. Therefore, these estimates are represented to be reasonable rather than correct in an absolute sense. An attempt to quantify the sensitivities of important derived parameters with respect to major uncertainties has been made and extensive parametric results are presented in Chapter IX.

## VIII.B FUSION SYSTEM DEFINITION

### VIII.B.1 Plasma Engineering Basis

The plasma engineering model used to estimate the performance of the tandem mirror fusion driver for both reference design concepts is based upon the Axi-Cell end plug configuration with 20 tesla hybrid barrier coils and a central cell plasma  $\beta$  of 70%. The later quantity is limited by interchange MHD stability considerations. The fusion physics basis is discussed in more detail in Chapter II. An artists conception of the Axi-Cell configuration is shown in Figure VIII.B-1. The end plugs themselves are rather complex, but in comparison with other magnetic fusion options, the linear central cell of the tandem mirror reactor provides distinct advantages with respect to nuclear design, operation and maintenance of the blanket modules, and layout of the energy transport system and the reactor building. The linear blanket geometry, combined with the low (3 Tesla) central cell field, allows the use of efficient liquid metal coolants which might not be desirable in other fusion systems.

Although the two blanket module designs presented in Chapters IV and V were based upon a 2 m first wall radius (and a  $2 \text{ MW/m}^2$  neutron wall loading) as a design basis, a 1.5 m first wall radius was chosen for the reference plant designs. The choice of a lower wall radius resulted arbitrarily because a detailed end plug magnet configuration had been previously developed for a 1.5 m radius<sup>3</sup> while none existed for the 2 m radius. As a result of the decrease in wall radius, the central cell length was increased from 97 m to 129 m. The length of the end cell magnet configuration is 40 meters.

A summary of the fusion driver power flow data, as generated by TMPC and input to TMRDC, is shown in Table VII.B-1.

VIII-3

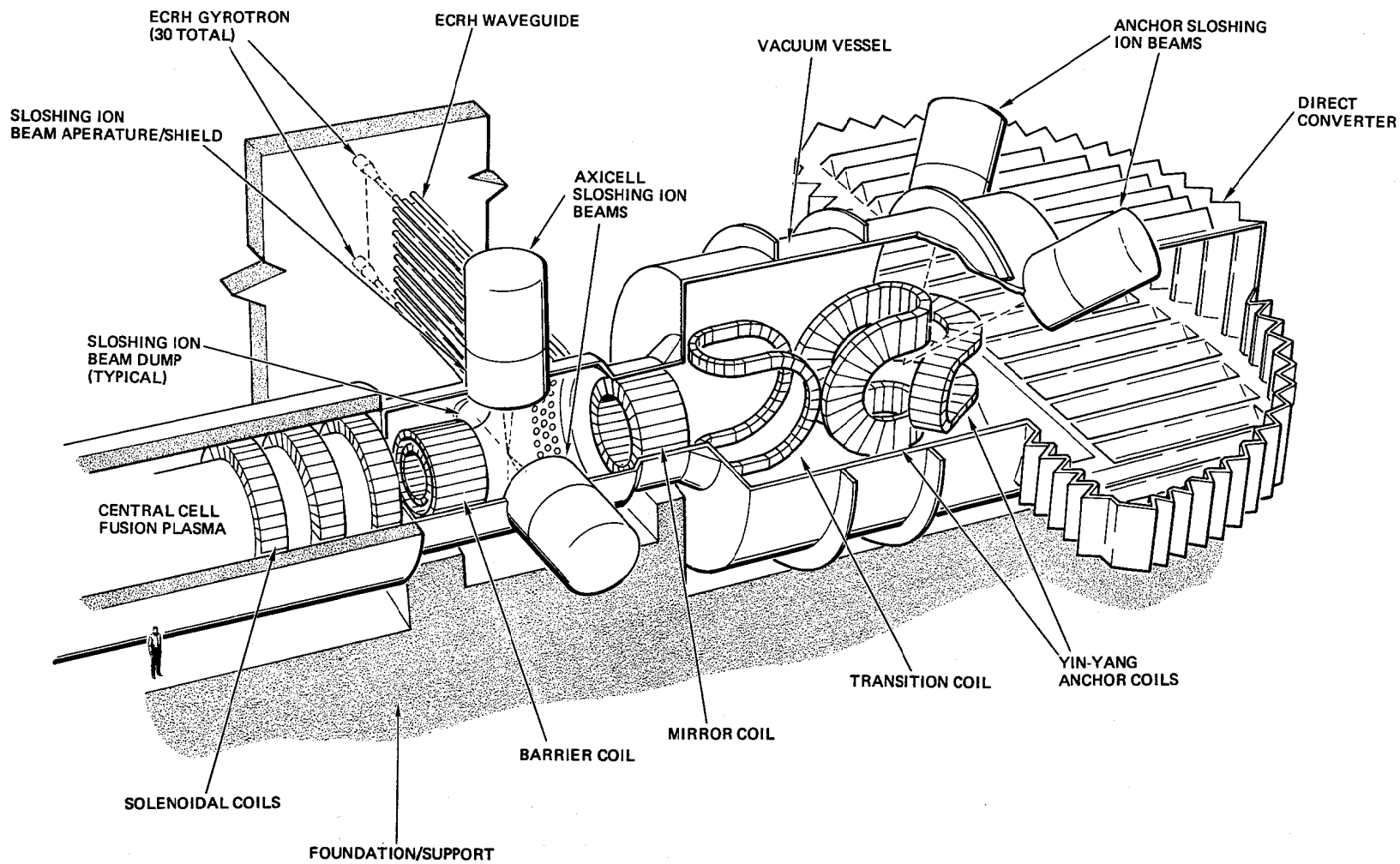


FIGURE VIII.B-1. Tandem mirror reactor axi-cell configuration.

TABLE VII.B-1. Fusion plasma power flow data.

Fusion power	3000 MW
Plasma Q <sup>a</sup>	15.3
Net injected power absorbed in plasma	196 MW
Net injected power trapping fraction	0.605
Gross injected power	324 MW
RF heating power	59 MW
Neutral beam power	265 MW
Neutron wall loading	2.0 MW/m <sup>2</sup>

<sup>a</sup> 20T barrier coil in axi-cell configuration with 1.5 m first wall radius and 129 m central cell length

#### VIII.B.2 Fusion Component Technologies Performance and Cost Basis

The estimated performance and cost of a TMHR plant is largely dependent upon assumptions concerning several key fusion subsystems: neutral beams, microwave (rf) heating systems, magnets, and direct energy conversion systems. In this section we summarize the fusion component performance and cost parameters used in our analysis and discuss the motivation leading to their choice. As mentioned above, these parameters reflect the performance and present dollar cost of fusion component technologies to be used in a 10<sup>th</sup> of a kind facility which might operate during the 2025-30 timeframe. The reader is referred to Chapters III and IX for a more complete discussion of the fusion component technologies and an analysis of the sensitivities in overall performance to uncertainties in the cost and performance of the various subsystems.

Our assumptions regarding the fusion subsystem efficiencies and direct cost parameters are presented in Tables VIII.B-2 and VIII.B-3 respectively. The variations shown in these tables indicate a reasonable range of eventual outcomes for specific subsystems.

TABLE VIII.B-2. Fusion component power flow parameters.

	Base	(Variations)
Neutral beam wall plug efficiency	0.60	(.30 to .80)
Fraction of unconverted neutral beam thermal power input to thermal converter power cycle	0.70 <sup>a</sup>	(0.0)
RF wall plug efficiency	0.50	(.3 to .6)
Fraction of unconverted RF thermal power input to thermal converter power cycle	0.70 <sup>a</sup>	(0.0)
Plasma dump direct conversion efficiency	0.50	(.35 to .65)
Fraction of unconverted plasma dump thermal power input to thermal converter power cycle	0.50 <sup>a</sup>	(0.0)
Auxiliary electric power as fraction of fusion power	0.0433 <sup>b</sup>	

<sup>a</sup> Thermal power assumed to be extracted at  $\sim 500^{\circ}\text{C}$  to enable efficient conversion to electricity

<sup>b</sup> Principal component is  $100 \text{ MW}_e$  for resistive power losses ( $I^2R$ ) in copper barrier coil at 20 Tesla

TABLE VIII.B-3. Fusion component direct cost parameters

	BASE	(VARIATIONS)
End cells (magnets, vessel, shielding), M\$	392	(+ 50%)
Neutral beam system, \$/W-output	1.5	(1 - 2)
RF system, \$/W-output	3	(1 - 5)
Central cell magnet system, M\$	141 <sup>a</sup>	(+ 25%)
Leakage plasma dump system (includes vacuum vessel, direct converter and pumping system), \$/W-input	0.13	(+ 50%)
Other (unspecified) costs, M\$	50	(+ 50%)

<sup>a</sup> Westinghouse contributed model with  
 conductor cost, \$/kg 50  
 structure cost, \$/kg 25

The neutral beam system performance estimates are based on projections made in Ref. 4 and the projections of beam line efficiencies for developed systems are summarized in Figure VIII.B-2 (a reproduction of Figure 14 of Ref. 4). Our base case assumes negative-ion beams at 60% (ave.) efficiency while our low technology case is based on a positive-ion system operating at 200 keV with 35% efficiency. A base case of 60% is conservative in that the predicted average efficiency is 77% (from Section III.A.1) where total injected power is 308 MW and total input (electric) power is 400 MW. The fraction (0.7) of unconverted neutral beam system thermal power available for thermal conversion to electricity (ie.,  $0.7 \times (1 - \eta_{nb})$  x electric power to drive neutral beams) is an educated guess. (5)

The motivation for using an RF system efficiency of 50% is discussed in Section III.A.1. The useful thermal fraction of 0.7 for the RF system was arbitrarily set to the neutral beam value.

Plasma dump system performance parameters are discussed in detail in Section III.A.4. The 50% efficiency value is based on results of the analysis discussed in that section.

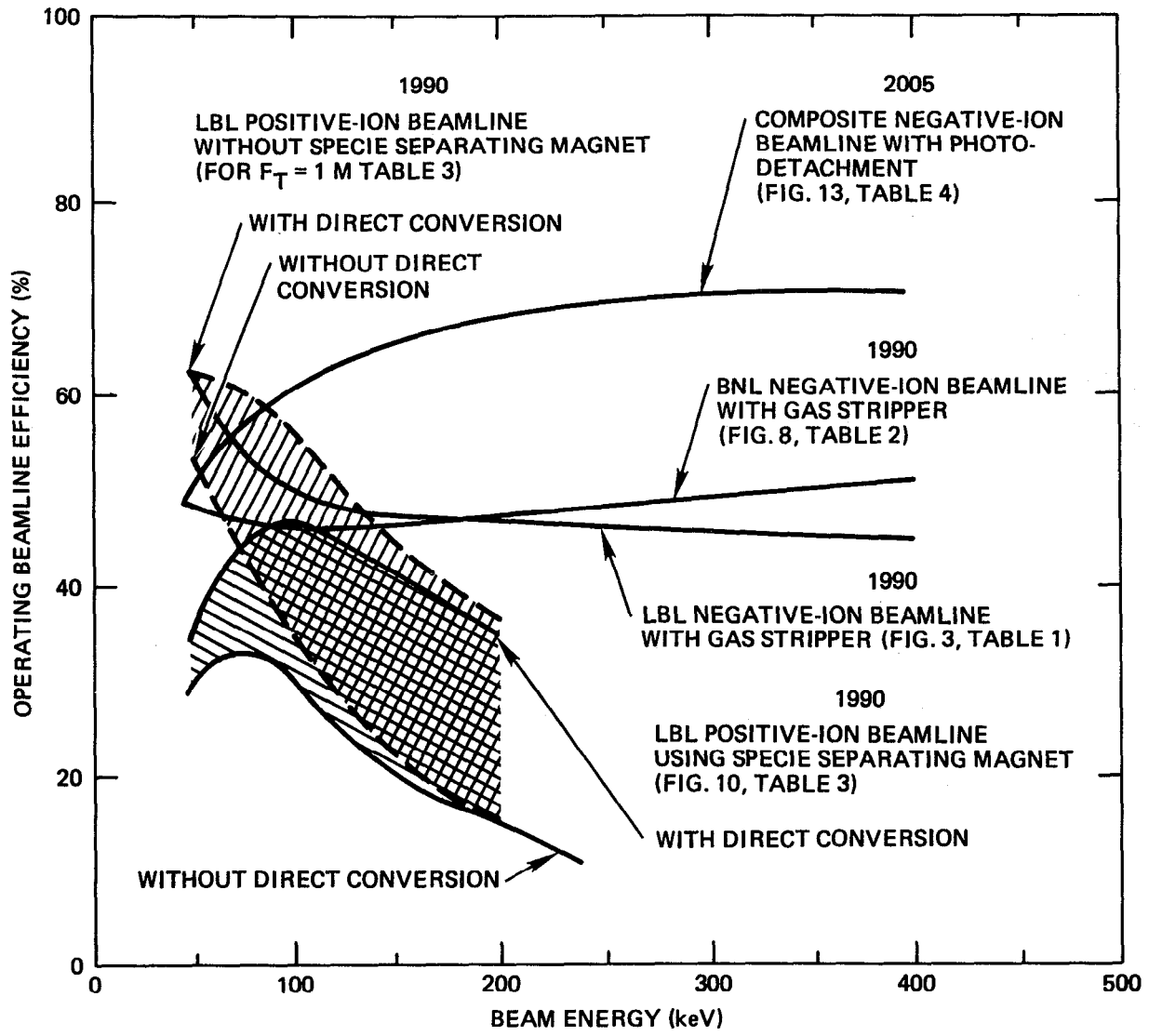


Figure VIII. B-2 Neutral Beam System Efficiency

The auxiliary power fraction is mainly intended to account for cryoplant power and for  $I^2R$  losses in the copper coils of the 20 T magnets. A 1% of fusion power requirement for the cryoplant (30 MWe equivalent for the 3000 MW<sub>f</sub> cases) is a guess that is considered conservative. The 3500 MW<sub>f</sub> STARFIRE has a 7 MWe cryoplant.<sup>6</sup> The requirement for the 20 T coil copper inserts derives from a preliminary estimate.<sup>7</sup>

The cost of the end cell (magnets, vessels, shielding) are based on preliminary estimates. The 20 T axi-cell cost estimate is discussed in Section III.A.2a.<sup>3</sup> In comparison, an axi-cell configuration with 14 T barrier coils would cost 20 \$/M less and would require 100 MW less magnet power, but would increase supplemental heating requirements more than a factor of two. A set of 14 vs. 20 T tradeoffs is discussed in Chapter IX. These favor the 20 T configuration.

Central cell magnet costs are calculated with a model Westinghouse originally developed for Tokamak studies and then modified for tandem mirror central cell applications. The modification was done for the EPRI-sponsored preliminary study on the feasibility of the fusion-fission hybrids.<sup>2</sup>

Central cell magnet costs were also estimated by scaling TMNS<sup>3</sup> costs with  $B^2$ , the magnet inner bore, and length. When results of the two methods of central cell magnet cost estimating were compared, we found to be substantially different. For example, for a TMNS-like case, the modified Westinghouse model predicted a coil cost of 23 M\$ and a total cost of 46 M\$ (cost + associated cryoplant) while the TMNS model predicted a coil cost of 74 M\$. The Westinghouse model is used in this study unless indicated otherwise. It is assumed the Westinghouse model is more representative of a commercial system. The conductor and structure unit costs used are based upon the PNL cost report.<sup>8</sup> The neutral beam system cost of 1.5 \$/W-output is also based upon PNL's cost report.<sup>8</sup>

The 3 \$/W estimate for microwave heating is lower than PNL's recommended value (5 \$/W),<sup>8</sup> but is motivated by recent studies and technological developments in the area of electron cyclotron resonance heating (ECRH). Most importantly, the development of advanced  $\sim 1$  MW Gyrotron tubes (largest current size is 200 KW) which feature less sensitive power supply regulation requirements will have potential to lower the rf heating cost to the 1.5 \$/W range.<sup>9</sup> In the absence of a detailed conceptual design

of a 1 MW or more system, we have not baselined rf power costs equal to neutral beam power costs (1.5 \$/W according to PNL cost report), but have reduced these somewhat relative to the PNL suggested values.

The cost of the leakage plasma dump system consisting of vacuum vessels, the ion direct converter, the electron dump, and pumping systems, is scaled from a reference case as a linear function of power capacity.

For the reference cases, the leakage plasma power ( $P_{\ell}$ ) is given by:

$$P_{\ell} \approx P_f (0.2 + 1/Q) = 3000 (.2 + 1/15.3) = 796 \text{ MW}$$

The reference case used for scaling is summarized below:

$$P_{\ell} = 1079 \text{ MW}$$

$$A_{DC} = 1009 \text{ m}^2 \text{ (area of direct converter)}$$

Costs (M\$)

DC panels	7.6
Power conditioning	38.6
Pumping system	12.4
Vacuum vessel	<u>46.8</u>
	105.4
Additional 1/3 for unspecified components	35.1
	<u>140.5</u>

$$\text{Unit cost} = 140 \text{ M\$}/1079 \text{ MW} = 0.13 \text{ \$/watt}$$

A more detailed description of the costing methodology is given in Section III.A.4.

The last cost parameter, called "other", is intended to account for items not accounted for in the named parameters. The value listed, 50 M\$, is an arbitrary estimate. Examples of items not specifically accounted for and thus are part of "other" are the cryosystem required for the end cell magnets, vacuum systems, fusion fuel handling systems, and the blanket fuel dump tanks (with associated possible cooling systems). The effects of uncertainties in the plant capital cost are discussed in Chapter IX. Other service systems, buildings, and site facilities costed by TMRDC are listed in Sections VIII.C and VIII.D.

## VIII.C PLANT CHARACTERISTICS

In this section we provide power flow and cost information for TMHR plants based upon the two reference blanket concepts. This information is used in the performance of the systems analysis presented in Chapter IX.

### VIII.C.1 Power Flow

Power flow information for the lithium/molten salt and beryllium/thorium oxide blankets is shown in Figures VIII.C-1 and VIII.C-2, respectively. Both systems utilize the same 3000 MW<sub>fusion</sub> driver (see Tables VIII.B-1 and VIII.B-2). Consequently, many of the power flow parameters are identical. In comparison, the lithium/molten salt blanket produces more electrical power, but less fissile fuel than the beryllium/thorium oxide blanket. As a result, the lithium/molten salt blanket TMHR produces 17% more net electrical power, but in symbiosis with its LWR client reactors, the overall system electricity production is 30% less than for the beryllium/thorium oxide blanket system. More detailed fuel cycle data for each blanket concept and various LWR fuel cycles is provided in Chapters VII and X.

### VIII.C.2 TMHR Direct Capital Cost

A rough costing analysis for each of the two reference blanket TMHR designs was performed using the TMRDC code. A breakout of this analysis for both systems, by major PNL cost account number,<sup>10</sup> is shown in Table VIII.C-1. Despite a larger heat transport system, the Be/ThO<sub>2</sub> TMHR achieves a 150 \$M lower direct cost. This results due to lower central cell magnet costs (smaller bore) and lower reactor plant equipment costs (single coolant). For both TMHR designs the cost for fusion reactor equipment (cost account 22.1) represents about 60% of the total direct capital cost.

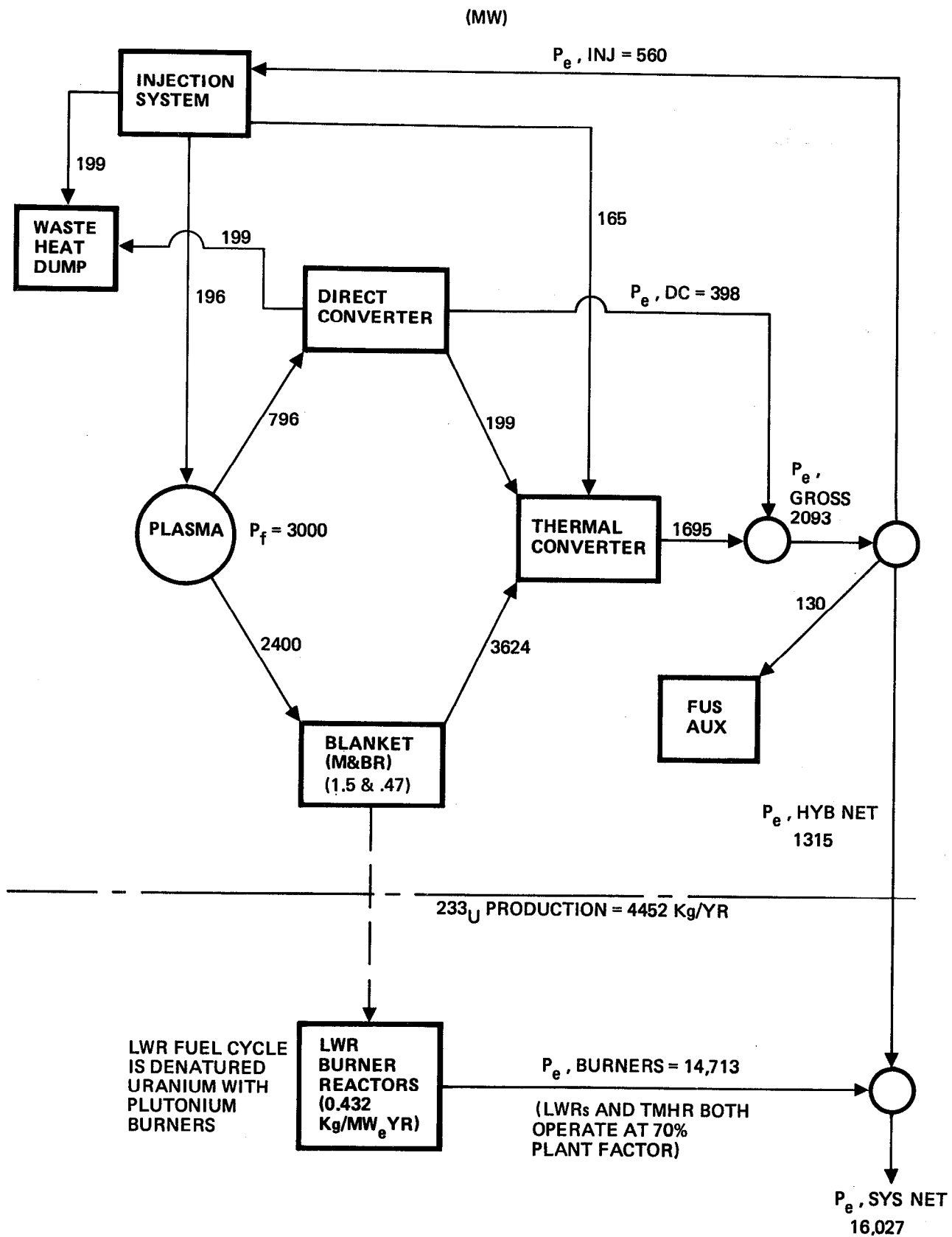


FIGURE VIII.C-1. System power flow for lithium/molten salt blanket TMHR.

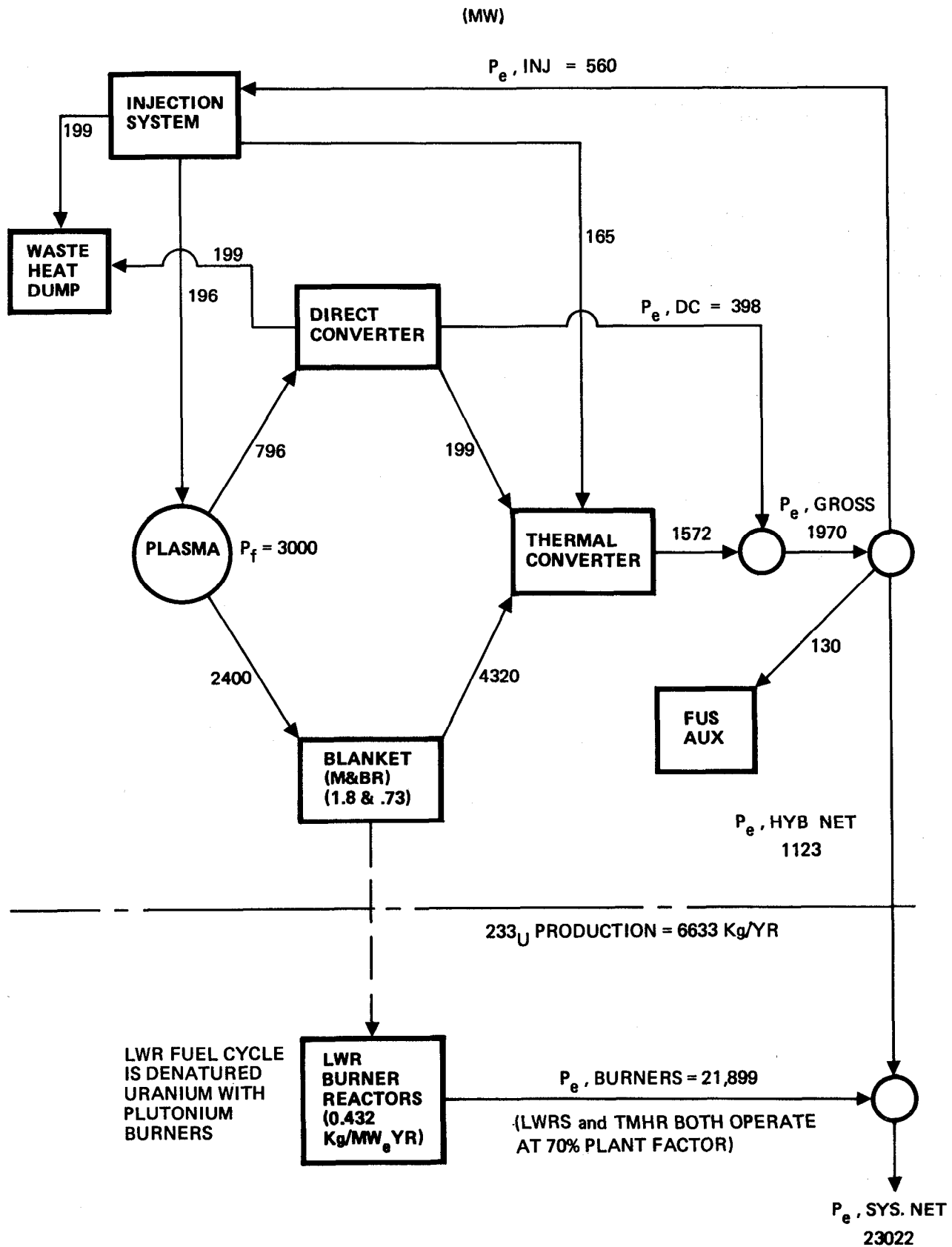


FIGURE VIII.C-2. System power flow for beryllium/thorium oxide blanket TMHR.

TABLE VIII.C-1. TMHR direct cost breakout by cost account number  
(\$ Million)

Account Number	Account Title	Blanket Type	
		Li/Ms	Be/ThO <sub>2</sub>
20	Land and land rights	5.0	5.0
21	Buildings and structures	337.9	337.2
21.1	Site improvements and facilities	12.5	12.5
21.2	Reactor containment building	106.2	99.6
21.3	Turbine generator building	47.0	46.1
21.4	Cooling system structure	7.1	7.8
21.5	Power supplies and energy storage	0.0	0.0
21.6	Other plant buildings	165.1	171.2
21.6.1	Reactor auxiliary building, R	22.2	22.5
21.6.2	Reactor auxiliary building, NR	5.5	5.6
21.6.3	Reactor service building	28.1	28.4
21.6.4	Steam generator building	35.0	40.2
21.6.5	Control building	19.4	19.5
21.6.6	Direct converter building	42.4	42.4
21.6.7	Misc. structures	12.5	12.6
22	Reactor plant equipment	1967	1764
22.1	Fusion reactor equipment	1627	1576
22.1.1	NA		
22.1.2	Blanket/shield	365.7	350.3
22.1.3	Magnets	532.5	496.2
22.1.3.1	End cell magnets	392.0	392.0
22.1.3.2	Central cell magnets	140.5	104.2
22.1.4	Plasma heating systems	574.6	574.6
22.1.4.1	Neutral beams (@ 1.5 \$/W)	398.1	398.1
22.1.4.2	RF heating (@ 3.0 \$/W)	176.5	176.5
22.1.5	NA		
22.1.6	Vacuum vessels	0.9	0.9
22.1.7	Other driver components	50.0	50.0
22.1.8	NA		
22.1.9	Direct converters (@ 0.13 \$/W)	103.5	103.5
22.2	Reactor plant equipment	339.4	188.7
23	Turbine plant equipment	227.2	237.2
23.1	Turbine generators	125.6	119.2
23.2	Main steam system	9.5	11.2
23.3	Heat rejection system	25.7	32.8
23.4	Condensing system	17.2	22.7
23.5	Feed heating system	30.2	33.2
23.6	Other equipment	19.0	18.1

TABLE VIII.C-1. TMHR direct cost breakout by cost account number (Continued)  
(\$ Million)

Account Number	Account Title	Blanket Type	
		Li/Ms	Be/ThO <sub>2</sub>
24	Electric plant equipment	<u>162.4</u>	<u>206.8</u>
24.1 thru 24.3	Switch gear and related equip.	23.3	36.4
24.4	Protective equipment	2.1	2.1
24.5 thru 24.6	Electrical bulks	133.6	164.9
24.7	Electrical lighting	3.4	3.4
25	Misc. plant equipment	<u>12.0</u>	<u>12.0</u>
90	TOTAL PLANT DIRECT CAPITAL COST	<u>2712</u>	<u>2562</u>

## REFERENCES FOR CHAPTER VIII

1. G. A. Carlson, et al., "Comparative End-Plug Study for Tandem Mirror Reactor," LLNL Report UCID-19271, December 1981.
2. "Preliminary Feasibility Assessment of Fusion-Fission Hybrids, EPRI Project RP-1463, Final Report," WFPS:TME-81-003, Westinghouse Electric Corporation for Electric Power Research Institute (1981).
3. C. C. Damm, et al., "Preliminary Design of a Tandem-Mirror-Next-Step Facility," Lawrence Livermore National Laboratory, Livermore, Ca, UCRL-53060 (1980).
4. J. H. Fink, "Neutral-Beam Injectors for 1990 and 2005," Lawrence Livermore National Laboratory, Livermore, Ca, UCRL-53112 (1981).
5. J. H. Fink, Lawrence Livermore National Laboratory, Livermore, Ca, Private communication.
6. "STARFIRE - A Commercial Tokamak Fusion Power Plant Study," Argonne National Laboratory, Argonne, IL, ANL/FPP-80-1, Vol. I (1980).
7. J. N. Doggett, Lawrence Livermore National Laboratory, Livermore, Ca. memorandum (1981).
8. S. C. Schulte, et al., "Fusion Reactor Design Studies - Standard Unit Costs and Cost Scaling Rules," PNL-2987, Pacific Northwest Laboratories (1979).
9. C. D. Henning, "The Economic Potential of Magnetic Fusion Energy," Lawrence Livermore National Laboratory, Livermore, Ca, UCRL-84938 (1981).
10. S. C. Schulte, et al., "Fusion Reactor Design Studies - Standard Accounts for Cost Estimates," PNL-2648, Pacific Northwest Laboratories (1978).



CHAPTER IX  
SYSTEMS AND ECONOMIC ANALYSIS

IX.A INTRODUCTION

IX.A.1 Overview

The suppressed fission tandem mirror hybrid reactor (TMHR) can be best understood and evaluated in the context of a symbiotic fusion fuel factory-fission burner electricity generation system. In this concept, shown in Figure IX.A-1, the fusion fuel factory is typically incorporated into a fuel cycle complex along with fuel reprocessing plants, fuel fabrication facilities and possibly a waste disposal facility. The entire fuel cycle complex could be located within a safeguarded area. The fissile fuel produced in the fusion fuel factory is recovered by reprocessing, mixed with fertile fuel, fabricated into fuel rods and shipped to the fission burner reactors. The spent fuel from the burner reactors is shipped back to the safeguarded fuel cycle complex where the remaining fissile fuel is separated from radioactive waste material which is processed for disposal. Typical fuel cycle complex configurations are discussed in more detail in Chapter X.

This chapter consists of five sections. Section IX.A is an introduction and discussion of several figures-of-merit for symbiotic electricity generation systems. These include the nuclear support ratio, the system electricity cost and the equivalent cost of mined  $U_3O_8$ . Sections IX.B,C,D, and E present the results of the TMHR systems analysis.

The basic analytical capability used to generate the results presented in Sections IX.B,C,D and E is shown in Figure IX.A-2. This capability is provided by three computer codes implemented on the Magnetic Fusion Energy Computing Network: the Tandem Mirror Physics Code (TMPC),<sup>1</sup> the Tandem Mirror Reactor Design Code (TMRDC),<sup>2</sup> and the economics analysis code (PERFEC).<sup>3</sup> Each of these codes has a distinct function. TMPC is used to estimate plasma engineering parameters (see Chapters II and VIII) associated with the fusion reactor configuration and power flow.

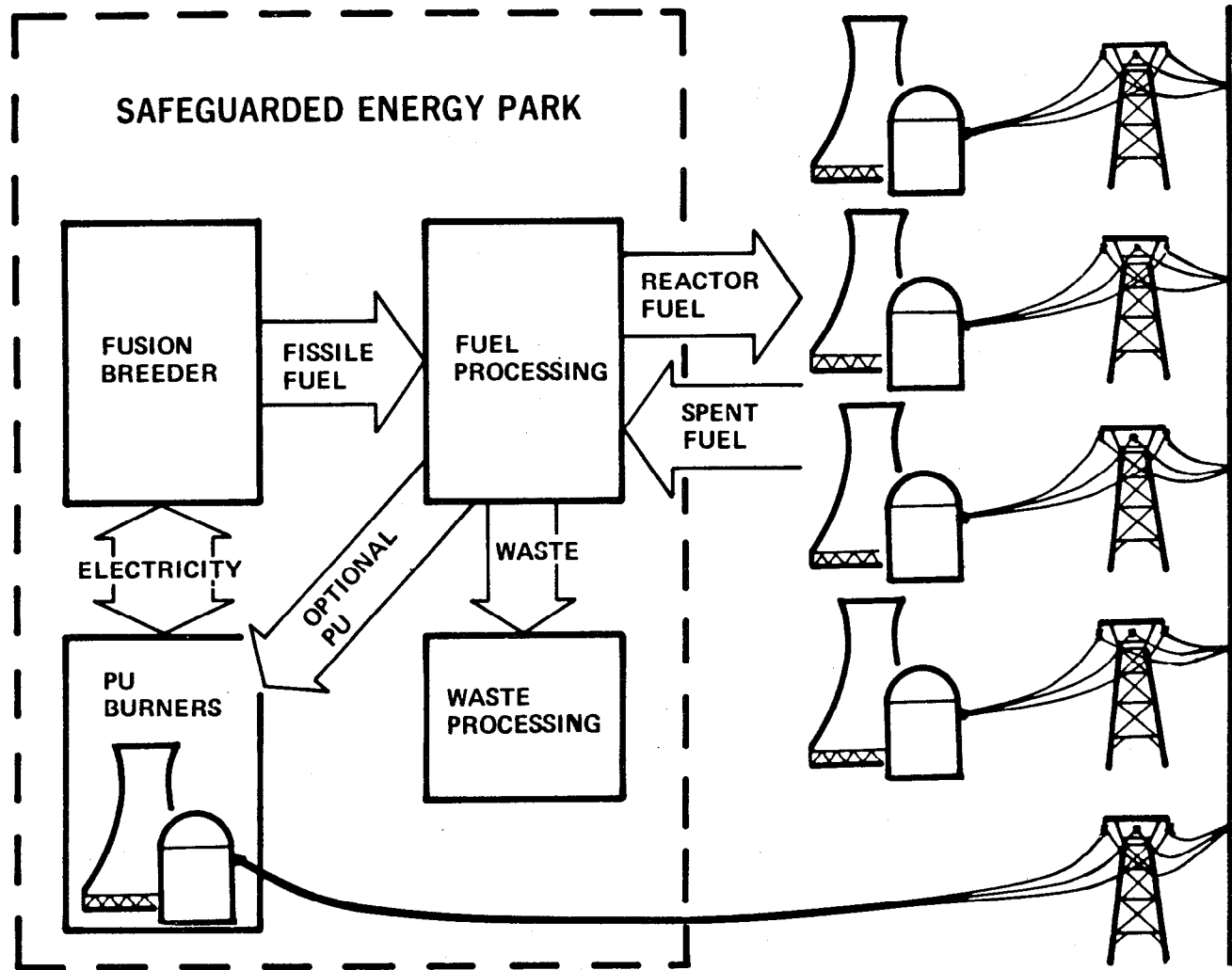
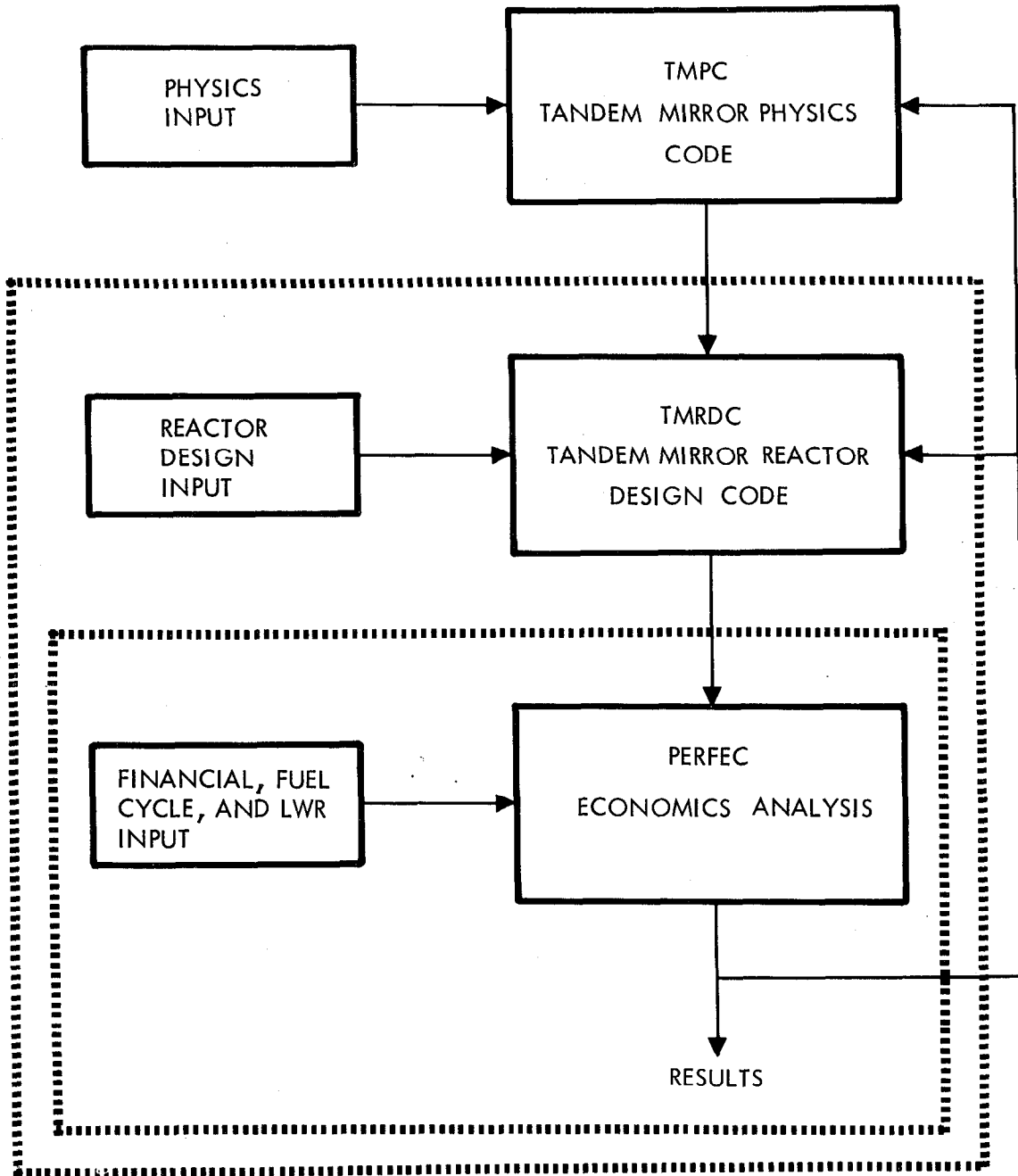


Figure IX.A-1. Fusion fuel producer - fission burner concept

Figure IX.A-2. TMHR/LWR systems modeling code capabilities



TMRDC is used to integrate these quantities into a reactor design and estimate the net TMHR power flow, fissile production, and direct cost (see Chapters III and VIII). PERFEC combines the TMRDC output with fission reactor, fission fuel cycle, and financial data to estimate the economic performance of the entire symbiotic electricity generation system. In performing the systems and economics analysis, the capital and operating costs of the entire electricity generation system are considered with respect to the production of one net product, electricity.

Each of the three codes may be utilized in a stand-alone mode or may be interfaced to the adjoining code. For instance, given a fixed set of inputs from TMRDC, PERFEC can be used to estimate the effects of parametric variations in the financial, fission fuel cycle, and/or LWR client data. In another mode, changes in plasma physics assumptions can be modeled using TMPC and the new results can be used to generate new TMRDC and PERFEC results. This capability provides a logical and straightforward mechanism to perform trade and optimization studies.

Section IX.B, "PERFEC Economics Analysis for a Suppressed Fission TMHR" provides a detailed description of the economics and performance characteristics of one typical TMHR driven electricity generation system. In this section the PERFEC methodology<sup>3</sup> is reviewed, input data relating to both the TMHR and its client LWRs is presented, a typical case is developed, and several parametric analyses are discussed. A fixed set of TMRDC cost and performance data is used (and not varied) in the Section IX.B PERFEC analysis.

Section IX.C, "Systems and Economics Analysis for Reference TMHR Designs", provides a description of the economics and performance of TMHRs based upon the Li/MS and Be/ThO<sub>2</sub> blanket designs. The performance and cost information presented in Chapters VII and VIII are used in this analysis and the PERFEC methodology introduced in Section IX.B is applied to estimate system figures-of-merit such as the cost of electricity and the equivalent cost of U<sub>3</sub>O<sub>8</sub>.

Section IX.D, "Technology Dependent TMRDC + PERFEC Parametric Economics Analysis for a Suppressed Fission TMHR" provides a parametric analysis to address the effects of uncertainties in the performance of key fusion subsystems modeled in the Tandem Mirror Reactor Design Code (TMRDC). In this analysis input parameters associated with the fusion physics and non-fusion technologies (eg., blanket, balance-of-plant, fuel cycle) are held fixed while the performance of selected fusion subsystems (eg., neutral beam electrical efficiency) is varied.

Section IX.E, "Plasma Physics Dependent TMPC + TMRDC + PERFEC Parametric Analysis", provides a parametric analysis to address the effects of uncertainties in the key plasma physics assumptions which are modeled in the Tandem Mirror Physics Code (TMPC). In this analysis non-plasma physics related input parameters (eg., electrical efficiencies of supplemental heating systems) are fixed, but plasma physics related quantities (eg., neutron wall loading, central cell beta, peak barrier coil B field) are varied. For example, in a wall loading optimization presented in Section IX.E, a lower wall loading (at fixed fusion power and first wall rating) results in a larger central cell and reduced neutral beam and rf power requirements (due to better plasma confinement at lower plasma density). In this case, calculated results are passed from the TMPC code to the TMRDC code, but the basic assumptions regarding the blanket configuration, subsystem efficiencies, etc. are unchanged.

#### IX.A.2 Discussion of System Figures-of-Merit

IX.A.2.a Nuclear Support Ratio. The nuclear support ratio, R, is defined as the nuclear power of the client fission reactors divided by the nuclear power of the TMHR (ie., fusion power  $\times (.8M + .2)$  where M is the blanket energy per source neutron divided by 14.1). As discussed in Chapter X, this quantity can be defined for both a "makeup only" mode of operation (considered in this chapter) and a "makeup plus inventory" mode of operation. In the latter case the support ratio is reduced, but regardless of the operational mode, a high nuclear support ratio is advantageous because only a small fraction of the symbiotic system's cost and electricity generation comes from the TMHR (typically, about 15% of the

overall capital cost and about 5% of the overall electricity generation). As a result of the high support ratio, system electricity costs can be relatively insensitive to uncertainties in the performance and cost of the fusion system while preserving a low average capital cost for the entire fusion-fission electricity generation system. Because a large fraction of the existing nuclear electric grid can be fueled from a small amount of fusion hybrid reactor capacity, TMHR's with high support ratios can have larger commercial impacts as earlier dates. These assertions are demonstrated in Section IX.B and Chapter X.

A symbiotic system with high support ratio may also offer a more diversion resistant fuel cycle because only a small fraction of the system energy needs to be generated in safeguarded fuel cycle centers where the fissile fuel is produced and processed. The majority of the electricity can be generated in a distributed system of LWRs using denatured, diversion-resistant fuel.<sup>4</sup> Since little power would be produced within the safeguarded area itself, these centers can be sited in remote areas.

Nuclear support ratios range from 4 to 60 depending upon the choice of fusion hybrid reactor and client thermal converter (eg., LWRs or advanced converter reactors such as HTGRs or CANDUs). The following nuclear support ratio estimates are representative of values which have resulted from hybrid reactor conceptual design studies performed during the last 10 years.<sup>5,6,7,8</sup>

- Hybrids with uranium fast fission blankets produce enough plutonium to support 4 to 6 LWRs.
- Hybrids with thorium fast fission blankets produce enough <sup>233</sup>U to support 8 to 12 LWRs or 14 to 28 advanced converters.
- Hybrids with uranium suppressed fission blankets produce enough plutonium to support 9 to 12 LWRs.
- Thorium suppressed fission blankets produce enough <sup>233</sup>U to support 10 to 20 LWRs or 35 to 60 advanced converters.

The variations in these support ratio estimates are dependent on the specifics of the fusion hybrid reactor designs, the type of client fission reactor, and fuel cycle choices. Blanket design parameters which significantly influence fissile fuel breeding include the fissile discharge

concentration, blanket coverage, first wall thickness, fuel burnup, and the relative concentrations of fuel, coolant, structure, moderators, and parasitic absorbers.

These nuclear support ratios can be put in perspective by comparing them to those of an LMFBR. LMFBRs can produce enough excess fissile fuel to support about one LWR of equivalent nuclear power.<sup>9</sup> Even so, the LMFBR must also produce fissile fuel to satisfy the fissile inventory requirement of additional LMFBRs. Consequently, LWR support is not a likely mode of LMFBR operation.

IX.A.2.b System Electricity Cost. System electricity cost is an important figure of merit for a fusion fuel factory-fission burner system because the only real product of the symbiotic system is electricity. A knowledge of the following quantities for both the TMHR and client fission burners is required to estimate system electricity cost.

- Fixed capital costs
- Variable operating costs
- Fissile fuel production and consumption
- Fissile fuel inventories
- Net thermal-to-electric conversion efficiencies

Given the above data, the PERFEC computer code may be used to estimate levelized (discount averaged) cost of electricity over the fixed operating lifetime of the hybrid and its fission reactor clients.

The system electricity cost is most useful when compared to a similar calculation of the cost of electricity produced by a "current technology LWR" fueled with <sup>235</sup>U derived from conventional mined uranium (see Section IX.B). Such a comparison is shown in Figure IX.A-3 for hybrid driven electricity generation systems featuring several generic blanket and fuel cycle options. As shown in the figure, these options reflect lower cost and improved power flow characteristics for the fast fission blankets relative to suppressed fission blankets. In this analysis the current technology LWR burns mined U<sub>3</sub>O<sub>8</sub> costing 100 \$/Kg (1980 dollars)

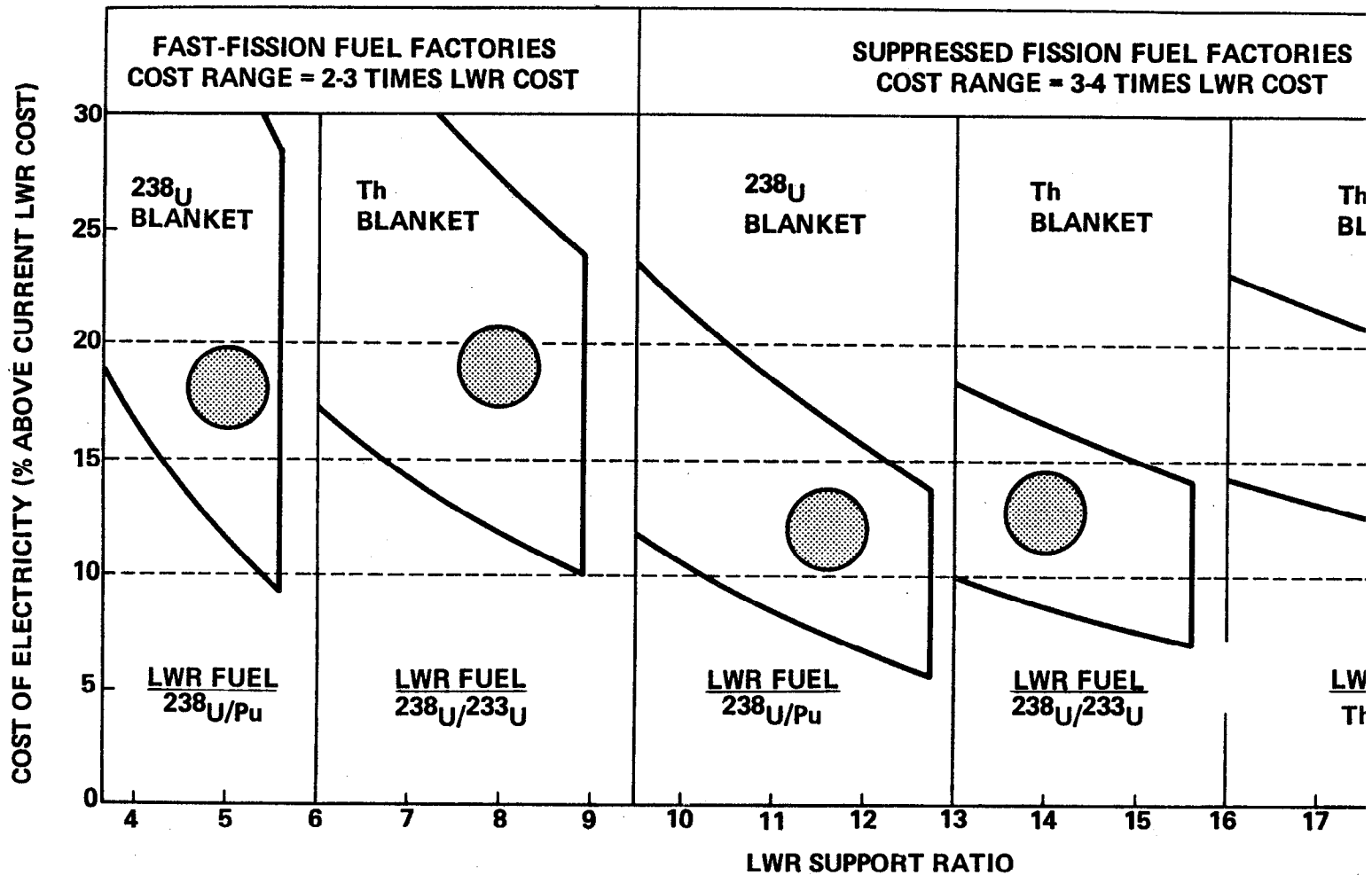
during its first year of operation \* and assumes fissile recycle via fuel reprocessing. As shown in the figure, most blanket/fuel cycle options have potential to provide electricity for less than 15% above the cost of electricity for the current technology LWR.

IX.A.2.c Equivalent  $U_3O_8$  Cost. Once the system electricity cost is known, it is possible to determine the bred fuel cost by subtracting the fusion fuel factory's electricity sales revenues from its operating expense. More importantly, the system electricity cost can be expressed in terms of an equivalent  $U_3O_8$  cost. This is the year zero  $U_3O_8$  price for which a new LWR, using mined  $U_3O_8$ , would generate electricity at the same levelized cost over its lifetime as the fusion fuel factory-fission burner system. Included in calculations for both the system electricity cost and the equivalent  $U_3O_8$  cost are cost and cost escalation estimates for uranium,\* uranium enrichment, fuel fabrication and fuel reprocessing.

Typical year zero equivalent  $U_3O_8$  costs (1980 dollars) are also shown in Figure IX.A-3. These indicate that equivalent  $U_3O_8$  costs of less than 200 \$/Kg (about 90 \$/lb) are possible. As shown in Section IX.B, these indicate economic breakeven for the hybrid in the 2000-2020 timeframe.

---

\*  $U_3O_8$  escalation assumed to be 3%/year above general inflation for 30 year subsequent plant life.



CIRCULAR AREAS DEFINE ESTIMATES OF THE MOST PROBABLE REGION OF CAPITAL COST AND LWR

Figure IX.A-3. The economics of typical fusion fuel factory - fission burner system

## IX.B PERFEC ECONOMICS ANALYSIS FOR A SUPPRESSED FISSION TMHR

In this section we consider the performance and economics characteristics of a typical suppressed fission TMHR in symbiosis with its LWR clients. Also, the LWR data base is described and parametric analyses which are independent of the particular TMHR design are presented. The TMHR considered in this analysis is based upon the 1979 molten salt blanket design<sup>7</sup> shown in Figure IX.B-1 rather than either the Li/MS blanket or Be/thorium oxide blanket developed during this study (the later systems are discussed in Sections IX.C, IX.D, and IX.E). However, the trends indicated by these analyses are generally applicable to all of the TMHR systems we have investigated and complement the technology dependent parametric results presented in Section IX.D and the tandem mirror physics dependent parametric results presented in Section IX.E.

The large data base used in this analysis originates from a variety of sources. Most importantly, we acknowledge tandem mirror hybrid design calculations performed during the 1979 tandem mirror hybrid study,<sup>7</sup> data resulting from the EPRI-sponsored "Preliminary Feasibility Assessment of Fusion-Fission Hybrids",<sup>2</sup> and the fuel cycle performance and cost results of NASAP<sup>9</sup> and other studies.<sup>10,11</sup>

In the TMHR study, a detailed analytical methodology for evaluating fusion breeder-fission converter reactor system economics incorporated into the digital computer code, PERFEC, has been used. This methodology is presented in Ref. 3. It is not specific to tandem mirror fusion-fission hybrid schemes, and is generally applicable to all types of symbiotic breeder-burner systems including those based on other fusion drivers and spallation neutron sources (accelerator breeders). The PERFEC methodology is briefly described in this section.

### IX.B.1 Typical TMHR Characteristics

To provide a case to illustrate the systems analysis, we have chosen a reference tandem mirror hybrid design based on the results of the 1979 suppressed-fission design investigated by LLNL.<sup>7</sup> The blanket design, featuring a beryllium neutron multiplier and a molten salt coolant and fertile fuel form is designated as the Be/MS TMHR. The tandem mirror

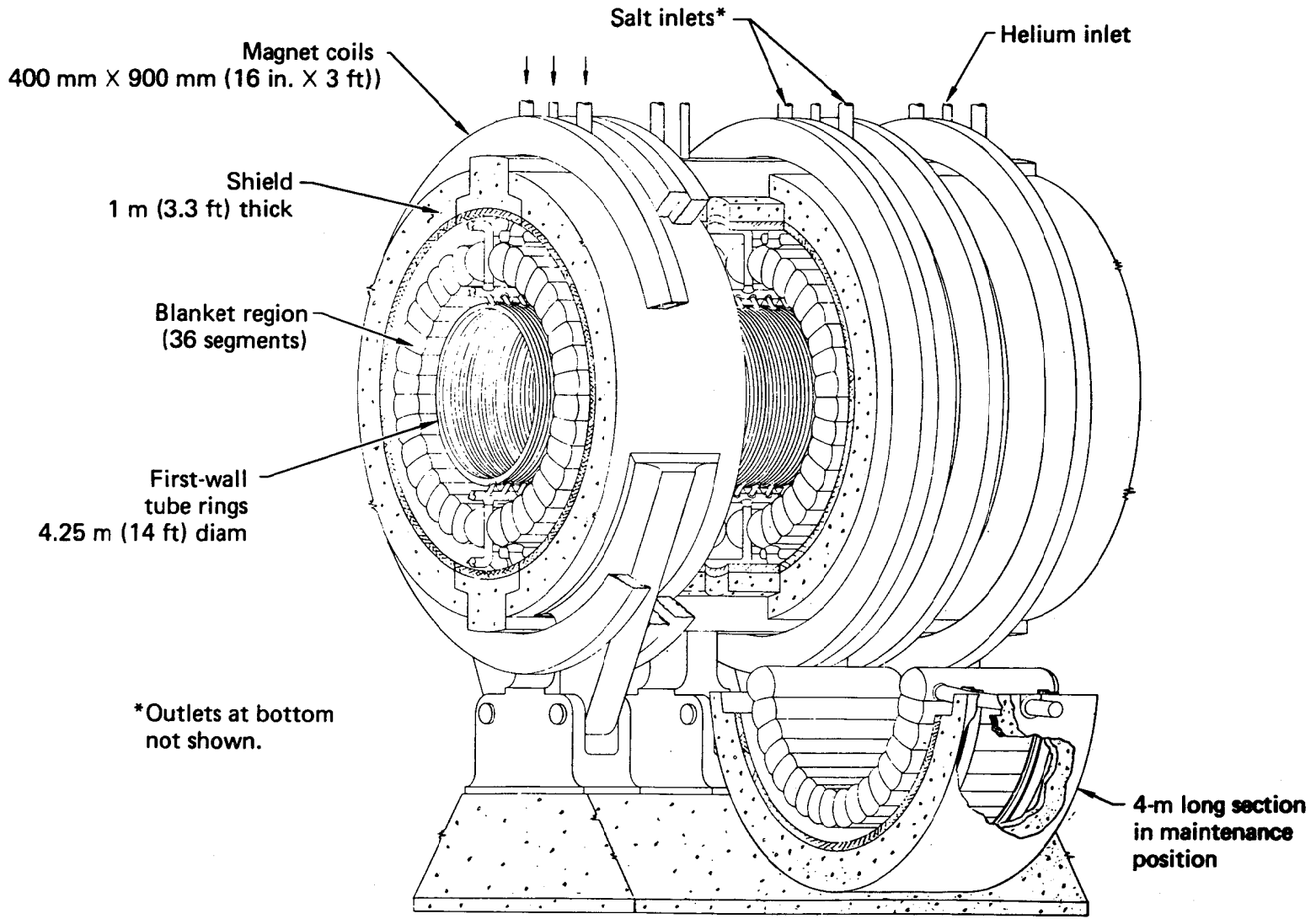


Figure IX.B-1. 1979 molten salt breeding blanket design with beryllium multiplier

driver is assumed to be operated in the thermal barrier physics mode with an A-cell configuration.<sup>7,12</sup> The cost and performance of this suppressed fission TMHR plant was estimated using the original version of the tandem mirror reactor design code (TMRDC) developed during the EPRI-sponsored "Preliminary Feasibility Assessment of Fusion-Fission Hybrids".<sup>2</sup> The original version of TMRDC differs from the latest version (used to generate the results shown in Chapter VIII) in that a simple physics model is included in the code. This model was eliminated in favor of the more complex TMPC model in later versions.<sup>1</sup>

The TMRDC performance and cost estimates are in most cases, highly uncertain. Therefore, such estimates are to be viewed as being reasonable rather than correct in an absolute sense. An attempt to quantify the sensitivities of important derived parameters with respect to major uncertainties has been made and extensive parametric results are presented at the end of this section.

IX.B.1.a Typical TMHR Performance. The performance for the Be/MS blanket TMHR input to, and calculated by, TMRDC is given in Tables IX.B-1 (code input) and IX.B-2 (output). As shown, the physics models in the code were normalized using a plasma Q, fusion power, and the first wall loading of 14.3, 3500 MW, and 1.6 MW/m<sup>2</sup>, respectively. However, the values of these quantities calculated for this case are 5.06, 2675 MW, and 2.6 MW/m<sup>2</sup>.

TABLE IX.B-1. Typical reference case input to tandem-mirror reactor design code (TMRDC)

Base Physics for Normalized Scaling Equations in Model

Central cell field, T	2.8
Central cell radius, m	1.29
Central cell $\beta$	0.4
Neutron energy current at plasma boundary, MW/m <sup>2</sup>	1.6
Plasma Q	14.3
Fusion power, MW	3500
Maximum field (barrier coils), T	12

Other Driver Component Input

Conversion efficiency of direct converter (DC)	0.6
RF heating overall efficiency	0.5
Driver auxiliary power, fraction of fusion power	0.01
Fraction of neutral beam power to the plugs	0.15
Energy of neutral beam to the plugs, keV	400
Trapped fraction of neutral beam in the plugs	0.2
Energy of neutral beam to the thermal barriers, keV	50
Trapped fraction of neutral beam in the thermal barriers	0.93
Plant availability factor	0.70

Typical Reference Case Physics Input Parameters

Fusion power, MW	2675
Neutron first wall loading, MW/m <sup>2</sup>	2.6
Central cell plasma $\beta$	0.4
Maximum barrier coil field, T	12

As discussed in Section IX.E, the plasma Q is highly dependent upon the input values for the fusion power and wall loading. The TMRDC results relating to power flow and fissile production given in Table IX.B-3 form the basic breeder electricity generation and fuel cycle performance input to the PERFEC economics code.

TABLE IX.B-2. Typical reference case output from tandem-mirror reactor design code (TMRDC)

Physics Parameters

Plasma Q	5.06
Central cell plasma radius, m	1.17
Central cell first wall radius, m	1.41
Central cell field, T	3.40
Central cell length, m	92.6
Neutral beam efficiency, plug/barrier	0.43/0.60

Hybrid Power Balance

Input power to plasma from rf and neutral beam, MW	529
Plasma power leaking to direct converter, MW	1064
Electric power from DC, MW	638
Useful thermal power from DC, MW	243
Power requirements for rf and neutral beam heating, MW (electric)	1143
Useful thermal power from rf and neutral beam heating, MW	429
Total useful thermal power from driver components, MW	672
Driver auxiliary electrical power requirement, MW (electric)	27
Total electric power requirement for driver, MW (electric)	1169
Blanket power, MW	3400
Gross useful thermal power, MW	4070
Gross electrical power, MW (electric)	2368
Net electric power, MW (electric)	1027

Fuel Cycle Performance

Annual fissile production, Kg/yr <sup>a</sup>	6060
Equilibrium fissile enrichment in thorium, %	0.25
In-blanket fissile inventory, Kg	3620
Out-of-blanket fissile inventory, Kg <sup>b</sup>	1420
Tritium breeding ratio	1.05

<sup>a</sup> includes plant capacity factor = 70%

<sup>b</sup> estimate includes 3 month cool off plus decay of <sup>233</sup>Pa to <sup>233</sup>U

IX.B.1.b Typical TMHR Economic Characteristics. The fusion breeder economics characteristics are described by two types of charges: fixed (indirect) charges associated with plant capital and variable (direct) charges associated with the fuel cycle and operation and maintenance. These are presented separately. All costs are given in 1980 dollars.

TABLE IX.B-3. Summary of performance parameters for PERFEC analysis of typical suppressed fission TMHR.<sup>a</sup>

Net electrical efficiency, KW (electric)/KW (nuclear)	0.26
Specific fissile fuel production, g/KW (nuclear) yr	2.20
Specific fissile inventory, g/KW (nuclear)	1.28

<sup>a</sup>Defined such that total nuclear power = (0.8 M + 0.2) times total fusion power

IX.B.1.b.(1) Annual Fixed (Indirect) Charges. Breeder fixed charges are given by the product of the total breeder capital cost at the beginning of plant operation and the total fixed charge rate. The latter consists of the various components shown in Table IX.B-4.<sup>13,14</sup> Note that the total fixed charge rate of 15.23% includes 7% inflation. This fixed charge rate is typical of private utility financing and is also applied to LWR capital costs.

The total breeder capital cost is computed as shown in Table IX.B-5. To obtain the total cost in 1980 dollars, the breeder direct cost is multiplied by a factor of 2.178 (2.052 for the LWR).<sup>13</sup> The direct capital cost of the beryllium/molten salt TMHR design discussed above was computed using the tandem-mirror reactor design code.

The fixed charges associated with this design are summarized in Table IX.B-6. These charges will be compared with similar charges for an LWR in Section IX.B.2.b.

IX.B.1.b(2) Breeder Variable (Direct) Charges. Breeder variable charges consist of both fuel cycle charges and operation and maintenance charges. These are computed for the first year of operation (i.e., year zero dollars) and are assumed to escalate in subsequent years according to the general inflation rate (7%/yr in this analysis). The year zero variable charges for the typical TMHR system are shown in Table IX.B-7.

TABLE IX.B-4. Fixed charge rate components.

Component	Charge rate, %
Capital recovery <sup>a</sup>	11.74
Income and property tax <sup>b</sup>	3.03
Salvage cost <sup>c</sup>	0.21
Miscellaneous and insurance	<u>0.25</u>
Total	15.23

<sup>a</sup>Plant lifetime = 30 years, bond fraction = 55%,  
bond return = 10%, stock return = 13%, inflation = 7%.

<sup>b</sup>Income tax rate = 50%, property tax rate = 1.5%,  
depreciation rate = 8.7%/yr.

<sup>c</sup>Decommissioning cost = 5% of original plant cost (1980 dollars).

TABLE IX.B-5. Total plant capital cost components.

	Breeder Multiplier	LWR Multiplier
Total direct cost <sup>a</sup>	1.00	1.00
Total indirect cost <sup>b</sup>	1.849	1.742
Time value of money <sup>c</sup>	<u>1.178</u>	<u>1.178</u>
Total	2.178	2.052

<sup>a</sup>1980 dollars.

<sup>b</sup>Field indirect cost multiplier = 1.2, home office cost  
multiplier = 1.2, contingency factor = 1.2 (hybrid) or 1.10  
(LWR), owner's cost factor = 1.07 (hybrid) or 1.10 (LWR).

<sup>c</sup>Inflation = 7%, escalation = 7%, construction period = 10 years.

TABLE IX.B-6. Summary of fusion breeder fixed (indirect) charges.

Direct cost, millions of dollars	2790
Indirect cost, millions of dollars	2369
Time-related cost, millions of dollars	918
Total capital cost, millions of dollars	6077
Specific cost, \$/kW(nuclear)	1544
Total annual charge at 15.23%/yr, \$/kW(nuclear)yr	235

Note that the assumed capital cost of the molten salt reprocessing plant (\$51 million direct costs) is included with the indirect costs since this facility is considered to be an integral part of the TMHR plant. This cost estimate was made prior to the results of the ORNL molten salt processing cost assessment, but is representative of later results (see Chapter VII). The molten salt processing costs are expected to be very low when compared to alternative processing technologies such as the conventional THOREX process. A first-order comparison of the levelized cost to reprocess thorium metal, thorium oxide, and molten salt fuels based on the same fissile throughput and average in-blanket  $^{233}\text{U}$  concentration in thorium was shown in Table VII.D-1.

It should be noted that the reprocessing cost per gram of bred fissile fuel is quite sensitive to the blanket design details. For instance, thorium oxide and thorium metal have different thermal properties (melting point, thermal conductivity, etc.), which will result in different  $^{233}\text{U}$  discharge assays when used in similar blanket configurations. In the case of a molten salt blanket, the fuel is continuously processed and the average  $^{233}\text{U}$  concentration in the blanket will be specified rather than the discharge concentration. A comparison of the reprocessing cost impact of the three types of fertile fuel will be given in the parametric sensitivity analysis.

Although included in Table IX.B-7, fissile inventory carrying charges are calculated implicitly, by PERFEC, using a self consistent method to determine the value of fissile material in the fusion-fission electricity generation system.<sup>3</sup> Fissile inventory carrying charges are given by the product of the fissile inventory (units: g/KW (nuclear)), the value of fissile material in the system (units: \$/g), and the fissile inventory carrying charge (units:  $\text{yr}^{-1}$ ). The latter quantity, 8.16 %/yr in this analysis, reflects the assumption that the cost of carrying fissile fuel is given by the difference between the cost of carrying fissile fuel (15.6%/yr) and the increased value of such fuel (7%/yr = general inflation rate). Fissile fuel is amortized over a one year period and is treated as a non-depreciating asset.

TABLE IX.B-7. Summary of fusion breeder variable (direct) charges in year zero

Annual processing cost, \$/kW(nuclear) yr <sup>a</sup>	0.68
Molten salt process cost, \$/kgHM	1.05
Fuel throughput, kgHM/kW(nuclear) yr	0.65
Fissile inventory cost, \$/kW(nuclear) yr	7.42
Operation and maintenance charge \$/kW(nuclear) yr	26.22
Total year zero variable charge, \$/kW(nuclear) yr	34.32

<sup>a</sup> Operation and maintenance cost of the fuel process plant. Its capital cost is factored into the overall plant fixed cost.

### IX.B.2 LWR Performance and Economics Characteristics

Although the LWRs discussed in this section are considered to be identical, they can be distinguished according to their operating fuel cycles. Two principal LWR types are considered: (a) plutonium burners and (b) denatured <sup>233</sup>U burners.<sup>4,10</sup> Another, more fuel efficient fuel cycle for LWRs, the denatured thorium fuel cycle, is also discussed. In all cases, spent fuel discharged from the LWRs is assumed to be reprocessed for the recovery of all fissile uranium and plutonium isotopes.

IX.B.2.a Fuel Cycle Considerations. For all cases considered in this analysis, both <sup>233</sup>U-burning LWRs and plutonium-burning LWRs are supported by the fusion breeder. In particular, for thorium blanket breeders, which breed only <sup>233</sup>U, some plutonium burners would also be included in the system. This occurs because ~205 kg of plutonium per GW(electric) year is produced in the client denatured uranium LWRs that are supported by the breeder.<sup>10</sup> This secondary plutonium is recovered in reprocessing and burned in plutonium burners. In effect, the thorium blanket supports both primary <sup>233</sup>U-burning uranium fuel cycle LWRs and secondary plutonium-burning LWRs. Thus, for thorium blanket systems, a synthesized, or mixed, LWR system is required to maximize the number of LWRs that can be supported by a breeder. For the denatured uranium fuel cycle, 30% of the supported LWRs burn plutonium. For the denatured thorium fuel cycle, 14%

of the supported LWRs burn plutonium. It is important to note that, although it is possible, we have not considered mixed  $^{233}\text{U}$ -Pu fuel cycles in a single LWR. Rather, our systems are composed of the two LWR types shown in Table IX.B-8.

TABLE IX.B-8. LWR generation mix (fraction of generating capacity)

Fuel Cycle Designation	LWR Type	
	Primary $^{233}\text{U}$	Secondary $\text{Pu}_f$
Denatured uranium	0.70	0.30
Denatured thorium	0.86	0.14

IX.B.2.b LWR Performance and Economic Characteristics. The performance characteristics of the mixed (or synthesized) LWR reactor systems, which couple to the reference TMHR system, are given in Table IX.B-9. These data, as well as the LWR economics data, have been derived from various sources including the EPRI's "Technical Assessment Guide," the DOE's NASAP reports, fuel cycle studies generated at ANL, fuel reprocessing studies performed by Exxon Nuclear Company, and information provided by Bechtel.<sup>14,9,10,11,13</sup> However, in many cases, it has been necessary to revise, blend, renormalize, or cost escalate the source data to provide for a consistent treatment in this analysis.

In this analysis, all LWRs are assumed to operate at 70% of rated plant capacity [1000 MW(electric), 3000 MW(nuclear)] and all are assumed to be batch loaded such that one-third of the fuel is replaced each reload. The fuel burnup and specific power densities are assumed to be 33,000 kWd/kg (35,300 kWd/kg for denatured thorium) and 33.3 kW/kg, respectively. Note that the denatured uranium fuel cycle requires 31% more fuel than the denatured thorium fuel cycle. However, its total fissile inventory is 28% lower (due to lower fissile enrichment).

The economic characteristics of the LWRs modeled in this paper are given in Tables IX.B-10 and IX.B-11. Table IX.B-10 is a summary of LWR fixed charges (analogous to Table IX.B-6 for the breeders). A comparison of Tables IX.B-6 and IX.B-10 indicates that on a unit thermal power basis, the typical TMHR fusion breeder considered in this analysis is 4.1 times as costly as an LWR. Table IX.B-11 is a summary of the year zero LWR variable charges (analogous to Table IX.B-7 for the breeders). All of the LWR fuel processing costs listed refer to the processing of uranium oxide and thorium oxide fuels. The most important difference between the various fuel cycles is the fuel reprocessing cost. The reason for higher thorium oxide reprocessing costs is discussed in Section VII.B.<sup>11</sup> In comparison with the breeders, on a unit nuclear power basis, year zero LWR variable costs are ~60% of the breeder costs. After year zero, LWR variable costs are assumed to escalate at the general inflation rate, 7%/yr.

TABLE IX.B-9. Summary of LWR performance parameters.

	Fuel Cycle	
	Denatured Uranium	Denatured Thorium
Nuclear support ratio with Be/MS TMHR	15.3	20.0
Specific fissile consumption, g/kW(nuclear) yr	0.144	0.110
Annual fissile consumption, kg/yr <sup>a</sup>	302	231
Fissile enrichment, %	2.6	3.2
In-core fissile inventory, g/kW(nuclear)	0.57	0.80
Out-of-core fissile inventory, g/kW(nuclear) <sup>b</sup>	0.16	0.22

<sup>a</sup>Includes plant capacity factor = 70%

<sup>b</sup>Assumes a total of two years required to fabricate fresh fuel and reprocess spent fuel.

TABLE IX.B-10. Summary of LWR fixed (indirect) charges

Direct cost, millions of dollars	552
Indirect cost, millions of dollars	410
Time-related cost, millions of dollars	171
Total capital cost, millions of dollars	1133
Specific cost, \$/kW(thermal)	378
Total annual charge at 15.23%/yr, \$/kW (nuclear)yr	57.5

TABLE IX.B-11. Summary of LWR variable (direct) charges in year zero

	Fuel Cycle	
	Denatured Uranium	Denatured Thorium
Annual processing charge, \$/kW(nuclear) yr <sup>a</sup>	7.93	9.22
Fuel reprocessing cost, \$/kgHM	281	475
Fuel fabrication cost, \$/kgHM	665	807
Fuel transportation cost, \$/kgHM	16.8	16.8
Back end fuel cycle cost, \$/kgHM	61.3	61.3
Total unit processing cost, \$/kgHM	1024	1260
Fuel throughput, kgHM/kW(nuclear) yr <sup>a</sup>	0.0077	0.0073
Fissile inventory cost, \$/kW(nuclear) yr	4.23	5.83
Operation and maintenance charge, \$/kW(nuclear) yr	6.41	6.41
Total year zero variable charge, \$/kW(nuclear) yr	18.57	21.46

<sup>a</sup> Includes 70% capacity factor

### IX.B.3 Symbiotic Electricity Generation System

The following quantities, for both the breeder and the client LWRs, required for systems economic analysis were provided above in Tables IX.B-1 through IX.B-11:

1. Fixed capital costs [\$/kW(nuclear) yr]
2. Variable operating costs [\$/kW(nuclear) yr]
3. Fuel consumption (LWR) and production (breeder) [g/kW(nuclear)]
4. Fissile inventories [g/kW(nuclear)]
5. Net nuclear-to-electric conversion efficiency [kW(electric)/kW(nuclear)].

IX.B.3.a Methods of Analysis. Referring to the right side of Figure IX.A-1, we note that the only real product of the combined fusion breeder-fission converter system is electricity. We also note that, considering the TMHR fusion breeder and a consistent number of supported fission reactors, the closed energy system shown is entirely and exactly self-sufficient in fissile fuel. Thus, the sale of fissile fuel by the TMHR operator and the purchase of fissile fuel by the LWR converter operator can, for the moment, be treated as an internal transfer. In this case, it is reasonable and appropriate to define the system busbar electricity cost, mill/kW(electric) hr, as

$$S = 1000 C_{op}^{Tot} / E^{Tot}, \quad (1)$$

where  $C_{op}^{Tot}$  [\$/kW(nuclear) yr] is the total annual levelized cost of operating the closed energy system including capital, fuel cycle, fissile inventory, and operating costs, and  $E^{Tot}$  [kW(electric) h/yr] is the total annual electrical output of the closed energy system. The solution of Eq. (1) for the system electricity cost is developed and expanded in detail in Ref. 3.

For the purpose of simplicity in illustration, we can expand the system electricity cost given in Eq. (1) by assuming that costs associated with fissile inventory charges are known\* and by assuming that breeder and burner plant capacity factors are equal ( $\gamma^B = \gamma^C = \gamma$ ). In this case,

$$S \approx (C_{op}^B + RC_{op}^C) / [8.76\gamma(\eta_n^B + R\eta_n^C)], \quad (2)$$

where

- $C_{op}^B$  = total breeder plant operating cost (including capital, fuel cycle, fissile inventory, and operation and maintenance costs but not including revenues from fuel or electricity sales), \$/kW (nuclear) yr
- $C_{op}^C$  = total converter plant operating cost (again not including the cost of fissile fuel or revenues from electricity sales), \$/kW (nuclear) yr
- R = ratio of converter reactor nuclear power output to breeder reactor nuclear power output (i.e., support ratio)
- $\eta_n^{B,C}$  = net nuclear-to-electric conversion efficiencies of the breeder and converter, respectively (i.e., net electric/nuclear power)

---

\* The fissile inventory charges are implicitly calculated in PERFEC as they depend upon the system electricity cost and the cost of fissile makeup.

The above can be expanded to first order with respect to the system electrical support ratio,  $R\eta_{\eta}^C/\eta_{\eta}^B$ , as

$$S = \frac{1}{8.76\gamma} \left[ \frac{C_{op}^C}{\eta_{\eta}^C} + \frac{1}{R} \frac{\eta_{\eta}^B}{\eta_{\eta}^C} \left( \frac{C_{op}^B}{\eta_{\eta}^B} - \frac{C_{op}^C}{\eta_{\eta}^C} \right) \right] \quad (3)$$

Equation (3) is interesting because it indicates that the symbiotic system electricity cost can be represented as the fission converter electricity cost (not including fissile make charged),  $C_{op}^C/(8.76\gamma \eta_{\eta}^C)$  [mil/kW(electric) hr], plus an adjustment. This adjustment is inversely proportional to the electrical support ratio (typically between 5.8 and 38 for systems considered). Also, the adjustment is proportional to the difference between the TMHR operating cost (not including fissile sales),  $C_{op}^B/\eta_{\eta}^B$  [\$ /kW(electric) yr], and the fission converter operating cost,  $C_{op}^C/\eta_{\eta}^C$  [\$ /kW(electric) yr]. It is apparent that the adjustment can be arbitrarily close to zero by increasing the support ratio, but such improvements are not necessarily of economic benefit if achieved by implementing a more costly fuel cycle (e.g., denatured thorium) or a more costly advanced converter reactor, which increases the value of  $C_{op}^C$  significantly.<sup>6</sup> The system busbar electricity cost is the most important system parameter and the system with lowest electricity cost is always the most desirable in economic terms.

The strategy, therefore, is to first determine the cost of electricity for the entire system of a TMHR fusion breeder and its client LWRs. Once the system electricity cost is determined,<sup>3</sup> it is possible to determine the bred fissile cost by subtracting the breeder's electricity sales revenue from its operating expense. Given the fissile cost, the cost of the fissile makeup and the fissile inventory carrying charges for the fission reactors can be determined. The cost of fissile fuel circulated in the system,  $C_{fiss}^B$  (\$/g), is an important parameter in analyzing the economic merits of a fusion-fission electricity generation system. In particular, if averaged over the plant lifetime, the LWR operator can but conventionally processed fissile (i.e., mined, milled, converted, and enriched), for less than the bred fissile cost, the fusion breeder will not be economical.

Unfortunately, such a comparison is not possible in practice because the fusion breeder produces nearly pure  $^{233}\text{U}$  or plutonium, which cannot be directly compared in value with enriched  $^{235}\text{U}$ .

Instead, we can equate any calculated symbiotic electricity cost with the cost of producing electricity using a current technology LWR (see Section IX.A.2.b) and conventional mined  $\text{U}_3\text{O}_8$  fuel during the same 30 year operating lifetime (see Table IX.B-12 for current technology LWR fuel cycle data). In this case, the levelized cost of conventional  $\text{U}_3\text{O}_8$  that yields the same levelized electricity cost as the symbiotic calculation is the breakeven, or equivalent, levelized  $\text{U}_3\text{O}_8$  cost for the hybrid. The levelized cost of generating electricity in a conventional LWR with fuel reprocessing versus the year zero cost of  $\text{U}_3\text{O}_8$  for a 10%/yr  $\text{U}_3\text{O}_8$  cost escalation rate (or 3%/yr real escalation above 7%/yr general inflation) is shown in Figure IX.B-2. The  $\text{U}_3\text{O}_8$  cost escalation rate is important because the levelized cost calculation takes into account the  $\text{U}_3\text{O}_8$  requirements over the entire 30-year plant life. For example, the figure may be interpreted to indicate that, with reprocessing and recycle, a \$200/kg of  $\text{U}_3\text{O}_8$  cost when the LWR first operates (year zero) translates to a 13% increase in electricity costs over the cost of electricity for the same reactor with a \$100/kg  $\text{U}_3\text{O}_8$  cost at the beginning of operation. At the 10%/yr escalation rate, it is expected that  $\text{U}_3\text{O}_8$  will cost \$220/kg after the first year of operation and \$242/kg after the second year, etc.

#### IX.B.3.b Systems Economics Results for Typical Suppressed Fission TMHR.

The economics methodology, which is described in Section IX.B.3.a, and is discussed in detail in Reference 3, has been applied to the typical suppressed fission TMHR and LWR data presented in this paper. The results of our analysis for all of these systems are shown in Table IX.B-13. Referring to this table, we note that, despite a 24% lower support ratio, the denatured uranium fuel cycle is marginally preferred over the denatured thorium fuel cycle based on economics considerations. This occurs because the large fissile inventory and high fuel processing costs of the denatured thorium fuel cycle mix more than offset the large fuel consumption of the denatured uranium fuel cycle mix (See Tables IX.B-9 and IX.B-11).

TABLE IX.B-12. Data for current technology LWR with reprocessing and conventional U<sub>3</sub>O<sub>8</sub> fuel<sup>a</sup>

Fissile consumption, g/kW(thermal) yr <sup>b</sup>	0.180
Fissile inventory, g/kW(thermal)	0.907
Fuel fabrication cost, \$/kg	235
Fuel transportation cost, \$/kg	16.8
Enrichment cost, \$/kg	315
Reprocessing cost, \$/kg	281
Back end fuel cycle cost, \$/kg	61.3
Total unit processing cost, \$/kg	1163

<sup>a</sup> Other data are similar to client LWRs. The U<sub>3</sub>O<sub>8</sub> costs are assumed to escalate 10%/yr (3% above general inflation) over the 30 year LWR plant lifetime

<sup>b</sup> at 100% plant capacity.

TABLE IX.B-13. Symbiotic system results for typical TMHR<sup>a</sup>

	Fuel Cycle Type (includes plutonium burners)	
	Denatured Uranium	Denatured Thorium
Levelized electricity cost, mill/kW (electric)·hr	54	55
Electricity cost, % above current LWR <sup>b</sup>	9.2	12.5
Levelized fissile cost, \$/g	143	142
Levelized equivalent U <sub>3</sub> O <sub>8</sub> cost, \$/kg <sup>c</sup>	520	598
Year zero equivalent U <sub>3</sub> O <sub>8</sub> cost, \$/kg <sup>c</sup>	171	196

<sup>a</sup> All costs in 1980 dollars.

<sup>b</sup> Current technology LWR levelized electricity cost is 49 [mill/kW (electric)·h] (with reprocessing and U<sub>3</sub>O<sub>8</sub> feed cost = \$100/kg).

<sup>c</sup> Assumes 10%/yr U<sub>3</sub>O<sub>8</sub> cost escalation (includes 7%/yr general inflation) and recycling of uranium and plutonium in LWR fuel reprocessing.

Although the higher support ratio for the denatured thorium system is attractive, the preservation of PUREX reprocessing technology for the denatured uranium system is also attractive and we have chosen the latter as our reference fuel cycle.

The Be/MS suppressed-fission tandem mirror hybrid considered in this analysis and the denatured uranium/plutonium burning LWRs result in attractive performance. For this system, the cost of electricity is <10% above the current technology LWR electricity cost (i.e., \$100/kg  $U_3O_8$  with reprocessing) and the year zero breakeven cost of  $U_3O_8$  is only \$171/kg (\$78/lb). If the current cost of  $U_3O_8$  is \$30.5/lb (1980 dollars),<sup>15</sup> the above results imply that when the cost of  $U_3O_8$  increases 2.5 fold, fuel produced in the TMHR could provide an economic benefit to the LWR operator over the 30 year operating life of the LWR plant.

These results are sensitive to the real escalation rate of  $U_3O_8$  during the time frame that LWRs would be fueled by the TMHR. This sensitivity is shown in Figure IX.B-2. Referring to this figure, we see that a higher real escalation rate of 5%/yr leads to an equivalent  $U_3O_8$  cost of only \$127/kg (\$58/lb) while a lower real escalation rate of 2%/yr increases the equivalent  $U_3O_8$  cost to \$195/kg (\$88/lb). Recent projections of  $U_3O_8$  costs performed in conjunction with the NASAP studies are shown in Figure IX.B-3 (References 2 and 9). These indicate that for low, medium, and high nuclear power growth scenarios, the price of  $U_3O_8$  in 1980 dollars could reach the reference value of \$78/lb during the years 2004, 1998 and 1993 respectively. If the equivalent year zero  $U_3O_8$  cost were \$120/lb, the breakeven years would be 2005 for the high growth case and 2017 for the medium growth case. The price of  $U_3O_8$  is expected to peak at only \$95/lb for the low growth case and the hybrid option is most likely not appropriate in this case, since, as discussed in Chapter X, its effect will be to promote an accelerated growth pattern for nuclear power.

#### IX.B.4 Exploring Uncertainties

Although the system electricity costs presented in Section IX.B.3 are encouraging, it would be misleading to indicate that cost, performance, and economics parameters are known to an acceptable degree of accuracy.

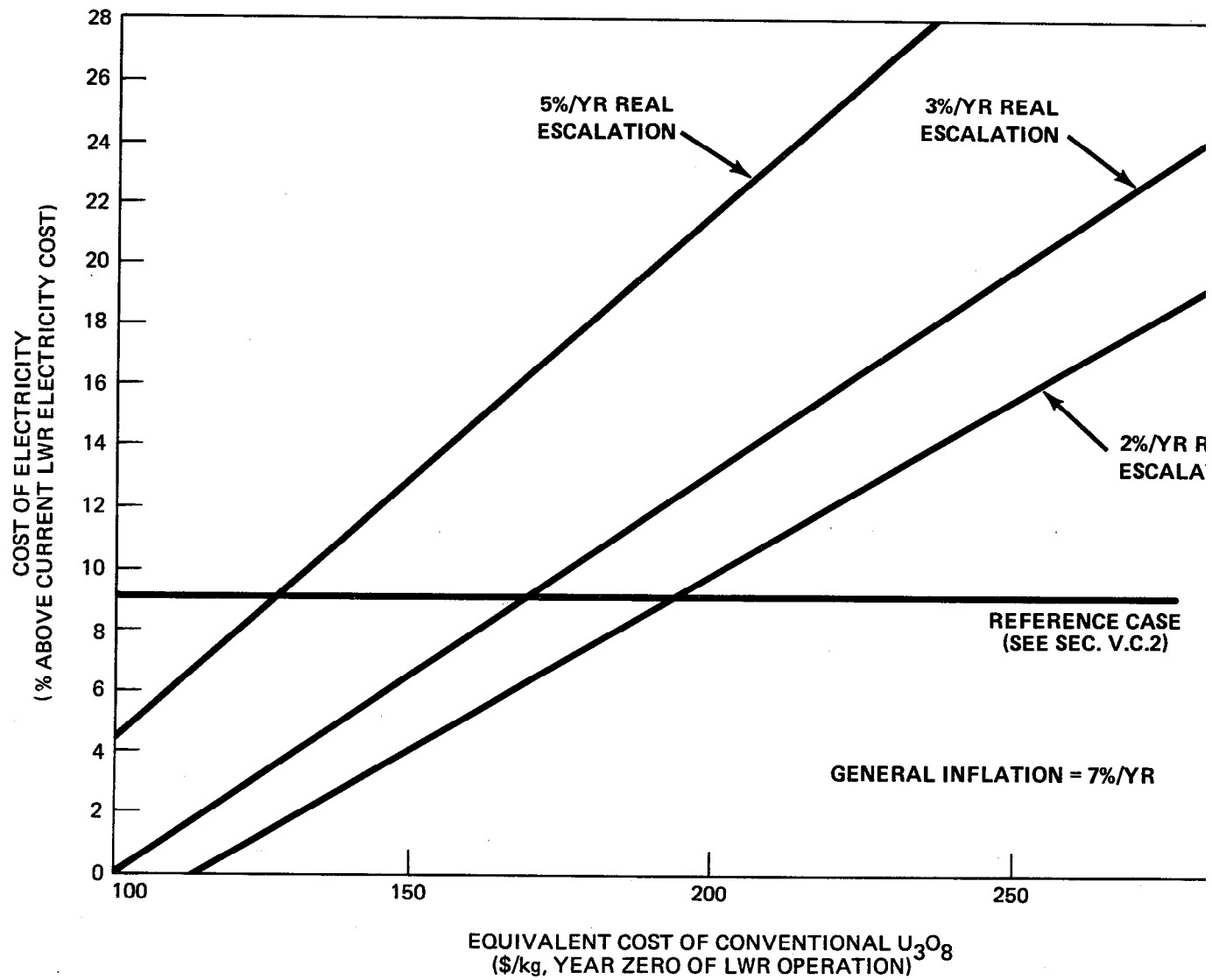


Figure IX.B-2. The LWR electricity cost versus equivalent  $U_3O_8$  costs.

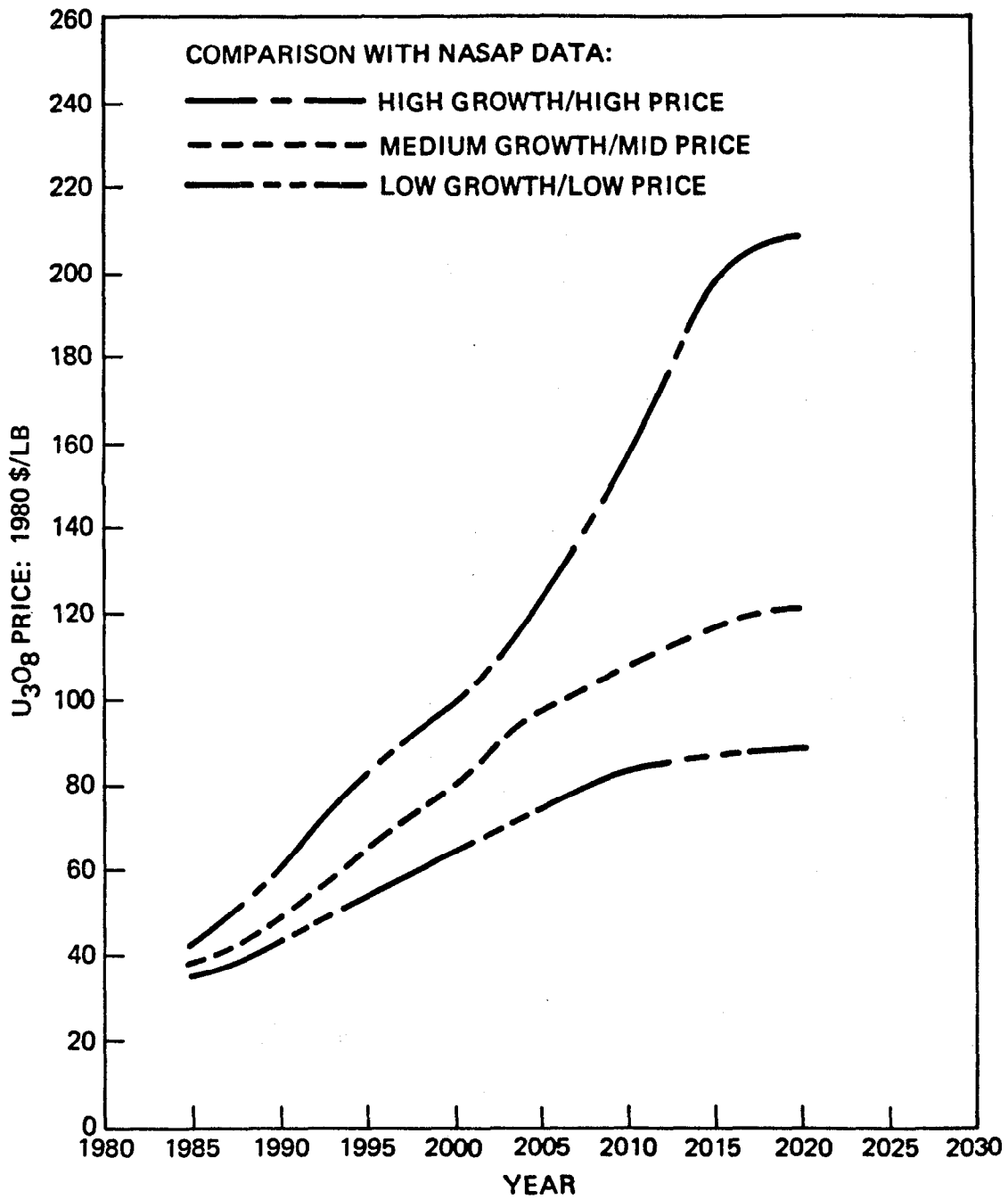


Figure IX.B-3. NASAP U<sub>3</sub>O<sub>8</sub> price projections versus year for different nuclear growth rates and prices.

In particular, we might expect that while the LWR data are reasonably accurate and well known, fusion breeder data are largely uncertain (despite the best efforts in conceptual design and costing). Fortunately, as is shown in the following discussion, system electricity costs are quite insensitive to uncertainties on the fusion breeder side of the system.

This observation is demonstrated in Figure IX.B-4. This figure shows the system electricity cost relative to the current technology LWR electricity cost (\$100/kg of  $U_3O_8$ , 10%/yr  $U_3O_8$  cost escalation reprocessing) as a function of the normalized breeder capital cost. The figure indicates that a 50% increase in breeder capital cost (to over six times the LWR cost) would result in only a 14% increase in the cost of electricity.

The sensitivity of the system electricity cost and breakeven  $U_3O_8$  cost to the TMHR fuel cycle cost is shown in Figure IX.B-5. In this figure, we compare the three fuel forms discussed earlier (see Table VII.D-1). As shown, the cost of electricity is quite insensitive to the breeder fuel form. However, the difference in breakeven  $U_3O_8$  cost for the thorium oxide and molten salt cases is significant [about \$50/kg (\$23/lb)] and could delay the breakeven date for commercial viability of the TMHR by 5 to 10 years. System electricity cost is also quite insensitive with respect to relatively small changes in the breeder fuel production and breeder net electricity production, as shown in Figures IX.B-6 and IX.B-7. In the case of breeder fuel production, the figure shows that the economic figures of merit are sensitive to large decreases in fissile breeding. For the reference system (denatured uranium) a 50% decrease in fissile production [to 1.1 kg/kW(nuclear)·yr or  $F = 0.4 \text{ }^{233}\text{U/fusion neutron}$ ] results in a 20% increase in the cost of electricity and a breakeven  $U_3O_8$  cost of \$340/kg (\$154/lb). The latter represents a 3.4-fold increase in the price of  $U_3O_8$  that is only projected to occur under high demand growth scenarios. For  $^{233}\text{U}$  production levels below 1.1 kg/kW (thermal)·yr, prices climb steeply and the fusion breeder option becomes less attractive.

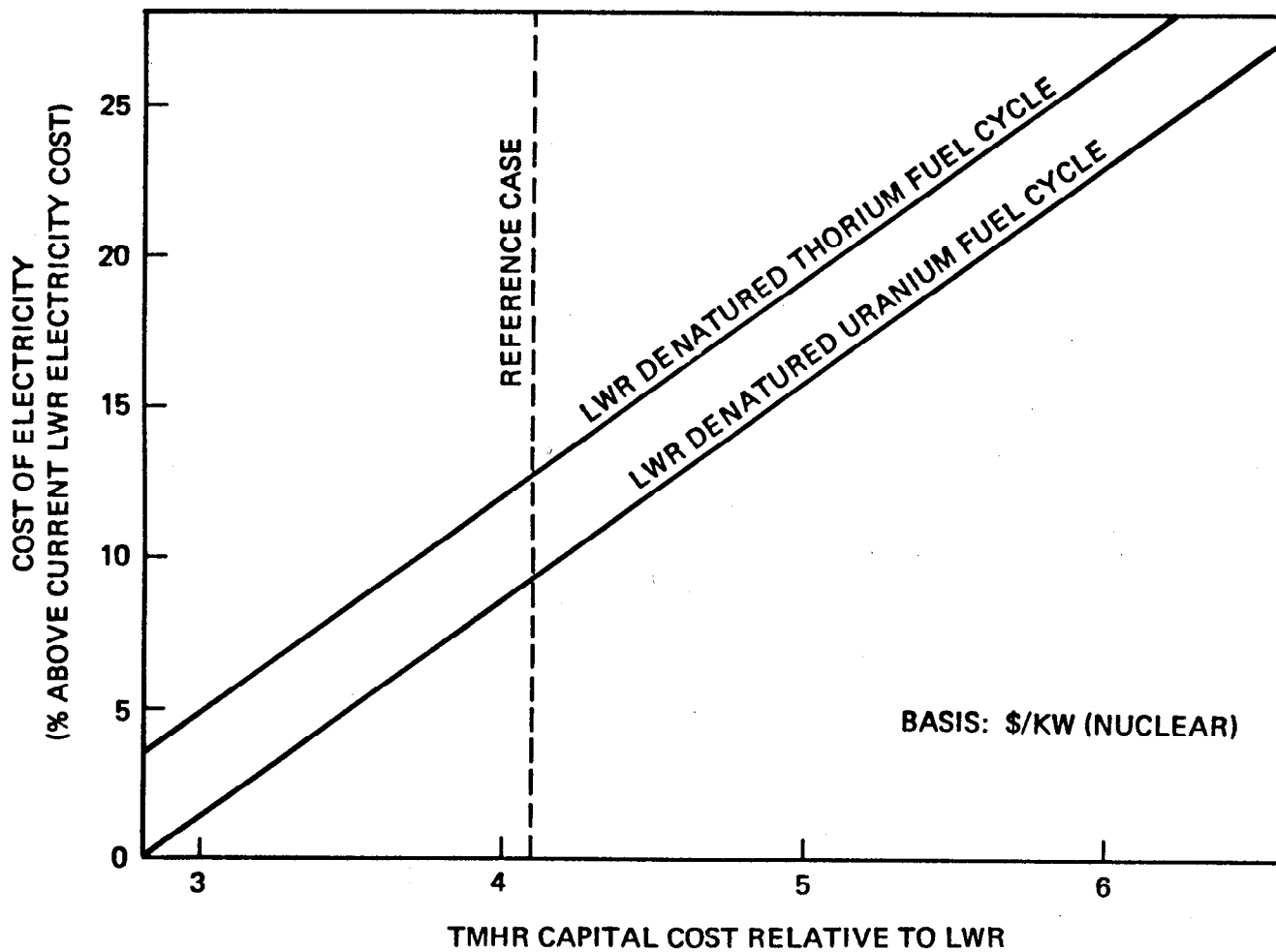


Figure IX.B-4. System electricity cost versus TMHR capital cost.

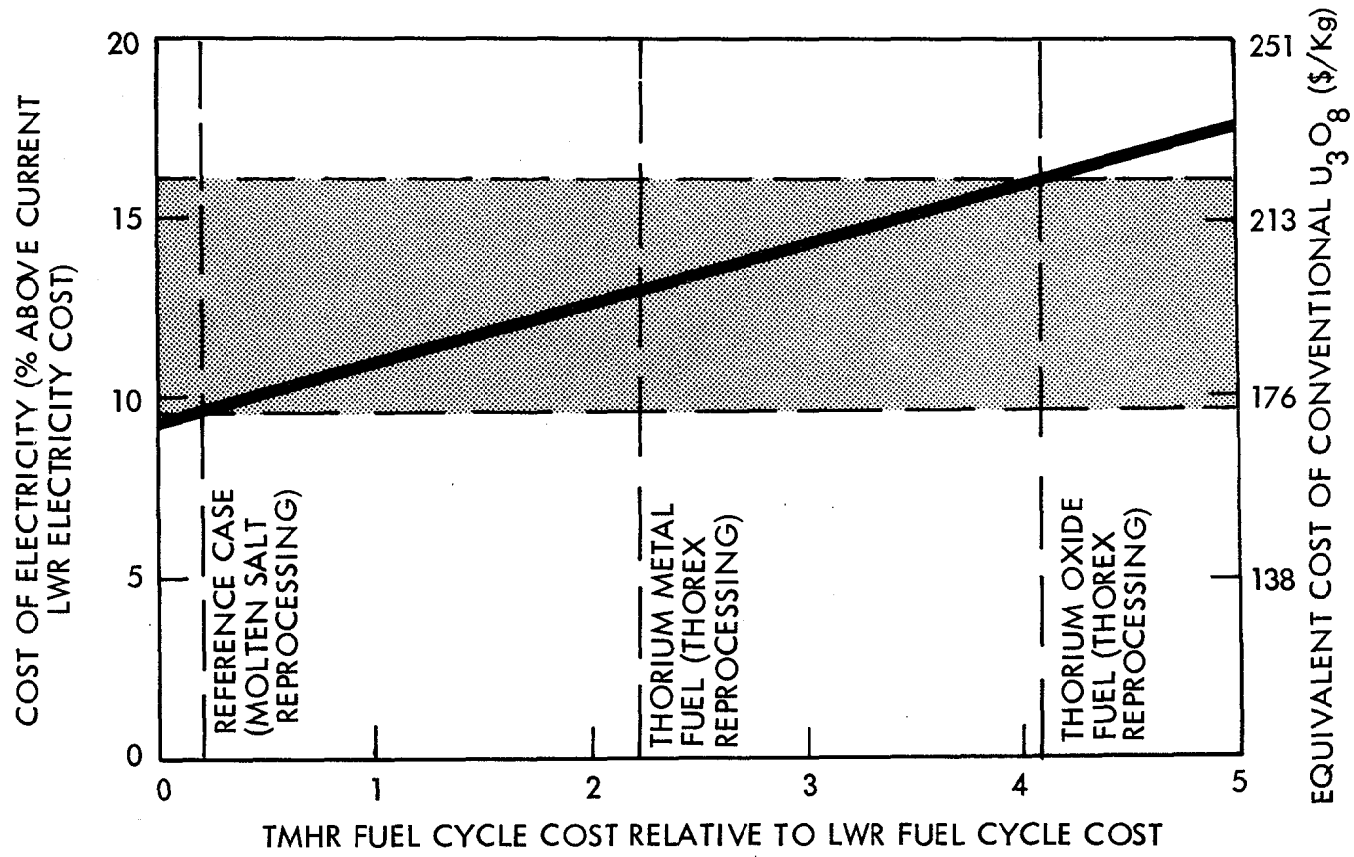


Figure IX.B-5. System electricity cost versus TMHR fuel cycle cost.

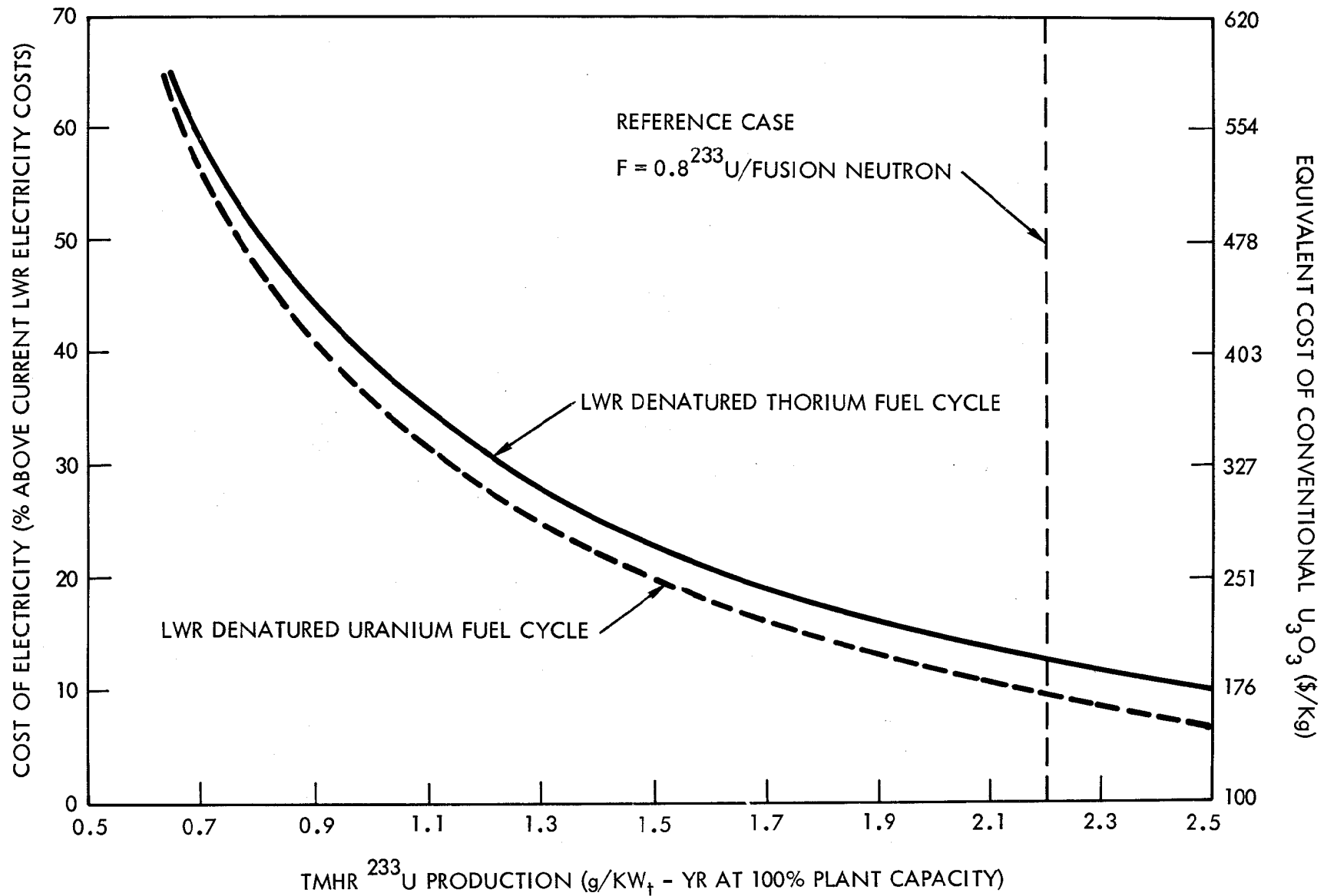


Figure IX.B-6. System electricity cost versus TMHR fissile production rate

In the case of breeder electricity production, the sensitivities are somewhat lower. Figure IX.B-7 indicates that, for the reference TMHR, a 50% decrease in electrical production (expressed as the net electrical efficiency) results in a 4% increase in the cost of electricity and a breakeven  $U_3O_8$  cost of \$206/kg (\$93/lb). In the "fuel factory mode" (i.e., not net electrical production), the cost of electricity becomes 19% above the current LWR electricity cost and the breakeven  $U_3O_8$  costs become \$244/kg (\$111/lb). Based on these results, the fuel factory mode of operation seems viable. Nevertheless, a hybrid with net electrical consumption (i.e., net efficiency less than zero) might not be viable; particularly for institutional and operational reasons.

The above results indicate the following order of importance regarding sensitivities to design uncertainties for the reference system:

1. fuel breeding
2. TMHR capital cost
3. TMHR fertile fuel form (breeder fuel cycle cost)
4. TMHR net electrical efficiency.

In all, the hybrid system demonstrates a great degree of economic "robustness" in its response to large changes in expected performance.

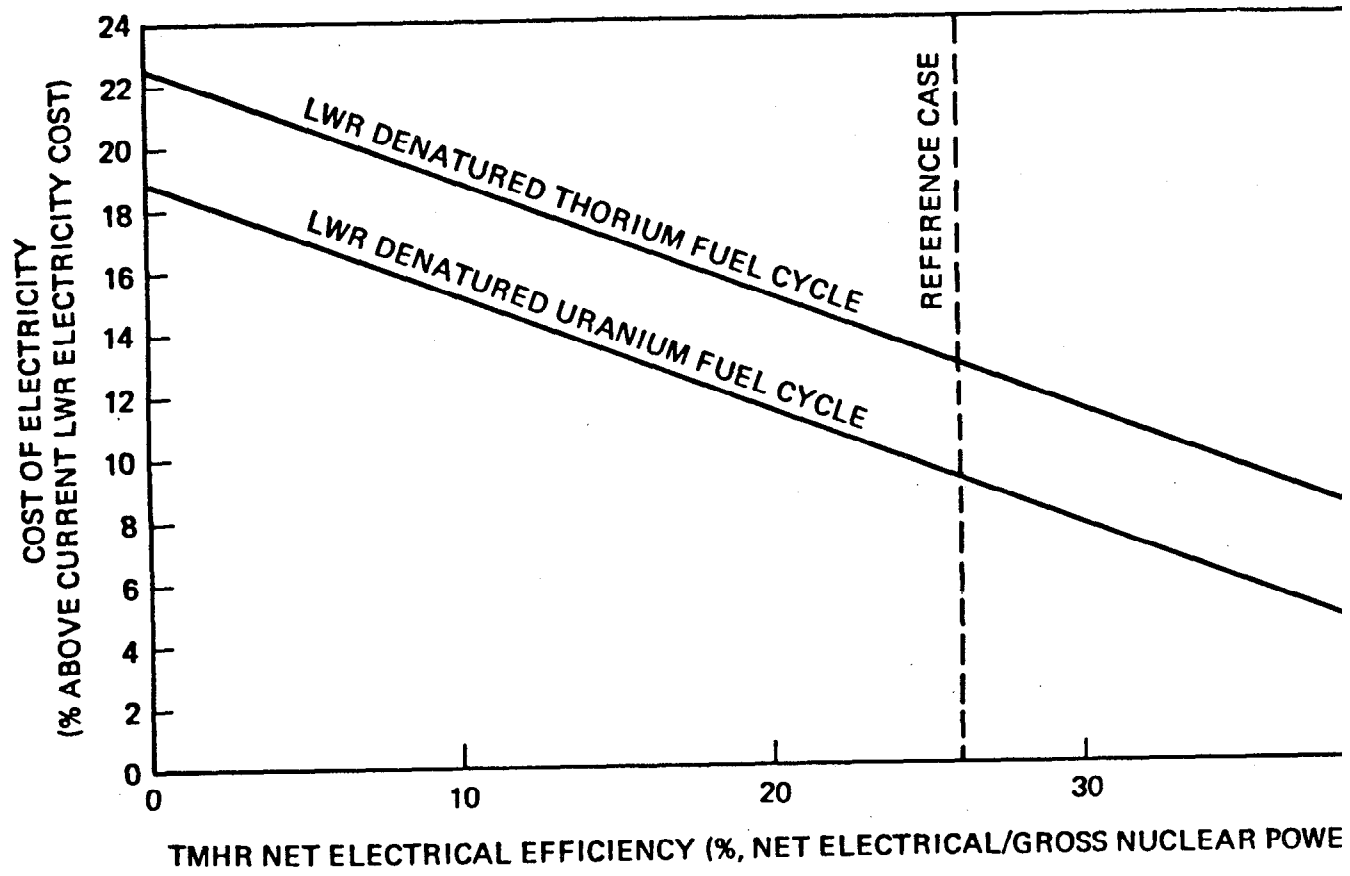


Figure IX.B-7. System electricity cost versus TMHR electrical efficiency

## IX.C SYSTEMS AND ECONOMICS ANALYSIS FOR REFERENCE BLANKET CONCEPTS

In this section we consider the performance and economics characteristics of fusion-fission electricity generation systems utilizing suppressed fission TMHR plants based upon the lithium/molten salt and beryllium/thorium oxide reference blankets developed during this study. With the exception of the TMHR specifications, all data and methods relating to this analysis are identical to those presented in Section IX.B. In particular, denatured uranium fuel cycle LWR clients are assumed. Parametric studies utilizing the results presented in this section as a starting point are presented in Sections IX.D and IX.E while fuel cycle center concepts based upon the reference TMHR designs with LWR clients are presented in Chapter X.

### IX.C.1 Reference TMHR Characteristics

Fuel cycle and power flow specifications relating to the two reference TMHR designs were presented in detail in Chapters VII and VIII. These were reduced to a minimum number of key parameters for input to the PERFEC economics analysis code and are presented in Table IX.C-1.

TABLE IX.C-1. Key performance parameters for reference TMHR plant designs.

	Blanket Type	
	Li/MS	Be/ThO <sub>2</sub>
Net electricity efficiency, kW(electric)/kW(nuclear)	31.1	22.8
Specific fissile fuel production, g/kW(nuclear) yr	1.51	1.93
Specific fissile inventory, g/kW(nuclear)	1.12	0.78

In this table all quantities are normalized to the nuclear power rating of the TMHR. This quantity is defined as:

$$\text{Nuclear Power} = \text{Fusion Power} \times (0.8M + 0.2)$$

where M, the fusion neutron energy multiplication is

$$M = \text{Blanket Energy Per Fusion} / 14.1 \text{ MeV}$$

As discussed in Chapter VIII, both reference TMHR designs utilize the same 3000 MW<sub>fusion</sub> driver but differ with respect to the type of breeding blanket and power conversion system. M values for the Li/MS and Be/ThO<sub>2</sub> blankets are 1.51 and 1.80, respectively.

In comparing the two designs, we first note that the Li/MS TMHR is more efficient in electricity production than the Be/ThO<sub>2</sub> TMHR. This difference can be attributed to a more efficient thermal conversion cycle due to a higher coolant outlet temperature (650°C vs. 450°C) and lower coolant pump power requirements. Regarding fissile production, although the Be/ThO<sub>2</sub> TMHR produces 49% more fissile fuel per unit of fusion power, its higher M value (1.80 vs. 1.51) leads to only a 28% improvement over the Li/MS TMHR per unit of nuclear power. The lower fissile inventory of the Be/ThO<sub>2</sub> system is attributable to a lower in-blanket inventory which results due to a very low fertile fuel volume fraction in the blanket.

The direct capital cost of both reference TMHR plants was presented in Chapter VIII. To obtain the total (direct plus indirect) capital cost for these systems we use the method discussed in Sections IX.B (Table IX.B-5). The plant capital cost is summarized in Table IX.C-2.

Note that the cost of the associated fuel processing plant is included in the total direct cost. This feature reflects our belief that the fuel throughput for each suppressed fission TMHR will be large enough to support a dedicated (economy-of-scale) fuel reprocessing facility. If such facilities are owned by the TMHR operator a cost savings will accrue because the operators capital dominated annual cost for such facilities will not escalate as quickly as the general inflation rate over the plant life. Conversely, if the fuel processing is a service which is purchased from a private supplier it is more reasonable to treat the entire fuel processing charge as a quantity that escalates at the general inflation rate (7%/yr in this analysis).

TABLE IX.C-2. Summary of reference TMHR charges

	Blanket Type	
	Li/MS	Be/ThO <sub>2</sub>
TMHR direct cost, millions of dollars	2711	2561
Fuel processing plant direct cost millions of dollars	75	541
Total direct cost, millions of dollars	2786	3102
Indirect cost, millions of dollars	2365	2634
Time related cost, millions of dollars	917	1020
Total capital cost, millions of dollars	6068	6756

TABLE IX.C-3. Key cost parameters for reference TMHR plant designs

	Blanket Type	
	Li/MS	Be/ThO <sub>2</sub>
TMHR specific capital cost, \$/kW(nuclear)	1397	1134
Total specific capital cost, \$/kW(nuclear)	1436	1374
Annual indirect capital charge at 15.23%/yr, \$/kW(nuclear) yr	219	209
Year zero direct operation and maintenance charge, \$/kW(nuclear) yr	25	24

A summary of the fixed (indirect) and variable (direct) cost inputs to PERFEC is shown in Table IX.C-3. As shown, the cost of both reference TMHRs (including fuel processing) is similar, but the cost of the Li/MS TMHR is 23% above that of the Be/ThO<sub>2</sub> TMHR when the fuel processing plant is not included. This results because the Li/MS blanket produces less power and utilizes a more costly, two coolant, power conversion system. The year zero direct charges shown in the table are a guess based upon PNL recommendations.<sup>16</sup>

#### IX.C.2 System Economics Results for Reference TMHR Designs

The economics methodology used in Section IX.B has been applied to the reference Li/MS and Be/ThO<sub>2</sub> TMHR designs using the performance and cost characteristics described in Section IX.C.1. The results of this analysis are shown in Table IX.C-4.

TABLE IX.C-4. Symbiotic system results fro reference TMHR designs<sup>a</sup>

	Blanket Type	
	Li/MS	Be/ThO <sub>2</sub>
Levelized electrical cost, mill/kWe hr	56	54
Electricity cost, % above current LWR <sup>b</sup>	13	9
Levelized <sup>233</sup> U cost, \$/g	168	141
Levelized equivalent U <sub>3</sub> O <sub>8</sub> cost, \$/kg <sup>c</sup>	613	512
Year zero equivalent U <sub>3</sub> O <sub>8</sub> cost, \$/kg <sup>c</sup>	201	168

<sup>a</sup> All costs in 1980 dollars.

<sup>b</sup> Current technology LWR levelized electricity cost is 49 [mill/kW(electric) hr] (with reprocessing and U<sub>3</sub>O<sub>8</sub> feed cost = \$100/kg)

<sup>c</sup> Assumes 10%/yr U<sub>3</sub>O<sub>8</sub> cost escalation (includes 7%/yr general inflation) and recycling of uranium and plutonium in LWR fuel reprocessing.

Referring to the table we note that, despite a lower net electrical efficiency, the Be/ThO<sub>2</sub> TMHR, in symbiosis with its LWR clients, produces electricity at a slightly lower cost than the Li/MS TMHR system. Most importantly, the 168 \$/kg (76 \$/lb) year zero equivalent U<sub>3</sub>O<sub>8</sub> cost attributed to the Be/ThO<sub>2</sub> TMHR is 33 \$/kg lower than the year zero equivalent U<sub>3</sub>O<sub>8</sub> cost attributed to the Li/MS TMHR. The NASAP U<sub>3</sub>O<sub>8</sub> cost projections presented in Section IX.B (Figure IX.B-3) indicate that the cost of U<sub>3</sub>O<sub>8</sub> will reach 76 \$/lb between 1993 and 2005. For electricity generation beginning during this period, the Be/ThO<sub>2</sub> TMHR (if available) and its LWR clients could produce electricity (over a 30 year lifetime) for the same cost as a conventionally fueled LWR. Assuming a 3%/yr real U<sub>3</sub>O<sub>8</sub> escalation rate (i.e., 1980 dollars) we would expect the Li/MS TMHR to achieve economics breakeven 6 years later than the Be/ThO<sub>2</sub> TMHR (i.e., before 2015).

The economic performance for both of these systems is encouraging in the sense that economic breakeven is possible when the cost of conventional  $U_3O_8$  feed in 1980 dollars increases 2.5 fold.\* The latter condition requires only a modest real escalation of  $U_3O_8$  costs over the next  $\sim$  20-30 years. Considering the calculated cost of electricity from the symbiotic electricity generation system, we know of no other advanced electricity generation option (including the LMFBR) which could be as attractive. In particular, an LMFBR or other advanced option which costs significantly more than an LWR will also produce electricity at a higher cost. The TMHRs described above cost 3-3.5 times as much as an LWR, but because they provide fuel for many LWRs (eg., 10.4 for Li/MS, 13.5 for Be/ $ThO_2$ ), the resulting electricity cost is only about 10% above that obtainable in a current technology LWR fueled with conventional  $U_3O_8$  at near-current prices. Recent LMFBR cost estimates are  $\sim$  1.4 times those of an LWR.<sup>15</sup>

As described in Section IX.A, the results for the reference designs presented in this section are the subject of extensive parametric variations in Sections IX.D and IX.E.

---

\* Current cost of  $U_3O_8$  is about 30.5 \$/lb in 1980 dollars.<sup>15</sup>

#### IX.D TECHNOLOGY DEPENDENT TMRDC + PERFEC PARAMETRIC ANALYSIS FOR A SUPPRESSED FISSION TMHR

When the performance and costs of the fusion driver components are varied as indicated in Tables VIII.B-2 and VIII.B-3, the economics of the system, composed of the fusion breeder and its support fission burners are affected. Examples of the magnitude of these effects will be shown by using the axi-cell (20T case) physics and the Li/MS blanket as base cases. As a starting point, a detailed breakout of the reference TMHR power flow performance and the cost of plant components was provided in Section VIII.C. For this base case, the fusion components (called fusion reactor equipment in Table VIII.C-1) account for 60% of the total direct cost of the fusion breeders.

Variations of fusion component performance and cost around the base case result in the system economic variations listed in Tables IX.D-1 and IX.D-2. Variations in the neutral beam efficiency, from 60% to 30%, give the largest cost increase of any single component performance parameter; a 4.1% increase in system electricity cost, and an 18% increase in year zero equivalent  $U_3O_8$  costs. When all components are reduced to their minimum performance, system electricity cost and equivalent  $U_3O_8$  cost increase 8.4 and 36%, respectively. When all components are increased to their maximum performance, system electricity cost and  $U_3O_8$  costs are reduced by 2.2 and 9.0%, respectively. The effects of component performance variations on the year zero equivalent  $U_3O_8$  cost are shown graphically in Figure IX.D-1.

Turning to variations in component costs, a 50% increase in end cell magnets resulted in the largest cost increase of any component; a 2.4% and a 10% increase in system electricity cost and  $U_3O_8$  cost, respectively. When all component costs are changed to their maximum, system electricity and  $U_3O_8$  costs increase 7% and 30%, respectively. For the optimistic case, the cost of electricity and the equivalent  $U_3O_8$  cost decrease 7% and 30% respectively.

Neutral beam efficiency was found to have the largest effect on system economics of any single variation. But in all cases the bottom line system electricity cost is quite insensitive to variations; the system is quite robust.

TABLE IX.D-1. System economics vs. fusion component performance

Performance Change	FB Direct Cost (M\$) <sup>a</sup>	FB Net Power (MWe)	System Power Cost <sup>b</sup> (mils/kwh)	U <sub>3</sub> O <sub>8</sub> Cost <sup>c</sup> (\$/kg)
None (base case)	2711	1315	55.7	201
$\eta_{NB} = 0.3$ (vs 0.6)	2767	997 (-.242) <sup>d</sup>	58.0 (.041)	236 (.180)
$\eta_{RF} = 0.3$ (vs 0.5)	2721	1259 (-.043)	56.1 (.007)	207 (.035)
$\eta_{DC} = 0.3$ (vs 0.5)	2720	1219 (-.073)	56.3 (.011)	210 (.050)
All waste heat from NB, RF, DC	2664	1169 (-.111)	56.2 (.009)	209 (.045)
All of above	2683	528 (-.598)	60.4 (.084)	274 (.363)
Optimistic, $\eta_{NB} = .8, \eta_{RF} = .6,$ $\eta_{DC} = .65$	2685	1504 (.144)	54.5 (-.022)	182 (-.090)

<sup>a</sup>Cost variations do not include increased component costs at lower efficiency (ie., power supplies for neutral beams and rf)

<sup>b</sup>Levelized costs from PERFEC analysis

<sup>c</sup>Year zero breakeven costs from PERFEC analysis

<sup>d</sup>Fractional changes in parentheses

TABLE IX.D-2. System economic vs. fusion component cost variations

Cost Change	FB Direct Cost (\$M)	System <sup>a</sup> Power Cost (mils/kwHe)	U <sub>3</sub> O <sub>8</sub> <sup>b</sup> Cost (\$/kg)
None (base case)	2711	55.7	201
End cell magnet cost + 50%	2907 (.072) <sup>c</sup>	57.1 (.024)	222 (.104)
NB cost = 2 \$/W (vs. 1.5)	2844 (.049)	56.6 (.017)	215 (.069)
RF cost = 5 \$/W (vs. 3)	2829 (.044)	56.5 (.015)	214 (.065)
Center cell magnet cost + 25%	2746 (.013)	55.9 (.004)	205 (.020)
Plasma dump system cost + 50%	2763 (.019)	56.1 (.007)	207 (.030)
Other costs + 50%	2736 (.009)	55.9 (.003)	204 (.015)
All of the above increases (pessimistic case)	3270 (.206)	59.6 (.070)	262 (.303)
Optimistic case <sup>d</sup>	2152 (-.206)	51.8 (-.070)	140 (-.303)

<sup>a</sup>Levelized costs from PERFEC analysis

<sup>b</sup>Year zero breakeven costs from PERFEC analysis

<sup>c</sup>Fractional charges in parenthesis

<sup>d</sup>Beneficial variations in Table VIII.B-3

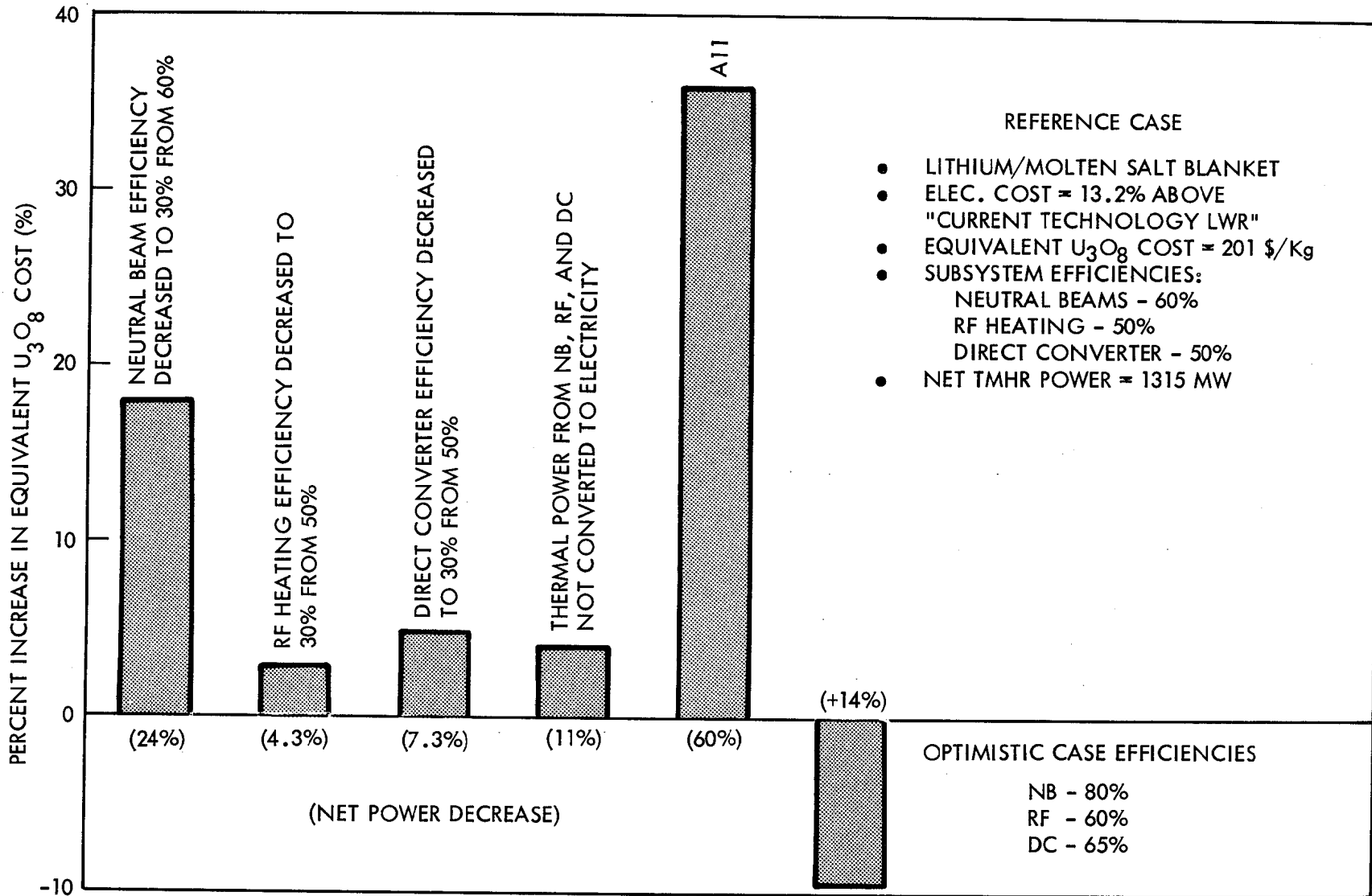


Figure IX.D-1. Effects of variations in fusion subsystem performance on the equivalent costs of  $U_3O_8$

## IX.E PLASMA PHYSICS DEPENDENT TMPC + TMRDC + PERFEC PARAMETRIC ANALYSIS

### IX.E.1 Overview

In this section, we present results from the coupling of the physics code (TMPC),<sup>1</sup> the fusion reactor design code (TMRDC),<sup>2</sup> and the fissile fuel cycle economics code (PERFEC).<sup>3</sup> For the purpose of determining system sensitivities to changes in physics input variables, the year zero equivalent cost of  $U_3O_8$  and the levelized cost of electricity produced by the breeder/burner system are used as figures of merit. The case used as a starting point is a case with slightly better performance ( $Q \approx 16.3$ ) than the baseline used for the reference TMHR cases (i.e.,  $Q \approx 15.3$ , in Chapter VIII and Sections IX.C and D). This case was discovered by additional optimization after the baseline case had been frozen.

The physics sensitivities and baseline case are the same as those presented in Section II.D. One important variation, which effects the system economics, involves a parametric survey of different operating points on the plasma gain vs. wall loading ( $Q, \Gamma$ ) curve. In this section, we also examine the changes in system economics when maximum magnetic field strength, fusion power, neutral beam injection energy (and charge state of ion which is neutralized), central cell beta value, and fraction of cold plasma at the thermal barrier are changed. The two "low technology" axicell cases described in Section II.D are evaluated here with respect to their economic potential. The MFTF-B/TMNS A-cell thermal barrier end cell configuration is considered, and economic performance assessed. For these TMNS cases, the costing is changed to be consistent with the TMNS study report.<sup>17</sup>

Finally, we analyze a pure fusion case incorporating a blanket similar to the blanket which was used for the WITAMIR-I tandem mirror design.<sup>18</sup> A comparison is made between the stand-alone levelized cost of electricity produced by this system and that produced by the breeder/burner system.

Parametric analyses are an important ingredient in the TMHR economic analysis because, among other things, such analysis can be used to determine the optimum operating point of a tandem mirror hybrid. When the study began, a baseline wall loading of  $2 \text{ MW/m}^2$  was specified. This

choice was based upon our previous experience in which system cost minimizes at this wall load. The minimum is obtained as a tradeoff between supplementary heating costs and costs associated with lengthening the central cell. At low Q, the central cell is compact, but neutral beams and microwave gyrotrons which provide plasma heating are costly. At high Q, heating is less expensive, but the central cell is long and, for example, many magnets may be needed. We find in this study that the optimum wall loading is lower than  $2 \text{ MW/m}^2$ , and is a function of the maximum magnetic field strength in the plug,  $B_{\text{max}}$ . At a  $B_{\text{max}}$  of 20 T, the optimum occurs at  $1.6 \text{ MW/m}^2$  (at the baseline 1.5 meter first wall radius). At a  $B_{\text{max}}$  of 14 T, the minimum cost occurs at  $1.3 \text{ MW/m}^2$ . The reasons for the optimum occurring at lower wall load is the desirability of operating at high Q, induced by the high cost of supplementary heating in the end cells. Previous studies (1979 hybrid study) assumed that the cost of end cell heating was fairly modest, \$.50/watt.<sup>7</sup> The estimates used in the present study is \$1.50/watt for neutral beams, and \$3.00/watt for ECRH.

The results presented in this section have also shown the importance of high magnetic field strengths and have deemphasized the need for high neutral beam injection energies (i.e., neutral beams produced by negative ions) for the axicell end plug configuration. The cost of bred fissile material and the system electricity cost are both strong functions of  $B_{\text{max}}$ , but are not nearly as sensitive to reducing the injection energy. This result does not provide enough basis to conclude unequivocally that the hybrid does not require negative ion neutral beams. Nevertheless, the present state-of-the-art plasma and systems modeling of the fusion driver based on the axicell end-cell configuration indicates that good system performance can be obtained using only positive ion beam technology.

## IX.E.2 System Parametrics

As discussed above, an interesting variation involves a determination of the sensitivity of the year zero equivalent cost of  $U_3O_8$  and the levelized symbiotic electricity cost of changing the point on the Q versus  $\Gamma$  operating curve. Figures IX.E-1 and IX.E-2 show the year zero  $U_3O_8$  cost and the levelized symbiotic electricity cost as a function of wall loading, respectively. Both the beryllium/thorium oxide and the lithium/molten salt blankets are shown, as well as two values of magnetic field strength in the barrier coil; 14T and 20T.

Several points should be made regarding these figures. First, note that the reference systems described in earlier sections do not operate at the wall loading which yields the lower cost. For the 20T case and a 2 m first wall radius the minimum occurs at about  $1.8 \text{ MW/m}^2$  and, for the 14T case, the minimum occurs at  $1.5 \text{ MW/m}^2$ . The reference baseline ( $2 \text{ MW/m}^2$ ) was chosen based on previous experience. This experience was gained at a time when supplementary heating was assumed to be inexpensive ( $\sim \$0.50/\text{watt}$ ). When plasma heating costs are low, high Q is not nearly as important, and the minimum cost shifts to higher wall loading. When heating costs are high compared to central cell costs, (as is true in the present study) high Q is important. This makes the optimum wall load shift to a lower  $\Gamma$  value (higher Q). Since the 14T axicell case has a Q value which is lower than the 20T case for the same wall loading, the 14T case optimizes at a lower  $\Gamma$  value.

Another important result may be obtained from these figures. The sensitivity of costs on wall loading at wall loadings higher than the optimum is much greater at lower maximum magnetic fields. This occurs because the 14T case operates at a lower Q where system costs are more sensitive to supplementary heating. Note also that for wall loads less than the optimum, the sensitivity at both values of  $B_{\text{max}}$  is similar. This occurs because the turnup of the curve in this regime is due to rising central cell costs, which are similar for both cases.

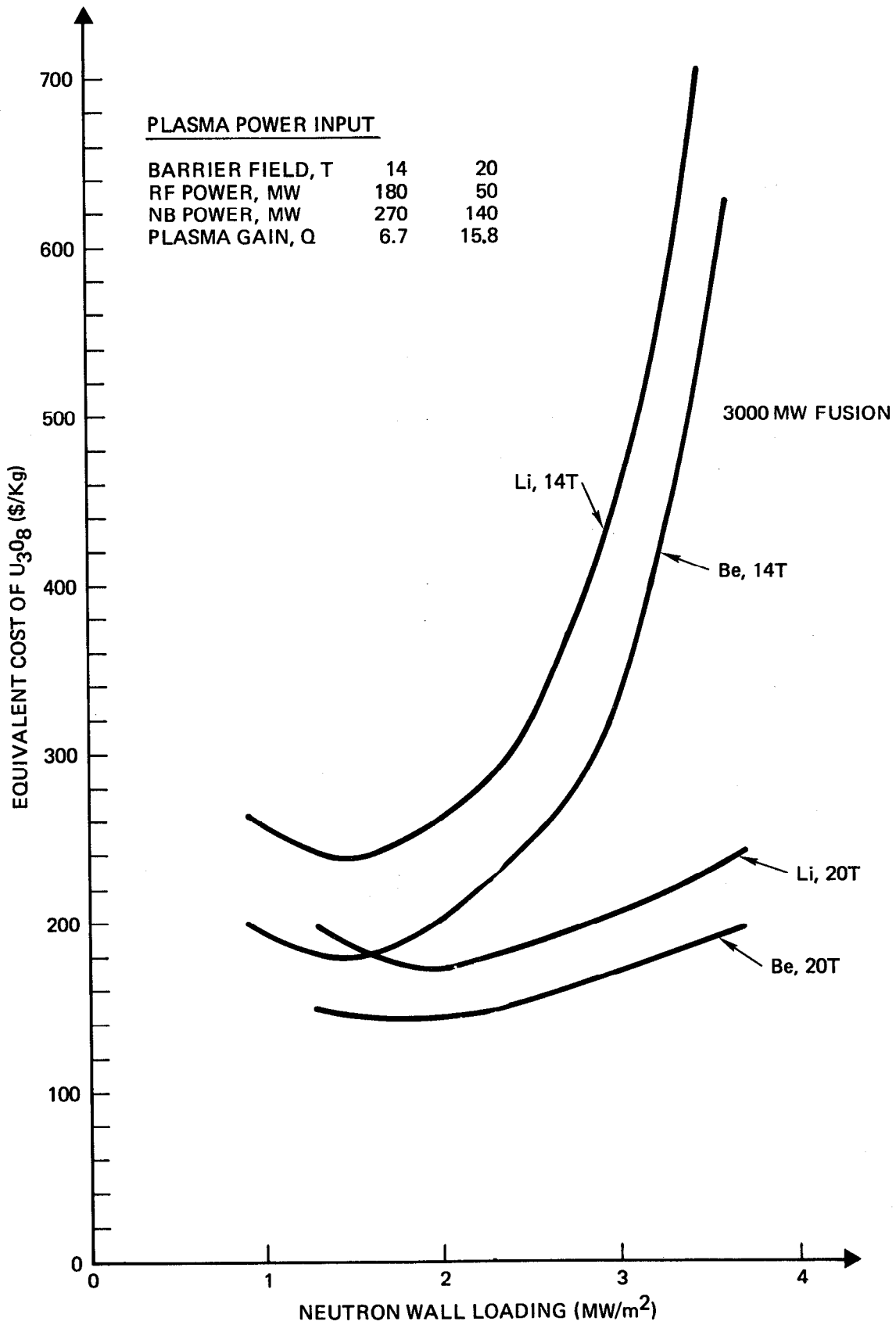


Figure IX.E-1. Comparison of equivalent  $U_3O_8$  cost vs. wall loading for different maximum magnetic field strengths and blanket designs

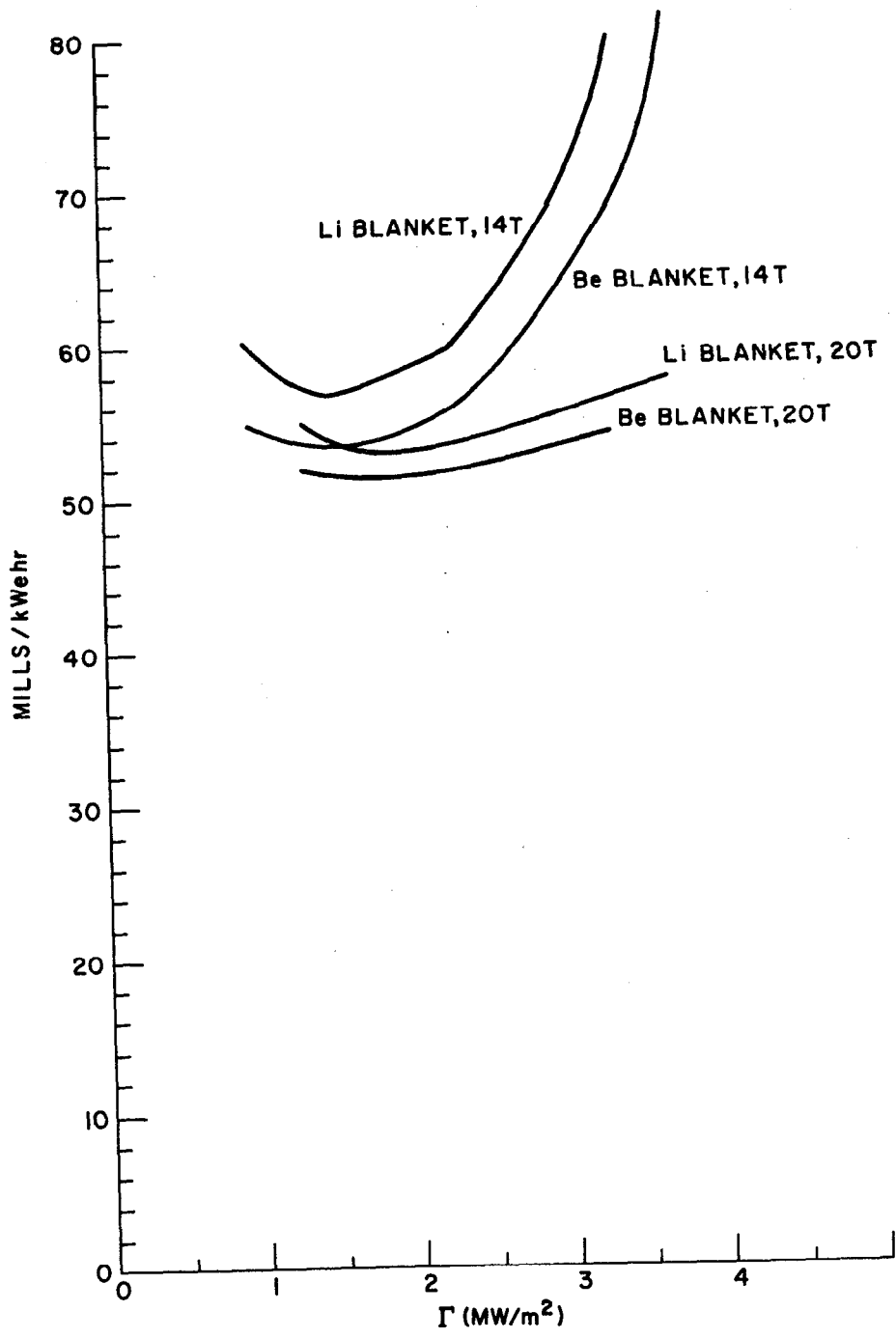


Figure IX.E-2. Levelized symbiotic cost of electricity as a function of wall loading, treating  $B_{max}$  as a parameter

Figures IX.E-3 and IX.E-4 show the sensitivity of equivalent  $U_3O_8$  cost and system electricity cost on variations in central cell beta value,  $\beta_{cc}$ . Curves such as these indicate what happens if the interchange criterion used to predict a MHD stable beta is too optimistic. Beta values around 20% are typical of the pessimistic MHD ballooning criterion (Section II.G.2). The cost penalty in going from 70% down to about 40% is not particularly severe for the hybrid, but dropping to still lower beta values indicates a considerable cost increase. Note that the lithium blanket has a greater sensitivity to changes in  $\beta_{cc}$  than does the beryllium blanket. This results because of the larger amount fissile material produced by the hybrid using the beryllium blanket. This support ratio related result is typical of the results obtained when other parameters are varied.

It is important to assess the impact of changing magnetic field strengths and beam injection energies on hybrid economics. Table IX.E-1 shows four beryllium blanket cases. Shown in the table are the baseline case with a 20T barrier coil, a case where a 14T barrier coil is used, a "low technology" case where a 12T barrier coil and 200 keV positive ion neutral beams are used, and a case where positive ion beam technology is used, but the 20T coil with copper insert is reinstated. The "low technology" case also assumes physics pessimism in that central cell beta is assumed to be 40% rather than the normal 70%. The breeder direct capital cost ( $C_{BR}$ ), neutron wall loading ( $\Gamma$ ), plasma gain ( $Q$ ), year zero equivalent  $U_3O_8$  cost ( $C_{U_3O_8, yr0}$ ), and levelized cost of symbiotic electricity ( $C_{elec, lev}$ ) are used as figures of merit.

To model the positive ion neutral beam system, the efficiency has been lowered from the nominal 60% to about 35% (see Section IX.D). The cost of the neutral beams has been estimated using two methods. The first is to assume that the \$1.50/watt of delivered power to the plasma remains constant. This is consistent with the assumptions advanced in the Battelle costing study (Section IX.D).<sup>20</sup> The other method assumes that the cost per watt delivered to the plasma increases by the factor that the beam efficiency decreases, modeling the expectation that power supplies (which drive beam cost) need to produce more electrical power for a given beam power.

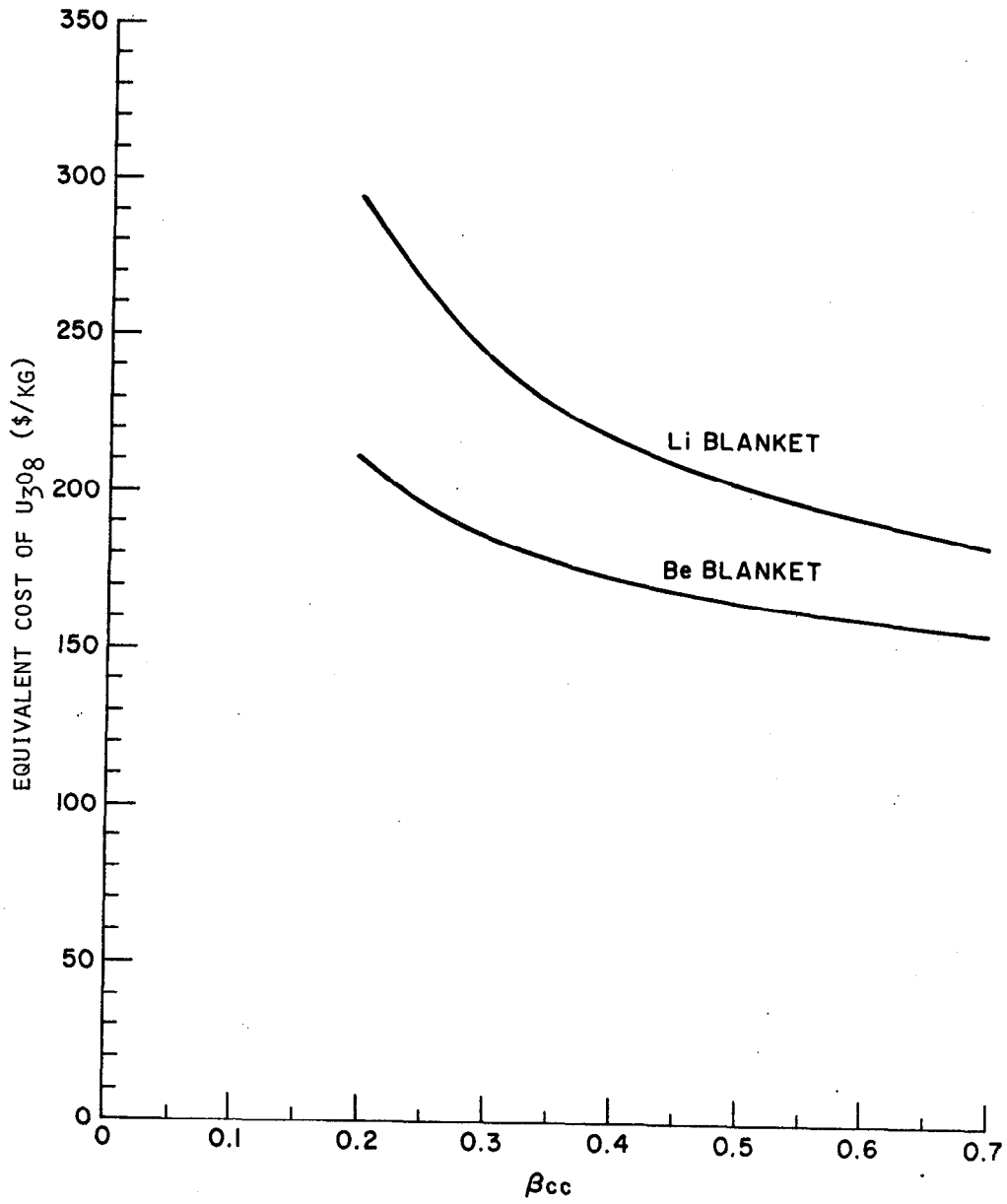


Figure IX.E-3. Sensitivity of equivalent  $U_3O_8$  cost to  $\beta_{cc}$  variations  
 $(r_{cc}^2 B_{cc} \sqrt{1-\beta_{cc}} = \text{constant}, B_{cc}^2 \beta_{cc} = \text{constant}, B_{\text{max}} = 20T)$

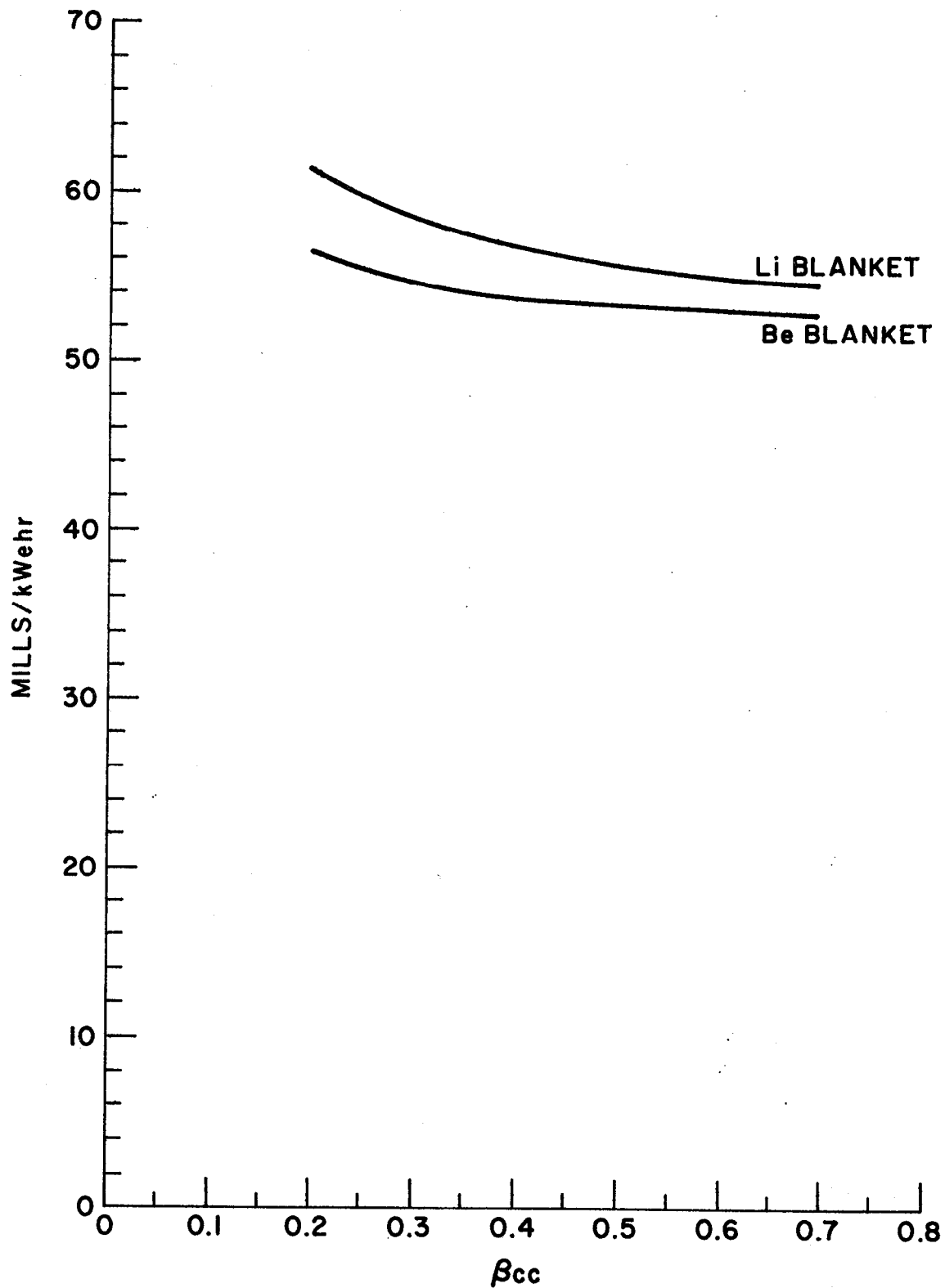


Figure IX.E-4. Levelized symbiotic cost of electricity as a function of central cell beta value.

$$(B_{\max} = 20T, r_{cc}^2 B_{cc} \sqrt{1-\beta_{cc}} = \text{constant}, B_{cc}^2 \beta_{cc} = \text{constant})$$

TABLE IX.E-1. Hybrid cost and performance parameters when magnet and neutral beam parameters are changed. Beryllium blanket used here.

	1980 Dollars						
	$B_{\max}$ (T)	$E_{inj}$ (keV)	$C_{BR}$ (\$B)	$C_{U_3O_8, yr0}$ (\$/kg)	$C_{elec, lev}$ (mills, kV(e)hr)	Q	$\Gamma$ (MW/m <sup>2</sup> )
Baseline	20	250	2.4	158	53.	16.3	2.3
14T barrier coil	14	250	3.2	229	57.5	6.7	2.3
"Low Technology"	12	200	4.9	481	74.	3.3	1.4
Positive ion N.B.	20	200	2.5 (2.8)*	174. (194)	54. (55)	16	2.3

\* Parenthesis indicate effects of neutral beam cost scaling as inverse of beam efficiency (see text).

There is a large increase (~45%) in the equivalent cost of  $U_3O_8$  by going from 20T to 14T, and a large increase (~200%) in going from 20T to the 12T (with lower  $\beta_{cc}$ ) low technology case. Notice that the penalty for going to positive ion technology is not severe, if the cost per delivered watt remains fixed; capital cost rises about 4%, cost of  $U_3O_8$  rises only 10%, the symbiotic electricity cost rises only 2%. This result may suggest that positive ion neutral beam technology may be sufficient for the hybrid. The cost numbers in parenthesis are those which correspond to the case when the cost per watt of neutral beams is increased by the ratio of efficiencies. These costs are somewhat higher; capital cost rises 16%, equivalent  $U_3O_8$  cost is 23% higher and the electricity cost rises about 4%. Note that the net electric power drops from 1170 MW to 930 MW when the neutral beams are less efficient.

Figures IX.E-5 and IX.E-6 show the sensitivity of costs to changes in fusion power,  $P_{fus}$ , for both blanket designs. Economy of scale is clearly apparent as the 400 MW driver makes fuel at about half the price as the 2000 MW driver. As fusion power changes, so will the cost of fissile fuel. This results because, for a fixed end cell cost, the cost of providing fewer fusion neutrons increases as the driver cost remains nearly constant with decreasing power. Other factors, such as a fixed central cell tritium breeding requirement to provide for end cell losses, increase the net cost of fissile fuel bred.

Figure IX.E-7 shows the variation in the equivalent cost of  $U_3O_8$  for the beryllium/thorium oxide blanket as the sloshing beam injection energy is varied. The cost per unit power of neutral beam as well as neutral beam efficiency are held fixed in this calculation. This is intended to model the situation where negative ion neutral beams are used at all energies, and only the energy of the particles are varied. Recall from Section II.D,  $Q$  was quite insensitive to  $E_{inj,a}$  until the energy got so low that confinement was poor (Figure II.D-3). This result is reflected in the cost of  $U_3O_8$ . The lithium blanket yields similar results.

Figure IX.E-8 shows the sensitivity of  $U_3O_8$  cost to changes in the fraction of cold electrons at the midplane of the thermal barrier,  $F_{ec}$ . As was mentioned in Section II.D, this parameter measures the effectiveness of the thermal barrier. Better performance is obtained at lower  $F_{ec}$ . From this figure, it can be seen that the  $U_3O_8$  cost only increases by about 10% when  $F_{ec}$  is increased by almost an order of magnitude. This is a fortunate fact, because the value of  $F_{ec}$  required for microstability and hot electron particle balance has not as yet been established, although it is expected to lie within the range surveyed in Figure IX.E-8.

The hybrid costing parametrics presented thus far have been based on a fusion driver using the "axicell" end cell configuration. It is of interest to determine the costing sensitivities when the more familiar TMNS-like A-cell configuration is used. Figure IX.E-9 shows the A-cell year zero equivalent cost of  $U_3O_8$  as a function of wall loading for both blanket types. Costing information for these cases was obtained directly from the TMNS report.<sup>19</sup> The major changes were the cost of ECRH (increased from \$3/watt to

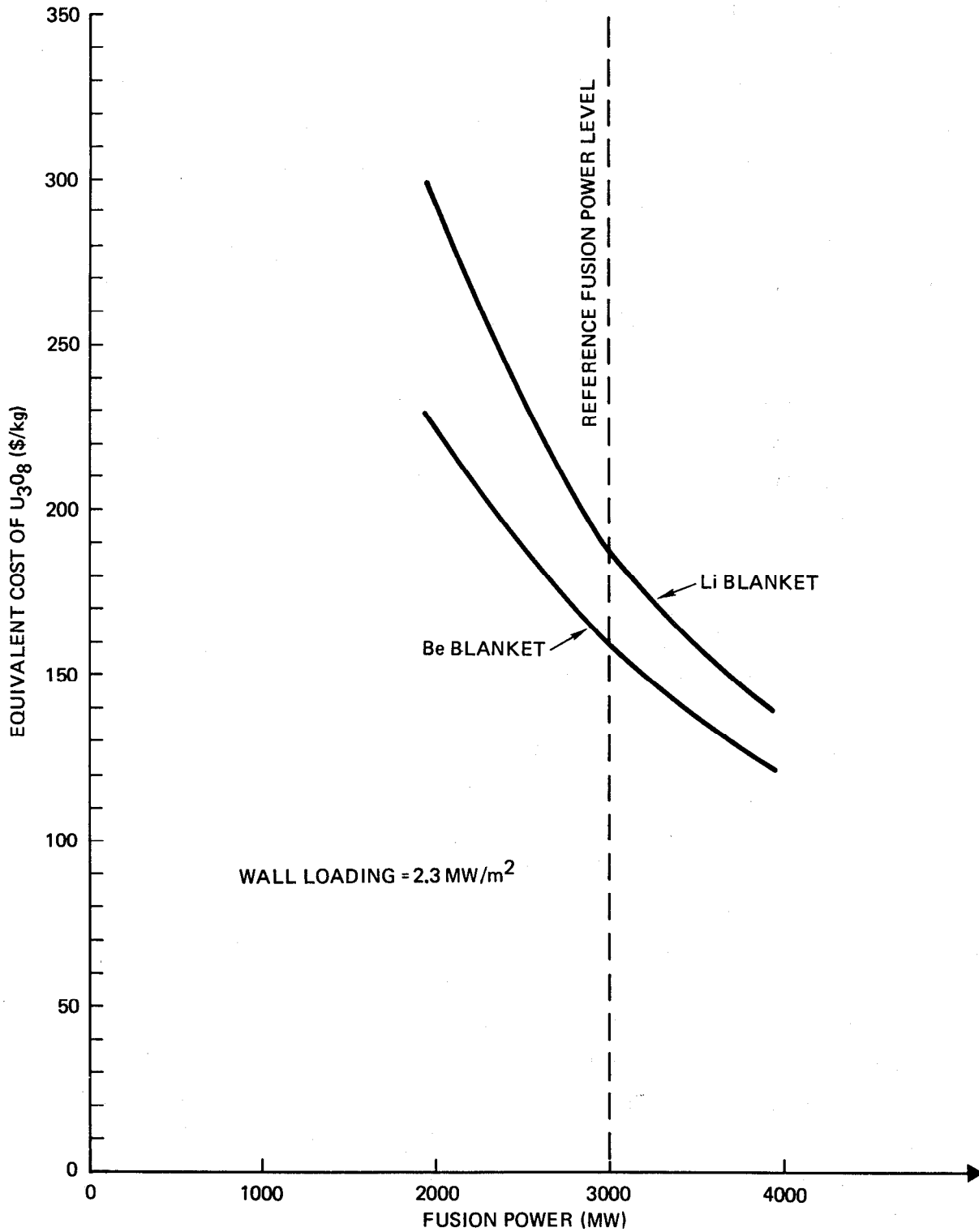


Figure IX.E-5. Year zero equivalent  $U_3O_8$  cost as a function of fusion power

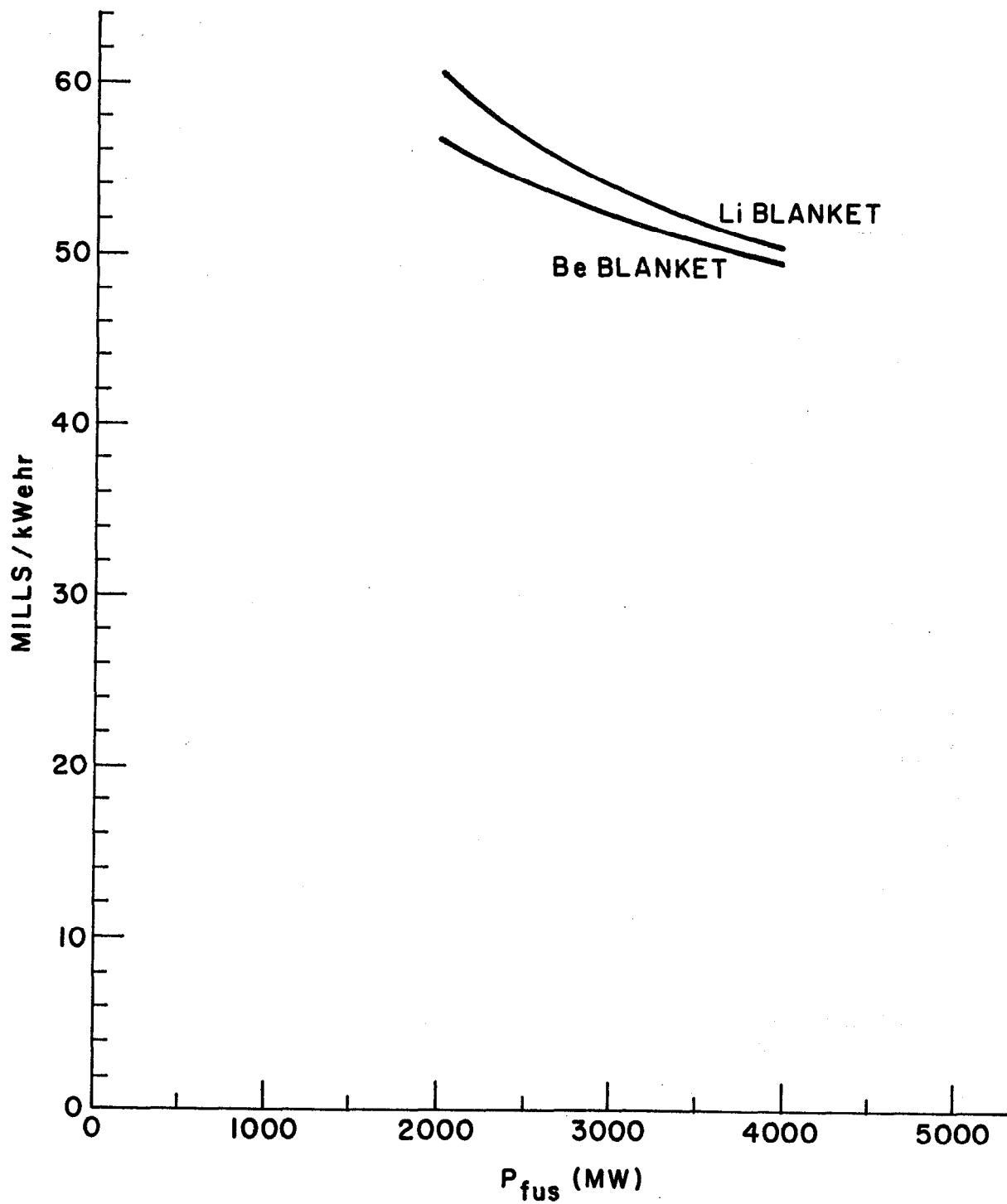


Figure IX.E-6. Levelized symbiotic cost of electricity as a function of fusion power

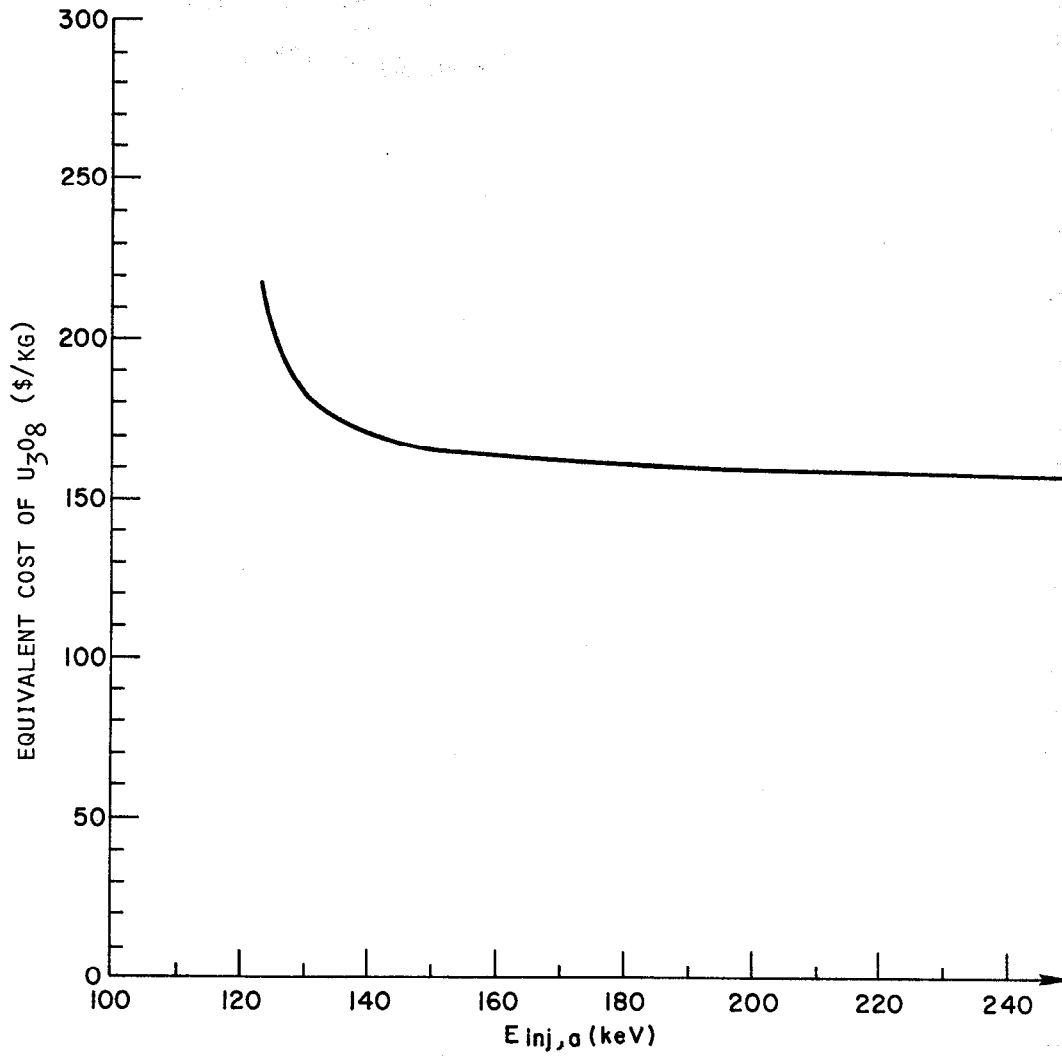


Figure IX.E-7. Equivalent  $U_3O_8$  cost as a function of sloshing beam injection energy (Be blanket)

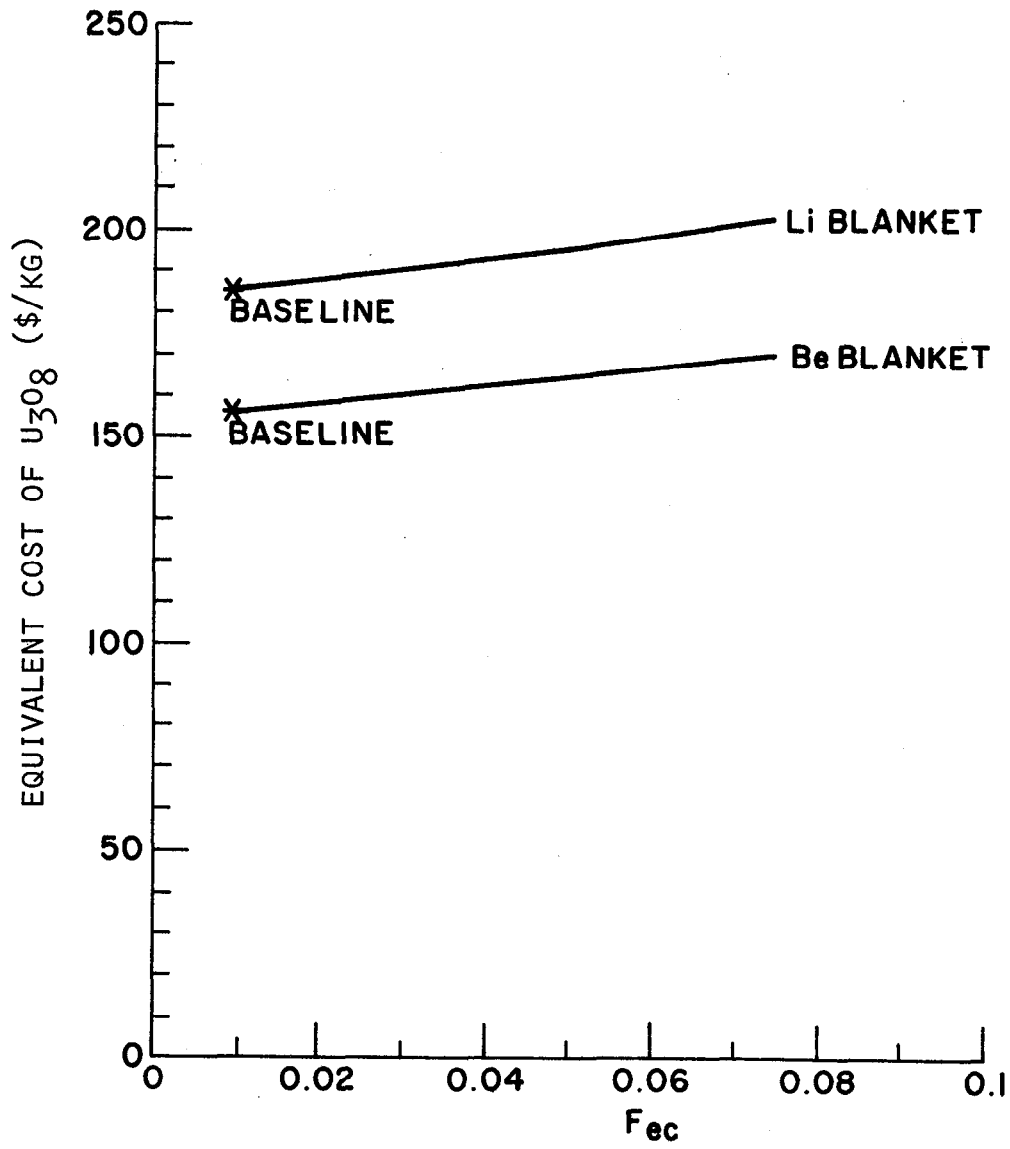


Figure IX.E-8. Equivalent  $U_3O_8$  cost as a function of  $F_{ec}$

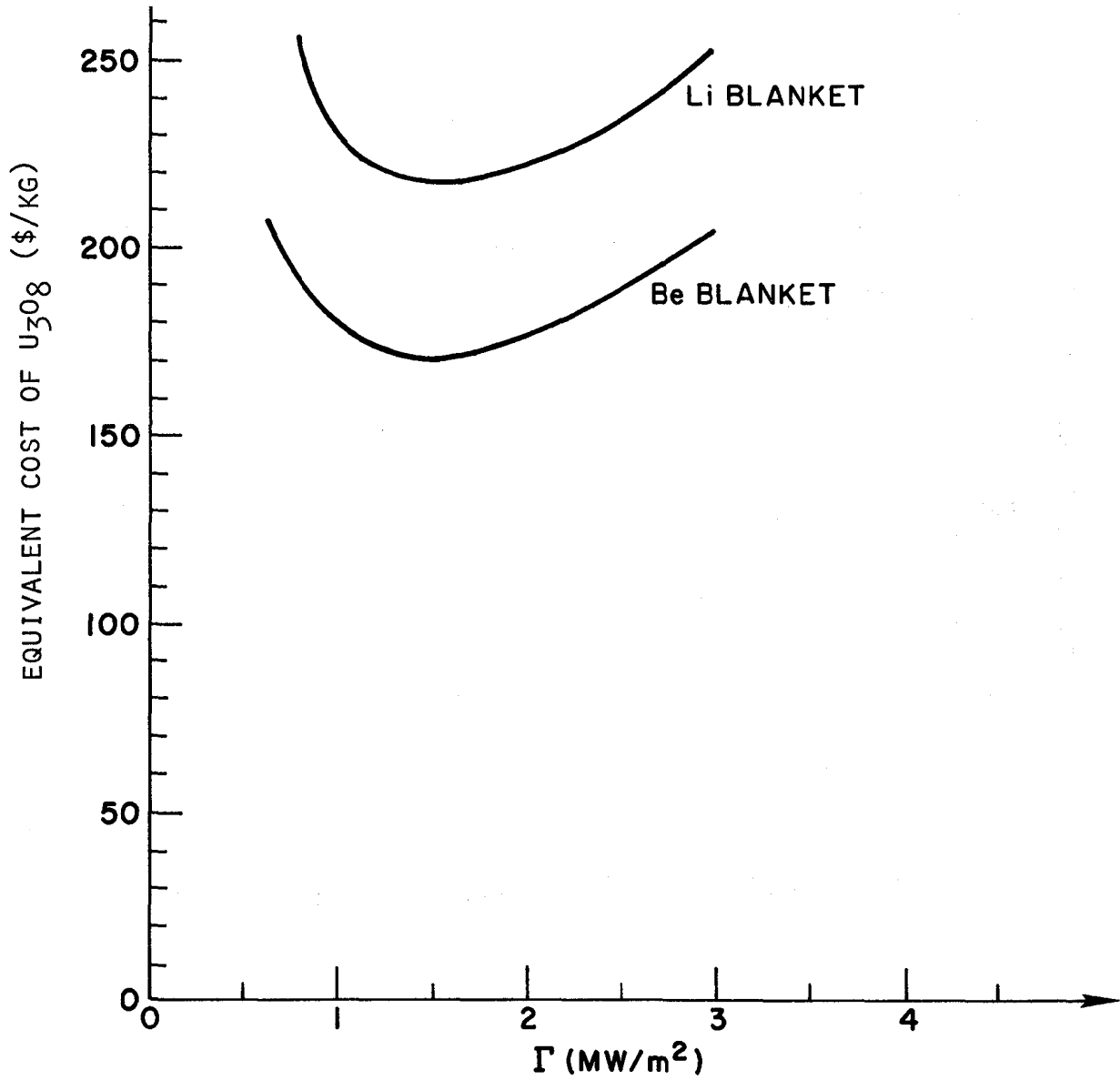


Figure IX.E-9. Equivalent cost of  $U_3O_8$  for TMNS end cells and costing as a function of wall loading ( $P_{fus} = 3000$  MW)

\$5/watt of delivered power), and the end plug magnet set cost (assumed to be \$453M). Also, since fusion power generated in the end cells is much greater in the case of the A-cell configuration (see Section II.I), more tritium breeding must be accomplished in the central cell and the net number of fissile atoms produced per fusion neutron was appropriately reduced. As can be seen from the figure, the optimum wall load occurs of about  $1.5 \text{ MW/m}^2$  and is very similar to the 14T axicell case with approximately the same absolute cost. This optimum cost is about 15% higher than the 20T axicell case.

### IX.E.3 Pure Fusion Comparison

It is of interest to compare the system performance (i.e., electricity costs) of a pure fusion power plant with the performance of a fusion hybrid breeder/LWR burner. The blanket chosen for the pure fusion driver is similar to that used for the WITAMIR-I reactor design. Figure IX.E-10 shows such a comparison with the plasma gain,  $Q$ , as independent variable, and the normalized levelized cost of electricity as the figure of merit. The normalizing factor is the levelized cost of electricity of a current technology LWR when the cost of  $\text{U}_3\text{O}_8$  reaches \$100/lb (see Section IX.B). The neutron wall loading at the minimum first wall radius is shown as a set of X's. The cost competitiveness of the hybrid is evident in this figure; both the lithium and beryllium blankets are within 20% of LWR costs, even with the poor  $Q$  value of around 7.5. With better performance, (i.e., the baseline case of  $Q \sim 15-16$ ), the curve is rather flat, with symbiotic electricity costs only 7-12% higher than competing LWR costs. Pure fusion suffers greatly with low  $Q$  and, even at the optimum  $Q$  of around 30, pure fusion electricity costs about 2.3 times as much as LWR electricity.

Another important area which breeder/burner electricity generation systems and pure fusion reactors should be compared is the sensitivity of their electricity cost to changes in the central cell beta value deemed stable to perturbations of the plasma column. Figure IX.E-11 shows the normalized costs of fusion and symbiotic electricity generation as a function of central cell beta,  $\beta_{cc}$ . The sensitivity of symbiotic electricity cost is quite mild, whereas the pure fusion electricity cost is sensitive to changes in  $\beta_{cc}$ , for all values of  $\beta_{cc}$ .

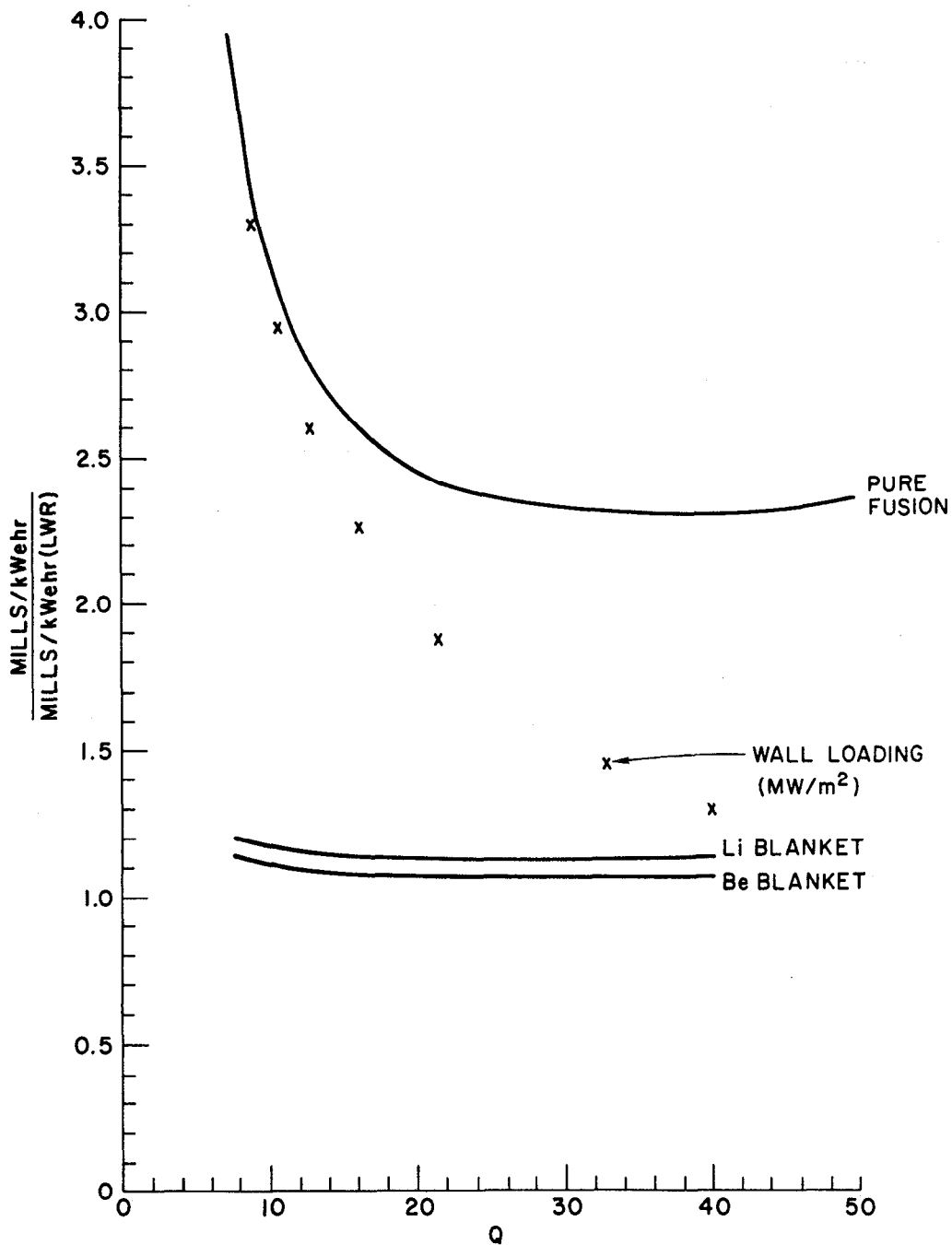


Figure IX.E-10. Comparison of normalized levelized cost of electricity for pure fusion and the hybrid ( $Q = Q(\text{wall loading}, \Gamma)$ )

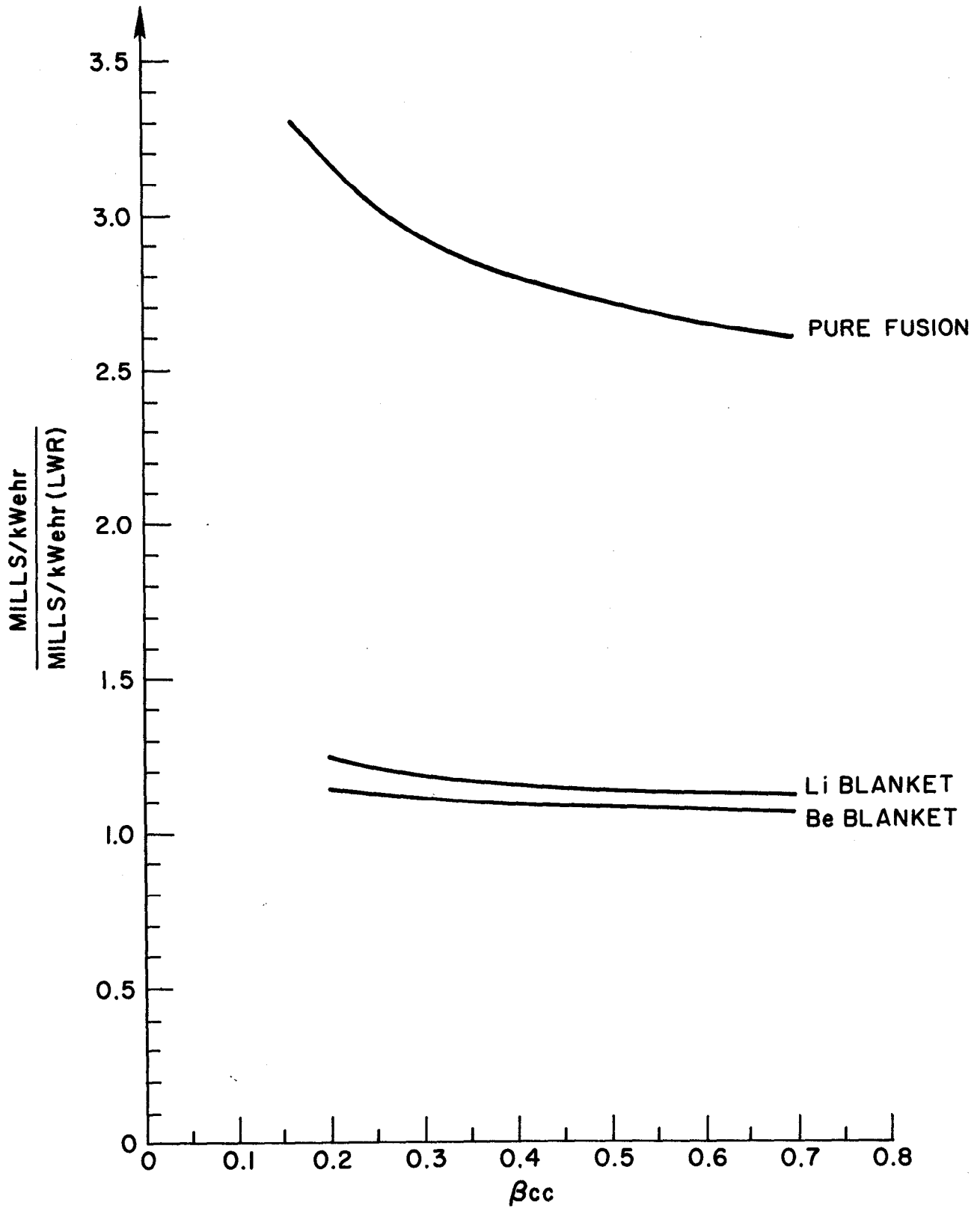


Figure IX.E-11. Sensitivity of normalized levelized cost of electricity on  $\beta_{cc}$  for pure fusion and the hybrid/LWR system

#### IX.E.4 Summary

The most important results from this section can be summarized as follows:

(1) The high cost of supplementary heating relative to costs associated with lengthening the machine drive the hybrid to higher Q and lower wall loading than had been previously suspected. This results in a Q increase from 4 to about 16, since our estimates for the cost of heating have quadrupled since the 1979 hybrid study.

(2) The impact of going to lower neutral beam injection energies, even using positive ion neutral beam technology, is quite mild compared to the great sensitivity of performance to changing the magnetic field in the barrier coil.

(3) The levelized cost of electricity for the hybrid/LWR system is from 7 to 20% higher than current technology LWR electricity costs which correspond to a  $U_3O_8$  cost of \$100/kg. The exact number depends upon the point on the (Q, $\Gamma$ ) performance curve at which the machine operates.

(4) Using published costs for a fusion driver based on the TMNS A-cell end plug configuration, a moderately competitive hybrid/burner system can be defined.

(5) The electricity cost of the fusion breeder/LWR burner system is much less expensive than that of pure fusion. From our modeling of a fusion driver using a WITAMIR-I blanket, we find that pure fusion optimally produces electricity at just over twice the cost of an LWR at the time which a hybrid could be introduced competitively.

## REFERENCES FOR CHAPTER IX

1. G. A. Carlson, et. al., "Comparative End Plug Study for Tandem Mirror Reactor," LLNL Report UCID-19271, December 1981.
2. D. I. Chapin et.al., "Preliminary Feasibility Assessment of Fusion Fission Hybrids," WFPS TME-81-003, Westinghouse Fusion Power Systems Department (1980).
3. D. H. Berwald and J. A. Maniscalco, "An Economics Method for Symbiotic Fusion-Fission Electricity Generation Systems," Nucl. Tech./Fusion, 1, 128 (1981).
4. T. H. Pigford, C. S. Yang, and M. Maeda, "Denatured Fuel Cycles for International Safeguards," Nucl. Tech., 41, 46 (1978).
5. Proc. Second Fusion/Fission Energy Systems Review Meetings, Washington, D.C., November 2-3, 1977, CONF-771155, USDOE (1978).
6. D. L. Jassby, Ed., Proc. 3rd U.S./USSR Symp, Fusion-Fission Reactors, Princeton (1979)
7. R. W. Moir, Ed., "Tandem Mirror Hybrid Reactor Design Study," UCID-18808, Lawrence Livermore National Laboratory (Sept. 29, 1980).
8. J. A. Maniscalco et.al., "Laser Fusion Driven Breeder Design Study, Final Report," Contract DE-AC08-79DP40-11, TRW Systems and Energy for the U.S. Department of Energy (1980).
9. "Nuclear Proliferation and Civilian Nuclear Power: Report of the Nonproliferation Alternative Systems Assessment Program," DOE/NE-0001, U. S. Department of Energy (1979).
10. Y. I. Chang et al., "Alternative Fuel Cycle Options: Performance Characteristics and Impact on Nuclear Power Growth," ANL-77-70, Argonne National Laboratory (1977).
11. R. E. Tomlinson et.al., "The Economics of Reprocessing Alternative Nuclear Fuels," ORNL/Sub-7501/4, Exxon Nuclear Company for Oak Ridge National Laboratory (1979).
12. D. E. Baldwin, B. G. Logan, and T. C. Simonen, "Physics Basis for MFTF-B," UCID-18496, Lawrence Livermore National Laboratory (1980).

REFERENCES FOR CHAPTER IX (Continued)

13. W. O. Allen, informal calculations, Bechtel Corporation (1978-1980).
14. "Technical Assessment Guide," EPRI-PS-1201-SR, Electric Power Research Institute (1979).
15. Nuclear News, December, 1981.
16. S. C. Schulte, et.al., "Fusion Reactor Design Studies-Standard Accounts for Cost Estimates," PNL-2648, Pacific Northwest Laboratories (1978).
17. C.C. Damm, et.al., "Preliminary Design of a Tandem Mirror-Next-Step Facility," Lawrence Livermore National Laboratory, UCRL-53060 (1980).
18. B. Badger, et.al., "WITAMIR-I: A Tandem Mirror Reactor Design Study", UWFD-400, University Wisconsin (1980).
19. S.C. Schulte, et.al., "Fusion Reactor Design Studies - Standard Unit Costs and Cost Scaling Rules," PNL-2987, Pacific Northwest Laboratories (1979).

CHAPTER X  
ELECTRICITY GENERATION SYSTEM CHARACTERIZATION

X.A INTRODUCTION

In this chapter we characterize the symbiotic electricity generation systems consisting of TMHRs, their client LWRs, and associated fuel cycle facilities. Section X.B is a characterization of the TMHR role in a fuel cycle center and a self-consistent description of the number and type of reactors that might be associated with such a center, the net electricity generation, and the number and types of fuel processing facilities that might be required. Section X.C is a characterization of various deployment scenarios for the TMHR. The latter analysis is an attempt to define the potential nuclear energy generation impact with and without the TMHR and makes comparisons with other alternative options including the LWR alone, the LWR with LMFBRs, as well as the fusion electric option.

## X.B. SYMBIOTIC ELECTRICITY GENERATION SYSTEM CHARACTERIZATION

### X.B.1 Overview

In this section we characterize two types of TMHR/LWR symbiotic electricity generation systems: (1) a "static" system in which the TMHR provides only make-up fissile material for LWRs (i.e., LWR fissile inventories originate from mined uranium) and (2) a constant growth system in which the TMHR also supplies LWR fissile inventory requirements such that the combined system fissile inventory (and therefore, capacity) can grow at some fixed annual rate (e.g., 10%/yr).

### X.B.2 Symbiotic Electricity Generation Systems where TMHR Supplies Makeup Fissile Only

X.B.2.a. Overview. In this section we consider the following four TMHR/LWR combinations:

- Beryllium/thorium oxide blanket TMHR with LWR denatured thorium (and secondary plutonium) fuel cycle clients
- Beryllium/thorium oxide blanket THMR with LWR denatured uranium (and secondary plutonium) fuel cycle clients
- Lithium/molten salt blanket TMHR with LWR denatured thorium (and secondary plutonium) fuel cycle clients
- Lithium/molten salt blanket TMHR with LWR denatured uranium (and secondary plutonium) fuel cycle clients

A more detailed description of the LWR fuel cycles has been given in Chapter IX.

### X.B.2.b Beryllium/Thorium Oxide Blanket TMHR Fuel Cycle Center Description.

It is of interest to define the minimum size and characteristics of a fuel cycle center which contains TMHR breeders, their fuel cycle facilities, and the fuel cycle facilities associated with a self-consistent number of client LWRs. The size of such a fuel cycle center will be determined by two constraints:

- All fuel cycle facilities should be large enough to benefit from economies of scale
- The total number of fuel cycle centers should be small (perhaps 3-5 in the U.S.)

In Figure X.B-1 a fuel cycle center concept for the reference beryllium/thorium oxide blanket TMHR with LWR denatured thorium (and plutonium) fuel cycle clients is shown. In this configuration three TMHRs supply 19890 Kg/yr of  $^{233}\text{U}$  (70% capacity factor) to support 86 1 GWe LWR clients<sup>1,2</sup> for a total electrical output of about 90 GWe. The plutonium produced by 74 of these LWRs is sufficient to support an additional 12 1 GWe LWRs (or, alternatively it could be stockpiled for LMFBR inventories as discussed in Section X.C). The TMHRs each have dedicated fuel fabrication and reprocessing facilities (1326 MT/yr thorium each) and the LWR reprocessing/fabrication throughput is 1885 MT/yr. Of this, about 285 MT/yr is associated with the plutonium burners (i.e., PUREX) and about 1600 MT/yr is associated with the  $^{233}\text{U}$  burners (i.e., THOREX).

All facilities are large enough to benefit from economies of scale with the possible exception of the fuel cycle facilities for the plutonium burners. If several such fuel cycle centers were to exist, economies of scale for the plutonium burner fuel cycle facilities could be achieved by concentrating such facilities in only one of 4 or 5 fuel cycle centers.

It is anticipated that low level wastes generated in the reprocessing and fuel fabrication facilities would be disposed on-site, but that high level wastes would be shipped elsewhere for permanent disposal. Although not shown, the facility described above would require on the order of 100 MT of mined thorium per year for makeup (2% losses assumed).

A similar fuel cycle center concept where LWR denatured uranium fuel cycle clients are utilized instead of denatured thorium fuel cycle clients has also been considered. In this case a smaller total of 66 LWRs can be supported (including 20 plutonium burners), but since none of the LWR fuel is thorium oxide based, the need for THOREX reprocessing of LWR fuel is eliminated and PUREX reprocessing (1535 MT/yr uranium) can be used exclusively for these fuels. In comparison with THOREX, the PUREX process is considered to be closer to commercial viability and less expensive. The net electrical output for this three TMHR driven system would be 69 GWe.

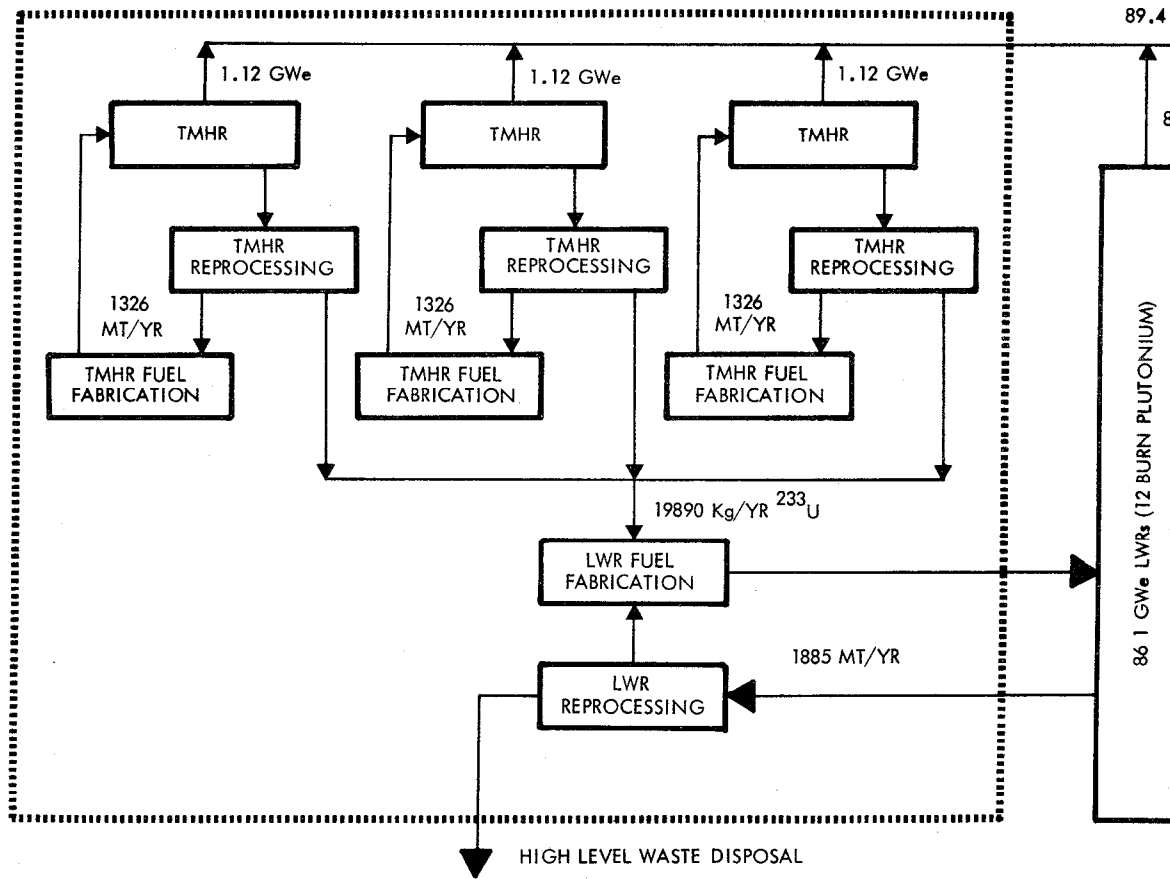


Figure X.B-1. Fuel cycle center concept for beryllium/thorium blanket TMHR with LWR der (and plutonium) clients.

X.B.2.c Lithium/Molten Salt Blanket TMHR Fuel Cycle Center Description. In Figure X.B-2, a fuel cycle center configuration similar to that shown in Figure X.B-1, but for the lithium/molten salt blanket TMHR, is shown. In comparison with the case for the beryllium/thorium oxide system, the figure shows that, due to a lower fissile production rate, a total of four TMHRs are needed to provide a similar, but slightly lower, total electricity generation of about 82 GWe. Another difference between the two blankets is the elimination of TMHR fuel fabrication for the molten salt blanket. Although the heavy metal throughput associated with the molten salt TMHR (5400 MT/TMHR-yr) is very large, it is not unreasonable (see Section VII.B.2).

A denatured uranium client LWR case was also considered for the molten salt blanket TMHR. In this case 74 LWRs (including 22 plutonium burners) are supported by five TMHRs. The LWR reprocessing/fabrication throughput is 1720 MT/yr uranium and the net electrical output for this five TMHR driven system would be 80 GWe.

X.B.3 Symbiotic Electricity Generation Systems where TMHR Supplies both Makeup and Fissile Inventory for Client LWRs

When the TMHR is initially introduced, its likely role will be to provide makeup fissile for already existing LWRs. However, if the TMHR is to be an attractive long term option it must provide a means to expand the symbiotic electricity generation system to meet future growth in electrical demand and/or enable nuclear power to play an increasing role in meeting demand. To accomplish this goal, the TMHR must provide fissile material not only to satisfy makeup requirements, but to satisfy initial inventory requirements for new LWRs added to the system.

When the TMHR also supplies fissile inventories, the LWR nuclear support ratio, R, will decrease and will be a function of several reactor and growth rate dependent quantities. In particular, R is given by

$$R = \frac{\alpha F_b - \gamma I_b}{\alpha F_c + \gamma I_c} \quad (1)$$

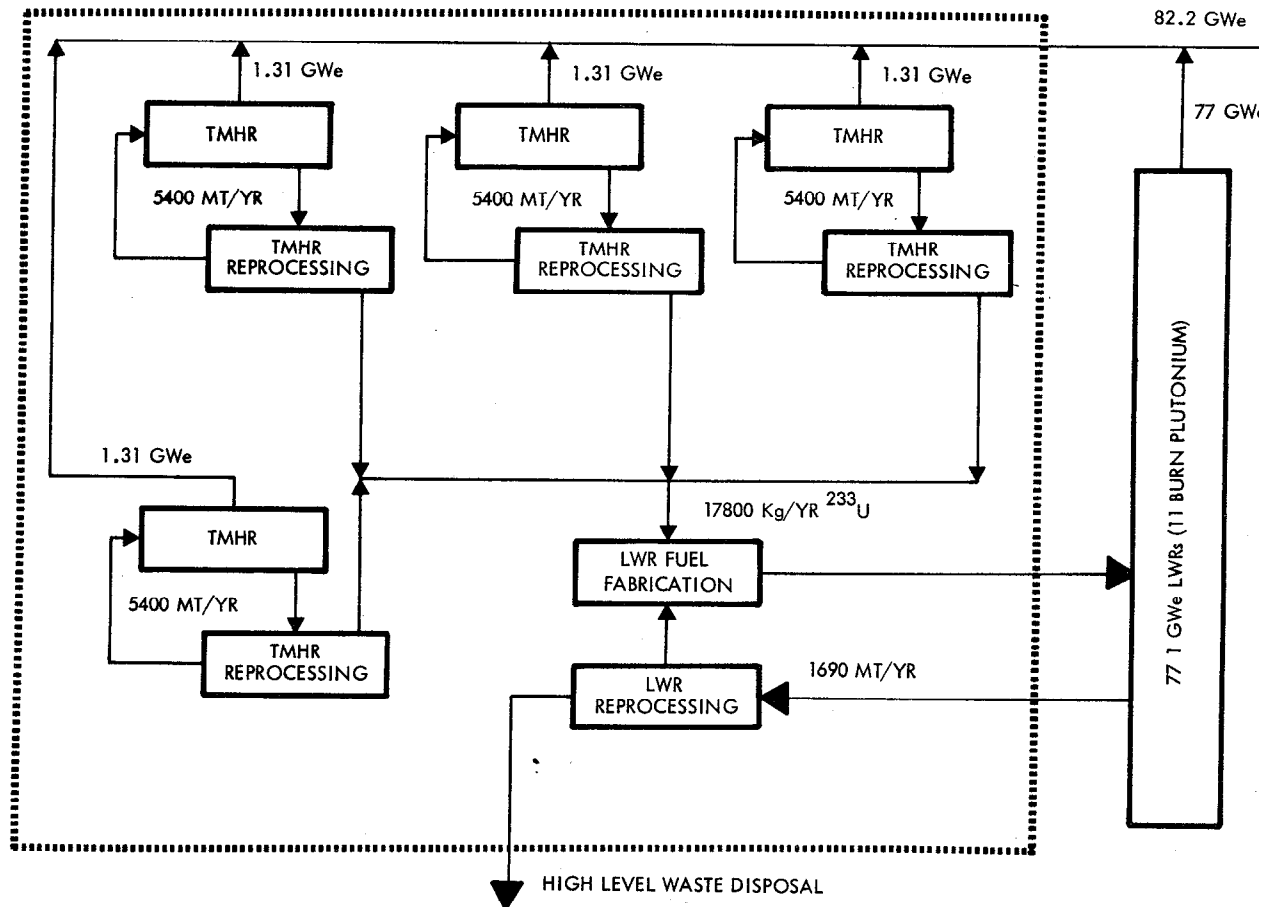


Figure X.B-2. Fuel cycle center concept for lithium/molten salt blanket TMHR with LWR clients (and plutonium) clients.

where:

- $\alpha$  = the average plant capacity factor (0.7 in this analysis),
- $F_b$  = TMHR fissile fuel production rate,  $\text{g/kW}_{\text{Nuclear}}\text{-yr}$
- $\gamma$  = annual rate of growth (e.g., 0.1 represents 10%/yr growth or a 7.27 yr double time)
- $I_b$  = TMHR equilibrium fissile inventory,  $\text{g/kW}_{\text{nuclear}}$  (i.e., the fissile inventory required in the TMHR blanket and fuel processing plant before the TMHR reaches equilibrium  $^{233}\text{U}$  production levels)
- $F_c$  = LWR fissile consumption rate,  $\text{g/kW}_{\text{nuclear}}\text{-yr}$  (a composite number including the plutonium burners)
- $I_c$  = LWR equilibrium fissile inventory,  $\text{g/kW}_{\text{nuclear}}$  (also a composite)

Considering the above model, a TMHR driven electricity generation system consists of a given number of TMHRs and a corresponding LWR nuclear capacity (given by the product of R and the TMHR nuclear power). The entire system can grow at the rate specified by  $\gamma$  if both the TMHR and LWR capacities are expanded at the designated rate (i.e., by new construction).

Using the above model and data provided in Table X.B-1<sup>1,2</sup> the support ratio, as a function of growth rate for the four reactor/fuel cycle combinations discussed in Section X.B.2, may be calculated. As shown in Figure X.B-3, the support ratio is quite sensitive to the required growth rate and decreases from as high as 17.5 (for zero growth) to as low as 2.4 (when 25% growth is required). As expected, the highest support ratios are achieved in cases using the beryllium/thorium oxide blanket but, surprisingly, the denatured uranium fuel cycle cases achieve a higher support ratio than the denatured thorium fuel cycle cases when the required growth rate is more than 8%/yr (9 year doubling time). The latter effect occurs because the fissile inventory associated with the denatured thorium fuel cycle is greater than that of the denatured uranium fuel cycle.

TABLE X.B-1. Fusion breeder and LWR fissile flow and inventory data.

	$F_b$	$F_e$	$I_b$	$I_c$
Be/ThO <sub>2</sub> Fusion Breeder	1.926	X	0.776	X
Li/MS Fusion Breeder	1.506	X	1.120	X
LWR (denatured thorium) <sup>a</sup>	X	0.110	X	1.020
LWR (denatured uranium) <sup>a</sup>	X	0.144	X	0.734

<sup>a</sup>Fuel cycle performance data includes secondary plutonium burner LWR clients as discussed in text.

Choosing a typical example from the figure, for a 10%/yr growth rate and case 2 (Be/ThO<sub>2</sub> and denatured uranium), the nuclear support ratio, R, is 7.3. In this case, one 4920 MW<sub>nuclear</sub> TMHR will support 12 (= 7.3 x 4920/3000) 3000 MW<sub>nuclear</sub> (1 GW<sub>e</sub>) LWRs. These require a heavy metal (uranium) throughput of 280 MT/yr. Therefore, 5 TMHRs with their fuel cycle facilities and 60 LWRs sharing a reprocessing and fuel fabrication plant (1400 MT/yr throughput) might be associated with one fuel cycle center which produces 65 GW<sub>e</sub> of power. Since bred fuel is committed for expansion, this fuel cycle center (including all of its facilities) can expand at the average rate of 10%/yr and will be self-sufficient in fissile fuel. In particular, double the number of TMHRs could support twice as many LWRs in 7.3 years without using any enriched uranium to provide fissile inventories.

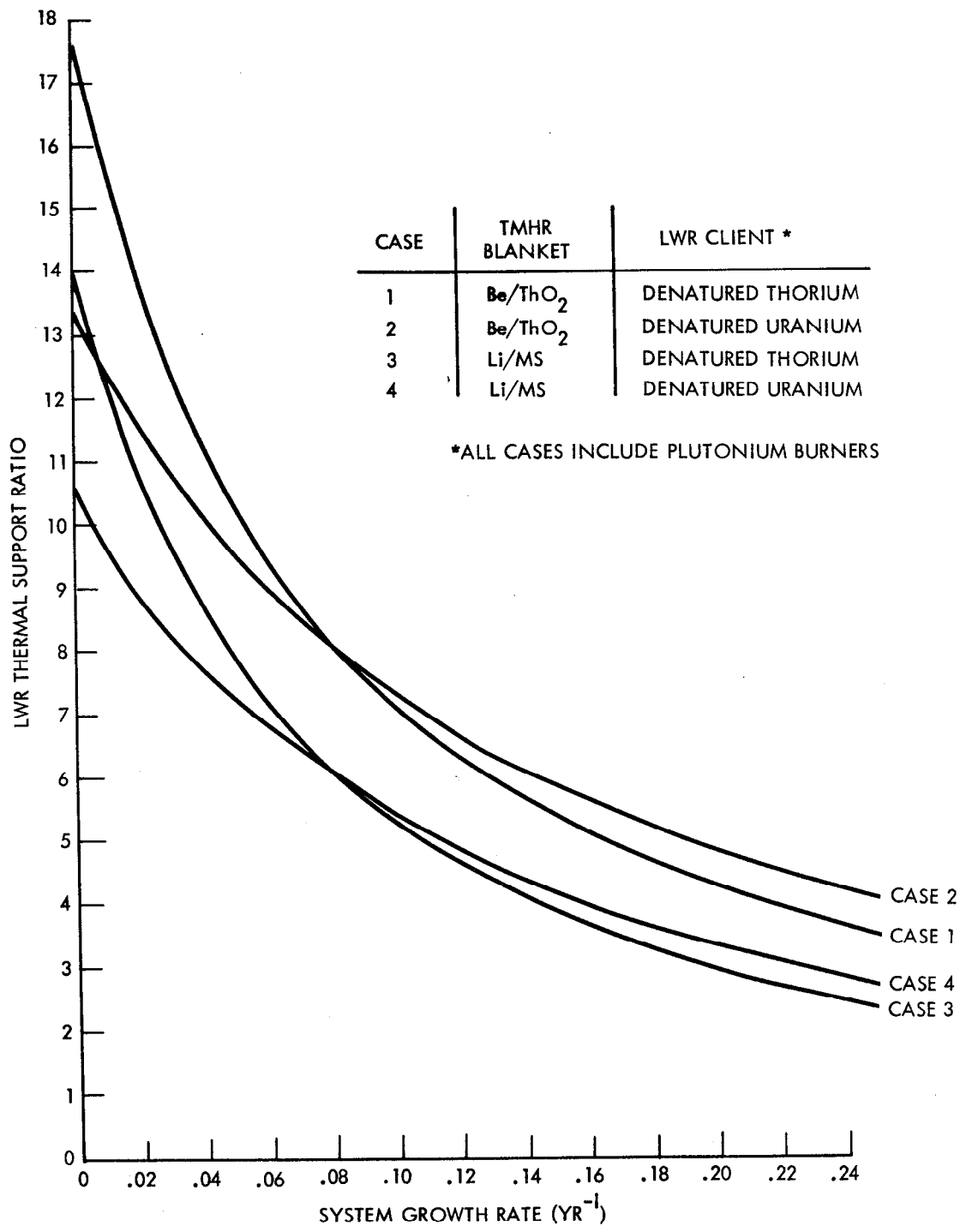


Figure X.B-3. LWR thermal support ratio versus system growth rate for four cases.

## X.C TMHR DEPLOYMENT MODELS AND CONSIDERATIONS\*

### X.C.1 Introduction

In the 2050 timeframe, all of our relatively inexpensive gas, oil, and conventional  $U_3O_8$  resources will, most likely, be exhausted. Considering the remaining resources which appear to be able to supply a substantial fraction of electrical energy in this timeframe (i.e., coal, shale oil, nuclear power with breeding), our ability to provide sufficient electrical generation capacity via the use of fossil fuels could be limited by one or more of the following circumstances:

- Limits on permissible  $CO_2$  generation due to the combustion of fossil fuels (i.e., the greenhouse effect)
- Use and/or preservation of fossil feedstocks for synthetic fuels, plastics, fertilizers, pharmaceuticals, or other chemicals
- Other environmental restrictions relating to effluent emissions, mining restrictions, or occupational health concerns
- An inability to develop these resources as quickly as they are needed
- Export commitments
- Excessive cost (possibly due to one or more of the above)

Similarly, a gross expansion in the need for electrical generation (e.g., due to the introduction of electrical vehicles) is possible.

Under the above circumstances, it is prudent to consider an important set of long range deployment questions which address the possible need for nuclear power (of all varieties) to provide a major fraction (~50%) of the U.S. electrical demand by the middle of the next century. In this context, the question of whether the TMHR can have a significant impact upon the overall level of nuclear power generation that is achievable is relevant.

---

\* This work results from an independent IR&D project performed at TRW, but is included in the TMHR report due to its applicability and general interest.

We will consider a TMHR which can produce enough fissile fuel to supply the makeup requirements of 17 LWRs of equivalent nuclear power. By providing fissile fuel for existing LWRs, the TMHR could operate in the same mode as current uranium enrichment facilities and can be located in a few remotely sited fuel cycle centers. Since only 6 TMHR fusion fuel factories would be required to provide fissile makeup for up to 170 LWRs (see Table X.B-1), a confirmation of the commercial feasibility of a fusion fuel factory option, before conventional  $U_3O_8$  resources for new LWRs begin to become scarce, could accelerate LWR deployment by removing the current requirement to secure  $U_3O_8$  resources for new plants for their entire 30 year operating lifetimes prior to commitment to plant construction. Thus, the TMHR can provide a means to economically preserve the LWR option.

If fusion is used to make fuel for existing fission reactors, it might have a significant impact on our energy needs in an earlier timeframe than alternate options (in particular, the LMFBR) even though fusion technology is less developed. To illustrate this assertion, a comparison of the TMHR and LMFBR with respect to their respective roles in the electricity generation system, development timescale and deployment is made. To begin, the primary product of the LMFBR is electricity, while the primary product of the TMHR is fissile fuel to be used in fission reactors. This difference in the fuel/power ratio of TMHR fusion fuel factories and fission breeders should be stressed because it delineates different missions for the two reactor technologies.

In the case of the LMFBR, commercial demonstration and deployment on an aggressive schedule is needed to positively influence projected electricity generation shortfalls in the post 2000 timeframe. The extent of this positive impact is a strong function of the LWR growth rate, the capital cost differential between the LMFBR and the LWR, and the speed at which LMFBRs can be constructed and brought on-line. The Electric Power Research Institute (EPRI) has estimated an ambitious schedule for LMFBR commercial demonstration and deployment.<sup>3</sup> Assuming a decision is made to proceed with an aggressive LMFBR program, the following assumptions were made:

- The commercial feasibility of an LMFBR could be demonstrated between 1993 and 1996.
- The first commercial plant could be started as early as 1995 and go into full power operation between 2005-2010.
- The second through sixth commercial LMFBR plants (1.5 GW<sub>e</sub> each) could be ordered between 2013 and 2017 and completed 8 to 10 years later. In this mode, the LMFBR by 2020 would account for about 10 GW<sub>e</sub> (or less than 1% of the total installed capacity).

This inability to rapidly impact electrical generation requirements is common to any new power producer be it a fission breeder, fusion, or solar. Four decades are typically required to develop a new electrical generation option. Twenty years are needed to take a new option from the laboratory stages of development to commercial feasibility and twenty more years are needed to commercially introduce and expand the demonstrated option to a point where it can have a substantial impact. Specifically, the new power producer cannot contribute something approaching 5% of the total electric demand until more than 25 years after commercial demonstration.

Fusion technology and thus the TMHR is at least 10 to 15 years behind the LMFBR. However, fusion is sufficiently mature that an engineering demonstration plant for a fusion fuel factory could be started in the late 80s and completed by the mid 90s. Extrapolating from that with the same schedule used by EPRI for the LMFBR implies that the commercial feasibility of a TMHR fusion fuel factory could be demonstrated between 2003 and 2006; the first commercial fusion fuel factory could be started as early as 2005; and full power operation as early as 2015 appears to be reasonable. Thus, in 2015 with an LWR support ratio of 17, the demonstration plant and the first commercial fusion fuel factory (3000 MW<sub>t</sub> each) could provide fuel for as much as 34 GW<sub>e</sub> (or about 6%) of the nuclear generating capacity in 2020, representing a much larger impact than the 3 GW of installed LMFBR capacity which could be operating in the same timeframe.

## X.C.2 Reference Cases

To further quantify the potential energy impact of the TMHR, we must project the U.S. electrical demand into the next century and make some assumptions about fission reactor deployment and uranium resources. The electrical demand projection shown in Figure X.C-1 follows the Electric Power Research Institute's<sup>3</sup> intermediate growth projection through 2020 and then a lower growth rate of 1.5%/year thereafter. The EPRI intermediate forecast assumes that electrical generation requirements will increase at the rate of 4.4%/year from 1979 to 2000 and 2.8%/year from 2000 to 2020. The installed generating capacity required to meet these growth rates increases from 540 GW<sub>e</sub> in 1980, to about 1280 GW<sub>e</sub> in 2000, and 2220 GW<sub>e</sub> in 2020. These electrical growth rates are tied to a much lower total energy growth of 2.0%/year with the added assumption that electrical energy will continue to account for a large fraction of the total energy - increasing from 32% in 1978 to 48% in 2000 and 57% in 2020.

The guidelines and assumptions used to project nuclear energy growth in the first half of the next century are presented in Table X.C-1.<sup>1,2,3</sup> To begin, our goal of 250 GW<sub>e</sub> of LWR capacity in 2000 lies near the midrange of low and high projections of 150 and 300 GW<sub>e</sub> respectively. An LWR installed capacity of 150 GW<sub>e</sub> would result if the nuclear option is to be phased out by restricting the ordering of new plants. The high nuclear case of 300 GW<sub>e</sub> represents the maximum number of nuclear power plants that can reasonably be in service by 2000. It requires a healthy growth of new plant orders, increasing to 20 per year in the 1990's and beyond.

Four nuclear technology options are considered in an attempt to define which combinations of conventional and advanced reactors can satisfy the above generation goals. The cases considered are as follows:

- Case 1: LWR only
- Case 2: LWR and LMFBR
- Case 3: LWR and TMHR
- Case 4: LWR, LMFBR, and TMHR

In cases 2 and 4, the benefit of the doubt is given to the LMFBR. For example, it is assumed that the LWRs burn up to 3.0 million metric tons of U<sub>3</sub>O<sub>8</sub>. This is at the high end of estimates of economically recoverable

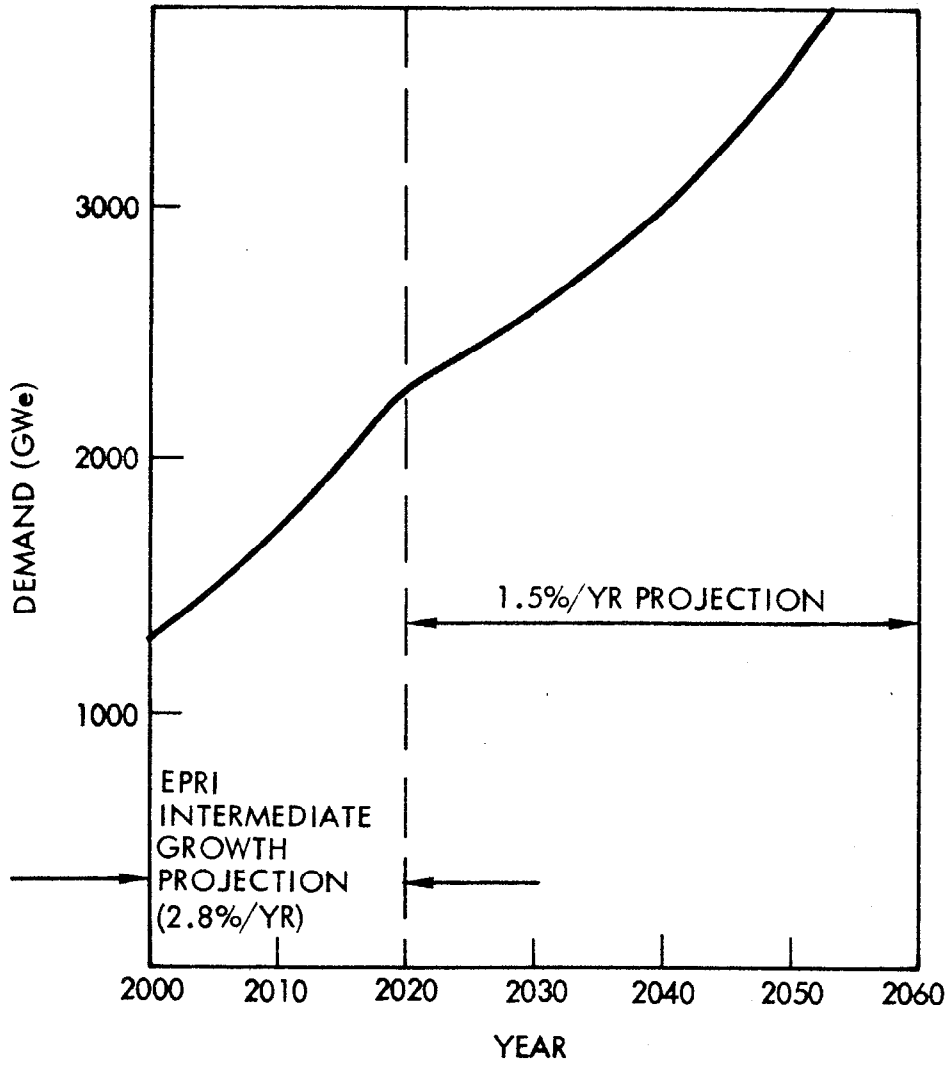


Figure X.C-1. Electrical demand (2000 - 2060).

TABLE X.C-1. Guidelines and assumptions.

---

Nuclear Generation Goals and Assumptions

- 250 GW<sub>e</sub> of LWR capacity in 2000 (20% of demand)
- 1735 GW<sub>e</sub> total nuclear capacity in 2050 (50% of demand)
- Requires overall nuclear growth rate of 3.95%/yr
- All reactors operate with 70% average plant capacity factor

LWR Assumptions

- LWR mix consists of both <sup>235</sup>U burners fueled by mined and enriched U<sub>3</sub>O<sub>8</sub> (tails assay = 0.1%) and <sup>233</sup>U burners (for cases 3 and 4)
- <sup>235</sup>U burners (low enriched uranium with reprocessing and recycle)
  - <sup>235</sup>U makeup requirement = 570 kg/GW<sub>e</sub>-yr
  - Plutonium production = 161 kg/GW<sub>e</sub>-yr. The plutonium produced in LWRs is recycled in plutonium burning LWRs (cases 1 and 3) or recovered and stockpiled for use in LMFBRs (cases 2 and 4)
  - Initial core fissile inventory = 1760 kg
  - U<sub>3</sub>O<sub>8</sub> resource limit = 3 million MT
- <sup>233</sup>U burners (denatured thorium fuel cycle with reprocessing and recycle)
  - <sup>233</sup>U makeup requirement = 300 kg/GW<sub>e</sub>-yr
  - Plutonium production = 59 kg/GW<sub>e</sub>-yr (see above for usage)
  - Initial core fissile inventory = 1930 kg
- Utility must see a 30 year supply of fissile fuel (U<sub>3</sub>O<sub>8</sub>, bred <sup>233</sup>U, or both) to commit to the construction of a new LWR

TABLE X.C-1. (Continued.)

---

LMFBR Assumptions (Cases 2 and 4)

- Deployment
  - First commercial plant in 2005
  - 10 GW<sub>e</sub> in 2020
  - 25%/yr growth in LMFBR capacity after 2020 until 20 plants per year limit is reached
  - 20 plants per year until growth decreases to 10%/yr
  - 10%/yr thereafter
  - Above growth rates apply only until plutonium stockpile is consumed. In the absence of a plutonium stockpiled LMFBR growth is limited to a 15 year system compound doubling time
- Plant and fuel cycle description
  - 1.5 GW<sub>e</sub>, 4110 MW<sub>t</sub> (nuclear)
  - Breeding ratio = 1.32 (homogeneous core)
  - Plutonium production = 184 kg/yr
  - Initial core fissile inventory = 3200 kg

Fusion Fuel Factory Assumptions (Cases 3 and 4)

- Deployment
  - First commercial plant in 2015
  - Introduction scheme same as LMFBR
- Plant description
  - 1 GW<sub>e</sub>, 4000 MW<sub>t</sub> (nuclear)
  - <sup>233</sup>U production = 5920 kg/yr

reserves of  $U_3O_8$  in the U.S. which range from 1.8 to 3.5 million tons. It is also assumed that all of the LWR generated plutonium is recovered and stockpiled for use in LMFBRs. Finally, the LMFBR is deployed at a high rate of growth.

The results of this deployment analysis for case 1 is presented in Figure X.C-2. As shown, after 2000 the LWR deployment can increase such that in 2034 LWRs supply about 33% of the total electrical demand. However, after 2034 the  $3 \cdot 10^6$  MT  $U_3O_8$  resource is entirely committed, new LWR plants are not built, and the nuclear capacity decreases rapidly as plants built in the post 2005 time frame are retired. By 2050, nuclear power supplies only about 17% of the electrical demand.

As shown in Figure X.C-3, the situation is somewhat improved for case 2 with the addition of the LMFBR. In this case, the LMFBR begins to make a significant contribution to electricity generation in the same timeframe as the LWR contribution decreases due to  $U_3O_8$  limits. Nevertheless, the LWR capacity decreases quickly from 700  $GW_e$  in 2029 to 525  $GW_e$  in 2040 and the increasing LMFBR capacity is not great enough to offset the loss of LWR capacity. As a result, during the period 2030-2040, the total nuclear capacity remains at, or decreases slightly below 30% of the total electrical demand. In 2040, the nuclear fraction increases again, but in 2050 the nuclear fraction is only 36.5% of the electrical demand - or 73% of the 50% goal. Our results indicate that, for this case, the LMFBR/LWR system can supply 50% of the electrical demand after 2057.

The deployment of LWRs and TMHR fusion breeder reactors (case 3) is shown in Figure X.C-4. As shown, for this combination of reactor types, the fraction of electricity generated by nuclear power increases in every year through 2050 when the 50% goal is achieved. It is interesting to note that this system is not excessively stressed with respect to either the amount of  $U_3O_8$  resources consumed or the number of fusion breeders required. In total,  $2.2 \cdot 10^6$  MT of the  $3.0 \cdot 10^6$  MT  $U_3O_8$  limit are consumed by LWRs. The total required fusion breeder capacity through 2050 is 81 plants and, in 2050, LWRs provide 1654  $GW_e$  of electricity (nuclear support ratio = 15).

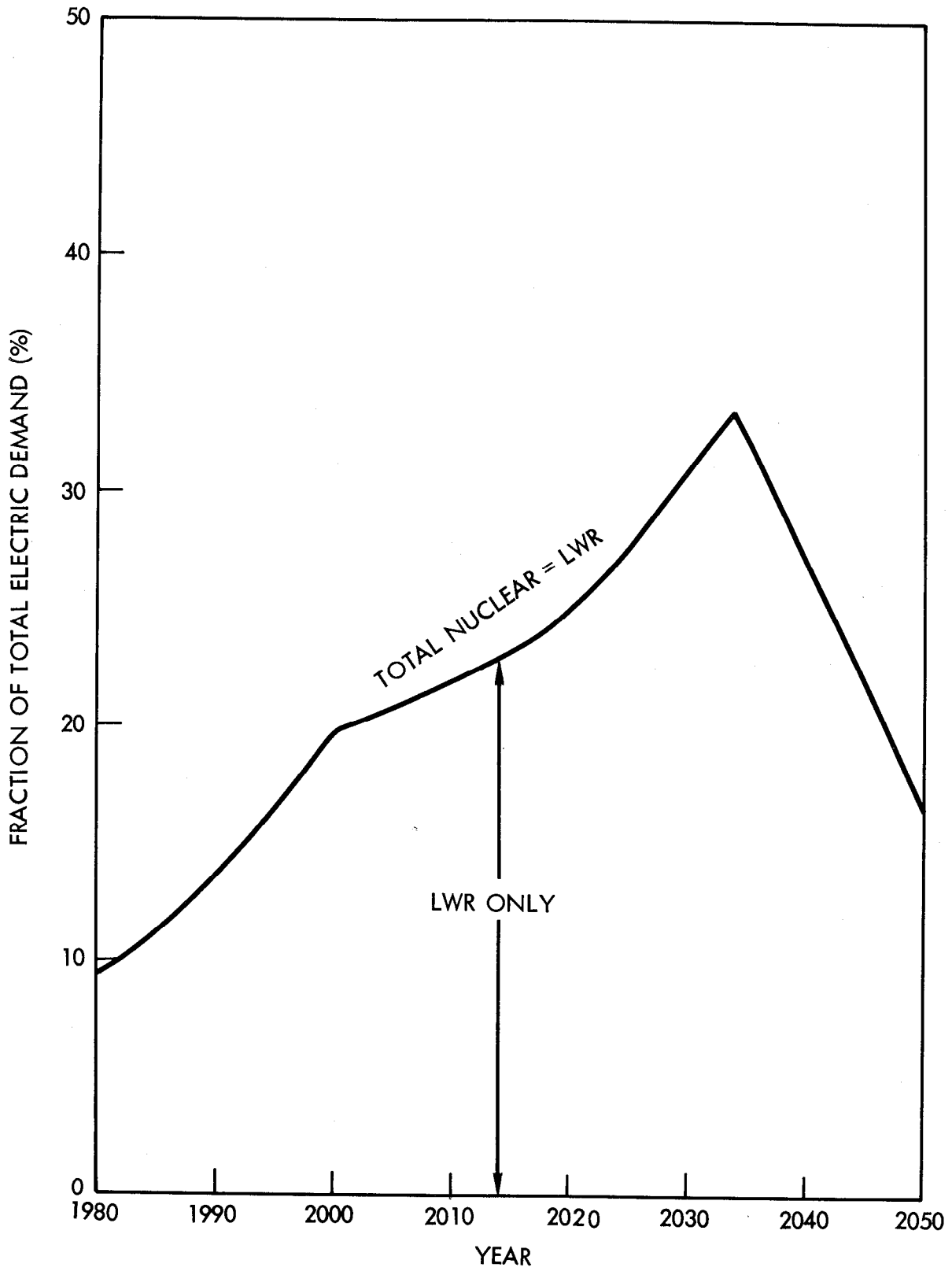


Figure X.C-2. Deployment case 1 (LWR with full recycle of uranium and plutonium).

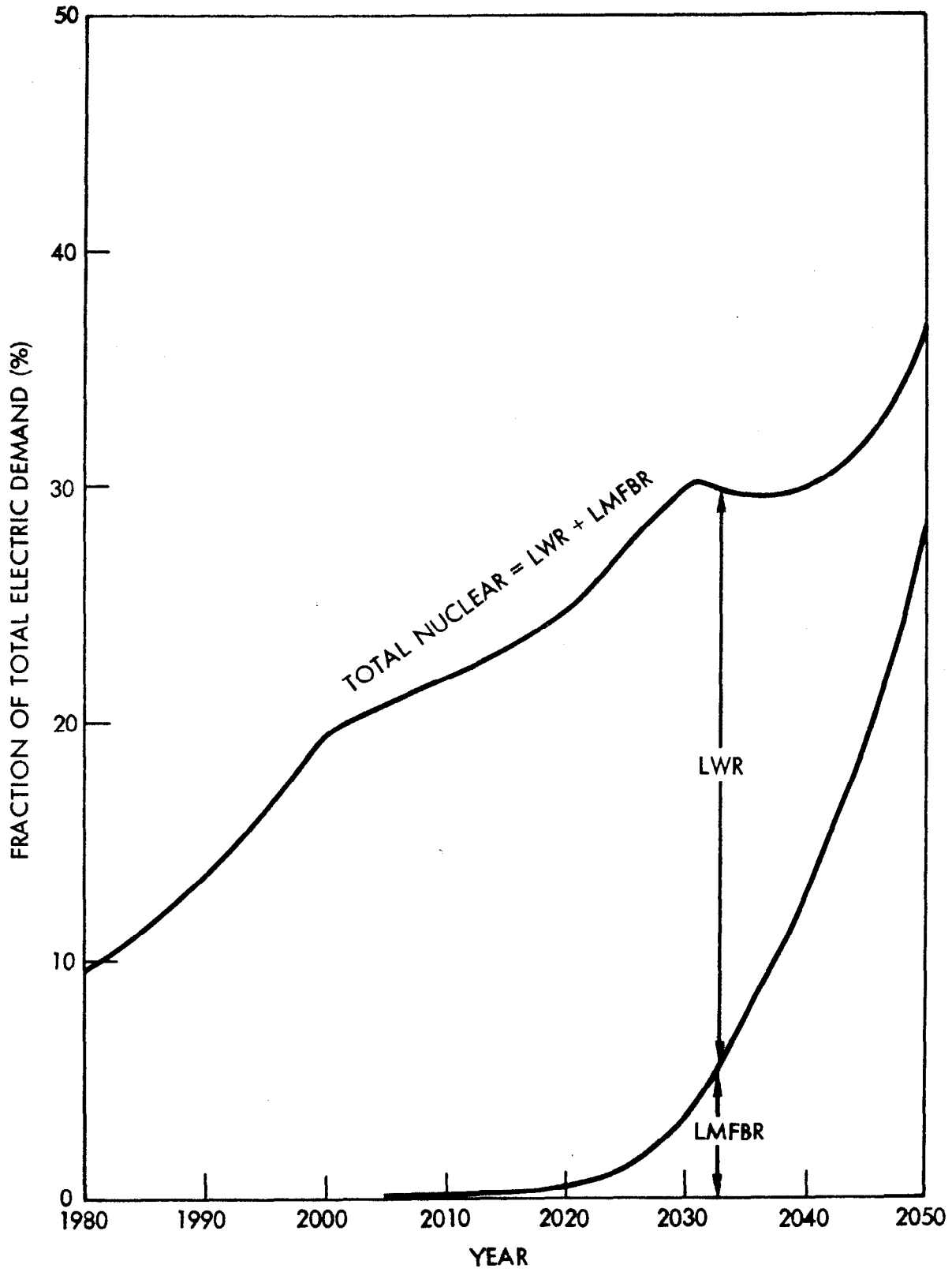


Figure X.C-3. Deployment case 2 (LWR and LMFBR).

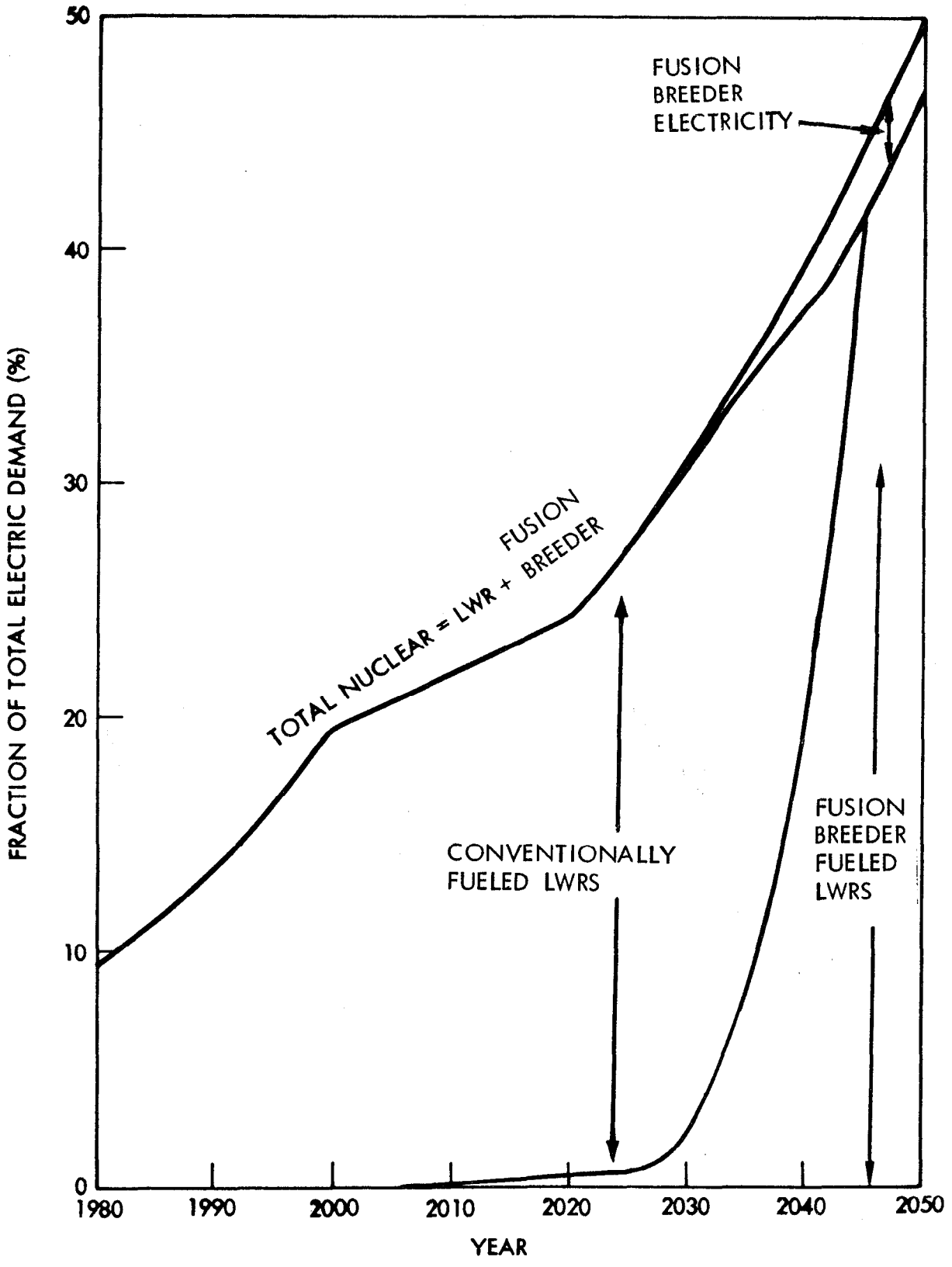


Figure X.C-4. Deployment case 3 (LWR and fusion breeder).

The deployment of LWRs, LMFBRs, and TMHRs (case 4) is shown in Figure X.C-5. As shown, this combination of reactor types also satisfies the 50% goal in 2050 without a decrease in the total nuclear fraction during any two successive years. In comparing this deployment scheme with case 3, several differences are apparent. First, slightly more  $U_3O_8$  is required ( $2.6 \cdot 10^6$  vs.  $2.2 \cdot 10^6$  MT) because plutonium is not recycled in the LWRs, but stockpiled for future LMFBR inventories. Even so, the LWRs dominate electricity generation until 2046. Most importantly, the number of fusion breeders required through 2050 is only 40. Therefore, the introduction of both fusion breeders and LMFBRs can reduce by about 50% the number of fusion breeders required to achieve the 50% goal.

### X.C-3 Parametric Results

The assumptions considered in the above analysis are typical of several recent studies and indicate a reasonable possibility that LWRs and LMFBRs alone will not be able to provide the quantities of nuclear power generation that could be required to satisfy demand during the first half of the next century. However, since many assumptions are required to perform such an analysis, these results do not conclusively demonstrate either that the fusion breeder can effectively remedy the situation, or that the LWR/LMFBR combination cannot meet demand. To better define the envelope of acceptable performance for all of the above combinations, a parametric analysis was performed.

The first set of results of this analysis are shown in Table X.C-2. For these analyses two conditions are required to achieve a successful combination of reactor technologies. First, the goal of providing 50% of electrical demand must be met, and, second, a successful scenario cannot result in a decrease in nuclear power generation during any year in the period 2000-2050. Given these conditions the following results are obtained:

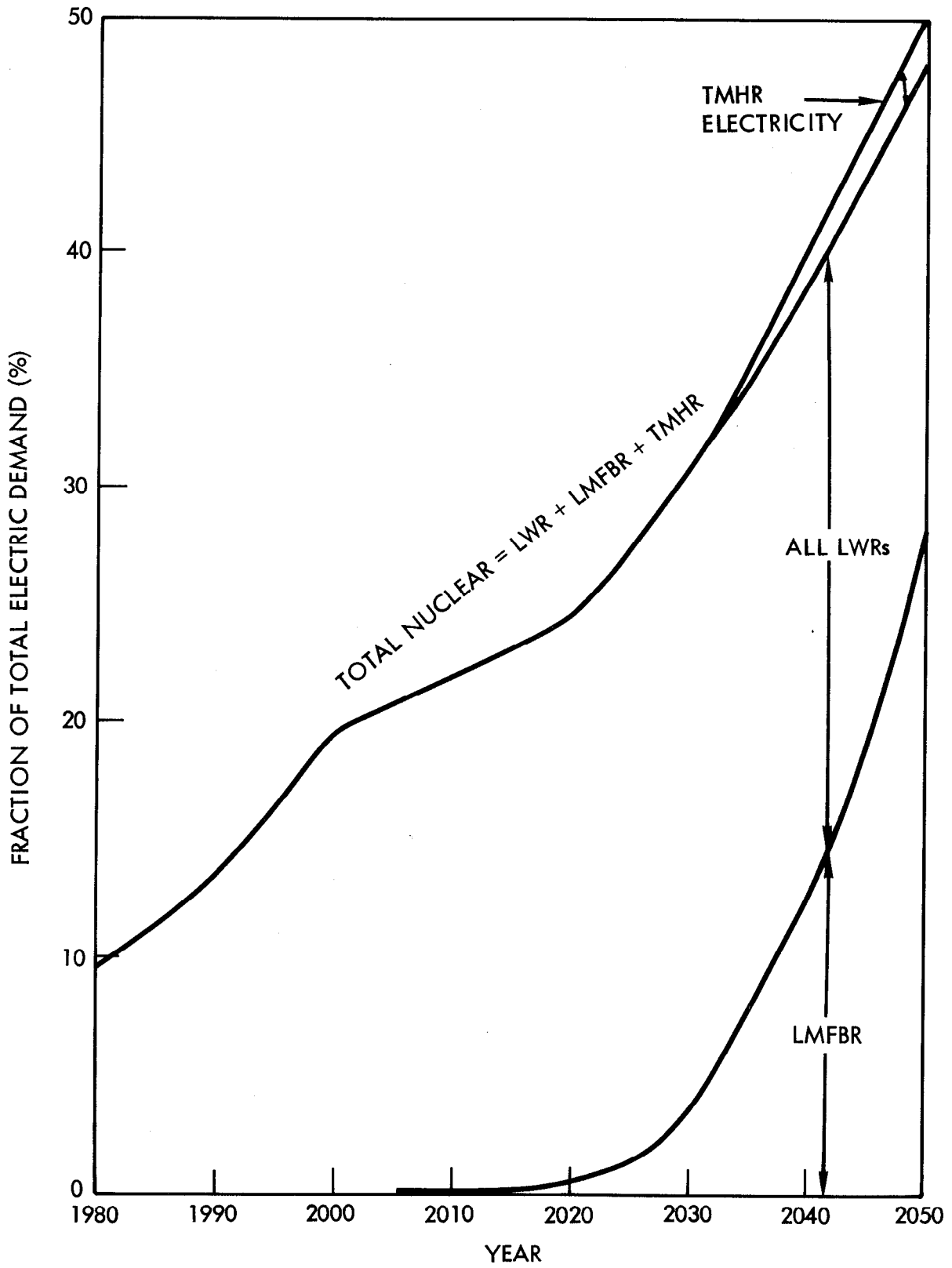


Figure X.C-5. Deployment case 4 (LWR, LMFB, and fusion breeder).

- An increase of  $1 \cdot 10^6$  MT in  $U_3O_8$  reserves improves the LWR/LMFBR combination (case 2), but does not lead to 50% of electricity generation in 2050

- A decrease in  $U_3O_8$  reserves by the same amount for the TMHR systems (cases 3 and 4) causes a slight decrease in total nuclear generation in the 2035 time frame, but the 50% goal in 2050 is possible

- Only the LWR/TMHR combination (case 3) appears able to provide 50% of the total demand as early as 2030. The LWR/LMFBR/TMHR combination (case 4) fails because plutonium which is needed by LWRs in the 2025-2030 period is stockpiled for later use in LMFBRs

- A decrease in the TMHR fuel production increases the number of fusion breeders deployed, but the above generation goals can be satisfied

TABLE X.C-2. Results of deployment parametric analysis (Part I).

<u>Parameter Varied</u>	<u>Successful Reactor Combinations<sup>a</sup></u>
• Reference case (see Table 1)	cases 3, 4 <sup>b</sup>
• Increase $U_3O_8$ resource from $3 \cdot 10^6$ MT to $4 \cdot 10^6$ MT	cases (2), 3, 4
• Decrease $U_3O_8$ resource $2 \cdot 10^6$ MT from $3 \cdot 10^6$ MT	cases (3), (4)
• Require nuclear to supply at least 50% of demand in 2030-2050 period	case 3
• Decrease fusion breeder fuel production by a factor of 2	cases 3,4

<sup>a</sup>( ) denotes cases in which the designated system is not successful, satisfies one of the two criteria, but not both.

<sup>b</sup> Number designations same as presented in text.

A second set of parametric results addresses variations in the assumed level of reactor technology (e.g., introduction dates) and the assumed growth rate of electrical demand. For these analyses varying levels of technology and demand are designed by the terms LOW, INTERMEDIATE, and HIGH. Assumptions associated with these technology and demand levels are given in Tables X.C-3 and X.C-4. The term INTERMEDIATE designates the reference cases described earlier (see Table X.C-1).

The results for this second set of parametric variations are shown in Table X.C-5. As shown, all of the HIGH technology cases (with the exception of Case 1, LWR only) can result in adequate performance as can all of the LOW demand cases. However, the HIGH technology cases provide very little lead time prior to commercialization (especially for the LMFBR) while the LOW demand cases project very little growth during the 2000-2020 period and no growth during the 2020-2050 period.

TABLE X.C-3. Technology variations.

<u>Technology Level</u>	
LOW	<ul style="list-style-type: none"> <li>● Delay LMFBR and fusion breeder introduction 10 years</li> <li>● Decrease LWR capacity in 2000 to 150 GW<sub>e</sub></li> <li>● Increase enrichment tails assay to 0.2%</li> </ul>
INTERMEDIATE	<ul style="list-style-type: none"> <li>● Reference case (see Table X.C-1)</li> </ul>
HIGH	<ul style="list-style-type: none"> <li>● Advance LMFBR and fusion breeder introduction 10 years</li> <li>● Increase LWR capacity in 2000 to 350 GW<sub>e</sub></li> <li>● Decrease enrichment tails assay to 0.05%</li> </ul>

TABLE X.C-4. Demand variations.

<u>Demand Level</u>	
LOW	<ul style="list-style-type: none"> <li>● Demand increases by 3.6%/yr during 1980-2000</li> <li>● 1%/yr during 2000-2020</li> <li>● No increase after 2020</li> <li>● 1660 GW<sub>e</sub> total demand in 2020-2050</li> </ul>
INTERMEDIATE	<ul style="list-style-type: none"> <li>● Reference case (see Table X.C-1)</li> </ul>
HIGH	<ul style="list-style-type: none"> <li>● Demand increases 5.2%/yr during 1980-2000</li> <li>● 3.6%/yr during 2000-2020</li> <li>● 1.5%/yr during 2020-2050</li> <li>● 4719 GW<sub>e</sub> total demand in 2050</li> </ul>

TABLE X.C-5. Results of deployment parametric analysis (Part II).

SUCCESSFUL CASES INDICATED	TECHNOLOGY LEVEL		
	LOW	INTERMEDIATE	HIGH
LOW	(2), 3, 4 <sup>a</sup>	2, 3, 4	2, 3, 4
INTERMEDIATE	None	3, 4	2, 3, 4
HIGH	None	3, 4	(2) <sup>a</sup> , 3, 4

<sup>a</sup>See Table X.C-2.

The four remaining cases indicate that if the technology level is LOW and demand is INTERMEDIATE or HIGH neither the LMFBR or the TMHR can meet ambitious generation goals (however the TMHR comes closest to our model). Finally, for cases with an INTERMEDIATE technology level and INTERMEDIATE or HIGH demand, the TMHR fusion breeder cases are successful while the LMFBR cases are not. Therefore, we conclude that the fusion breeder has a distinct advantage over the LMFBR regarding energy impact despite a later projected date of availability.

#### X.C-4 Fusion Electric vs. Fusion Breeder Deployment

An obvious point of comparison exists between the potential energy impact of fusion breeder driven electricity generation systems and pure fusion electricity generation systems. To perform a fair comparison it is only necessary to assume that pure fusion electric power plants can, despite an expected economic disadvantage, be introduced with the same deployment guidelines as the fusion breeder (see Table X.C-1). In this case (assuming the INTERMEDIATE demand scenario) fusion electric power could supply 0.3% of demand in 2030, 2.2% of demand in 2040, and 7.8% of demand in 2050. Consequently, we believe that the fusion breeder should be given serious consideration as a logical precursor to fusion electric plants which could begin to contribute significantly only in the 2050 timeframe.

## X.D CONCLUSIONS

A TMHR fusion fuel factory has the potential to produce unprecedented quantities of fissile fuel and the resulting high LWR support ratio leads to several important advantages with respect to energy generation impact and institutional acceptability. It reduces the number of TMHRs which must be deployed, and it enhances fusion's ability to rapidly impact our energy needs. Our results indicate that by producing fuel ~~for~~ LWRs, fusion can have a significant impact on our energy needs in an earlier timeframe than the LMFBR, even though the technology of fusion is not as developed as that of the LMFBR. We also believe that the fusion breeder/LWR option will be preferred by utilities over both pure fusion and the LMFBR. This preference can result because the bulk of electricity generation would be produced in conventional LWRs which will have been commercialized more than 50 years prior to significant deployment of any advanced alternative. Fusion breeders can be operated by the government or private interests in a mode similar to that of the present uranium enrichment facilities so that present utility operations need not be changed significantly.

The deployment analysis presented here has shown that the TMHR fusion breeder could be needed for nuclear power to provide a major fraction ( $\sim 50\%$ ) of the U.S. electrical demand by 2050. To preserve our ability to meet this ambitious nuclear goal, the feasibility of the fusion breeder should be demonstrated before the lack of an assured uranium supply begins to curtail LWR deployment. This could happen as early as 2005 and as late as 2025.

The above arguments apply to the current situation in the U.S. where domestic resources of coal and uranium provide some relaxation of the time to develop an inexhaustible source of energy. Many countries with less or none of these resources are compelled to develop the LMFBR on a much faster track.<sup>4</sup> In fact, studies<sup>5</sup> have shown that from a global point of view, the LMFBR cannot be developed and deployed fast enough to significantly impact the shortfall. Under these conditions, available plutonium reserves will become critical and the fusion fuel factory should be developed as rapidly as possible to both supplement and provide a backup to the LMFBR.

## REFERENCES FOR CHAPTER X

1. "Nuclear Proliferation and Civilian Nuclear Power: Report of the Non-Proliferation Alternative Systems Assessment Program," DOE/NE-0001, U. S. DoE (1980).
2. Y. I. Chang, et. al., "Alternative Fuel Cycle Options: Performance Characteristics and Impact on Nuclear Power Growth Potential," ANL-77-70, Argonne National Laboratory (1977).
3. "Overview and Strategy: 1980-1984 Research and Development Program Plan," PS-1141-SR, Electric Power Research Institute (1979).
4. C. P. L. Zaleski, "Energy Choices for the Next 15 Years," Science, March 2, 1979.
5. S. I. Abdel-Khalik, et. al., "Impact of Fusion-Fission Hybrids on World Nuclear Future," UWFDM-333, University of Wisconsin (1980).

## APPENDIX A

### ALTERNATIVE LIQUID METAL COOLED BLANKET OPTIONS

#### A.1 OVERVIEW OF SCOPING PHASE BLANKET OPTIONS

The selection of a reference liquid metal cooled concept was preceded by a scoping phase in which many concepts and a wide range of design options were investigated. Of the many concepts investigated by Westinghouse, one of the more attractive was the Packed Bed Blanket containing thorium metal spheres for the fertile fuel form with the use of liquid lithium as the neutron multiplier as well as the coolant. The blanket design considerations for the Packed Bed concept are discussed in Section A.1.a. The scoping phase options, and the logic that led to the selection of a reference design concept and rated the Packed Bed as the second ranked concept are summarized.

In addition to the Westinghouse scoping phase of the study, TRW, in a later effort, investigated various blanket configurations from the standpoint of nuclear performance and other feasibility related issues. In a preliminary attempt to combine the features of beryllium neutron multiplication with the design simplicity of liquid metal coolants, another Packed Bed design was conceived.

The TRW design uses beryllium as the neutron multiplier,  $\text{Li}_{17}\text{Pb}_{83}$  as the coolant and tritium breeding material and thorium metal as the fertile fuel. The single zone blanket configuration is similar to the breeding zone of the Westinghouse Packed Bed Concept but also adopts several of the design features of the reference lithium/molten salt blanket design (e.g., module length, mechanical configuration). The similarities will become apparent in the discussion of the Packed Bed Blanket with Beryllium Multiplier option in Section A.3.

##### A.1.a Design Considerations

The Packed Bed Blanket concepts evolved in parallel with the reference liquid metal cooled, fission suppressed blanket with molten salt as the fertile fuel form. The design guidelines were discussed in Section IV.B and

are tabulated in Table IV.B-1. During the scoping phase leading to the reference design selection, however, the magnet pitch was 2 m and the blanket module was 4 m long.

The original thermal/hydraulic and neutronic scoping analyses were based on the 4 meter module length. It was subsequently determined that the magnet pitch should be increased to 3.2 m and the module length to 6.4 m to provide the space required for the lithium coolant piping and still provide adequate room for shielding around the magnets for the reference design. While the thermal analysis, pressure drops, and lithium coolant pipe sizes were affected by adopting the longer module, the 1-D neutronic analysis was not since the analysis considered only the geometry at the center of the blanket and did not account for the end effects where the lithium coolant enters and leaves the blanket module. Although the reference design was subsequently reanalyzed to consider the effects of the longer length as well as 2-D neutronics performance, the alternate packed bed module was not. The 2-D neutronic analysis performed for the reference design (Section IV.D) accounted for the end effects and showed an 8% reduction in tritium breeding. Therefore, similar reductions in neutronic performance can be expected to result from 2-D analyses of the packed bed concepts.

#### A.1.b Identification of Scoping Phase Options

During the Initial Scoping Phase, various fuel forms, coolants, cooling systems and refueling mechanisms were considered. The options are listed in Table A-1.

Consideration of these possibilities and the basic design goals led to the following decisions:

- Use of liquid lithium\* in a front zone for first wall cooling, tritium breeding and to provide neutron multiplication.
- Use fuel pebbles, microspheres, or fluid fuels to permit on-line fueling and refueling, either continuously or by batch operation.

Following a preliminary screening and feasibility assessment, a number of coolant systems/blanket concepts were eliminated. The concepts that were

---

\*<sup>7</sup>Li (depleted to 0.2% <sup>6</sup>Li)

TABLE A-1. Tabulation of fuel, refueling and coolant options for TMHR blanket module concepts

---

Fuel material:	Thorium metal Thorium salt Thorium oxide/carbide/bismuthide
Fuel forms:	Liquid metal slurry Molten salt Solid salt Fuel pebbles Microspheres
Refueling mechanism:	Gravity aided flow Pumped fluid fuel
Coolant/cooling system:	Liquid lithium Liquid sodium Molten salt Heat pipes

---

eliminated are summarized in Table A-2. Among the initial blanket concepts, the five listed in Table A-3 were subjected to a comparative evaluation and were found to be relatively free of feasibility issues. All five concepts listed in Table A-3 had an inner liquid lithium zone for tritium breeding and neutron multiplication; the principal differences were in the outer, fissile breeding zone.

Three candidates for final concept selection emerged from these concepts - the reference design concept (similar to concept 3) identified as concept 3A and two versions of concept 1, identified as Concepts 1B and 1C.

Briefly, these three concepts had the following basic features:

- Concept 1C - A two-zone blanket (Figure A-1) with the inner zone of flowing liquid lithium for tritium breeding. The outer zone consists

TABLE A-2. Coolant system/blanket concepts that were eliminated during initial blanket concept selection.

Coolant system/ blanket concept description	Reason(s) for dropping concept
● Use of heat pipes for heat transport	<ul style="list-style-type: none"> <li>● Heat pipes require liquid metal working fluids in the temperature range established for TMHR. MHD effects limit heat transport capability</li> <li>● Tritium diffusion into heat pipes may limit heat pipe useful life</li> <li>● Tritium generation in pipes would limit useful life if Li is used</li> </ul>
● Simultaneous radial flow of liquid lithium & fuel pebbles	<ul style="list-style-type: none"> <li>● Nonuniform fluid velocities with continuously changing flow directions are expected to result in large MHD effects</li> <li>● Fluid flow phenomena are not readily amenable to analysis</li> <li>● Accelerated wall &amp; fuel pebble attrition may be encountered due to erosion</li> </ul>
● Simultaneous radial flow of liquid lithium and fuel particles	<ul style="list-style-type: none"> <li>● Velocity components transverse to the magnetic field may induce significant MHD losses leading to high blanket pressures &amp; high structural volume fractions</li> <li>● Fluid flow phenomena are not readily amenable to analysis</li> <li>● Accelerated wall &amp; fuel pebble attrition may be encountered due to erosion</li> </ul>
● Flow of liquid lithium through a stationary packed bed of fuel pebbles/particles	<ul style="list-style-type: none"> <li>● Large pressure drop (&gt;705 psi) and high blanket pressures leading to high structural volume fractions and poor neutronics performance</li> </ul>
● Continuous downflow of metallic fuel pebbles, heat exchanged externally	<ul style="list-style-type: none"> <li>● Accelerated fuel &amp; containment wall attrition due to erosion</li> </ul>

TABLE A-2. (Continued)

Coolant system/ blanket concept description	Reason(s) for dropping concept
<ul style="list-style-type: none"> <li>● Continuous downflow of metallic fuel pebbles, heat exchanged externally (Continued)</li> </ul>	<ul style="list-style-type: none"> <li>● Backwall requires separate cooling circuit</li> <li>● Unpredictable &amp; nonuniform void distributions</li> <li>● MHD effects not readily amenable to analysis</li> </ul>

of a stagnant bed of thorium fuel spheres immersed in liquid lithium or sodium and cooled by liquid lithium in axially aligned heat transport pipes. The inner (breeding) zone of liquid lithium flowing axially also serves as the first wall coolant. The coolant in both the inner region and outer fertile regions are supplied by common inlet and outlet manifolds.

- Concept 1B - A two-zone blanket (Figure A-2) similar to 1C, except that the coolant pipes in the fertile region are replaced by four circumferential annuli through which the lithium flows axially. The fuel spheres are loaded or removed by flowing circumferentially through the space between the coolant annuli.
- Concept 3A - A two-zone blanket (the reference design Concept of Figure IV.B-1) with an inner breeding zone of liquid lithium as in Concept 1, and an outer zone containing molten salt, which is circulated for fuel processing and self-cooling. This concept features a frozen salt layer to protect the steel container from molten salt corrosion.

These blanket concepts were evaluated considering criteria such as neutronics, design complexity/risk, economics, etc. to obtain an integrated figure-of-merit. Concepts 3A and 1C were judged superior to Concept 1B which had the complicated annular cooling regions. Although the overall rankings for 1C and 3A were relatively close, the economic advantage of processing molten salt fuel in Concept 3A and lower lithium coolant pressure led to the selection of

TABLE A-3. Blanket concepts retained in initial concept selection.

Concept No.	No. of Zones	Fuel	Fuel Form	Clad	Coolant	No. of Fluid/Fu Circuit
1	2	Th Metal	Spheres	None	Liquid Lithium/ Sodium	3
2	2	LM Fuel	ThBi <sub>2</sub> Slurry	None	Fluid Fuel/ Liquid Lithium	2
3	2	2 Phase Salt	Solid Salt In, Molten Salt Out	None Frozen Salt Liner	Liquid Lithium/ Molten Salt	2
4	2	LiF-BeF <sub>2</sub> -ThF <sub>4</sub>	Solid Salt	Graphite Lining	Liquid Lithium/ Sodium	3
5	1	LiF-BeF <sub>2</sub> -ThF <sub>4</sub>	Solid Salt	Graphite Lining	Liquid Lithium	2

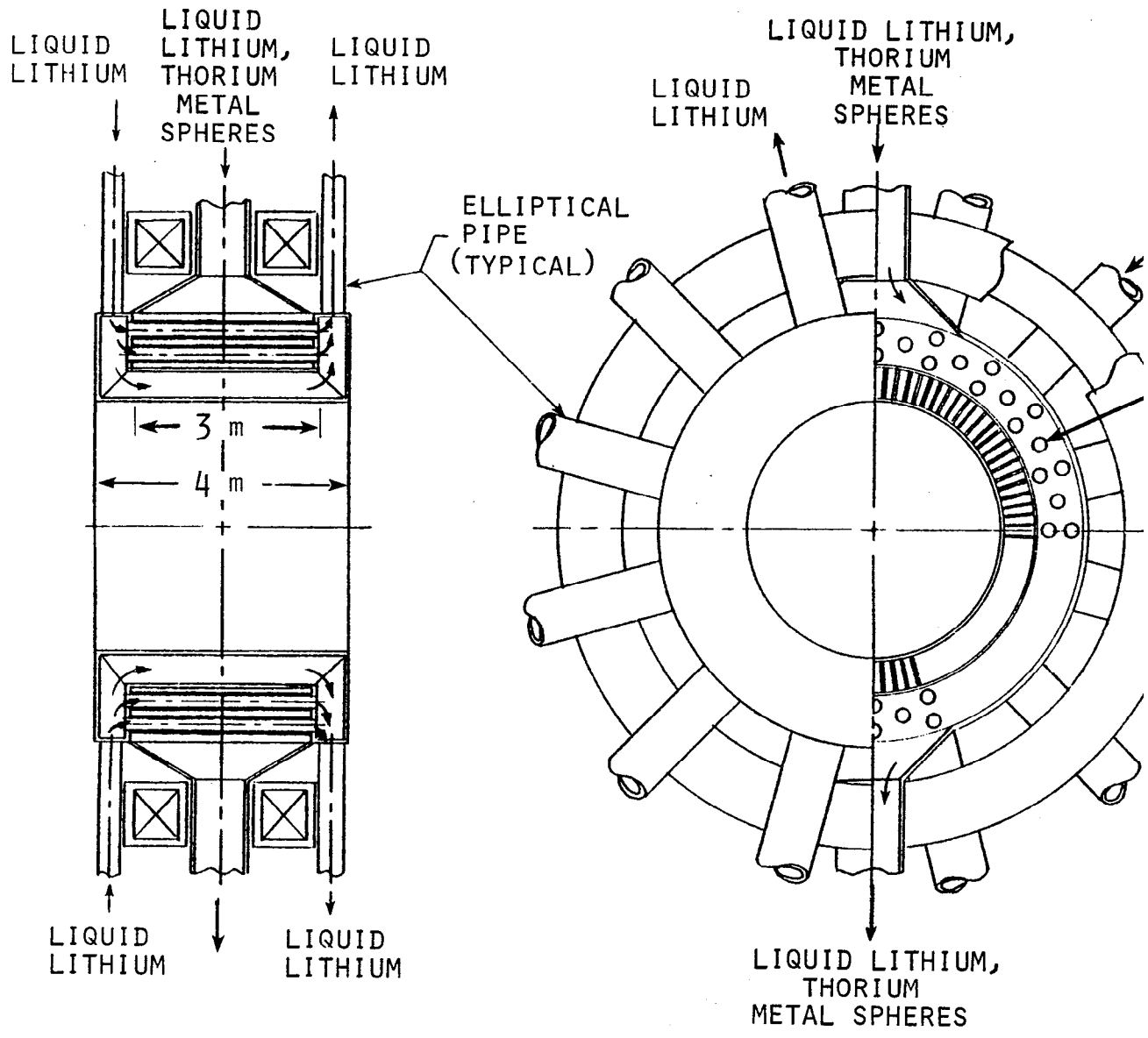


FIGURE A-1. TMHR liquid metal cooled-packed bed with lithium multiplier blanket concept for the TMHR (Concept 1C).



Concept 3A as the primary approach to be pursued by Westinghouse for the reference design of the blanket module. Because Concept 1C is ranked as a close second, it is judged to be worthy of possible further study in the future. In addition, the mechanical design of Concept 1C is, in many cases, directly applicable to the one zone beryllium packed bed design presented in Section A.3. The following section discusses the design and performance of this alternative blanket option.

## A.2 PACKED BED BLANKET WITH LITHIUM MULTIPLIER (WEC CONCEPT 1C)

### A.2.a Concept Description

A.2.a.(1). Overview. The packed bed concept, Figure A-1, is similar to the reference design described in Chapter IV in that both have essentially identical inner lithium zones. However, only 12 inlet and 12 outlet coolant pipes, elliptical in cross section, were provided in the concept 1C inner zone. Subsequent iterations for the reference design indicated that more smaller circular pipes (20 each for the inlet and outlet piping) were required to reduce the pressure drop (to reduce structure thicknesses) and minimize the space required to route the piping. In addition, the reduction in size of the pipes, together with the increase in magnet pitch and module length, enhanced fissile fuel production by providing a fertile fueled region which is a larger fraction of the total module length. Similar improvements would be expected to result from further iterations on the packed bed blanket design.

The outer zone contains a packed bed of thorium metal fuel spheres surrounded by liquid lithium. Stagnant lithium or sodium fills the voids between the spheres, providing good conduction for heat transport to the lithium coolant pipes which pass through the outboard fertile region. For fueling and refueling, the spheres are introduced from the top of the blanket, flow circumferentially through the outer region and are discharged at the bottom. Since the lithium and fuel flow during fueling and refueling are relatively slow, MHD effects on the pumping power can be made relatively small.

The outer zone is cooled by liquid lithium flowing through 60 coolant pipes passing axially through the thorium/lithium bed. The lithium coolant is manifolded to provide common headers to both zones of the blanket. This one coolant blanket represents an advantage in contrast to the reference design concept in which the 20 lithium inlet pipes feed only the inner blanket zone, but power generated in the outer zone is removed by a continuous circulation of the molten salt through intermediate heat exchangers as described in Section IV.E. The first wall and intermediate wall thicknesses shown in Figure A-3 were greater than those for the reference blanket concept for two reasons: the higher coolant pressure required to produce a greater liquid

lithium flowrate (to cool both the inner and outer zones); and the greater hydrostatic pressure exerted by the thorium spheres (compared to that of the molten salt). The design features for concept 1C and the reference design are summarized in Table A-4 to provide a ready basis for comparison.

A.2.a.(2). Mechanical Design and Thermal/Hydraulic Issues. Although the packed bed eliminates some issues and concerns associated with the molten salt reference design, there are additional feasibility issues which could affect the packed bed design.

One of these concerns is the possibility of bridging of the thorium spheres between the intermediate wall (between the inner and outer zones) and the inner row of coolant pipes (Figure A-3). The bridging, if it occurred, would be an impediment to flow of the spheres during charging/discharging of the fertile zone. This concern can be reduced if small spheres are used such that  $\sim 8$  spheres can fit side by side - the most constrained passage. However, the extent of the improvement requires further study. Because of the high density of the thorium, high contact stresses on the bottom of the blanket may cause the balls to yield and develop flat spots which might further impede the movement of fuel. This higher gravity head pressure of the alternate design requires a thicker wall between the two blanket zones, giving a penalty in neutronic performance. A possible fix for this issue would be to mix graphite balls with the thorium balls since only a small amount of thorium is required to achieve adequate breeding performance.

As in the reference design, the packed bed concept requires electrically insulated ducts and relatively large flow areas to reduce the flow velocity to keep MHD induced pressure drops within reasonable bounds. The flow area, in fact, is larger than that required for the reference design because of the additional flow required to cool the outer zone. Therefore the common lithium headers required to supply coolant to both zones are somewhat larger than those in the reference design. Because of the higher lithium flow rates, the MHD losses lead to a higher lithium coolant pressure (290 psia maximum vs. 200 psia, maximum). The end walls of the packed bed modules would also have to be redesigned and increased in thickness to withstand the coolant pressure, as was the case in the reference design.

TABLE A-4. Design features of the packed bed blanket module concept and the molten salt reference design.

	<u>Concept 1C</u>	<u>Reference Design</u>
Total Module Length	4 m	6.4 m
Length of Fertile Region	3 m	~ 5 m
First Wall Radius	2 m	2 m
Lithium Breeding Zone Thickness	~ 50 cm	~ 50 cm
Fertile Fuel Form	Thorium Metal Spheres	Molten Salt
Fertile Fueled Region Thickness	~ 80 cm	~ 80 cm
Coolant	Liquid Lithium	Liquid Lithium
First Wall Thickness	0.76 cm (0.3 in)	0.38 cm (0.15 in)
Equivalent Thickness <sup>a</sup>	Not Applicable	0.5 cm (0.2 in)
Lithium Zone Outer Wall Thickness	0.89 cm (0.35 in)	0.58 cm (0.23 in)
Equivalent Thickness <sup>a</sup>	Not Applicable	0.8 cm (0.3 in)
Stiffening Ribs Equiv. Thickness	1.65 cm (0.65 in)	~ 1.1 cm (0.45 in)
Lithium Coolant Pipes in outer zone -		
Quantity	60	Not Applicable
Size	17.9 cm (7.0 in) ID	Not Applicable
Thickness	0.38 cm (.15 in)	Not Applicable
Number of Inlet/Outlet Coolant Pipes Required	12 Each	20 each
Coolant Pipe Size	~ 0.5 x 0.8 m (elliptical)	~ 0.5 m Diameter
Outer Blanket Wall Thickness	3.81 cm (1.5 in)	3.8 cm (1.5 in)
Structural Material	Type 316 SS (Modified)**	Type 316 SS (Modified) <sup>b</sup>

<sup>a</sup>Actual Thickness of a flat plate having the name volume and length as the corrugated section

<sup>b</sup>Prime Candidate Alloy (PCA), Ref. 1

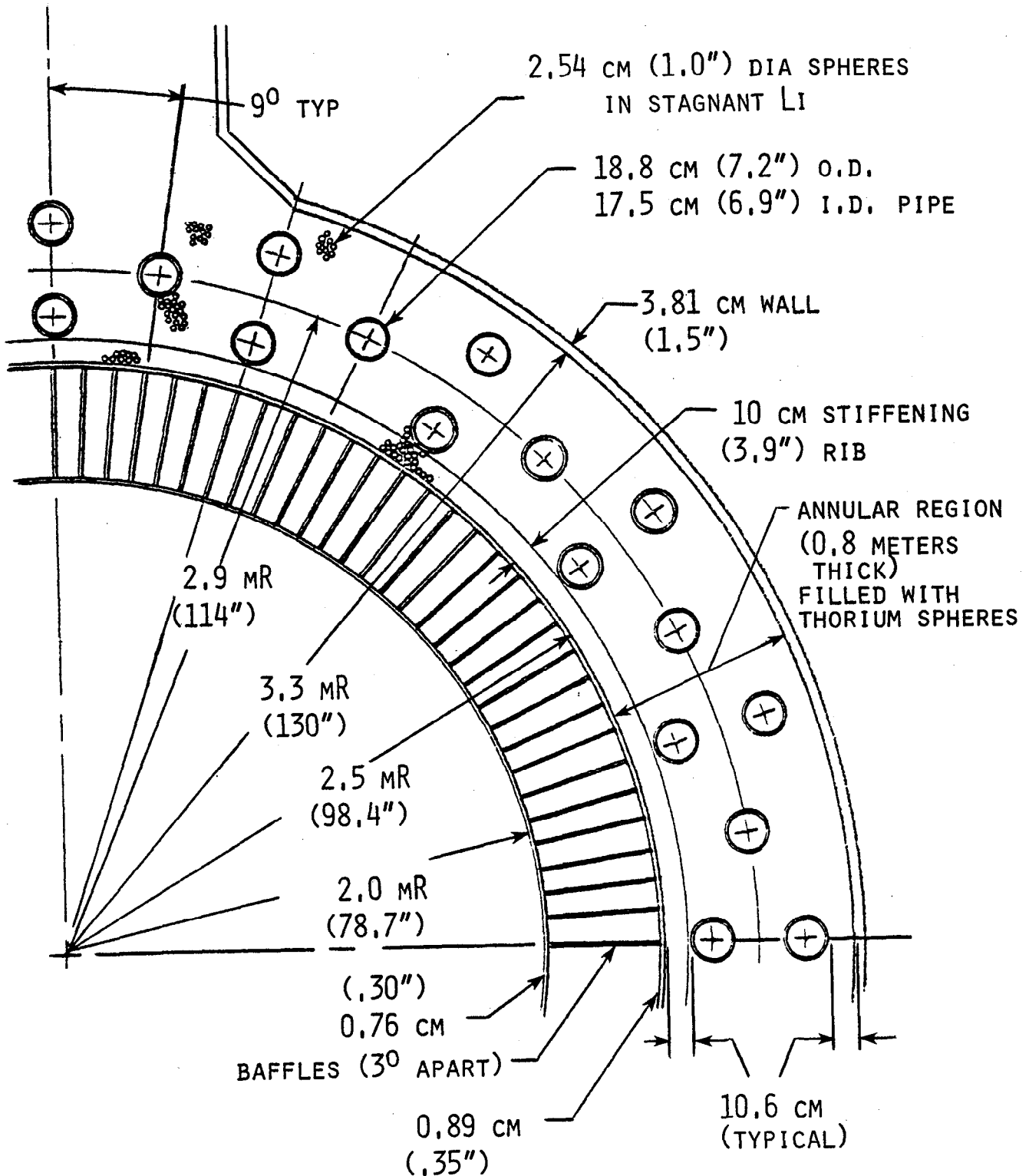


FIGURE A-3. Structural dimensions for TMHR liquid metal cooled-packed bed blanket module.

The maximum lithium temperature is kept the same for both concepts because of stainless steel material limitations, but if HT-9 is used instead of 316 stainless steel, higher temperatures ( $\sim 500^{\circ}\text{C}$ ) would be possible. If the choice of stainless steel is preserved, the  $400^{\circ}\text{C}$  maximum lithium coolant outlet temperature in the outer blanket region as opposed to the approximate  $600^{\circ}\text{C}$  temperature in the reference molten salt region will give an overall lower thermal performance for electrical power conversion.

A.2.a.(3). Neutronic Analysis and Issues. The neutronic analysis of the thorium metal sphere packed bed blanket with liquid lithium coolant and multiplier was performed with the TARTNP Monte Carlo code in one-dimensional cylindrical geometry. A schematic of the geometry and blanket zone thicknesses and material compositions is shown in Figure A-4. As the figure shows, the packed bed region of Th, Li, and steel was 80 cm thick, with the first 10 cm having a higher steel volume fraction to account for structural ribbing. Two key design parameters were varied during the analysis - the thickness of the lithium multiplier zone,  $\Delta_2$ , and the thickness of the first wall,  $\Delta_1$ . During the calculations the lithium was assumed to be depleted to 0.2%  $^6\text{Li}$ , and the revised ENDL cross section data set for the  $^7\text{Li}$  was used.

The results from the neutronic analyses for three different combinations of  $\Delta_1$  and  $\Delta_2$  are shown in Table A-5. The first two cases in the table have the same first wall thickness, 0.76 cm, but have different thicknesses for the front lithium zone. The following quantities are shown in the table:  $T_7$  = tritium production from  $^7\text{Li}$  (n,n',T) reactions, T = tritium breeding ratio, F = fissile atom production, and M = blanket energy multiplication factor; all are per fusion neutron. By increasing the thickness  $\Delta_2$  from 48 cm to 63 cm, the T value increased to 1.04, which was about the goal during the scoping phase. However, the total production rate of T+F stayed about the same even though  $T_7$  increased slightly. This was due to increased neutron absorption in the wall between the lithium and thorium zones for the thicker front lithium zone case.

To study the sensitivity to first wall thickness, another calculation was made in which the first wall was decreased by a factor of two. The comparison of these results is shown in the second and third cases of Table A-5.

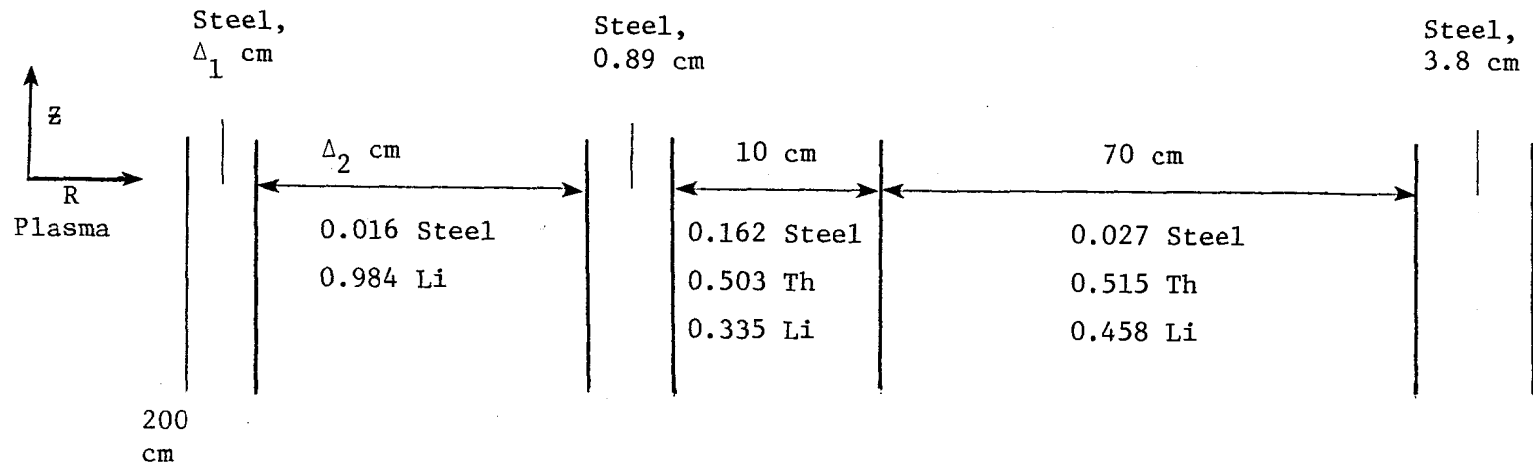


FIGURE A-4. TARTNP neutronic model schematic for Westinghouse packed bed blanket module concept.

TABLE A-5. Comparison of neutronic results for different variations of the packed bed blanket concept.

FIRST WALL THICKNESS $\Delta_1$	$^7\text{Li}$ Zone THICKNESS, $\Delta_2$	$T_7$	T	F	M	T + F	F AT T = 1.04	LEAKAGE
0.76 cm	48.4 cm	0.61	0.89	0.79	1.36	1.68	0.64	0.0045
0.76 cm	63.4 cm	0.65	1.04	0.63	1.28	1.67	0.63	0.0079
0.38 cm	63.4 cm	0.70	1.11	0.64	1.29	1.75	0.71	0.0098

Decreasing  $\Delta_1$  results in too high a T value, but the quantity T+F increases appreciably. Comparing F values at the same T of 1.04, one can see from the table that the fuel production increases by about 13% for the thinner first wall. It can also be noted that the leakage is very small, less than 0.01 neutrons, for all the cases.

The one-dimensional TARTNP results for this packed bed blanket are compared with a similar analysis for the reference blanket concept of lithium and molten salt in Table A-6. The results for this reference blanket are discussed in detail in Section IV.B of this report. This comparison of the two blanket concepts was done with identical front zones of lithium and the same first wall thickness. The only difference in the blankets was in the composition of the thorium blanket zones, as can be seen by comparing the diagrams in Figures IV.D-1 and A-4 for the two designs. As shown in Table A-6, the molten salt concept has a higher T but smaller T+F total. For the same T value, the table shows that the packed bed blanket has about a 5% higher F value than the molten salt blanket. Thus, there is a small difference between the two concepts with respect to fissile fuel production.

If the first wall thickness must be increased to accommodate the higher liquid lithium coolant pressures as discussed in the previous section, the neutronic performance will be penalized. This effect had not been considered in the original scoping study during concept selection.

TABLE A-6. Comparison of packed bed and molten salt blanket neutronic performance.

---

	<u>Packed Bed</u>	<u>Molten Salt</u>
T	1.04	1.13
F	0.63	0.51
T + F	1.67	1.64
M	1.28	1.21
F with T = 1.04	0.63	0.60

---

A.2.a.(4). Safety/Reliability Issues. Safety and reliability were not addressed in the scoping phase to the depth reported in Section VI.C for the reference design. In comparison with the molten salt blanket, the issues associated with a circulating radioactive coolant are eliminated, but the extra coolant circuit piping required to remove heat from the packed bed introduces an additional accident pathway and increases the probability for lithium leakage of coolant into fertile fueled region. From material compatibility considerations, the consequences are not expected to be critical since the leak would be into another region which also contains a liquid metal. In addition, the higher coolant pressure aggravates the consequence of a leak into the packed bed zone from the standpoint of increasing the buckling pressure on the intermediate wall between the inner and outer blanket zones. Finally a loss of the stagnant lithium, which acts as heat transfer medium in the packed bed, may cause melting of some thorium spheres. The magnitude of these effects, design features to mitigate such concerns, and impact on the safety/reliability were not assessed during this year's study.

A.2.a.(5). Fuel Cycle Issues. Although it is practical to reprocess the thorium metal fuel spheres, it is not as economically attractive as the molten

salt reprocessing previously discussed in Chapter VII. Therefore, a tradeoff exists between expected technology development requirements (more difficult for the molten salt) and expected economic benefits. Batch processing is a more probable approach since a constant movement of the spheres required for continuous processing could lead to fuel attrition and structural metal erosion. In addition, possible regions of constrained flow due to potential bridging may necessitate batch fuel reshuffling to redistribute the spheres as the fissile fuel inventory in the blanket increases at locations where sphere movement is restricted. It may be possible to extract the spheres, select those (by automation techniques) with adequate inventory and return those with low inventory to the blanket. An advantage of the packed bed blanket is that batch fuel management could be accomplished on-line by backfilling the outer region with liquid metal while balls are removed from the bottom.

#### A.2.b Overall Concept Evaluation

The Westinghouse packed bed is a relatively simple blanket concept using a conventional steel structure. Only one relatively low pressure coolant is used with a minimal number of coolant pipes (60) in the fertile fueled region. The consequence of a pipe leak into the outer zone may not be critical since a leak is into another region which also contains a liquid metal.

In common with the molten salt reference design (Section IV.D), lower neutronic performance can be expected when the design is subjected to a two-dimensional analysis. This is due to the module end effects when part of the outer zone fertile fueled region is replaced by the liquid lithium coolant headers. The module, in addition, should be analyzed with the greater 3.2 m magnet pitch (used for the reference design) which allows adequate space for both the piping and shielding around magnets. More smaller circular inlet/outlet pipes (perhaps 24 of each) should be considered to economize on space and maximize the length of the outer fertile fuel zone to improve neutronic performance.

In other respects the Packed Bed Blanket module is similar to the reference design. Electrically insulated ducts are required to reduce the

coolant pressure, reduce the structural wall thicknesses and improve neutronic performance. The module interface sealing problem (Section IV.B.3) is common to both designs.

The packed bed concept warrants further analysis and design effort to assess the full neutronic and thermal hydraulic performance of the concept as a possible nearer term technology back-up to the reference design.

### A.3. PACKED BED BLANKET WITH BERYLLIUM MULTIPLIER

#### A.3.a. Concept Description

A.3.a.(1). Overview. An alternate blanket concept, shown in Figure A-5, features a one zone randomly packed bed containing a mixture of beryllium and fertile pebbles (thorium or uranium) and a sodium heat transfer medium. The bed in the figure is cooled by axially directed tubes containing a lithium breeder/coolant. Several possible variations on this general design theme are possible including beds with and without cooling tubes (i.e., for a packed bed blanket without cooling tubes, the sodium would be replaced by lithium which would be pumped directly through the bed). In addition, at least one other coolant tube arrangement has also been proposed and lithium lead could be substituted for lithium.

This packed bed design is a preliminary attempt to combine the attractive features of beryllium neutron multiplication with the design simplicity associated with liquid metal coolants. The one zone blanket configuration is similar to the breeding zone of the Westinghouse packed bed design discussed earlier (note that the front zone containing liquid lithium is not included). To achieve high levels of fissile breeding, about 92% of the fertile spheres are replaced by beryllium spheres. The remaining fertile spheres are mixed with the beryllium spheres (fertile fuel is  $\sim$  4% of the total volume). Sodium is again used to enhance heat transfer. Fuel management for this design concept would be a batch process similar to that described for the Westinghouse packed bed design concept, but the beryllium and fertile spheres would be randomly mixed.

In this concept, beryllium swelling and refabrication are less of a concern because the beryllium spheres do not swell appreciably during the  $\sim$ 3 month exposure time. Also, it is possible to allow the pebbles to readjust to any swelling semi-continuously by removing some pebbles from the bottom and adding pebbles to the top. The beryllium pebbles can, therefore, swell significantly over several cycles. Their lifetime is limited only by possible losses in their physical integrity. These pebbles require no high tolerance machining and can, most likely, be refabricated using press sintering technology.

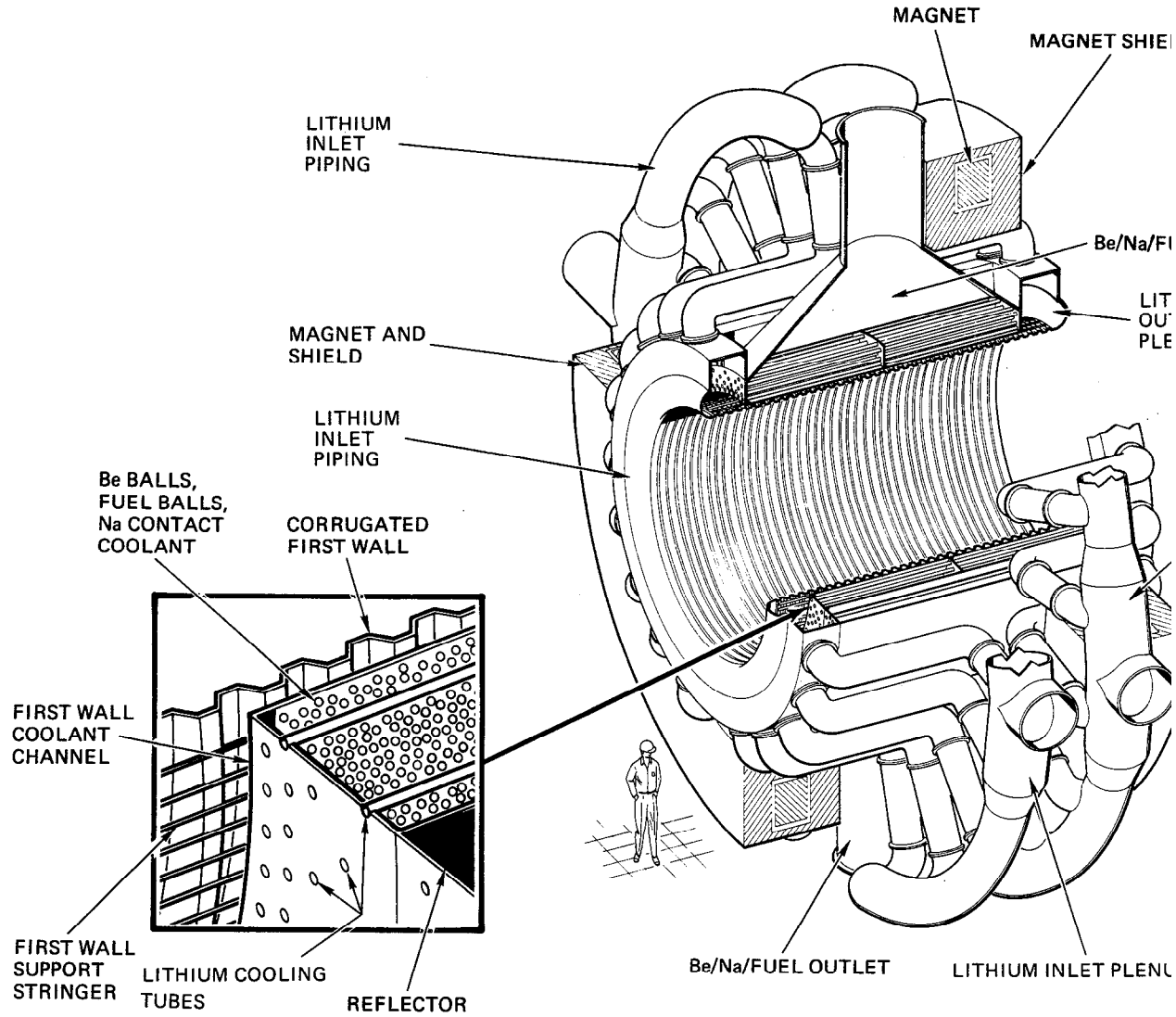


FIGURE A-5. Packed bed blanket with beryllium multiplier.

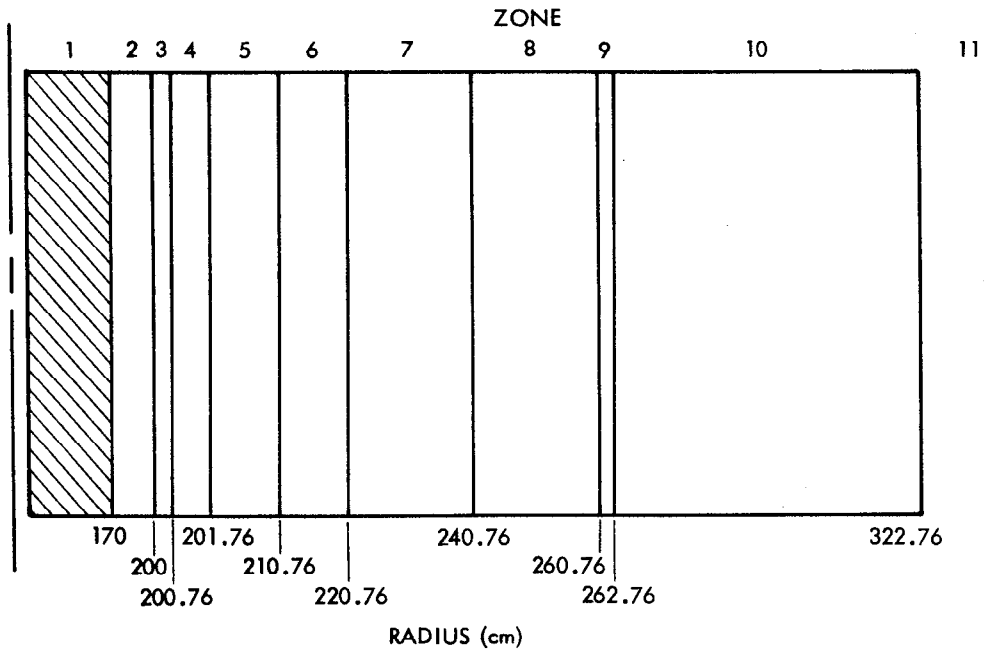
This design concept benefits due to the thermal characteristics of the Li coolant and Na heat transfer medium. Nevertheless, the reactive liquid metals cause some concern. To address this concern, a semi-passive dump tank system can be incorporated into the plant design philosophy (in addition to multiple barriers, inert cover gasses, etc.) and other safety systems can be adapted from the LMFBR program.

The potential benefits of this new design concept are excellent neutronics in a low risk mechanical design that offers conventional technologies.

A.3.a.(2). Neutronics Issues. A preliminary neutronics analysis using TARTNP was carried out for the one zone design. The objective was to scope neutronics performance as a function of blanket composition thickness. Both uranium and plutonium breeding designs utilizing thorium or uranium fertile fuel forms, respectively, were examined. Tritium and fertile fuel breeding performance were calculated. In addition, heating rates as a function of position were calculated for a thorium blanket. These calculations assumed a primary coolant of lithium lead ( $\text{Li}_{17}\text{Pb}_{83}$ ), but performance should be slightly superior in the case of a pure lithium coolant, which is the basis for the thermal analysis which following in Section A.3.a.(3).

The packed bed was modeled with TARTNP as a one-dimensional infinite cylinder. Separate radial regions were used to represent the first wall structure, a fuel zone (Be, fertile fuel, Na), a rear wall and a graphite reflector. Only neutrons were transplanted and gamma energies were assumed to be deposited locally. This model neglects effects in the blanket module end cells (see Figure A-5) as well as reactor end cell effects. In general, these can be expected to slightly reduce breeding performance (perhaps a five to ten percent decrease).

Some studies were performed using a fuel region of infinite thickness. This model is preferred for examining relative effects relating to various candidate blanket compositions. In most cases, the infinite radius model applies well to finite blankets since most nuclear reaction rates are peaked in the first 10 to 20 centimeters of the blanket. Figure A-6 shows the finite radius model and also the cylindrical geometry used in modeling the blanket. The multiple zoning in the fuel region was done to facilitate power profile calculations.



CYLINDRICAL SIMULATION OF ONE ZONE DESIGN

ZONE	DESCRIPTION	TOTAL THICKNESS (cm)
1, 2	PLASMA, VACUUM	200
3	Fe FIRST WALL	.76
4, 5, 6, 7, 8	FUEL REGION	60
9	Fe BACK WALL	2
10	GRAPHITE REFLECTOR	60
11	LEAKAGE ZONE	

NOTE: SOME SIMULATIONS DONE WITH INFINITE FUEL ZONE

Figure A-6. TARTNP one dimensional cylindrical simulation of one zone beryllium blanket.

Table A-7 is a summary of the results of the neutronic analysis for several different cases. Cases 1 through 3 relate to thorium blankets (<sup>233</sup>U breeders). Cases 1 and 2 represent infinite thickness fuel zone blankets. Where Case 1 represents the beginning of a fuel management cycle and case

two adds 0.25%  $^{233}\text{U}$  uniformly in the fuel region to represent possible end-of-cycle conditions. Case three represents the finite blanket shown in Figure A-6. Cases four and five relate to infinite fuel zone radius uranium blankets (plutonium breeders). The case five blanket contains 0.25%  $^{239}\text{Pu}$  to represent possible end-of-cycle conditions. The uranium blanket fuel contains about 0.20%  $^{235}\text{U}$  (representing depleted uranium).

TABLE A-7. Summary of neutronics analyses for the one zone beryllium blanket.

Volume Fractions, Volume Percent (%)	Case 1	Case 2	Case 3	Case 4	Case 5
	Infinite $^{232}\text{Th}$	Infinite $^{232}\text{Th}$ w/.25% $^{233}\text{U}$	Finite $^{232}\text{Th}$ w/.25% $^{233}\text{U}$	Infinite $^{238}\text{U}$	Infinite $^{238}\text{U}$ w/.25% $^{239}\text{Pu}$
$^6\text{Li}$	2.55	2.55	2.55	2.55	2.55
$^7\text{Li}$	--	--	--	--	--
Lead	12.45	12.45	12.45	12.45	12.45
Total Coolant	15.0	15.0	15.0	15.0	15.0
Beryllium	44.97	44.97	44.97	46.0	46.0
Sodium	32.24	32.24	32.24	32.85	32.85
$^{232}\text{Th}$	3.39	3.38	3.38	--	--
$^{233}\text{U}$	--	0.0085	0.0085	--	--
$^{238}\text{U}$	--	--	--	1.75	1.75
$^{235}\text{U}$	--	--	--	0.0035	0.0035
$^{239}\text{Pu}$	--	--	--	--	0.0044
Iron	4.4	4.4	4.4	4.4	4.4
Total Breeding Zone	85.0	85.0	85.0	85.0	85.0
Performance Per Fusion Neutron					
$^6\text{Li}(n,\alpha t), T$	1.174	1.171	1.164	1.169	1.176
$^{232}\text{Th}(n,\gamma)$	0.6475	0.6456	0.6409	--	--
$^{232}\text{Th}(n,f)$	0.0095	0.0093	0.0093	--	--
$^{233}\text{U}(n,\gamma)$	--	0.0008	0.0007	--	--
$^{233}\text{U}(n,f)$	--	0.0059	0.0058	--	--
$^{238}\text{U}(n,\gamma)$	--	--	--	0.6807	0.6855
$^{238}\text{U}(n,f)$	--	--	--	0.027	0.026
$^{235}\text{U}(n,f)$	--	--	--	0.003	0.003
$^{239}\text{Pu}(n,\gamma)$	--	--	--	--	0.0013
$^{239}\text{Pu}(n,f)$	--	--	--	--	0.0026
Net Fissile bred, F	0.6475	0.6389	0.6344	0.6807	0.6816
T + F	1.822	1.810	1.798	1.85	1.86
M	1.44	1.51	1.51	1.70	1.74

An important point of reference is illustrated by case 3, the 60 cm fuel region  $^{233}\text{U}$  breeding blanket. Since total breeding decreases by only about 0.02 relative to the infinite radius blanket, it follows that a 60 cm blanket is probably sufficient to fully utilize the fusion neutrons. The plutonium breeder cases (4 and 5) also produce excellent breeding. It should be noted that this breeding is accomplished with only about 50% of the fertile (i.e.,  $^{238}\text{U}$ ) concentration compared to the thorium blanket cases. This results because of capture cross section differences for the  $^{238}\text{U}(n,\gamma)$  and  $^{232}\text{Th}(n,\gamma)$  reactions. In particular,  $^{238}\text{U}(n,\gamma)$  has a much larger resonance capture cross section.

Figure A-7 presents a power profile through the thorium blanket for case 3. This is a plot of the average power density in six radial zones including the 0.76 cm thick iron first wall. The details of the power profile in the wall and the first few centimeters of the fuel zone are important and could be calculated more exactly. The calculation is expected to be conservative, however, because gamma ray transport is neglected. Including gamma ray transport will result in a reduction in locally deposited energy, especially in the first wall. The power profile was used in the next section as a heat source for the thermal hydraulic analysis.

In summary, the one zone beryllium blanket has excellent neutronics performance. Total breeding is about 1.8, and neutron energy multiplication is between 1.4 and 1.7, depending upon the choice of thorium or uranium as a fertile fuel form. Either  $^{233}\text{U}$  or  $^{239}\text{Pu}$  can be produced with only minor variations in blanket composition. Future studies should concentrate on several areas:

- Iteration with structural and thermal analysis to include changes in structure and composition
- Multi-dimensional and gamma transport calculations including end-of-the-module and end cell streaming effects
- Optimization studies to determine optimal dimensions, compositions, and fuel management schemes
- Calculation of radiation damage processes including atomic displacement rates and helium production
- Calculations with lithium replacing the lead-lithium coolant

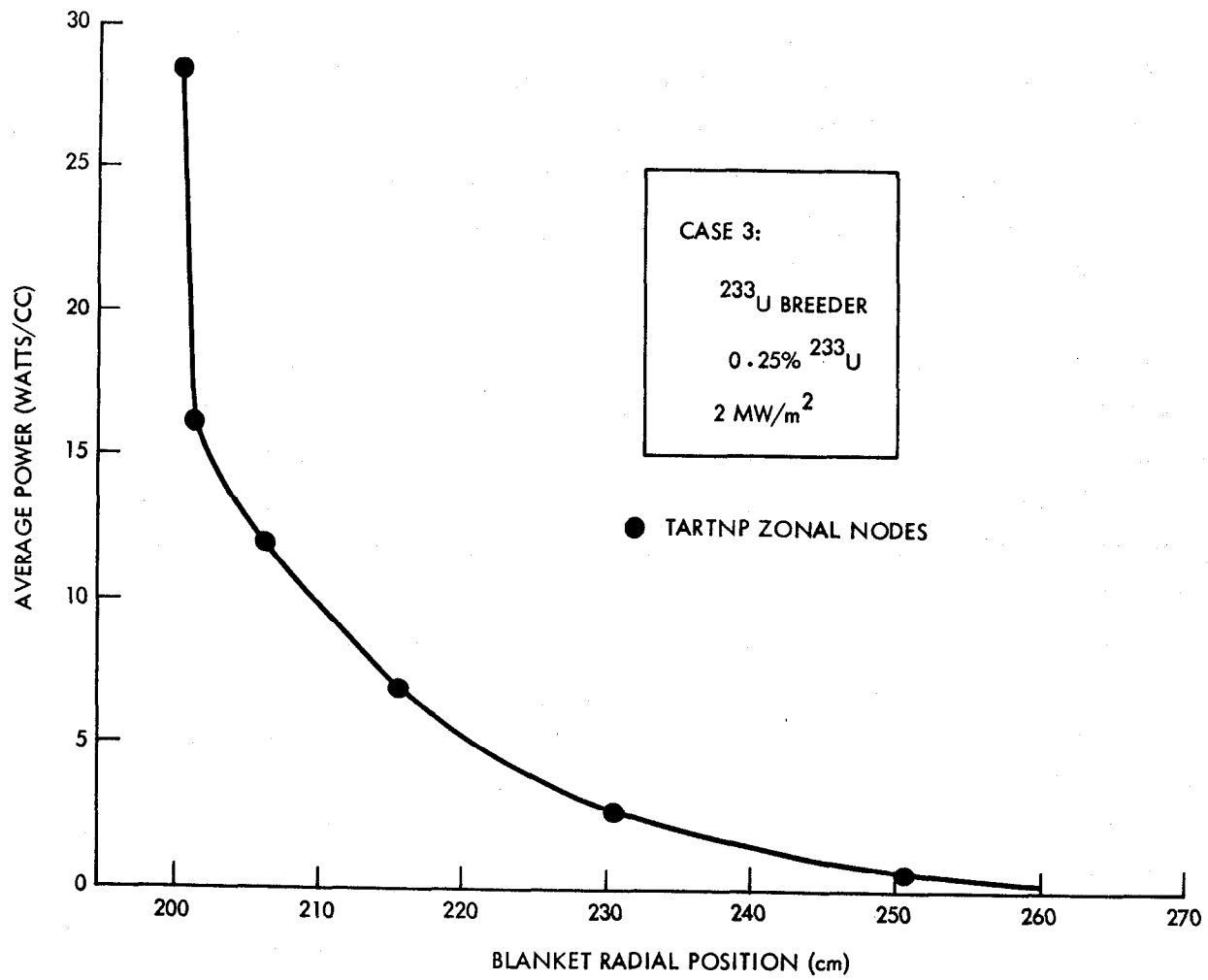


FIGURE A-7. Average nuclear power distribution in the one zone beryllium blanket.

A.3.a.(3). Mechanical Design and Thermal Hydraulics Issues. Mechanical design and thermal hydraulics analysis are interrelated tasks in that the physical configuration must insure structural integrity, operability, and adequate component longevity as well as removal of nuclear heat. The primary issues which must be addressed to achieve these goals include the following:

- Static and dynamic loads including thermal stresses and radiation damage induced effects
- Structural longevity in the radiation environment
- Materials compatibility
- Heat removal systems and blanket temperature distribution

Some of these issues have been addressed earlier in this report. In particular, the breeding module overall dimensions, piping and magnet arrangement, and mechanical design closely resembles that of the reference lithium/molten salt design and the reader is referred to Chapter IV for a general discussion. Similarly, the packed bed blanket is similar to that of the Westinghouse packed bed blanket discussed earlier in this Appendix. Future work should involve the development and integration of a self-consistent design.

The thermal hydraulics area is, however, considered to be critical to the design feasibility of the one zone packed bed blanket concept and is discussed below. Materials compatibility issues which relate to the mechanical and thermal hydraulic design are discussed in Section A.3.a.(4).

The thermal hydraulic design of the one zone, beryllium multiplier, pebble bed blanket requires consideration of several parameters. In particular, the major parameters affecting the thermal hydraulic design are power density (magnitude and distribution), thermal conductivity of the sodium-beryllium-thorium mix, coolant tube size and spacing, and liquid metal pressure drops. The magnitude of the power density is directly proportional to first wall loading, while radial attenuation of the heating profile is dependent on the nuclear properties of the blanket materials. Thermal conductivity is also dependent on blanket materials, but may be enhanced by convection in the sodium. The maximum tube spacing is limited by the maximum allowable temperature in the mix to preclude chemical reactions. The minimum tube spacing is constrained by the minimum pebble size; in

this analysis we have assumed that the minimum clearance between structural members in the blanket must be greater than 8 pebble diameters to prevent bridging of the pebbles which could result in constrained flow or packing. For a given spacing, tube size is constrained by the volumetric fraction of coolant assumed. Once the cooling tube and blanket geometry have been established, the liquid metal coolant velocity and inlet temperature will determine the temperatures of the tube walls and other blanket components. Although the coolant flow is primarily along magnetic field lines, liquid metal coolant heat transfer properties may be constrained by MHD induced effects. These effects can act to inhibit convection, force laminar flow in an otherwise turbulent regime, and increase the coolant pressure drop. Further study of MHD effects is required.

We have performed an analysis of the thermal hydraulic performance of the fertile region of the one zone, liquid metal cooled, packed bed, beryllium multiplier blanket (Figure A-5) using the coolant configuration shown in Figure A-8. A list of the critical design parameters is shown in Table A-8 while a tabulation of materials properties used in the analysis is given in Table A-9.

TABLE A-8. Thermal hydraulic design parameters for fertile region of the one zone beryllium multiplier pebble bed blanket.

---

Power Flow and Energy Deposition:

Fusion power	2900 MW <sub>t</sub>
Neutron wall loading	1.6 MW/m <sup>2</sup>
Power density profile	$2.46 \cdot 10^7 \exp[-7.1r] \text{ W/cm}^3$
Power collected in first wall coolant	522 MW <sub>t</sub> (21.2%)
Power collected in coolant tube row 1	431 MW <sub>t</sub> (17.5%)
Power collected in subsequent rows of coolant tubes	1509 MW <sub>t</sub> (61.3%)

TABLE A-8. (Continued.)

Blanket Volume Fractions:

Lithium	11.0%
Steel	4.4%
Beryllium	47.4%
Sodium	33.8%
Thorium (incl. $^{233}\text{U}$ )	3.4%

Configuration:

Central cell length	115 m
Number of modules	18
Module length	6.4 m
Length of fertile region per module	4.9 m
Coolant path length	4.9 m
First wall plenum thickness	0.5 cm
Clearance between first wall and first row of coolant pipes	4.5 cm
Clearance between coolant pipes in the first row	4 cm
Maximum beryllium and/or thorium pebble diameter	0.5 cm
Coolant pipe radius	1.5 cm
Number of first row coolant pipes	235
Number of coolant pipes in subsequent rows	~740

Operating Temperatures and Coolant Flow Parameters:

Coolant inlet temperature	230°C
Minimum structure temperature	265°C
Coolant outlet temperature	342°C
Maximum structure temperature at outside of first wall coolant plenum	365°C
Maximum structure temperature	375°C
Maximum temperature in sodium-beryllium-thorium bed	500°C
Axial coolant velocity in first wall	2.5 m/s
Axial coolant velocity in first row coolant tubes	3.1 m/s

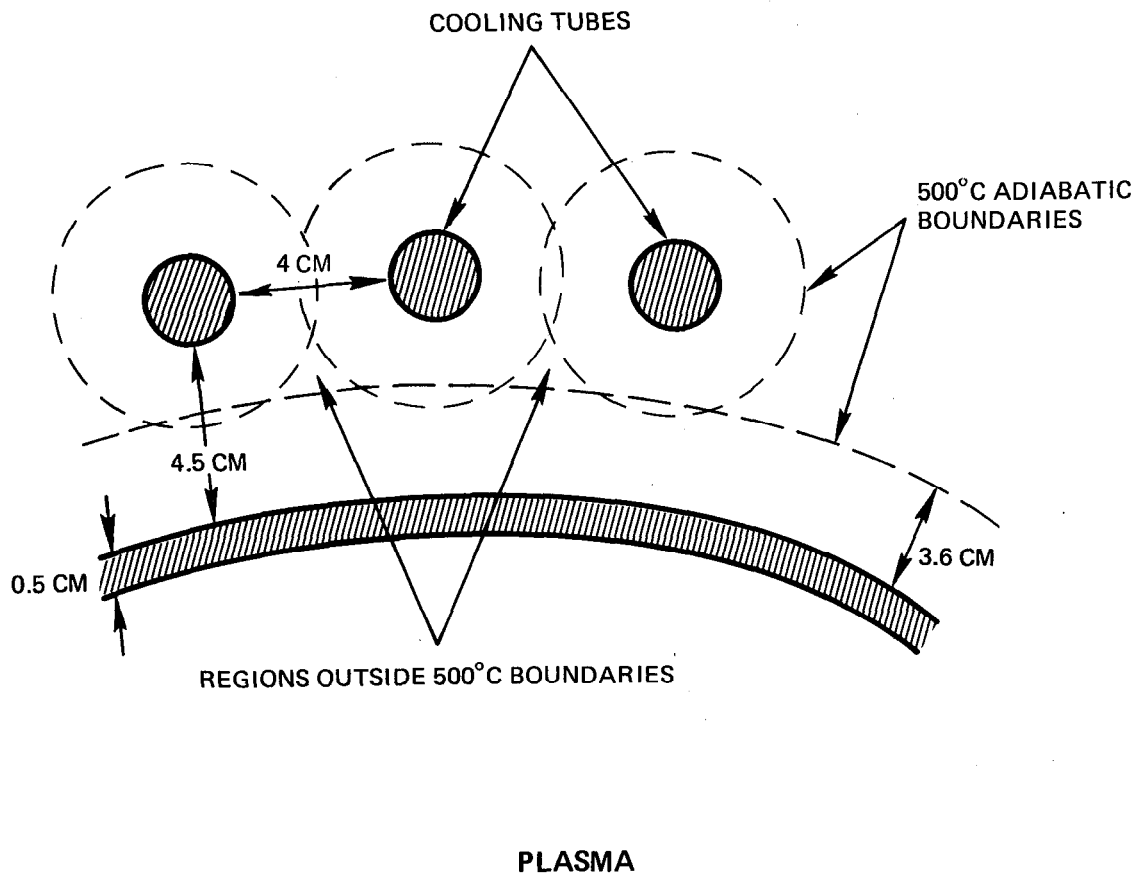


FIGURE A-8. Thermal hydraulic model for the one zone beryllium blanket coolant.

TABLE A-9. Heat transfer parameters for the one zone beryllium multiplier blanket.

---

Properties of sodium-beryllium-thorium mix:

Density	2050 Kg/m <sup>3</sup>
Heat capacity	1600 J/Kg°K
Thermal conductivity	70 W/m°K

Properties of Li<sub>17</sub>Pb<sub>83</sub> coolant:

Density	500 Kg/m <sup>3</sup>
Heat capacity	4190 J/Kg°K
Thermal conductivity	38.1 W/m°K
Viscosity	0.5 x 10 <sup>-3</sup> Kg/m·s
Prandtl number	0.065

---

As shown in Figure A-8 and Table A-8, the first wall loading is 1.6 MW/m<sup>2</sup> and the first wall is cooled by a 0.5 cm thick plenum of lithium. The lithium inlet temperature is 230°C and the outlet temperature is 342°C. Considering a coolant film drop, the maximum first wall temperature is predicted to be about 365°C at the coolant outlet.

The blanket power density is highest near the first wall, but pebble flow constraints prohibit the placement of coolant tubes close to the wall. For this reason, we use the first wall to cool the front region of the blanket. As shown in Figure A-8, the first wall plenum can cool 3.6 cm into the blanket before a 700°C temperature is reached. As such, it removes about 21% of the thermal power generated in the fertile region of the blanket and first wall.

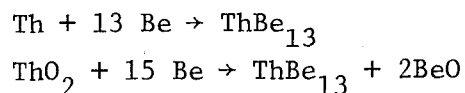
Similarly, 500°C isotherms were calculated for the first row of cooling tubes (same coolant inlet/outlet conditions) behind the first wall. When these 1.5 cm diameter tubes are placed 4.5 cm behind the first wall coolant plenum and 4 cm apart, the maximum allowable pebble diameter is 0.5 cm. In this configuration, our synthesis of one-dimensional heat transport calculations for the first row of tubes and first wall results in similar and compensating adjacent areas (1 cm<sup>2</sup> each) which would be

~230°C. Temperatures approaching 500°C result in many portions of the first ten or twenty centimeters of the blanket. The following discussions are relevant to any blanket concept which includes the same materials at elevated temperatures (~500°C). Section V.C contains related information about the beryllium blanket concept, which faces many of the issues mentioned here.

Careful design is required at elevated temperatures to limit the effects of agents which promote the degradation of structural integrity. In this section, the compatibility of the various materials which have been proposed for use in a one zone beryllium blanket containing thorium fuel is considered. The effects of commonly present impurities is also assessed. Following this, a solution to the possible problem of beryllium attack on structural components and fertile fuel will be described.

Liquid-Solid Interactions. Table A-10 summarizes acceptable operating temperature ranges with respect to solubility for several candidate coolants and blanket materials without considering the possible effects of impurities. Since many active damage mechanisms require the movement of one species through the coolant to attack another, solubility data is quite important and is a logical first step in addressing materials compatibility issues. Based upon this matrix of liquid-solid reactions, and experimental observations\* of beryllium attack on stainless steel through sodium at ppb concentrations and temperatures in the range of 600°C, a conservative design philosophy limiting the beryllium and thorium temperatures to less than 500°C and limiting the steel structure temperature to less than 400°C was adopted. As shown in the preceding section, the 500°C limit has the consequent effect of limiting the steel temperature to less than 375°C - a temperature range which should result in potentially excellent resistance to all life-limiting damage mechanisms to a stainless steel structure.

Solid-Solid Interactions. Beginning with beryllium solid-solid reactions, it has been observed that beryllium will react with thorium or thorium oxide to produce the intermetallic compound,  $\text{ThBe}_{13}$ .<sup>2,3</sup> The reactions are:



---

\* Jack Devan (ORNL) personal communication (December, 1981)

slightly under and above the 500°C maximum allowed temperature. This is considered to be tolerable because the "overcooled" regions would be expected to aid in the cooling of the "undercooled" regions with the result that a maximum temperature of about 500°C can be attained throughout the blanket.

In the above configuration, the first row of coolant tubes consists of 235 individual tubes (each 4.9 m long) which remove 17.5% of the power from a 3.9 cm thick radial zone which begins 3.6 cm outside of the first wall. The maximum bulk coolant velocity in the coolant tubes is 3.1 m/s.

Since it is recognized that (due to the strongly peaked power profile in the blanket) the thermal hydraulic design of the first wall plenum and first row of cooling tubes is most critical, we have not analyzed subsequent banks of coolant tubes which remove less power per tube and can operate with lower flow rates, larger spacings, or greater temperature margins. A more advanced design could use the outer rows to superheat coolant exiting the first wall and inner rows.

This brief analysis is approximate, but we believe that a more detailed analysis will further confirm the feasibility of the thermal hydraulic design. In future studies, a two dimensional thermal analysis should be performed in order to determine the full effect of the overlapping cooling regions in our analysis. A more detailed neutronics analysis, including gamma transport (which should spread more of the heat deeper into the blanket, relieving the first tube bank and plenum), needs to be included. An analysis of MHD effects also needs to be performed to determine the lithium coolant pressures necessary in the blanket, as these impact the amount of structure required. Finally, a better definition of the minimum pebble size needs to be determined.

A.3.a.(4). Materials Compatibility Issues. The major factor influencing materials issues in the one zone beryllium blanket (and many fusion concepts) is high temperature (500°C) in the inner regions of the blanket. Although the first wall and coolant tube structure might operate below 375°C for maximum power densities close to 23 watts/cm<sup>3</sup> (at 1.6 MW/m<sup>3</sup> neutron wall loading), it is difficult to reduce the maximum temperature in the packed bed below 500°C. This is especially true since the lithium coolant has a melting point of 180°C and cannot be used as a coolant below

TABLE A-10. Maximum operational temperature ranges and solubility information for materials compatibility in the one zone beryllium blanket.

Coolant	$\text{NaNO}_2\text{-NaNO}_3\text{KNO}_3$	Li	Na	$\text{Li}_2\text{ Be F}_4$	He
Stainless steel <sup>a</sup>	400 - 500	500 - 600	500 - 600	500 - 650	750
Ferritic steel	500	500	500	500	
TZM		650		700	
Hastelloy N	400 - 500			700	
Beryllium solubility		insoluble at 600°C <sup>b</sup>	insoluble at 700°C <sup>b</sup>	insoluble <sup>c</sup>	insoluble
Thorium solubility		insoluble at 600°C	insoluble at 800°C	insoluble <sup>c</sup>	insoluble

<sup>a</sup>Above 500°C special precautions must be taken with stainless steels because of their susceptibility to stress corrosion cracking. Radiation damage may also reduce the maximum temperature of operation.

<sup>b</sup>This is the solubility without taking into account the effect of the impurities C, N, or O.

<sup>c</sup>Beryllium and thorium will oxidize in the presence of tritium ions that might be formed.

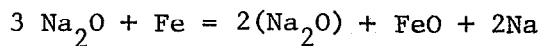
The extent of reaction of beryllium with thorium is a function of the temperature and the degree of contact between them. Darwin and Buddery<sup>2</sup> report that for powders of thorium and beryllium which are mixed and then sintered, considerable intermetallic compound formation took place with coincident swelling and void formation. Numerous intermetallic thorium compounds<sup>7</sup> can also be formed with iron, nickel, and chromium—but at temperatures which are high compared with the low structural temperatures of the packed bed blanket.

Beryllium also forms a wide range of solid solutions and intermetallic compounds with the major carbon steel and stainless steel constituents, that is, iron, chromium, and nickel.<sup>2,3,4,5</sup> Because of the difference in size of the beryllium atom as compared to the lattice parameters of the other metals mentioned, the diffusion of beryllium probably occurs by an interstitial rather than a substitutional mechanism.<sup>5,6</sup> This is an important point because diffusion coefficients for interstitial transport ( $\sim 10^{-8} \frac{\text{cm}^2}{\text{sec}}$  at  $500^\circ\text{C}$ ) are generally orders of magnitude greater than diffusion coefficients for substitutional transport ( $\sim 10^{-19} \frac{\text{cm}^2}{\text{sec}}$  at  $500^\circ\text{C}$ ).

For contact between large pieces of beryllium with other metals (thorium or structure), the extent of reaction is quite a bit smaller than in the case of sintered powders, but reaction layers on the order of ten to one hundred microns are observed (typical conditions:  $500\text{--}700^\circ\text{C}$  for 30 days). At the proposed operating temperature ( $500^\circ\text{C}$ ) of the bed, thin reaction layers may be formed over a short period of time ( $\sim 1$  month). For extended periods of time, and especially when the reactor may go through temperature cycles, the intermetallic reaction layers may tend to spall off, leaving a relatively new surface at which reaction can occur. This process may impact the fertile fuel residence time in the packed bed, but a more thorough investigation confirming the existence of the problem, its potential consequences, and possible solutions (e.g., beryllium and/or thorium coatings) is required. At lower temperatures, the problem of intermetallic compound formation is substantially reduced. At the proposed structural operating temperature of the packed bed ( $375^\circ\text{C}$ ), it is expected to be a minor problem requiring attention only on a longer timescale (years).

Effects of Impurities. The most active impurities in liquid metal systems are oxygen, carbon, and nitrogen. Oxygen solubility in the liquid metals increases with temperature.<sup>8,9</sup> The solubility of oxygen in liquid sodium, as a function of temperature is reported by Minushkin and Kissel.<sup>10</sup> Mansteller, et. al.,<sup>8</sup> give the solubility of oxygen in liquid sodium-potassium alloys as a function of temperature. For the lithium-oxygen system, solubility of oxygen as a function of temperature is given by Smith and Natesan.<sup>9</sup> In liquid sodium and liquid lithium, the oxygen is thought to exist as Na<sub>2</sub>O and Li<sub>2</sub>O, respectively. The stability of the oxides of the liquid metals decreases with increasing atomic weight of the metal and it is more difficult to remove oxygen from a liquid lithium system than it is from a liquid sodium system.<sup>8</sup> Oxygen levels for most liquid metals except lithium can be kept below 10 ppm. For lithium, difficulty is experienced in reducing oxygen levels to below 50 ppm.

The corrosion of iron due to oxygen in a liquid metal system is thought to proceed via the following reaction<sup>11</sup>:



The corrosion of chromium is thought to proceed in a similar way. The above equation illustrates why apparent solubilities of metals in liquid sodium are functions of the oxygen concentration. These corrosion reactions are reversible and, in the colder sections of a liquid metal system, deposition of metals can take place. Because of this reversibility, oxygen behaves like a catalyst in that, for the overall process, it is not consumed. Therefore, even low levels of oxygen concentration may not be tolerable over a long period of time.

According to Darwin and Buddery,<sup>2</sup> beryllium shows good corrosion resistance in liquid lithium, liquid sodium, and eutectic liquid sodium-potassium alloy. Shunk,<sup>5</sup> however, reports that beryllium is soluble in lithium (3000 ppm at 732°C). The discrepancy between the reported behavior of beryllium in liquid lithium is probably due to dissolved oxygen. When oxygen is present in a liquid metal, it can combine with beryllium to form beryllium oxide. Beryllium oxide does not adhere to beryllium metal and high corrosion rates can occur,<sup>2,12</sup> especially when convective transport processes take place.

The solubility of carbon in liquid metals is a function of the oxygen concentration as carbon is transported in the liquid metal as CO.<sup>13,14</sup> Nevzorov<sup>13</sup> observed high pressures developed in stainless steel containers containing liquid sodium and carbon steel. These high pressures were presumably due to the formation of carbon monoxide gas.

Carbon steels are decarburized by liquid metals while stainless steels are carburized. The carbon released from the carbon steels into the liquid metal is an undesirable impurity as it will combine with other metals in the cooling system to form carbides.<sup>13</sup>

A case in point is the carburization of stainless steel. The carbon participating in the process may be present as an impurity in the liquid metal,<sup>15</sup> or, as Fontana and Greene<sup>16</sup> point out, enough carbon is present in stainless steels to cause localized carburization at grain boundaries. Whatever its source, carbon combines with chromium at grain boundaries to form precipitates of chromium carbide ( $\text{Cr}_{23}\text{C}_6$ ). Chromium imparts corrosion resistance to stainless steel and so with the loss of chromium along the grain boundaries, a greater susceptibility to intergranular attack occurs. Low carbon stainless steels (e.g., 304L) may be used to reduce the self-carburization problem.<sup>15</sup>

Since carburization/decarburization problems became most important when the temperature of the steel exceeds 500°C, it appears that the proposed blanket has superior features in this respect. Nevertheless, Nevzorov<sup>13</sup> reports that critical changes in the mechanical properties can occur above this temperature. At higher temperatures ( $\sim 700^\circ\text{C}$ ), a preferential loss of nickel and chromium in stainless steel takes place.<sup>17,18</sup> A loss of nickel leads to a change of the austenite ( $\gamma$ -fcc.) structure to the ferrite ( $\alpha$ -bcc) structure.<sup>11</sup>

An advantage to using stainless steels over carbon steels is that stainless steels tend not to contaminate the reactor environment with carbon. A disadvantage is that stainless steels have a lower thermal conductivity than carbon steels and hence thermal stresses are greater. Ferritic stainless steels containing a maximum of 0.5 wt% Ni are expected to be more resistant to irradiation damage.

Other metals with which carbon can react are beryllium and thorium. The solid solubility of carbon in beryllium is reported to be very low.<sup>5</sup> The carbon-thorium system shows solid solubility and intermetallic compound formation, but the short fuel residence time in the packed bed blanket (~4 months) will limit the extent of carbon-thorium reactions.

In the temperature range 500-700°C, the solubilities of iron, nickel, and chromium in liquid sodium are less than 0.1 ppm by weight. Dissolved oxygen can make the apparent solubilities quite a bit larger.<sup>11</sup> In liquid lithium, a similar behavior is exhibited by the above metals when nitrogen is present.<sup>8</sup> In liquid sodium, it has been found that nitrogen is lost from stainless steel in the hot leg of a sodium test loop.<sup>20</sup> Presumably the nitrogen is transported to other parts of the system where it can form nitrides.<sup>14</sup> The loss of nitrogen from stainless steel is reported to have adverse effects on the mechanical properties of the steel.<sup>20</sup>

Summary of Chemical Compatibility Issues. It appears that in terms of materials compatibility, the major areas of concern for the beryllium packed bed design will be:

- Solid state reactions of beryllium with the other metals in the system. Possible transport of beryllium to the steel through sodium is also a concern.
- Interactions of impurities such as C, O, and N, that are present in the liquid metal coolant or heat transfer medium, with the other components of the bed.

Concerning the solid state reactions, their consequence is largely unknown for the proposed system. However, one possible solution to the problem of beryllium solid state reactions is the development of coating materials for the beryllium pebbles. Possible methods of coating application are electroplating, electroless plating, flame spraying, ion implantation, and plasma spraying. The coating techniques require some surface preparation of the beryllium so that a good mechanical bond can be achieved with the coating material. Of these techniques, it appears that flame spraying may be the easiest accomplished. Surface preparation for this technique can be achieved by sand blasting. Because of the suspected role played by oxides and oxygen in the interactions between

materials in a liquid metal environment, flame sprayed oxides, although otherwise attractive, should be carefully evaluated before serious consideration as coating materials. Other desirable candidates for flame sprayed coating materials appear to be zirconium, vanadium, and molybdenum. Impurities in the liquid metal can, most likely, be adequately controlled. The low operating temperature of structural components in this blanket design is a distinct advantage with respect to all temperature dependent mechanisms (both chemical and irradiation related).

One area which requires additional investigation is the role of convective transport on the rates at which material interactions occur. For the packed bed, convective flow will arise from the density gradients in the heat transfer medium due to temperature differences throughout the bed. This convective flow should be modeled to some extent to determine the magnitude of the flow, and then, small scale experiments could be set up to get a quantitative grasp on the rates of transport of the species of concern.

The rates at which solid-solid reactions occur in the packed bed environment also need to be determined. As mentioned before, the extent of beryllium attack will depend on the amount of contact, the mechanical integrity of the reaction layers formed, and possible beryllium transport through sodium. Small-scale experiments in this area would also be desirable if this blanket concept is pursued further.

A.3.a.(5). Fuel Cycle Issues. Although detailed consideration of fuel cycle and fuel management issues for the one zone packed bed blanket has not been given, these issues seem solvable based upon past work.<sup>21</sup> In particular, the proposed blanket is quite similar to the packed bed blanket discussed in Appendix Section A.1, and the associated issues are also similar. Both blankets derive from a similar blanket design proposed for the TRW HYLIFE Hybrid reactor.<sup>21</sup> In the final report of that study, detailed fuel cycle discussions as well as the preliminary design of a pebble transport system are presented. The design of a thorium metal reprocessing plant, also performed in conjunction with the HYLIFE Hybrid Study (by Bechtel), is repeated in Section VII.B of this report.

An important advantage for the proposed packed bed design is the ability to continue operation of a particular module (and the entire device) while batch fuel management operations proceed. This can be accomplished by backfilling the stagnant bed to maintain the sodium level although the pebbles might be removed. It is also possible that, since most structural components are actively cooled by the lead-lithium, the module could be operated with no sodium or pebbles.

A.3.a.(6). Safety Considerations. A detailed safety analysis considering a loss of coolant or loss of coolant flow event for the one zone, thorium fueled, beryllium packed bed blanket design has not been performed, but some general observations are important:

- A dump tank is required to remove the beryllium and thorium pebbles as well as the sodium. This tank and the required valving system should be of simple design and can, most likely, be cooled using natural convection to remove decay heat.

- The lithium coolant and the sodium can operate at low pressure.

- Conventional liquid sodium safety systems (e.g., cover gas, concrete liners, etc.) would be employed.

- The blanket would be expected to survive a loss of coolant flow event in isolated tubes with little consequence. However, a loss of sodium level event would be serious if the level of pebbles were higher than the sodium level. This type of event should be avoided by the design of active and/or passive safety and monitoring systems.

- A pressure relief system to address a lithium leak into the low pressure sodium filled bed might be adopted.

- Other safety considerations are similar to those presented in Chapter VI.

#### A.3.b. Overall Concept Evaluation

The one zone, beryllium multiplier, pebble bed blanket appears to be feasible and worthy of future consideration. The neutronic performance is excellent for either  $^{233}\text{U}$  or plutonium breeding and does not appear to be particularly sensitive to uncertainties. The mechanical design is quite

simple and utilizes conventional structural materials operated at low temperature and pressure. The thermal hydraulic design requires further refinement, but the general coolant concept appears to be able to limit maximum temperatures to an acceptable regime. Several issues have been raised in the area of chemical compatibility, but these are generic to all beryllium and/or liquid metal systems and do not appear to be fundamentally difficult. Similar conclusions can be drawn regarding the required reactor safety and fuel management technologies.

The highest priority feasibility areas requiring further resolution are as follows:

- A better understanding of MHD effects for this blanket concept including the possibility of pumping the coolant directly through the bed to eliminate the coolant tubes. Up to ~300 psia is tolerable.
- The possible need of inert coatings for beryllium (and possibly thorium). Some techniques have been proposed.
- A better understanding of the effects of impurities in liquid metal systems. Control seem possible.
- Improved designs of safety and pebble management systems.

REFERENCES FOR APPENDIX A

1. STARFIRE - A Commercial Tokamak Fusion Power Plant Study, Argonne National Laboratory, Argonne, IL., ANL/FPP/80-1 (1980).
2. Darwin, G.E., and Buddery, J.H., Beryllium, Academic Press Inc., New York, Chapter 8 (1960).
3. Elliot, R.P., Constitution of Binary Alloys, First Supplement, McGraw-Hill, New York (1965).
4. Hansen, M., Constitution of Binary Alloys, McGraw-Hill, New York (1958).
5. Shunk, F.A., Constitution of Binary Alloys, Second Supplement, McGraw-Hill, New York, p 110-115 (1969).
6. Nowich, A.S., and Burton, J.J., Diffusion in Solids, Academic Press, New York (1975).
7. Smith, J.F., Carlson, O.N., Peterson, D.T., and Scott, D.T., Thorium: Preparation and Properties, Iowa State University Press, Ames, Iowa (1975).
8. Mausteller, J.W., Tepper, F., and Rodgers, S.J., Alkali Metal Handling and Systems Operating Techniques, Gordon and Breach, New York (1967).
9. Smith, D.L., and Natesan, K., "Influence of Nonmetallic Impurity Elements on the Compatibility of Liquid Lithium with Potential CTR Containment Materials," Nuclear Technology, 22, 392 (1974).
10. Minushkin, B., and Kissel, G., "Solubility and Reactions of Oxygen in Sodium," in Corrosion by Liquid Metals, ed. by Draley, J.E., and Weeks, J.R., Plenum Press, New York (1970).
11. Weeks, J.R., and Isaacs, H.S., "Corrosion and Deposition of Steels and Nickel-Base Alloys in Liquid Sodium," in Advances in Corrosion Science and Technology V.3, ed. by Fontana, M.G., and Staehle, R.W., Plenum Press, New York, p 16 (1973).
12. Epstein, L.F., in NASA-AEC Liquid Metals Corrosion Meeting V.I., NASA SP-41, p. 27 (1963).
13. Nevzorov, B.A., Corrosion of Structural Materials in Sodium, AEC-TR-6984, Chapter 5 (1970).
14. Weeks, J.R., "Corrosion in Liquid-Metal Cooled Reactors," in Materials and Fuels for High-Temperature Nuclear Energy Applications, ed. by Simnad, M.T., and Zumwalt, R., MIT Press, Cambridge, p. 345 (1964).

REFERENCES FOR APPENDIX A (Continued).

15. Ruther, W.E., Cloar, T.D., and Strain, R.V., "Materials-Compatibility in EBR-II," in Corrosion by Liquid Metals, Draley, J.E., and Weeks, J.R., eds., Plenum Press, New York, p. 90,92 (1970).
16. Fontana, M.G., and Greene, N.D., Corrosion Engineering, McGraw-Hill, New York, p. 58 & 59 (1978).
17. Hopenfeld, J., "Corrosion of Types 316 Stainless Steel with Surface Heat Flux in 1200<sup>o</sup>F Flowing Sodium," in Corrosion by Liquid Metals, Draley, J.E., and Weeks, J.R., eds., Plenum Press, New York (1970).
18. Roy, P., Dutina, D., and Comprelli, F., "The Evaluation of Particulates Deposited in Flowing Non-Isothermal Sodium Systems," in Corrosion by Liquid Metals, Draley, J.E., and Weeks, J.R., eds., Plenum Press, New York (1970).
19. Cowan, R.L. II, and Tedmon, C.S. Jr., "Intergranular Corrosion of Iron-Nickel-Chromium Alloys," in Advances in Corrosion Science and Technology, V.3., ed. by Fontana, M.G., and Staehle, R.W., Plenum Press, New York, Chapter 3 (1973).
20. Shields, S.A., Bagnall, C., and Schrock, S.L., "Interstitial Mass Transfer in Sodium Systems," in Chemical Aspects of Corrosion and Mass Transfer in Liquid Sodium, ed. by Jansson, S.A., The Metallurgical Society of America, New York, p. 157 (1973).
21. Maniscalco, J.A., et. al., "Laser Fusion Breeder Design Study Final Report," Report No. DOE/DP/40111-1, TRW (1980).



APPENDIX B  
ALTERNATIVE GAS-COOLED BLANKET OPTIONS

B.1 OVERVIEW

B.1.a Design Considerations

The general considerations for the selection of the reference gas-cooled blanket concept include neutronic performance, heat transfer, mechanical design, temperature-material compatibility and safety. The beryllium-based pressure tube hybrid blanket design concept was suggested for further evaluation because of superior neutronic performance. Three beryllium blanket concepts were further identified as potential candidates for hybrid application in addition to the one chosen as the reference design concept. These are illustrated in Fig. B-1 and are described below. As seen in Fig. B-1 all these blanket concepts consist of three regions between the first wall and the pressurized vessel (coolant plenum). The first region in all three concepts is a neutron multiplying and tritium breeding region which is composed of beryllium, lithium material and metal structure. The thorium material is placed behind the first neutron multiplication and tritium breeding region. A graphite reflector region is placed behind the thorium fertile region. Since these design concepts are based on the fertile dilution approach, a moderating material is needed in the thorium fertile region. Graphite is proposed for that purpose in one of the design concepts, Concept I, where the beryllium inventory is to be a minimum. The Concept II blanket design employs beryllium as the moderating material in the thorium fertile region, which also acts as an additional neutron multiplying region to achieve better neutron multiplication. These two design concepts utilize two approaches to suppress fission reactions in the hybrid blanket, namely fertile behind the fusile region (fast fission suppression) and fertile dilution. As the bred fissile material accumulates, the thermal fission reaction becomes significant in the beryllium blanket where the neutron energy is highly moderated. Therefore, the Concept III blanket design was introduced. As shown in Fig. B-1, the Concept III blanket design is the same as the Concept II blanket design except that in the Concept III blanket design a small amount of lithium material is placed in both the fertile and reflector regions to suppress the thermal neutron flux and aid in tritium breeding.

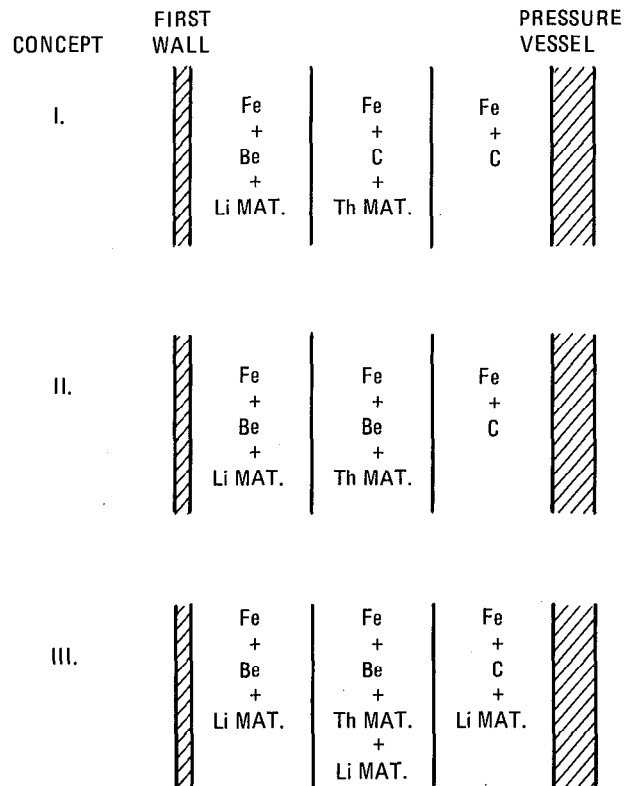


FIGURE B-1. Schematics of gas-cooled blanket design concepts for the Tandem Mirror Hybrid Reactor using beryllium neutron multiplier.

### B.1.b Scoping Phase Options

Neutronics scoping calculations were performed for several blanket designs based on the above-mentioned blanket concepts using the one-dimensional code ANISN and the DLC-37 nuclear cross section library. Figures B-2 and B-3 show the blanket models representing the Concept I and III blanket designs for the neutronics scoping calculations. As shown in Fig. B-2, the Concept I blanket consists of a 1 mm iron-based steel first wall (Zone 3), a tritium breeding and neutron multiplication zone (Zone 4), a 1 mm steel second wall (Zone 5), alternating zones of graphite and fertile material (Zones 6-13), a 0.2 m graphite reflector zone (Zone 14), and a 30 mm iron zone (Zone 15). Zone 4 consists of 1% Fe, 4% lithium and 95% beryllium (80% dense), all by volume. The fertile material zones (Zones 7, 9, 11 and 13), are composed of 3.4% Fe, 12.7% Th, 77.8% C and balance of void, the homogenized composition of an array of fertile material (thorium metal balls) and metal tubes (which are 11 mm O.D. with a tube wall thickness of 0.5 mm). There are four arrays of such tubes, each 40 mm apart and separated by the graphite matrix. The schematic of the fertile-in-tubes design for the Concept I blanket is illustrated in Fig. B-4. Immediately behind the alternating zones of graphite and fertile tubes is a graphite reflector (Zone 14) which is thick enough to assure full utilization of the fusion neutrons in the breeding zones. The 30 mm iron zone (Zone 15) following the graphite reflector is included in the blanket calculation to account for the net structural material composing the helium plenum and blanket supporting structure. In the scoping study for this design (and other designs to be described later), the thickness of the beryllium zone immediately behind the first wall and the  $^6\text{Li}$  content in lithium were the only parameters varied. All other parameters were determined preliminarily based on neutronics and mechanical design considerations and kept constant during the scoping study.

The Concept II blanket (not shown), is a modification of the Concept I design. In this design the graphite material in Zones 6-13 of the Concept I blanket shown in Fig. B-2 is replaced by beryllium material. All others are kept the same. Note that the neutronic models for the Concepts I and II blankets do not include the helium coolant, hence the neutronic results

ZONE		RADIUS (m)
		0.0
1	PLASMA	
		1.70
2	VACUUM	
		2.00
3	(IRON) FIRST WALL	
		2.001
4	1% Fe + 4% LITHIUM + 95% Be (80% DENSE)	
		2.001+X
5	(IRON) SECOND WALL	
		2.002+X
6	1% Fe + 99% C	
		2.042+X
7	3.4% Fe + 12.7% Th + 77.8% C	
		2.053+X
8	A	
		2.093+X
9	B	
		2.104+X
10	A	
		2.144+X
11	B	
		2.155+X
12	A	
		2.195+X
13	B	
		2.206+X
14	A	
		2.406+X
15	Fe	
		2.436+X

A - THE MATERIAL COMPOSITION IN THIS ZONE IS SAME AS THAT IN ZONE 6  
B - THE MATERIAL COMPOSITION IN THIS ZONE IS SAME AS THAT IN ZONE 7

FIGURE B-2. Schematic of a one-dimensional blanket model representing a Concept I blanket design for neutronic calculations.

ZONE		RADIUS (m)
		0.0
1	PLASMA	
		1.70
2	VACUUM	
		2.00
3	(IRON) FIRST WALL	
		2.001
4	2% Fe + 4% Li <sub>17</sub> Pb <sub>83</sub> + 84% Be (80% DENSE) + 10% HELIUM	
		2.001+X
5	12.7% Th + 4.9% Fe + 63.0% Be (80% DENSE) + 10% Li <sub>17</sub> Pb <sub>83</sub> + BALANCE HELIUM	
		2.012+X
6	A	
		2.042+X
7	B	
		2.053+X
8	A	
		2.093+X
9	B	
		2.104+X
10	A	
		2.144+X
11	B	
		2.155+X
12	A	
		2.165+X
13	2% Fe + 4% Li <sub>17</sub> Pb <sub>83</sub> + 84% C (90% DENSE) + 10% HELIUM	
		2.465+X
14	Fe	
		2.495+X

A - COMPOSITION IN THIS ZONE IS SAME AS THAT IN ZONE 4  
B - COMPOSITION IN THIS ZONE IS SAME AS THAT IN ZONE 5

FIGURE B-3. Schematic of a one-dimensional blanket model representing a Concept III blanket design for neutronic calculations.

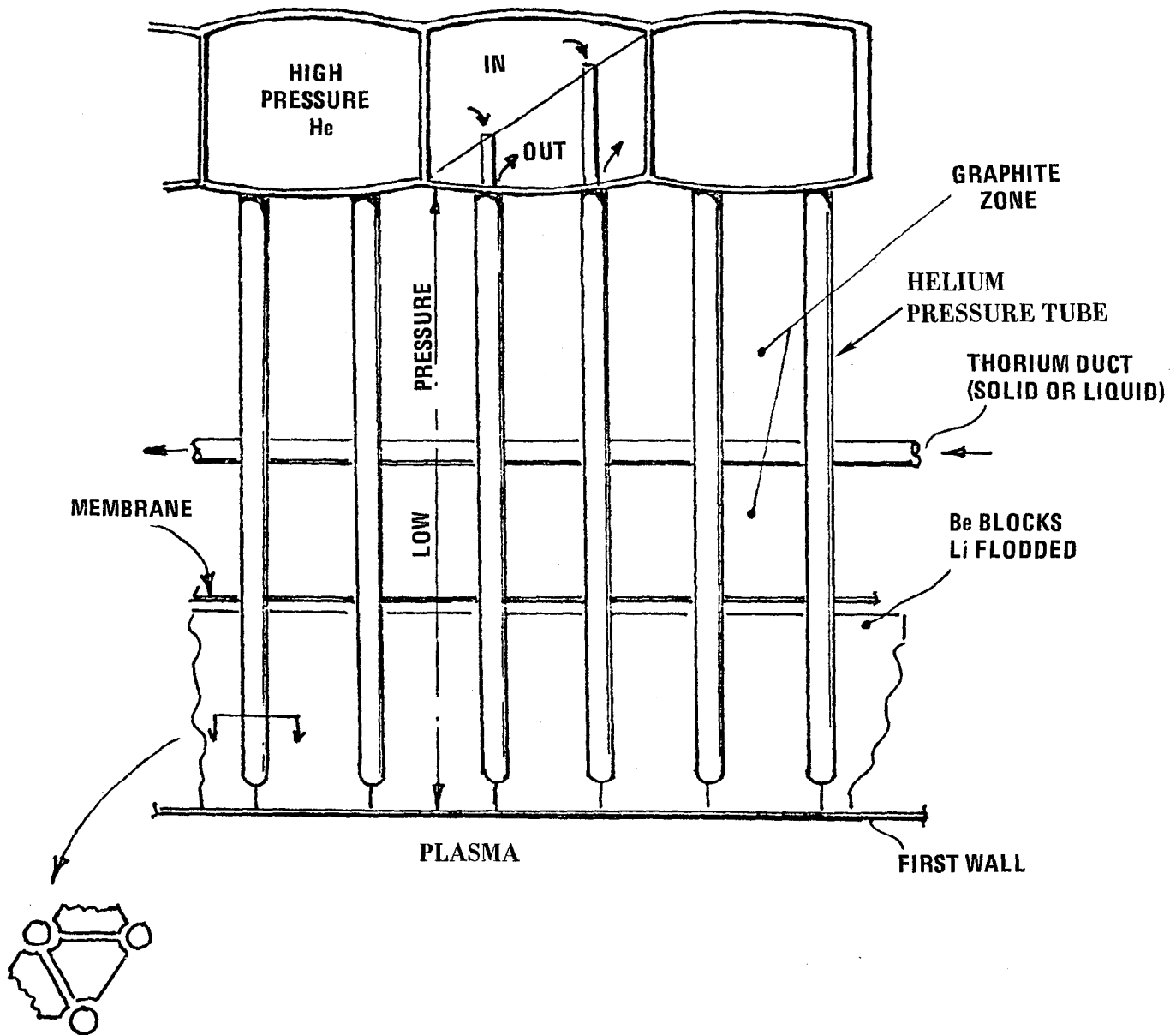


FIGURE B-4. Schematic of a fertile-in-tubes blanket concept coupled with the concentric helium pressure tube cooling design.

obtained may not reflect realistic blanket dimensions. However the performance trends and features should present the general characteristics of these blanket designs.

Figure B-3 depicts schematically the one-dimensional neutronic model for the Concept III blanket. The blanket design configuration of the Concept III blanket is almost identical to that of the Concept II blanket except that in the Concept III blanket, the alternating zones of beryllium and fertile tubes and the graphite reflector zone also contain lithium material. Thus, the zone immediately behind the first wall is repeated and alternates with the fertile zones. There are three additional changes in the Concept III blanket as compared to the Concept II blanket. In the Concept III blanket, the breeding material is  $\text{Li}_{17}\text{Pb}_{83}$ , helium coolant is included in the calculational model, and structural volume fractions are increased.

## B.2 FERTILE IN-TUBES BLANKET DESIGNS

### B.2.a Neutronic Performance Considerations

Tritium production rates, mostly from  ${}^6\text{Li}(n,\alpha)\text{T}$  reactions, and fissile atom production rates (U-233 + Pa-233) are shown in Figs. B-5 through B-7 for the Concept I, II and III blankets, respectively, as a function of first beryllium zone thickness and for several  ${}^6\text{Li}$  contents in lithium. Two noteworthy points can be made regarding the neutronic characteristics for this class of beryllium blankets based upon the results shown in Fig. B-5 through B-7:

1. When the first beryllium zone becomes thicker, the tritium breeding ratio increases for all blankets. The total fissile atom production (U + Pa) rate decreases for all blankets except the Concept I blanket where it increases initially as the beryllium zone becomes thicker due to the increase of beryllium  $n,2n$  reactions. It reached a maximum at about 60 mm of beryllium zone and then decreases because of the steady increase of neutron absorption in  ${}^6\text{Li}$  in the beryllium zone.

2. The increase of percent  ${}^6\text{Li}$  in lithium increases the tritium breeding performance. However at the same time, the fissile atom production rate decreases.

The total breeding rates (U + Pa and tritium) for all blankets are also strongly affected by the beryllium zone thickness and percent  ${}^6\text{Li}$  in lithium. They are shown in Figs. B-8 through B-10 for Concept I, II and III blankets, respectively. In general, a thicker beryllium zone and a higher percentage of  ${}^6\text{Li}$  in lithium produces a higher total breeding rate. In other words, for the same total fissile atom and tritium breeding, a higher percentage  ${}^6\text{Li}$  in lithium can be traded for a thinner beryllium zone. This is quite an important characteristic of the beryllium blanket design since beryllium is a relatively scarce material and its neutron multiplication utilization should be maximized. It is noted that, when comparing the total fissile and tritium breeding for different percentages of  ${}^6\text{Li}$  in lithium, the lithium material used in Concepts I and II is liquid lithium and that used in Concept III is  $\text{Li}_{17}\text{Pb}_{83}$  (which contains less lithium than liquid lithium).

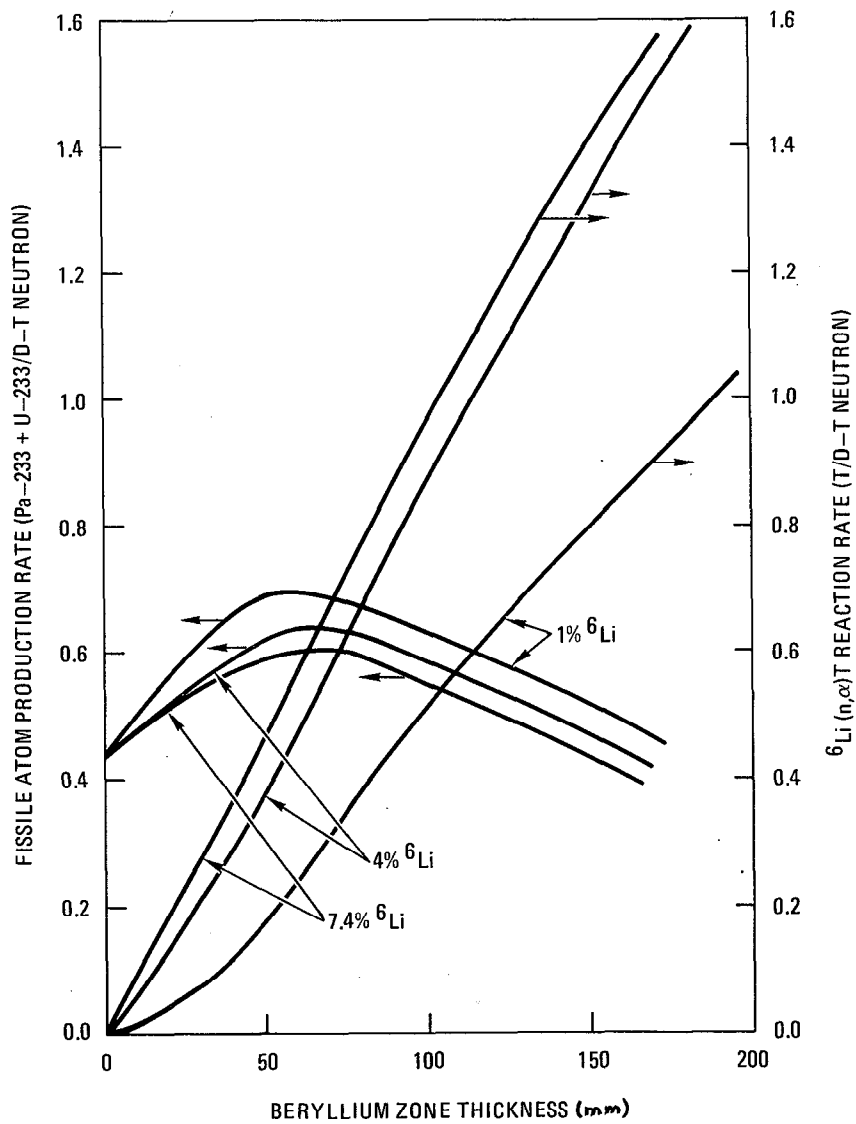


FIGURE B-5. Tritium production (mostly  ${}^6\text{Li}(n,\alpha)\text{T}$ ) and fissionable atom production rates as a function of beryllium zone thickness for the Concept I blanket. They are plotted for 1%, 4% and 7.4% (natural lithium)  ${}^6\text{Li}$  in lithium.

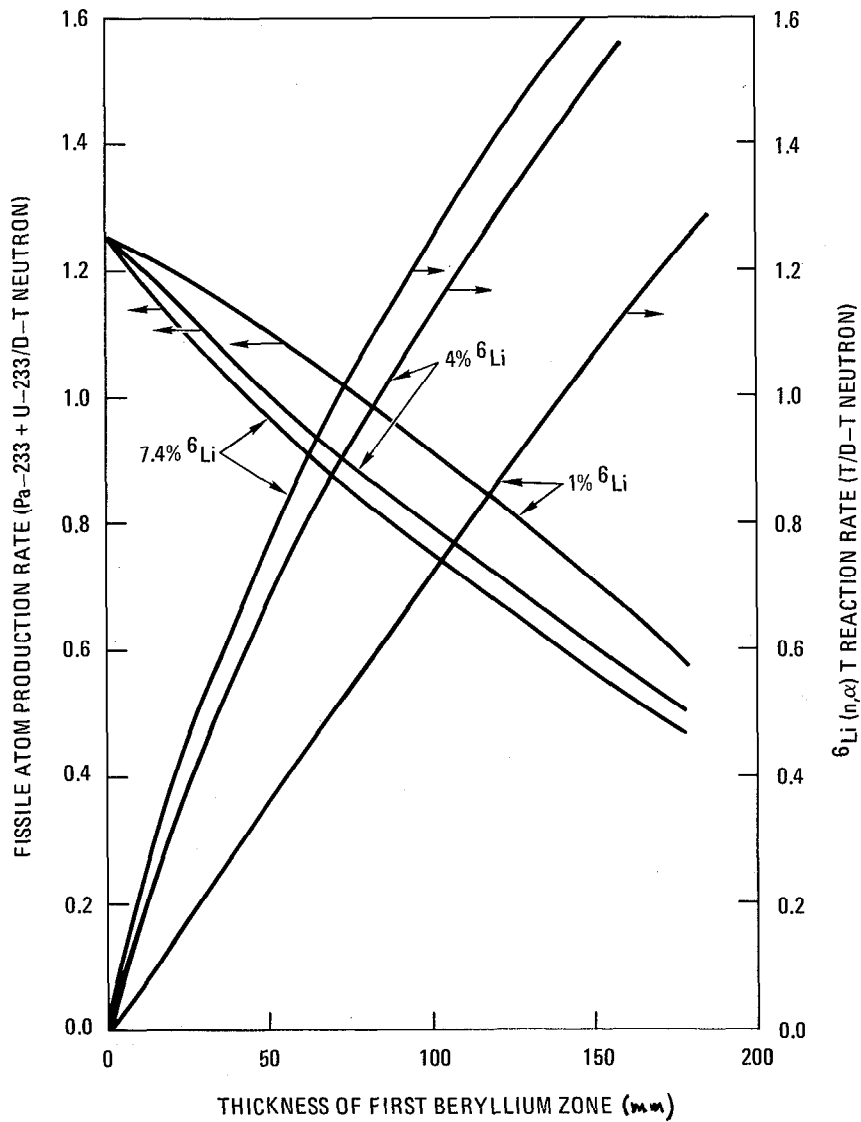


FIGURE B-6. Tritium production (mostly  ${}^6\text{Li}(n,\alpha)\text{T}$  and fissile atom production rates in the Concept II blanket displayed as a function of the first beryllium zone thickness. Curves shown here are for 1%, 4% and 7.4%  ${}^6\text{Li}$  in lithium.

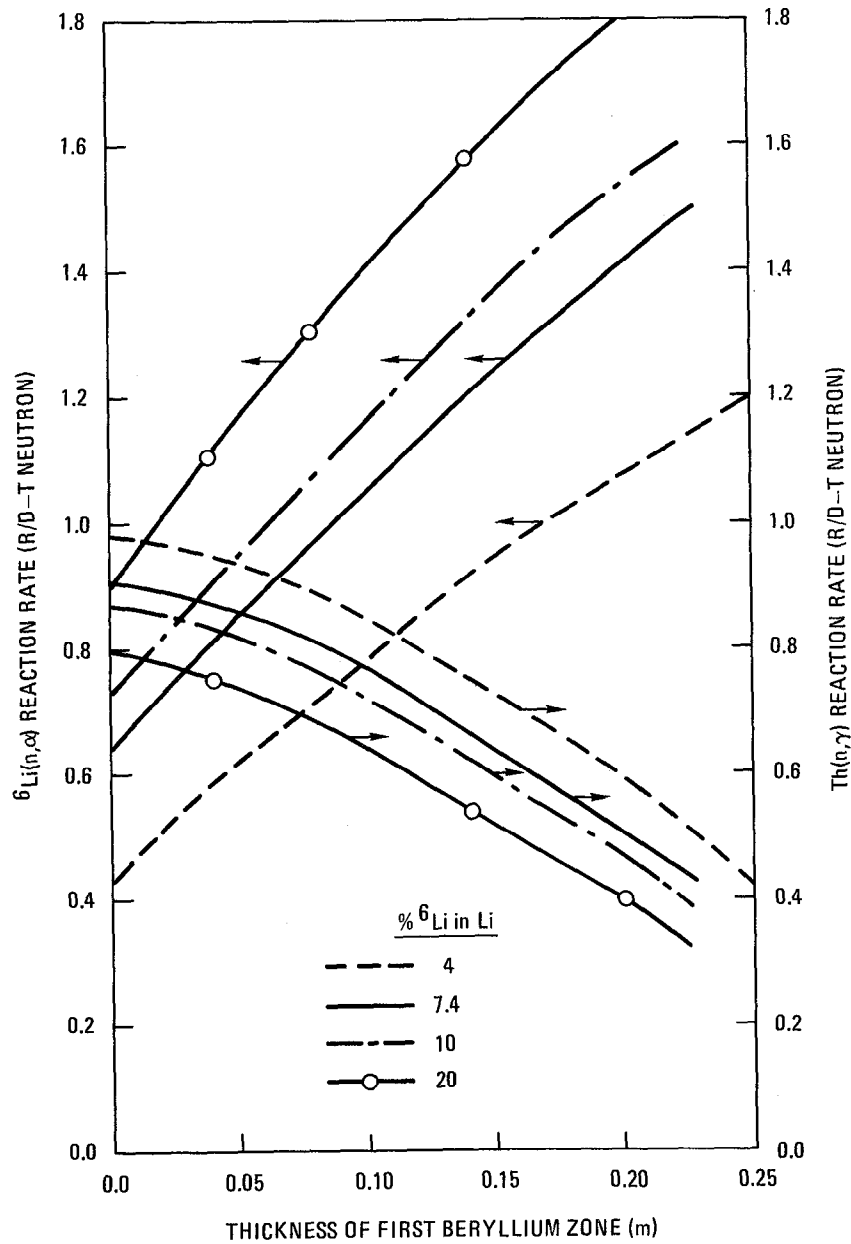


FIGURE B-7. Tritium production (mostly  ${}^6\text{Li}(n,\alpha)\text{T}$ ) and fissile atom production rates in the Concept III blanket as a function of first beryllium zone thickness. They are displayed for four  ${}^6\text{Li}$  contents in lithium, 4%, 7.4%, 10% and 20%.

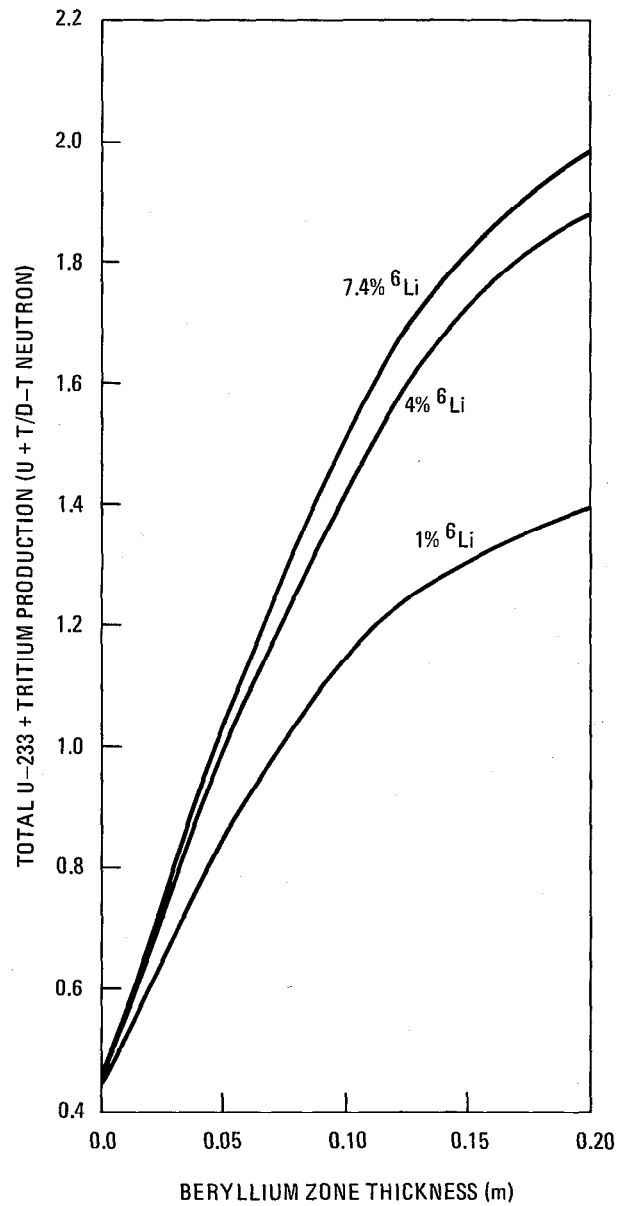


FIGURE B-8. Total fissile atom and tritium production rates for the Concept I blanket as a function of beryllium zone thickness. Note that they are given for 1%, 4% and 7.4% (natural lithium)  $^6\text{Li}$  in liquid lithium.

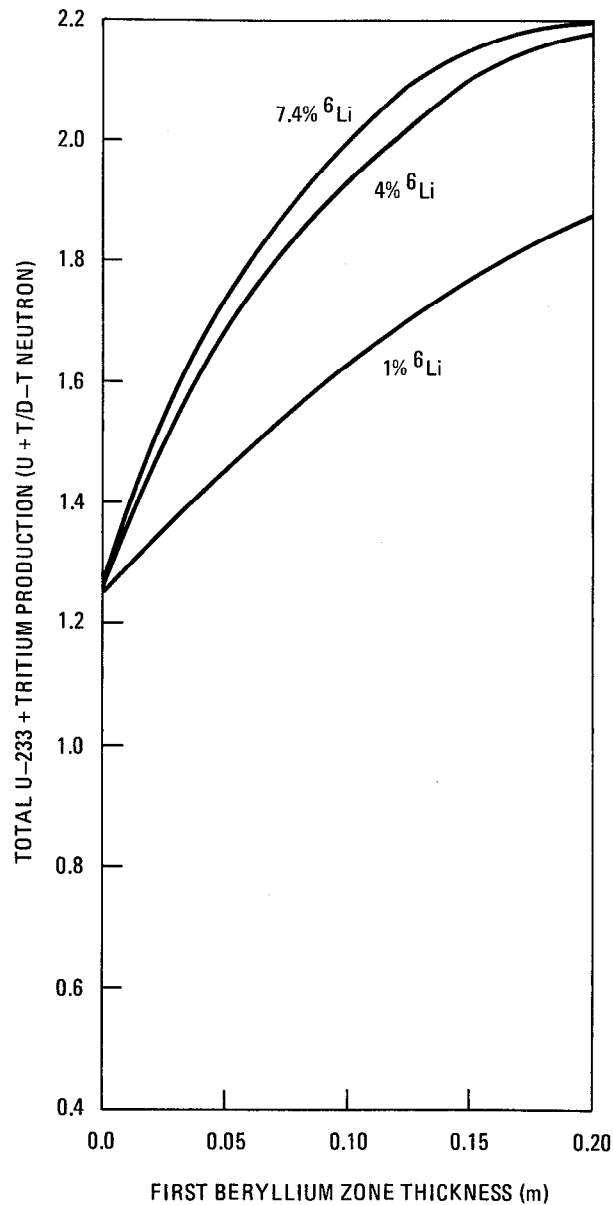


FIGURE B-9. Total fissile atom and tritium production rates for the Concept II blanket as a function of first beryllium zone thickness. Note that they are given for 1%, 4% and 7.4% (natural lithium) <sup>6</sup>Li in liquid helium.

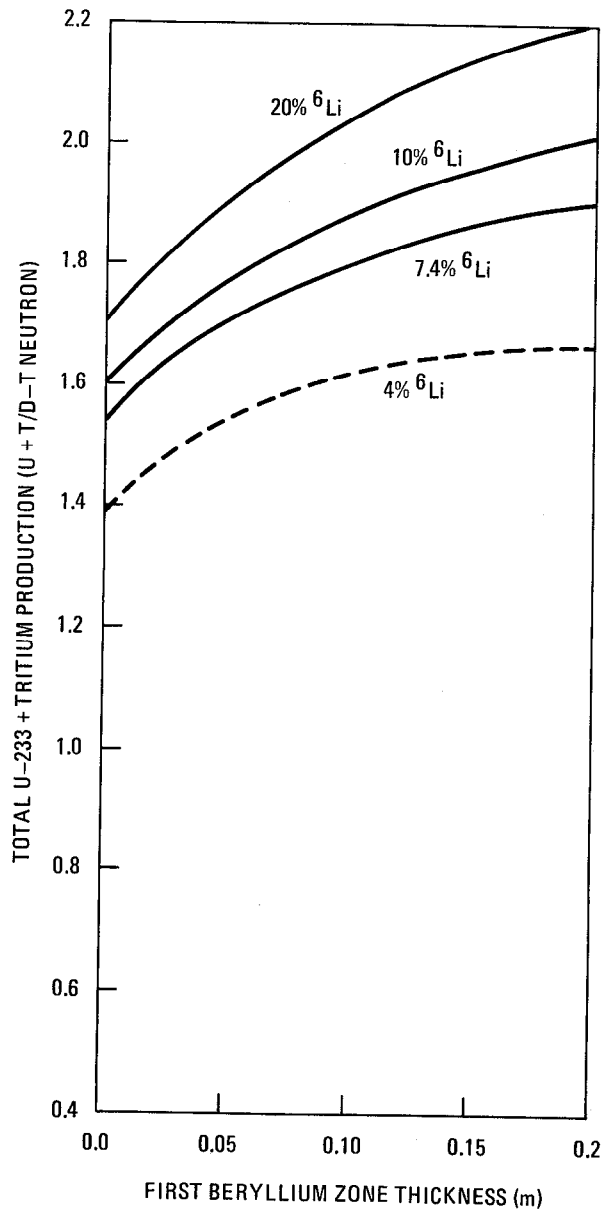


FIGURE B-10. Total fissile atom and tritium breeding rate for Concept III blanket as a function of first beryllium zone thickness. They are given for 4%, 7.4% (natural lithium), and 20%  ${}^6\text{Li}$  in lithium. Note that the lithium material used here is  $\text{Li}_{17}\text{Pb}_{83}$  eutectic.

The most important consideration in designing a D-T fusion reactor at the conceptual stage is that the reactor should breed adequate tritium to supply its own fuel. Based on this consideration, the fissile atom production rate and thus the total fissile and tritium breeding are determined from Figs. B-5 through B-10 and are tabulated in Table B-1 for all blankets with a tritium breeding ratio of 1.10. From this table, we see that the Concept II and III blankets produce more fissile atom per D-T neutron than the Concept I blanket as expected. The Concept II and III blankets behave very similarly in producing fissile atoms and tritium. The difference shown here is principally because the Concept III blanket assumes 2% iron-based steel structure in the breeding zones whereas the Concept II blanket assumes only 1% structure in the breeding zones. However the neutron population in the Concept III blanket is also more efficiently utilized because of the introduction of lithium material in the fertile and reflector zones. This is revealed in the need of thinner total beryllium zones in the Concept III blanket compared to that in the Concept II blanket. Notice that the presence of lithium-lead eutectic in the fertile and reflector zones also suppresses the thermal fission reaction which is an important concern as the bred fissile atom accumulates in the blanket.

From the above results, we conclude that Concept II and III blankets may offer the best performance for the fissile fuel production, but important feasibility concerns regarding the fertile-in-tubes blanket will be described from the mechanical design and the thermal-hydraulics viewpoints.

#### B.2.b Thermal-Hydraulic Design Considerations

The design approach in circulating solid fertile material in tubes has the distinct advantages for direct control of the fertile material and possibly the bred tritium. However, from the heat transfer point of view, possible problems in dealing with high material temperatures can be present because of high volumetric power generation in the tubes and possibly high thermal contact resistance between the moving thorium balls/pellets and the tube wall. These problems were identified and studied by using a 1-D heat transfer model based on cylindrical geometry.

TABLE B-1. Beryllium zone thickness, fissile atom production and total breeding rate for beryllium blanket Concepts I, II and III (all blankets product 1.10 tritons per D-T neutron).

	Blanket Design		
	Concept I	Concept II	Concept III
First beryllium zone thickness (m)	0.12	0.09	0.04
Total thickness of beryllium zones (m)	0.12	0.30	0.20
Fissile atom production (U+Pa/n)	0.51	0.81	0.75
Total fissile atom and tritium breeding rate (U+Pa+T/n)	1.61	1.91	1.85

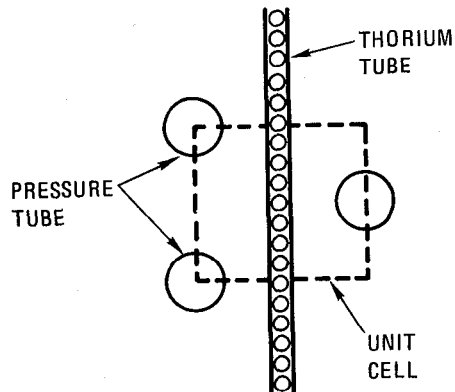
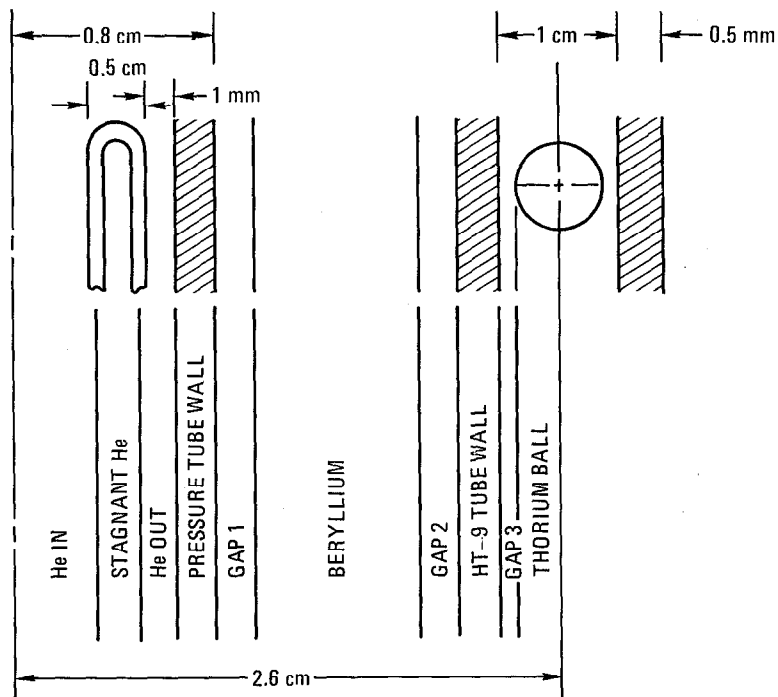


FIGURE B-11. Pressurized tube and thorium ball containing tube configuration. This unit cell is used in the heat transfer evaluation.

Figure B-11 shows the configuration of the unit cell for the pressurized cooling tube and the thorium containing tube, aligned orthogonally to each other in the blanket. A schematic that shows the different regions between the thorium ball and the pressurized cooling tube centerline is also illustrated in Fig. B-12. The dimensions of different zones are indicated. The heat flux at the HT-9 wall of the thorium tube was first estimated by energy balance from knowing the volumetric power generated in the thorium ball and the HT-9 wall. The heat-transfer between the thorium containing tube wall and the pressurized cooling tube were then performed by using cylindrical geometry heat-transfer equations as discussed in Section V.E. From neutronics results, Fig. B-13 shows the maximum volumetric power generation in the thorium metal,  $\text{Li}_{17}\text{Pb}_{83}$  eutectic and beryllium metal for the Concept II and III blankets. They were used for the scoping calculation.

Table B-2 summarizes the results from the heat transfer calculations showing the maximum temperatures for the thorium metal ball, thorium containing tube wall, the beryllium metal and helium pressure tube. Two cases and five options were evaluated. Corresponding to design concepts discussed in B.2.a, Concept II has lithium and Concept III has  $\text{Li}_{17}\text{Pb}_{83}$  in the alternating fertile tube and beryllium zones, respectively. The five options are separated by the assumptions of different heat transfer mechanism in various gaps. When stagnant helium was assumed in the gap, conduction heat transfer was considered. When convective helium was assumed in the gap, a convective heat transfer coefficient of  $3000 \text{ W/m}^2\text{-K}$  was assumed.

The results show that active heat removal between various gaps are required. The reduction of contact resistance either by convective helium or by liquid metal  $\text{Li}_{17}\text{Pb}_{83}$  is essential to maintain acceptable material temperatures. Options 4 and 5 have reasonable temperatures because of lower volumetric power generation in addition to the improvement in contact resistance. High pressure helium is required for generating high convective heat transfer coefficient. Thus, for the purpose of not requiring high pressure gas in the thorium containing tube, option 5 is the most reasonable choice. However it has the complication of circulating thorium metal balls in a tube containing  $\text{Li}_{17}\text{Pb}_{83}$  and more study is needed in this area.



MATERIALS:

COOLANT	He
STRUCTURAL	HT-9
FERTILE	Th-METAL OR ThO <sub>2</sub>
GAPS 1,2 and 3	STAGNANT He or CONVECTIVE He OR Li <sub>17</sub> Pb <sub>83</sub>

COOLANT CONDITIONS:

50 ATM HELIUM  
 T<sub>IN</sub> - 250°C  
 T<sub>OUT</sub> - 450°C

FIGURE B-12. One-dimensional calculation schematic and dimensions for the ball in-tube configuration.

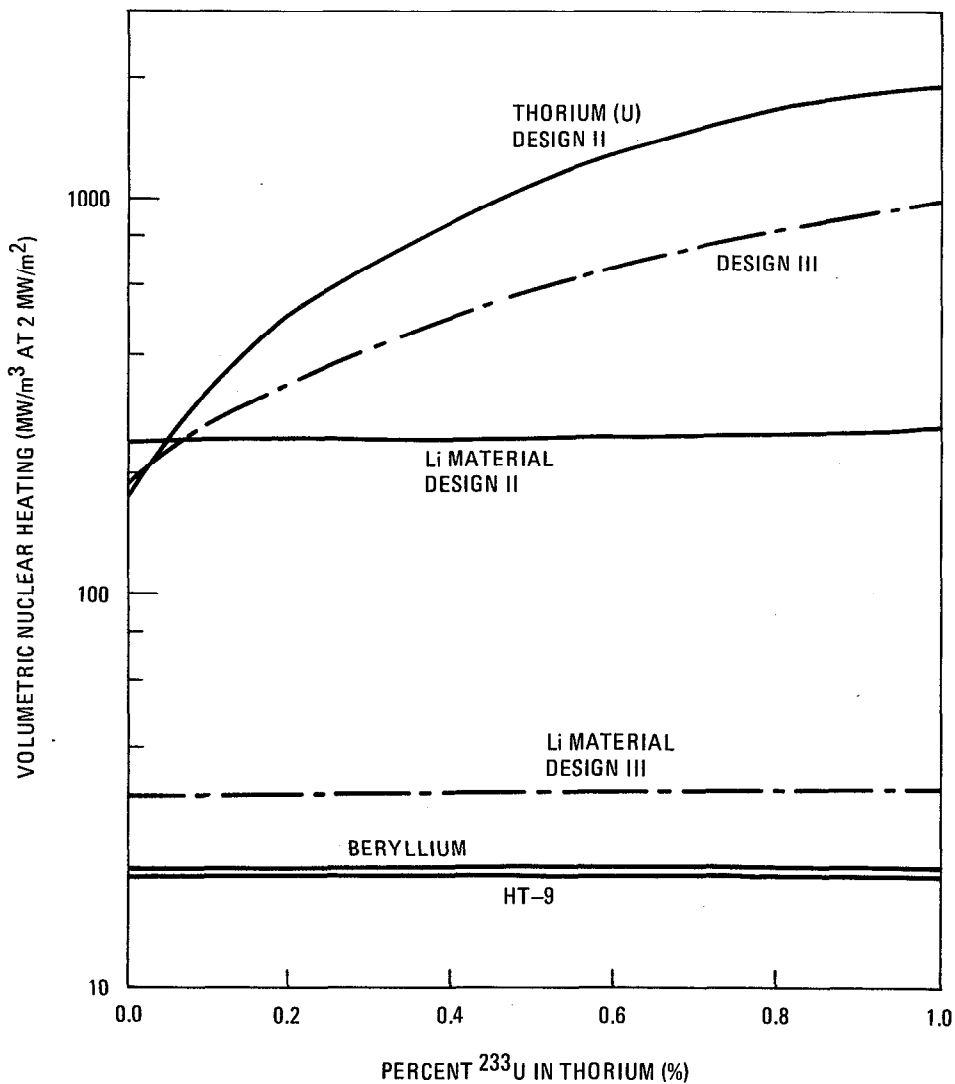


FIGURE B-13. Maximum volumetric nuclear heating rates in thorium structural beryllium and lithium materials depicted as a function of accumulated U-233 content in thorium and for design II and III blankets. Note that in the heat transfer calculations, the heating rates at 0.2% in thorium were used. The neutron wall loading is 2 MW/m<sup>2</sup>.

TABLE B-2. Maximum temperature distribution comparisons: (thorium me

	OPTIONS	$\dot{q}'''$ (MW/m <sup>3</sup> )	GAPS 1 & 2 (Be-ZONE)	GAP 3 (Th-TUBE)	T (Th) (°C)	T <sub>WALL</sub> (Th) (°C)	T (E) (°C)
CONCEPT II	1.	500	STAGNANT HELIUM	STAGNANT HELIUM	6386	4951	21
	2.	500	STAGNANT HELIUM	CONVECTIVE HELIUM	5164	4951	21
	3.	500	CONVECTIVE HELIUM	CONVECTIVE HELIUM	1271	1058	7
CONCEPT III	4.	340	Li <sub>17</sub> Pb <sub>83</sub>	CONVECTIVE HELIUM	685	540	4
	5.	340	Li <sub>17</sub> Pb <sub>83</sub>	Li <sub>17</sub> Pb <sub>83</sub>	589	540	4

### B.2.c Mechanical Design Considerations

The mechanical design concerns pertinent to the ball-in-tube alternate design are listed as follows:

1. Large number of mechanical gates to control ball flow.
2. Penetration of thorium ball tube through the blanket base walls.

The walls are in complex motion during reactor life and the tube would restrain this unless special flexing entries are made.

3. Reliability of ball flow and consequence of hung-up ball.
4. Difficulty of mechanical gating and fluid control if a ball contacting medium is required to flood the ball tube.

Regarding concern number 3, our safety modeling indicated that, due to high power generation in the balls themselves, a hung-up ball would melt within several minutes following a loss of coolant or loss of heat transfer capability event. These concerns represent considerable tasks in overcoming the design difficulties and the fertile-in-tubes concept was not pursued.



## APPENDIX C

### UPDATED BERYLLIUM/MOLTEN SALT BLANKET DESIGN CONCEPTS

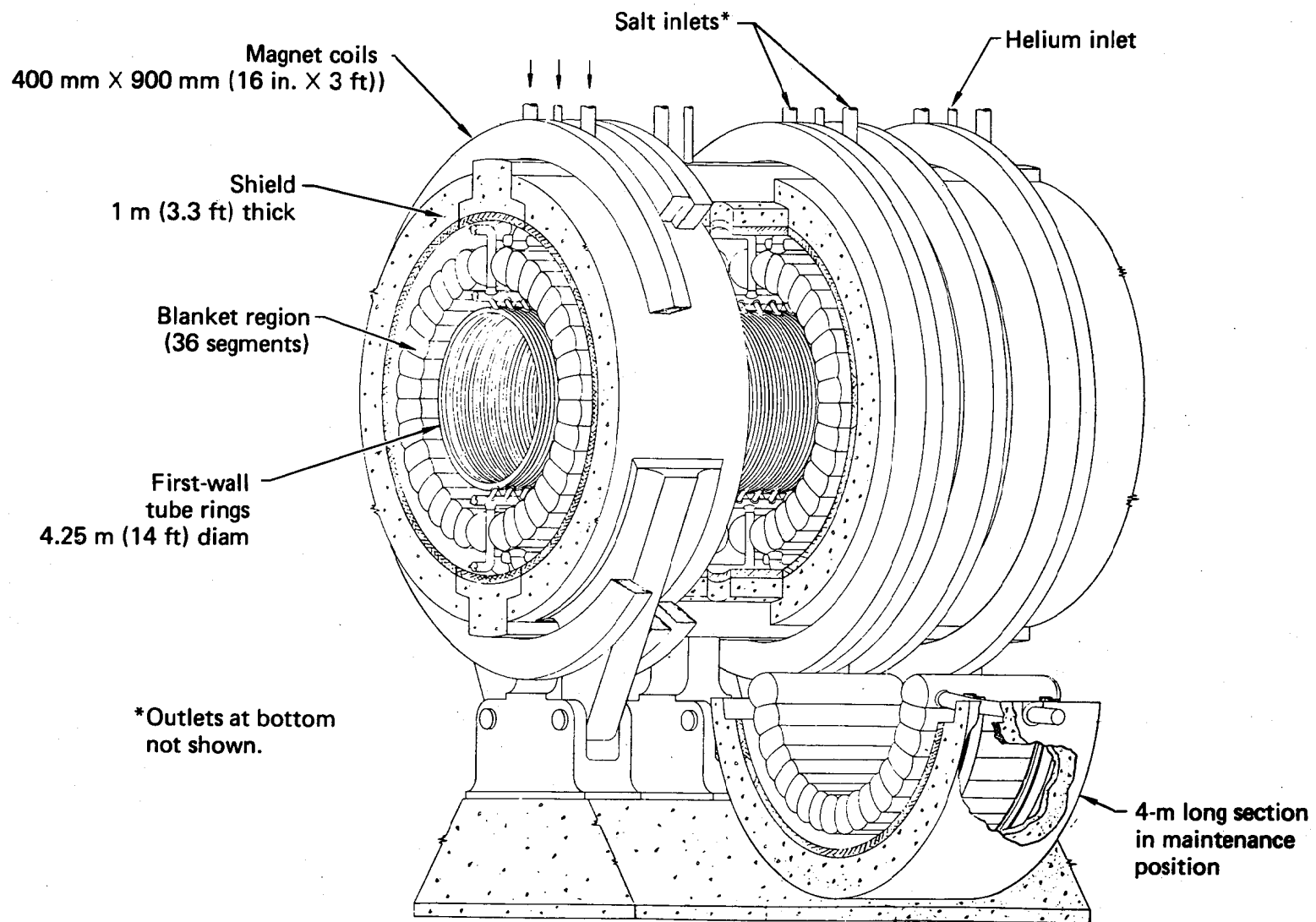
The combination of beryllium (Be) and molten salt (MS) for a fissile breeding, fission-suppressed blanket is still attractive if materials concerns can be circumvented, because beryllium gives the highest fissile breeding ratio (F), and molten salt, the lowest cost reprocessing. For the two-blanket concepts examined in this year's study, the Be/ThO<sub>2</sub> blanket has a F of 0.73 and a reprocessing cost of 46\$/g U233, while the lithium/molten salt has an F of 0.49 and a reprocessing cost of 3.1\$/g. Combining the advantage of the Be and MS would be the most desirable.

Our first try at conceptualizing a Be/MS blanket (1979 study)<sup>1,2</sup> was based on Be for neutron multiplication and the ORNL molten salt breeder reactor program technology base for materials and chemical processes. Based on the ORNL work, we initially chose Hastelloy N for structure and graphite as cladding for the Be. Unfortunately, radiation damage problems preclude using Hastelloy, at least near the first wall. TZM was chosen to replace Hastelloy, but TZM has welding problems that require further development, so its choice was also unattractive. The 1979 Be/MS reference blanket design is shown in Figs. C-1 and C-2.

Adapting the frozen salt wall concept to the Be/MS blanket would allow the use of conventional structural materials, such as SS-316, for salt containment, thus circumventing a major feasibility issue encountered in the 1979 Be/MS design. TZM might be all right for internal structure; graphite was another possibility.

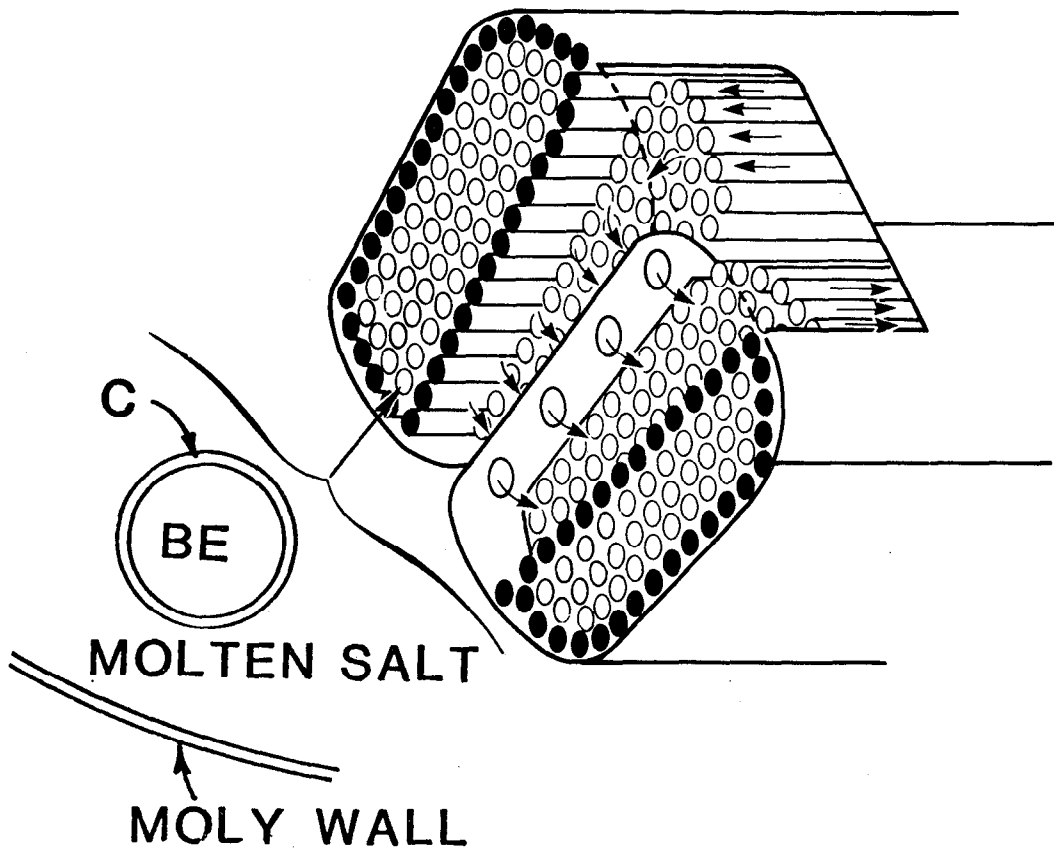
Another major feasibility issue with the initial Be/MS blanket was radiation damage (mainly swelling) of the beryllium and its graphite coating. A combination of factors are combining to alleviate the potential effects of swelling. One is the idea of having free standing (or more accurately floating in MS, C-coated, or other material such as Mo) Be spheres that can adjust for swelling and can be dumped or replaced when necessary. Recladding the balls, or even just patching the existing cladding, may be sufficient. We might even be able to come up with a "ball" design that can accommodate all the swelling. Swelling in Be is predicated to saturate at 10% (see Section V.C.1.e). The desired packing fraction may be achieved by using spheres with two or three different diameters.

C-2



72-127-0

FIGURE C-1. 1979 beryllium/molten salt reference blanket design.



72-128-0

FIGURE C-2. Cutaway of the 1979 beryllium/molten salt reference blanket design.

Another mitigating factor is the possibility that cracks in the cladding may tend to be self-healing. Also MS does not wet graphite, so small cracks may not cause Be/MS contact.

The proposed Be/MS blanket is conceptually simple. It contains clad Be balls in a zone about 50-cm thick, surrounded by a graphite zone for additional moderation. Molten salt containing both  $\text{ThF}_4$  and  $\text{LiF}$  is pumped through both the Be and graphite zones. The molten salt is the coolant as well as a mobile, fertile fuel. The molten-salt-containing blanket structure is SS-316. The SS-316 is protected from the molten salt by a frozen salt layer, as in this year's Li/MS design. The frozen layer is maintained by a second coolant circuit keeping the SS-316 temperature below the freezing point of the salt ( $490^\circ\text{C}$  for 12 mole percent and  $550^\circ\text{C}$  for 27 mole percent  $\text{ThF}_4$  salt). The secondary coolant could be Li, as in the Li/MS design, but more benign coolants, such as He or  $\text{H}_2\text{O}$ , seem more attractive from a safety point of view. Flibe is a possibility, too. The Be/MS design does not require Li, as the Li/MS design does. By running the blanket structure cool, it could last a long time, maybe even for the entire reactor lifetime. The Be balls can be changed as required without blanket disassembly. Fissile and fusile fuels bred in the molten salt are continuously removed by the same molten salt processing used in this year's Li/MS blanket. If it turns out that the Be does not require frequent replacement, a more efficient geometry (than balls) could be used.

A schematic drawing of the update Be/MS design concept is shown in Figs. C-3 through C-6. The walls are cooled to keep the salt frozen to protect the steel from corrosion. The wall might also be coated with graphite.

Since the wall is made up of two layers, separately cooled, it serves as an independent first wall, as in the separate first wall of the 1979 Be/MS designs. Failure of either the vacuum boundary wall or the molten salt boundary wall, separately, need not expose the vacuum chamber to radioactive material contamination. Another feature of the design also coming out of this year's work is to use Hastelloy for all structural material and piping in the back of the blanket where the neutron flux is low. Thus the back of the blanket, piping, and heat exchangers are all MSRE-based technology, and hence can be considered available technology.

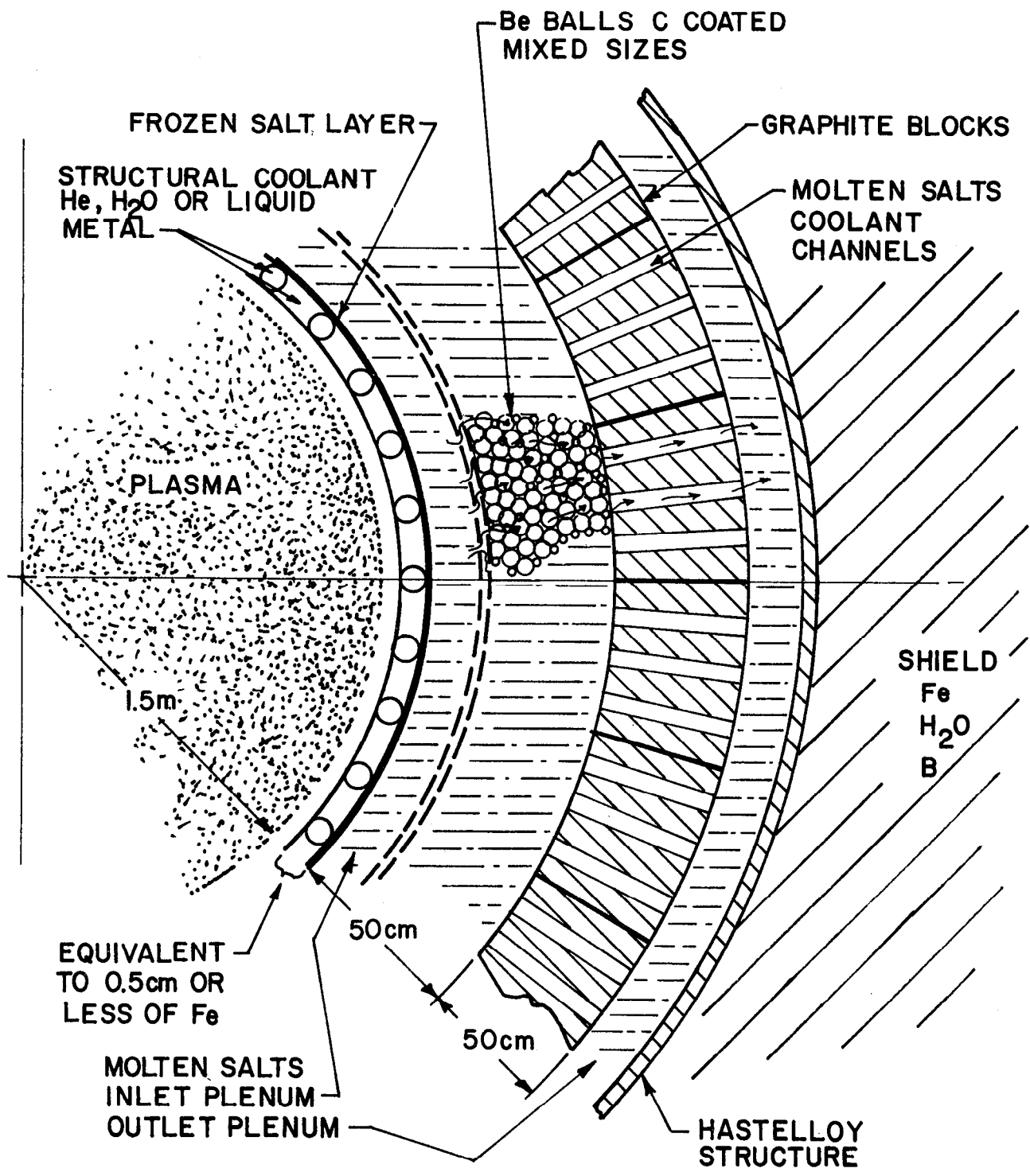


FIGURE C-3. Schematic arrangement of the updated 1979 beryllium/molten salt reference blanket design.

72-129-0

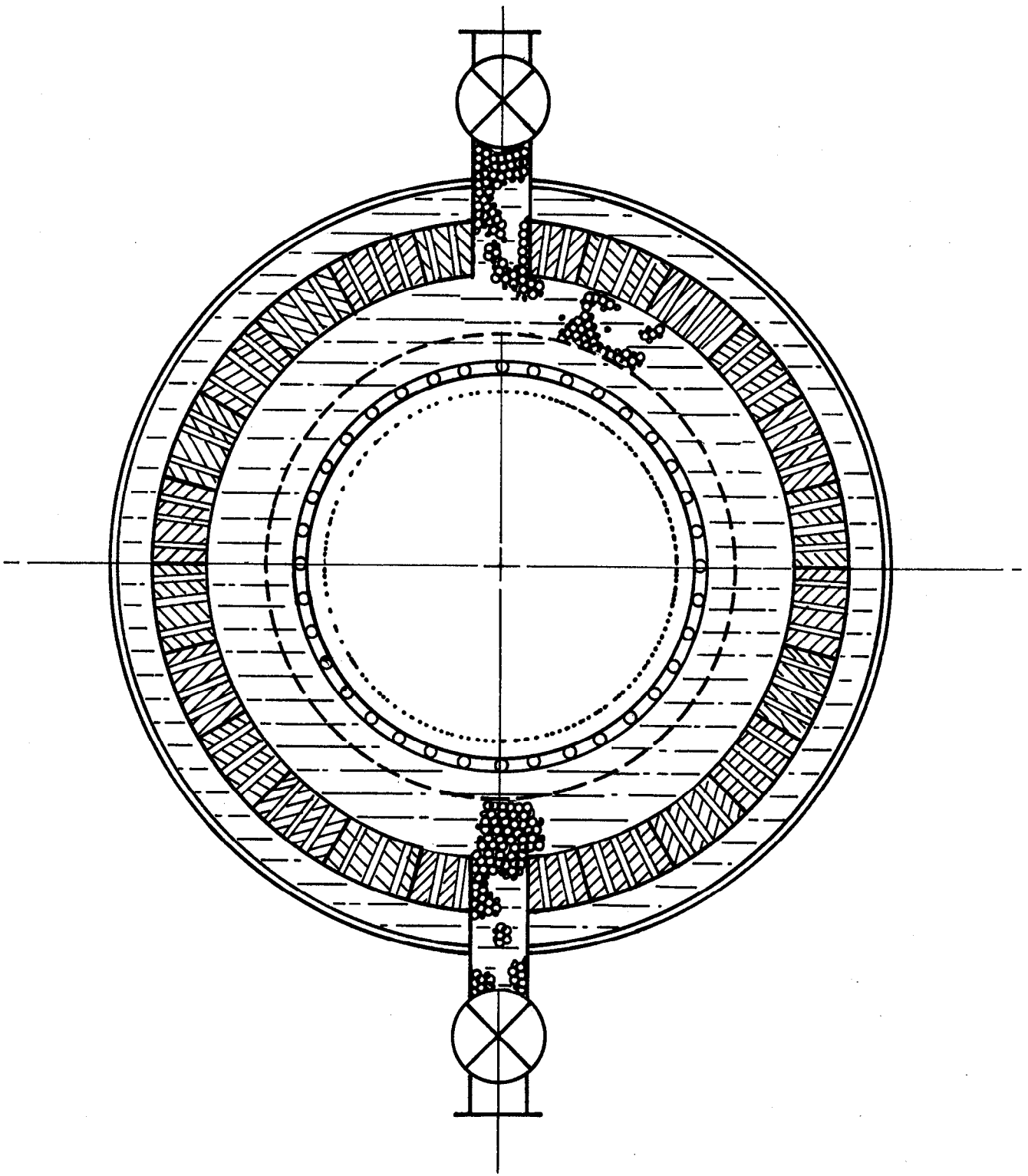


FIGURE C-4. Schematic arrangement of the Be ball transport.

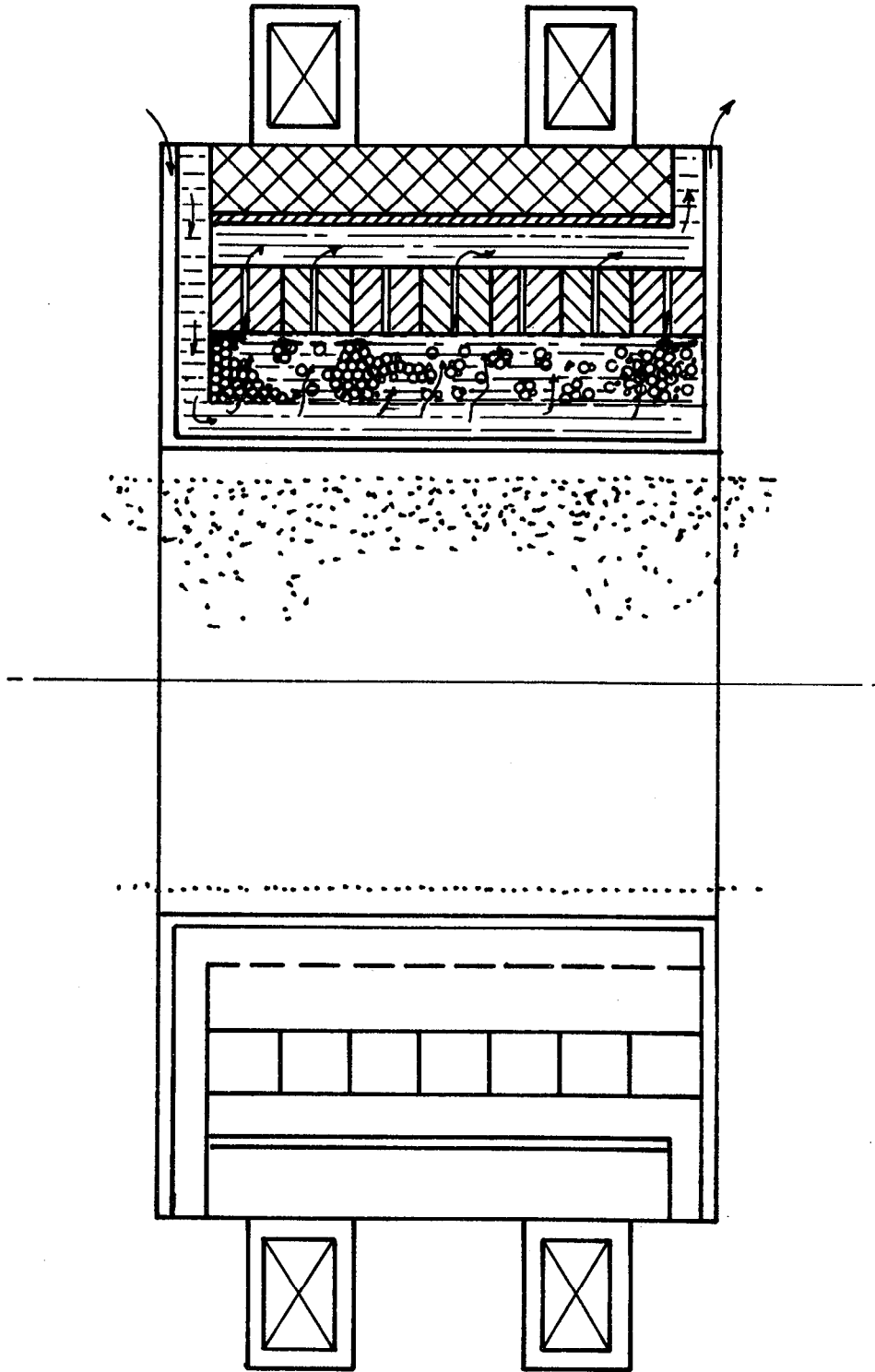


FIGURE C-5. Schematic arrangement showing radial molten salt coolant flow.

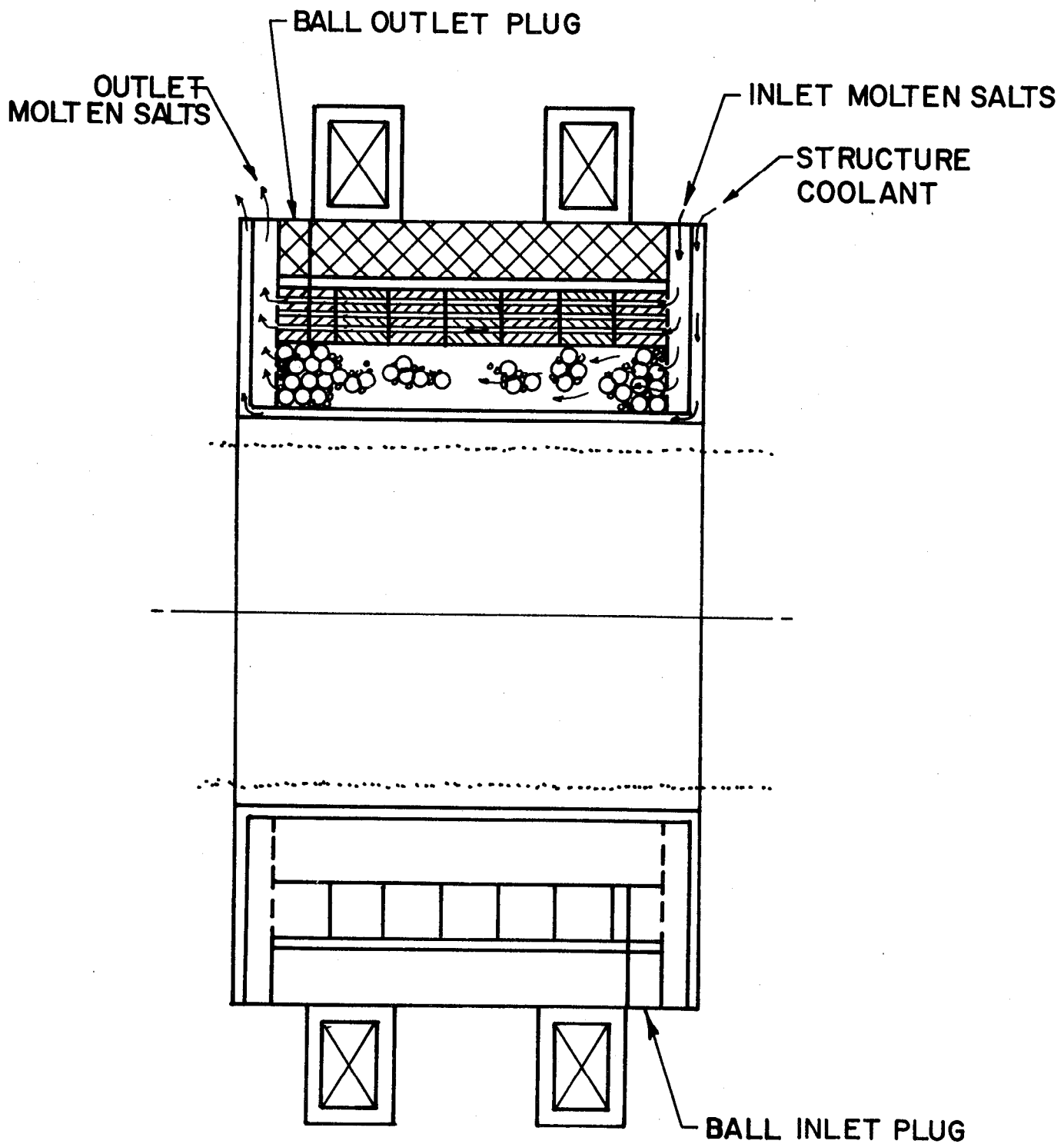


FIGURE C-6. Alternate molten salt flow and ball transport scheme (axial flow).

There are several key issues that may be go/no-go items. They are:

1. Cladding of Be that will adequately impede corrosion by the fluoride salt and accomodate swelling
2. A feasible mechanical design that will allow replacement of the Be, adequate heat removal, and avoid excessive galvanic enhanced corrosion due to MHD effects.
3. Maintaining a frozen salt layer on steel structure.

Other important questions are:

1. How best to remove T from molten salt.
2. How best to cool the structure.
3. Pressure drop in pebble beds.

The combination of beryllium and molten salt makes such an attractive fissile-breeding fusion-suppressed blanket, assuming we are successful in circumventing the materials concerns, that development of the Be/MS blanket should remain a goal of the fissile-breeding fusion-suppressed blanket program. Studies can provide the information needed to do cost benefit comparisons, including the cost of the development program. These comparisons would aid in choosing which blanket concepts should proceed on to the hardware stage of the development.

#### REFERENCES

1. J. D. Lee, "The Beryllium/Molten Salt Blanket," Lawrence Livermore National Laboratory, Report UCRL-82663 (1979); also published in Proceedings of the 3rd US/USSR Symposium on Fusion-Fission, Princeton, NJ (1979).
2. R. W. Moir et al., "Tandem Mirror Hybrid Reactor Design Study Annual Report," Lawrence Livermore National Laboratory, Report UCID-18808 (1980).